UNIVERSITÀ DEGLI STUDI DI MILANO

Department of Pharmaceutical Sciences
Doctoral programme in Pharmaceutical Sciences
XXXIV Cycle

Repurposing and morphing: a combined strategy to design multi target ligands

CHIM/08 – Medicinal Chemistry

PhD thesis of Angelica Artasensi
R12323

Supervisor: Prof. Laura Fumagalli

PhD Coordinator: Prof. Giancarlo Aldini

Academic Year 2020-2021

Abstract

Type 2 diabetes mellitus (T2DM) is one of the priority global health problems, which is characterized by dysregulation of carbohydrate, lipid, and protein metabolism and results from impaired insulin secretion, insulin resistance, or a combination of both. The global burden of diabetes had increased significantly since 1990[1], compelled to face this syndrome not only as a major threat to public health but also to socio-economic development.

The explosion of T2DM prevalence over the past half-century has paralleled that of the obesity epidemic[2]. The two inflammatory diseases are correlated since it has been shown that obesity induces immune cell changes in adipose tissue that affect insulin sensitivity[3,4]. Obesity and insulin resistance are two key drivers in the development of T2DM and are also connected to the development of both microvascular complications (including retinopathy, nephropathy, and neuropathy) and macrovascular complications (such as cardiovascular comorbidities). Other notable risk factors include a poor diet, low physical activity levels, and older age.

Multifactorial risk reduction strategies to normalize blood levels, lipid profile, and blood pressure are required to manage T2DM. Furthermore, it is also required continuous medical care, patient self-management for control of abnormal glucose levels.

Achievement of glycemic control requires a pharmacological approach that has progressed from biguanides and metformin to a wide spectrum of medications that seems to provide a beneficial effect on morbidity and mortality. Despite this, the target treatment goals are still not completely reached, so polypharmacological treatment is needed[5]. However, complex treatment regimens may lead to drug-drug interaction and/or poor patient adherence. Thus, novel antidiabetic drug classes capable of acting on several levels simultaneously are required. Nevertheless, in the state of metabolic disturbance, several major enzymes are abnormally expressed, thus they could be interesting targets in drug development. Hence, again, multimodal drugs, which could reduce hyperglycemia and concomitantly inhibit the progression of complications, may offer a valuable therapeutic option. The design of these multi-target ligands must focus on the selection of suitable targets, which must be well characterized and preferably implicated in different pathways of the disease, and on the optimization of the relative potency of the compound towards each interested protein[6]. To find new therapeutic compounds, a repurposing approach was applied on WB-4101, a well-known adrenergic ligand, to obtain potential dual ligands that would target different enzymes

involved in T2DM, namely Dipeptidyl Peptidase IV (DPP-IV) and Carbonic Anhydrase (CA-II and V). DPP-IV inhibitors prolong the half-life of the glucose-dependent insulinotropic polypeptide hormone (GIP) and the glucagon-like peptide 1 (GLP-1), two important regulators of post-prandial glycemic control[7]. On the other hand, CA inhibitors could be useful in the prevention of several common diabetic comorbidities.

WB-4101 has been chosen as a good "repurposable" candidate since previous computational studies showed that it conveniently fits into all these enzymes' pockets even if fails to interact with some key residues. To strengthen interactions towards the target enzymes, morphing WB-4101 has been required. Furthermore, this approach can lead to the design of more "drug-like" compounds with low molecular weight and with respect to Lipinski's rule of five.

Moreover, morphing would allow the modulation of the activity toward the old and new targets.

References

1. Saeedi, P. et al. Global and regional diabetes prevalence estimates for 2019 and projections for 2030 and 2045: Results from the International Diabetes Federation Diabetes Atlas, 9th edition. Diabetes Res. Clin. Pract. 157, (2019).
2. Wang, Y. C., McPherson, K., Marsh, T., Gortmaker, S. L. & Brown, M. Health and economic burden of the projected obesity trends in the USA and the UK. The Lancet vol. 378 815–825 (2011).
3. Weisberg, S. P. et al. Obesity is associated with macrophage accumulation in adipose tissue. J. Clin. Invest. 112, 1796–1808 (2003).
4. Xu, H. et al. Chronic inflammation in fat plays a crucial role in the development of obesity-related insulin resistance. J. Clin. Invest. 112, 1821–1830 (2003).
5. Artasensi, A., Pedretti, A., Vistoli, G. & Fumagalli, L. Type 2 Diabetes Mellitus: A Review of Multi-Target Drugs. Molecules 25, 1987 (2020).
6. Morphy, R., Kay, C. & Rankovic, Z. From magic bullets to designed multiple ligands. Drug Discov. Today 9, 641–651 (2004).
7. Irwin, N. New perspectives on exploitation of incretin peptides for the treatment of diabetes and related disorders. World J. Diabetes 6, 1285 (2015).

Table of contents

CHAPTER 1

Repurposing

Despite technological advancements and increased knowledge in the field of human diseases, the translation of these benefits into the drug development pipeline has been far slower than anticipated. The global pharmaceutical sector has several obstacles, such as high attrition rates, longer time to bring new pharmaceuticals to market, especially in particular therapeutic areas, and because of for regulatory requirements hurdle, all of which can add up to a greater cost. Due to the rising cost and length of time required for new drug development, it is estimated that less than a dollar of value is returned on average for every dollar spent on research and development (R&D), potentially making the pharmaceutical industry a less appealing investment option for investors[1].

In order to overcome the difficulties above mentioned drug repurposing (also called drug repositioning, reprofiling, or re-tasking) arise as a strategy for exploring new abilities to treat diseases/conditions beside the intended purpose with the aim to promote novel uses for known compounds[2]. Drug repurposing has accounted for over one-third of recent approvals, so that repurposed pharmaceuticals now account for roughly 25% of the pharmaceutical industry's yearly income[3].

A successful drug repositioning case is sildenafil citrate, now marketed as Viagra, which was originally developed as an antihypertensive drug, and repurposed by Pfizer for the treatment of erectile dysfunction. In 2012, it had a market-leading 47% share of the erectile dysfunction medicine market, with $2.05 billion in global sales[4]. Another effective example is Thalidomide: approved in 1957 and pulled from the market four years later due to the association to severe skeletal birth defects (phocomelia) in children born to women who took the drug during the first trimester of their pregnancy[5]. In recent decades, however, a more favorable aspect of thalidomide has emerged since it was found to be effective first in the treatment of erythema nodosum leprosum (in 1964) and decades later in multiple myeloma (in 1999)[6].

Table 1.1 shows selected successful drug repurposing examples along with the repositioning approaches employed, most of which so far have derived from an understanding of the pharmacology of the drug or retrospective analyses of the clinical effect of the drug when prescribed for its original indication.

Historically, drug repositioning cases are a result of an unintentional, serendipitous process and were

meant to find new scope outside the original indication, but drug repurposing strategies may also be applied as a business model by the pharmaceutical industry forward commercial exploitation. It is possible through the repositioning process to aim at changing price, patient population (drug racializing), and market share[7]. Moreover, the impact of drug repurposing holds many appeals: first, and perhaps most importantly, there is an enhanced chance for a successful launch. This is due to the larger amount of data/information available for the repurposed candidate since most of the preclinical testing, safety assessment, and, in some cases, formulation development have already been completed. These contribute also to save and to reduce the timeframe for preclinical, and phase I and II while regulatory and phase III costs may remain more or less the same.

Table 1.1 | **Some successful drug repurposing examples.**

Drug name	Original indication	New indication	Date of approval	Repurposing approach used	Comments on outcome of repurposing
Zidovudine	Cancer	HIV/AIDS	1987	In vitro screening of compound libraries	Zidovudine was the first anti-HIV drug to be approved by the FDA
Minoxidil	Hypertension	Hair loss	1988	Retrospective clinical analysis (identification of hair growth as an adverse effect)	Global sales for minoxidil were US$860 million in 2016 (Questale minoxidil sales report 2017; see Related links)
Sildenafil	Angina	Erectile dysfunction	1998	Retrospective clinical analysis	Marketed as Viagra, sildenafil became the leading product in the erectile dysfunction drug market, with global sales in 2012 of $2.05 billion8
Thalidomide	Morning sickness	Erythema nodosum leprosum and multiple myeloma	1998 and 2006	Off-label usage and pharmacological analysis	Thalidomide derivatives have achieved substantial clinical and commercial success in multiple myeloma
Celecoxib	Pain and inflammation	Familial adenomatous polyps	2000	Pharmacological analysis	The total revenue from Celebrex (Pfizer) at the end of 2014 was $2.69 billion (Pfizer 2014 financial report; see Related links)
Atomoxetine	Parkinson disease	ADHD	2002	Pharmacological analysis	Strattera (Eli Lilly) recorded global sales of $855 million in 2016
Duloxetine	Depression	SUI	2004	Pharmacological analysis	Approved by the EMA for SUI. The application was withdrawn in the US. Duloxetine is approved for the treatment of depression and chronic pain in the US
Rituximab	Various cancers	Rheumatoid arthritis	2006	Retrospective clinical analysis (remission of coexisting rheumatoid arthritis in patients with non-Hodgkin lymphoma treated with rituximab144)	Global sales of rituximab topped $7 billion in 2015
Raloxifene	Osteoporosis	Breast cancer	2007	Retrospective clinical analysis	Approved by the FDA for invasive breast cancer. Worldwide sales of $237 million in 2015
Fingolimod	Transplant rejection	MS	2010	Pharmacological and structural analysis	First oral disease-modifying therapy to be approved for MS. Global sales for fingolimod (Gilenya) reached $3.1 billion in 2017
Dapoxetine	Analgesia and depression	Premature ejaculation	2012	Pharmacological analysis	Approved in the UK and a number of European countries; still awaiting approval in the US. Peak sales are projected to reach $750 million
Topiramate	Epilepsy	Obesity	2012	Pharmacological analysis	Qsymia (Vivus) contains topiramate in combination with phentermine
Ketoconazole	Fungal infections	Cushing syndrome	2014	Pharmacological analysis	Approved by the EMA for Cushing syndrome in adults and adolescents above the age of 12 years
Aspirin	Analgesia	Colorectal cancer	2015	Retrospective clinical and pharmacological analysis	US Preventive Services Task Force released draft recommendations in September 2015 regarding the use of aspirin to help prevent cardiovascular disease and colorectal cancer

In addition, these benefits could lead to reduced risk and faster return on investment in the development of repurposed compounds, as well as lower average associated costs in case of failure. Furthermore, the evolution of related publications reflects the growing interest of academia in drug repurposing as shown in Figure 1.1.

Figure 1.1 | **Number of Scopus-indexed publications containing the terms 'drug' and 'repurposing' or 'drug' and 'repositioning' in their title, abstract, or keywords, versus year of publication.**

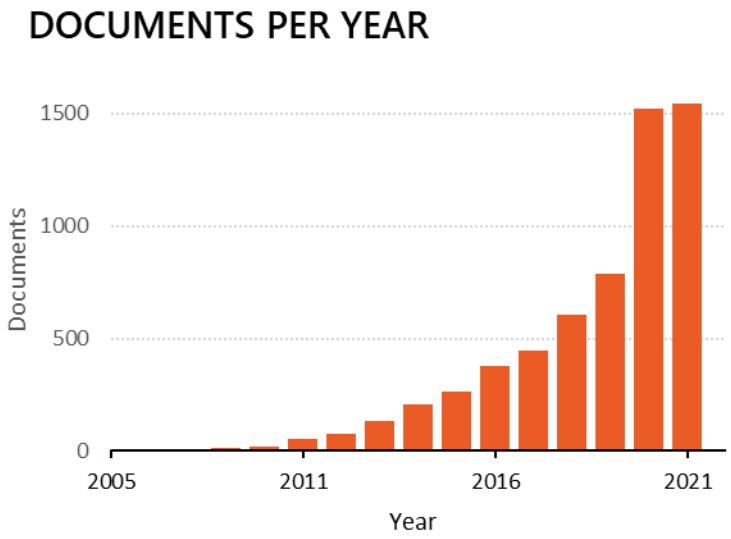

1.1 Enabling Tools and Technology

Typically, a general drug repurposing workflow starts with the identification of a candidate repurposable molecule. Given the amount and quality of evidence provided (i.e., 0–4, Table 1.2), a classification known as Drug Repositioning Evidence Level (DREL) has been proposed for drug repositioning projects, comparable to the classification approach used to measure medication–drug interactions.[8]

In practical terms, this classification suggests that as the evidence goes from *in vitro* research to animal and human investigations, the level of confidence rises, and those data having direct clinical significance are valued more highly.

Currently, there is no single, widely-adopted approach applied by the pharmaceutical industries for drug repurposing. In fact, most of the successful and best-known repositioning examples (e.g. Sildenafil, Thalidomide, Minoxidil, and Aspirin) were the result of serendipitous discovery.

Table 1.2 | **Classification of drug repurposing claims according to scientific evidence.**

Drug repositioning evidence level	Quality of scientific evidence
0	No evidence; includes *in silico* predictions without confirmation
1	*In vitro* studies with limited value for predicting *in vivo* /human situation
2	Animal studies with hypothetical relevance in man
3	Incomplete studies in man at the appropriatedose, e.g., proof of concept; very few cases orinference from medical records; some clinical effects observed
4	Well-documented clinical end points observed forthe repurposed drug at doses within safety limits

Nowadays, though, companies have implemented organized, systematic, data-driven efforts in the repurposing process, which integrate also computational science.

1.2 Computational approaches

The availability of high-performance computation and numerous databases has improved the capacity to design and validate automated workflows that can generate hypotheses for drug repurposing and rescue[9]. Furthermore, since new platform data sources become accessible, the literature database grows, and analytical methodology improves, so these strategies are projected to gain their value.

Various computational approaches can be used individually or in combination to systematically analyze different types of large-scale data to obtain meaningful interpretations for repurposing hypotheses.

The most commonly used computational approaches, together with drug repurposing examples, are discussed below

1.2.1 Signature matching

Signature matching compares a drug's distinct qualities, or "signature," with those of another drug, disease, or clinical phenotype[10]. This approach has been effective in identifying connections between diseases, genes, and drugs, involved in the same biological process by combining a large collection of gene expression data following drug treatment with a pattern-matching method. Three forms of

knowledge can be used to create a drug's signature: transcriptome (RNA), proteomic, or metabolomic data; chemical structures; and adverse event profiles (Figure 1.2).

Figure 1.2 | **The three general types of data that contribute to signaling matching.**

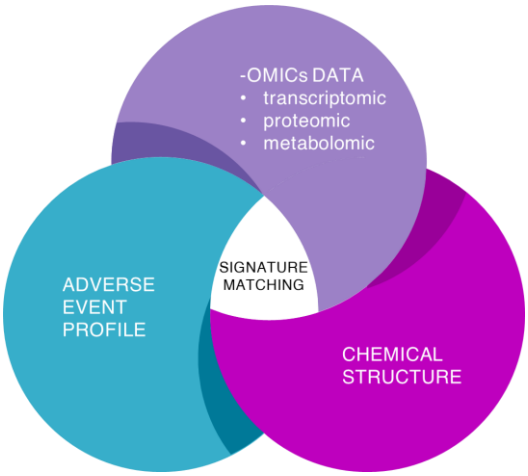

Matching transcriptomic signatures can be used to make drug-disease comparisons (estimating drug-disease similarity) and drug-drug comparisons (drug-drug similarity).

Initially, drug-disease comparison investigates gene expression profiles before and after treatment with a candidate drug. The results are then compared to the healthy expression profile and the disease-associated expression profile. This strategy is based on the signature reversion principle (SRP), which states that a drug that can reverse the hallmark of a gene expression pattern for a specific illness phenotype is very likely to be able to reverse the disease phenotype in consideration[11]. The drug-drug comparison technique, on the other hand, looks for compounds that have a comparable mode of action despite differences in chemical structures in order to discover a drug's therapeutic potential. This concept is known as guilt by association, and it can help identify alternate targets for existing medications as well as potential off-target effects that can be researched for clinical use. Regardless of how similar or dissimilar their chemical structures are, a common transcriptome signature between two medications could imply that they share a therapeutic application. Both drug-disease and drug-drug similarity approaches involve matching of transcriptomic signatures and therefore rely heavily on publicly accessible gene expression data like the US National Institutes of Health (NIH) Library of Integrated Network-based Cellular Signatures[12]. This enormous resource can be used along with other important public repositories of transcriptomic data, such as the Gene Expression Omnibus[13] and Array Express[14]. Besides that, chemical profiles are extremely important for drug repositioning, which compares chemical structures with respect to the biological activities of two different medications. This procedure is carried out to understand

chemical similarities and, as a result, to build a network based on shared chemical properties in order to forecast novel targets for existing medications. However, there are several drawbacks with the use of chemical similarity signature matching for drug repurposing, such as errors in chemical structures as well as physiological effects that exist beyond the structural relationship (for example, a metabolite of the original drug could be the active molecule) could limit the use of this approach in drug repurposing.

1.2.2 Computational molecular docking

Molecular docking is a structure-based computational strategy to predict binding site complementarity between the ligand (for example, a drug) and the target (for example, a receptor)[15]. If a receptor target implicated in a disease has previously been identified, various compounds could be tested against that target (conventional docking: one target and multiple ligands). Drug libraries, on the other hand, maybe tested against a variety of target receptors[16] (inverse docking: numerous targets and one ligand) to find new interactions that could be used for repurposing. Although it sounds very promising, the value of docking algorithms in predicting binding affinity has been questioned, and while the technology is getting better, there are still some variances between software packages and predictability limitations[17]. Moreover, there is a paucity of well-curated macromolecular target databases that provide precise structural information. Finally, challenges may arise also when 3D structures for some protein targets of interest are not available, especially because pharmacological targets are frequently membrane proteins that are difficult to crystallize.

1.2.3 Genome-wide association studies

Genome-wide association studies, also known as GWASs, aim to define genetic variants associated with common diseases, providing insights into disease biology[18]. The data obtained may also aid in the identification of novel targets, some of which may be shared between diseases treated by drugs and disease phenotypes studied by GWASs, resulting in drug repositioning. Following advancements in genotyping technology, the completion of the Human Genome Project, and diminishing genotyping costs, the number of GWASs performed has increased substantially over the last ten years. Sanseau and colleagues[18] expanded the National Human Genome Research Institute's (NHGRI) collection of published GWASs features and discovered that genes linked to diseases traits were more likely to code for druggable or biopharmable proteins than the rest of the genome.

However, there are hurdles to using GWASs data for drug repositioning, and its applicability is still uncertain. GWASs data do not give extensive pathophysiological information[19]. Furthermore, signals in gene-rich regions with strong linkage disequilibrium may make challenging to identify causal

genes and/or gene variants. Another difficulty is the lack of knowledge on the gene variant's direction of action; functional investigations will be needed to determine this before choosing whether an activator or suppressor is required to regulate the disease. It should also be mentioned that our current understanding of the human genome is still far from full and complete, and many more additional genes may be identified in the future[20].

1.2.4 Pathway or network mapping

Pathway mapping is a network analysis on drug or disease networks based on gene expression patterns, disease pathology, and protein interaction, providing the necessary information in exploiting drug repositioning opportunities[21]. Some of the signature matching studies discussed earlier also make use of the network analysis approach[22]. These studies are helpful when the identified potential targets found via GWAS or other methods are not immediately amenable to drug development. In such cases, a pathway-based method might provide information on genes that are either upstream or downstream of the GWAS-associated target, which could be exploited for repurposing[23].

1.3 Experimental approaches

1.3.1 Binding assays to identify target interactions

Analyses of drug targets and off-targets, as well as drug repurposing, have become natural bedfellows in an era of chemical biology for target validation. The Cellular Thermo Stability Assay (CETSA) method, for example, has been developed to map target engagement in cells using biophysical principles that predict thermal stabilization of target proteins by drug-like ligands with the appropriate cellular affinity[24]. Furthermore, proteomic techniques such as affinity chromatography and mass spectrometry have been used as approaches to identify binding partners for an increasing number of drugs[25]. Chemical genetics can also provide a better understanding of the relationship between binding and efficacy in the cellular context[26]. Many of these studies are based on high-throughput direct binding or catalytic assays developed by the pharmaceutical industry, in which small-molecule–kinase binding is investigated across the kinome using a variety of *in vitro* and increasingly organism-based assays to generate heat maps of biologically important interactions.

1.3.2 Phenotypic screening

Phenotypic screening can identify drugs that have disease-relevant effects in model systems without knowing the target(s) impacted. This strategy usually employs a variety of cell-based tests in a 96-

well format (*in vitro* phenotypic screens), but whole-organism phenotypic assays are also utilized in drug repurposing. Typically the models utilized are immortalized human cancer cell lines (CCLs), that have been studied against hundreds of compounds (both authorized and experimental) in high-throughput drug screens to see how they affect cell survival[27]. CCLs are, of course, unsatisfactory models since they may have acquired molecular modifications that provide selective benefits for *in vitro* growth and are frequently biased towards specific molecular subtypes[28]. Despite these limitations, studies based on CCLs have demonstrated that finding pharmacogenomic interactions can recapitulate therapeutic genomic markers that are currently in clinical usage, with a degree of correlation that is equivalent to what is seen in the clinic. More recently, phenotypic screening has been integrated with GWAS studies (PheWAS), increasing the likelihood of the repurposed drug[18]. The hypothesis is that human illnesses derive from a phenotypic and genetic overlap. Therefore, many traits are the result of the interactome: several genes interacting with one another through a network to generate a certain phenotype. Additionally, this strategy may be used in conjunction with electronic medical records to identify a large number of phenotypic correlations from real-world clinical data[29,30].

In Figure 1.3 are schematized the approaches that can be used in drug repurposing.

Figure 1.3 | **Approaches used in drug repurposing**

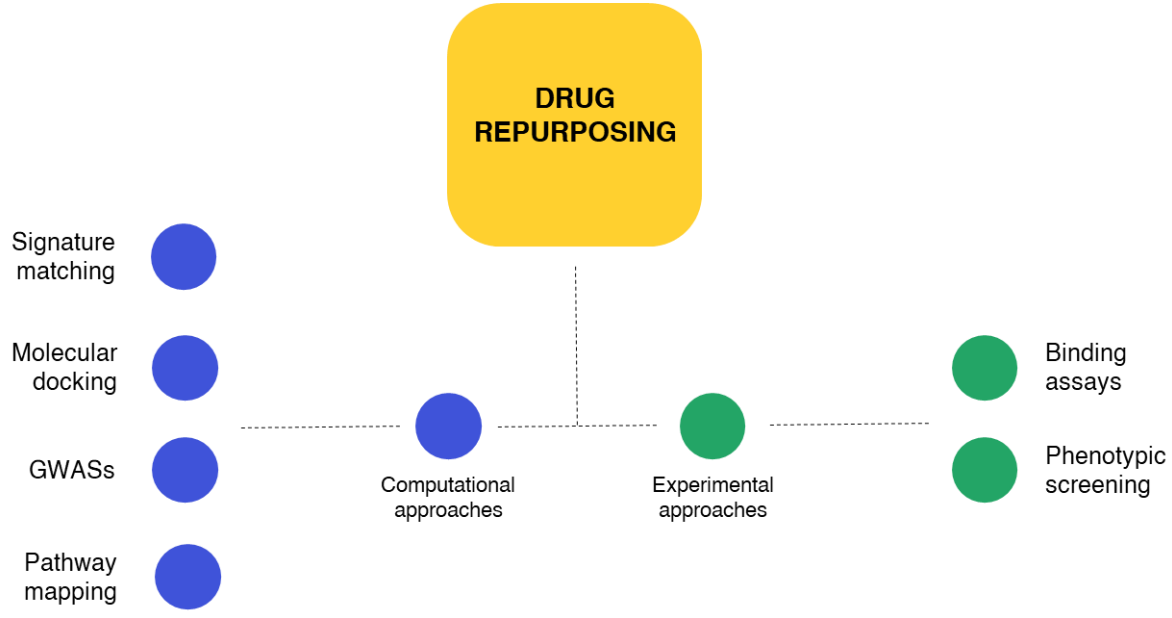

1.4 Retrospective clinical analysis

A systematic approach for analyzing clinical data is now increasingly suggested for identifying drug repurposing opportunities even though they have not been designed for that purpose. The best example of retrospective clinical analysis leading to the repurposing of a candidate molecule is

sildenafil[31]. Electronic medical records (EMRs), post-marketing surveillance data, and clinical trial data are all good places to look for retrospective clinical data[32]. EMRs have a massive quantity of structured and unstructured data on patient outcomes. Diagnostic and pathophysiological data, such as laboratory test results and drug prescribing information, are more structured; however, EMRs also contain a significant amount of unstructured data, such as clinical descriptions of patient symptoms and signs (which are important in defining disease phenotype) and imaging data. This vast quantity of data in EMRs might be utilized to discover medication repurposing signals; moreover, the massive volume of data in EMRs gives great statistical power. Other significant large data sources include post-marketing surveillance data and clinical trial data, however, their access may be restricted for commercial or confidentiality reasons. Nevertheless, more businesses are recognizing that allowing access to such a vast amount of data might help with drug development research. In fact, the EMA began providing direct public access to clinical trial data of pharmaceutical companies in October 2016[33], and has already published findings on six different drugs. Academics and researchers can utilize the data for independent reanalysis, which could lead to drug repurposing opportunities.

1.4.1 Collaborative models

Pharmaceutical companies and academia are increasingly realizing that new business models are required to propel the science of drug repurposing ahead. Therefore, new collaborative models that draw on the strengths of pharmaceutical companies biotechnology companies, academic researchers, venture capitalists, and others are needed if repurposing must be successful. By sharing data publicly in databases, drug repositioning efforts can be accelerated by using already existing data for the discovery of new drugs and targets. The Mechanisms for Human Diseases Initiative, which was launched in 2011 by the Medical Research Council (MRC) and AstraZeneca[34], and the Discovering New Therapeutic Uses for Existing Molecules initiative[35], which was launched in 2012 by the NIH–National Center for Advancing Translational Sciences (NIH–NCATS) in collaboration with partners, are two of the most important examples of this type of collaboration. Initially, the MRC–AstraZeneca collaboration identified 22 discontinued molecules for which AstraZeneca provided extensive information on the drug's potency, selectivity, pharmacology, pharmacokinetics, safety, and other features. The MRC's call for concept proposals received more than 100 submissions from 37 different UK universities, with 15 of them receiving funding from the MRC after peer review. In the first phase of the NIH–NCATS program, 57 molecules from eight different pharmaceutical companies were listed, and nine applications were funded in 2013, totaling $12.7 million. Academic researchers' enthusiasm for both of these programs demonstrated that they were viewed as

fascinating, once-in-a-lifetime possibilities to gain access to compounds that were previously unavailable to the public[34].

1.5 Potential barriers

With the development of new drugs, certain failures in late-stage development are unavoidable and sometimes are not related to the safety profile of the candidate like, for example, barriers related to intellectual property, regulatory consideration, and organizational hurdels[36]. Therefore, the design and successful implementation of well-thought-out repurposing methods can aid in the reduction of such issues while also adding significant value to pharmaceutical companies' pipelines. For example, companies usually submit plenty of other new patents during a product's life cycle to extend exclusivity, generally through line extensions (e.g., innovative formulations aimed at elderly patients rather than young patients) and repurposing. They can even claim that the chemicals produced by competitors are in the same drug class stifle their development efforts[37]. These legal issues could make patenting a new medical use and/or enforcing patent rights more difficult, reducing the incentives for drug repurposing. In this context, data exclusivity, which is a different way of acquiring market exclusivity than patenting a product, can be a key consideration, as patent exclusivity or remaining patent life. Regarding regulatory data exclusivity, the European Union provides 8 years of data protection plus 2 years of market exclusivity; if the originator develops a second indication during the 8-years data exclusivity period, an additional year of protection may be granted; the United States, on the other hand, grants an initial period of 5 years, which may be extended by 3 years for a new use[38]. Nonetheless, such extension of time may not be suitable to generate an acceptable return on investment, requiring additional economic incentives to make drug repurposing cost-effective. Given the hurdles outlined above, it may be necessary to assess how and to what degree intellectual property may be protected for a repurposed output at the start of the project. Some methods of increasing patentability include developing new formulations, dosage forms, or derivatives with a similar therapeutic effect, as well as securing exclusive marketing approval in new geographical areas[31]. Besides that, a legislative solution to these issues was unsuccessfully pursued in the UK through the Off-patent Drugs Bill (2015-2016). This proposal was intended to deal with the scenario in which a drug with an expired patent is proven to be effective for a new indication that is not covered by its license. Further to that, the British Generics Manufacturers Association (BGMA) has proposed a change to the R&D tax credits scheme that would allow any generics manufacturer with an appropriate marketing authorization to receive tax credits if they applied for a label extension in collaboration with an academic or non-profit partner[39]. Furthermore, out-licensing

or investigator-initiated studies may involve a support infrastructure and/ or legal agreements. Additionally, some organizational barriers may occur if the repurposed indication is not in the organization's primary disease area, or the compound has been discontinued in development, thus there is no longer an "active" project within the R&D division to provide focused support for the new indication. One approach to solving these challenges is to use external resources, or otherwise, funding routes can be considered when it would otherwise be impossible to do so within the company.

References

1. Pushpakom, S. *et al.* Drug repurposing: progress, challenges and recommendations. *Nat. Publ. Gr.* (2018) doi:10.1038/nrd.2018.168.
2. GNS, H. S., GR, S., Murahari, M. & Krishnamurthy, M. An update on Drug Repurposing: Re-written saga of the drug's fate. *Biomedicine and Pharmacotherapy* vol. 110 700–716 (2019).
3. Naylor, S., Kauppi, D. M. & Schonfeld, J. M. Therapeutic drug repurposing, repositioning and rescue: Part II: Business review. *Drug Discovery World* vol. 16 57–72 (2015).
4. Phillips, D. J. Pfizer's Expiring Viagra Patent Adversely Affects Other Drugmakers Too. *Forbes.com* https://www.forbes.com/sites/investor/2013/12/20/pfizers-expiring-viagra-patent-adversely-affects-other-drugmakers-too/?sh=3756030e68d4 (2013).
5. Vargesson, N. Thalidomide-induced teratogenesis: History and mechanisms. *Birth Defects Research Part C - Embryo Today: Reviews* vol. 105 140–156 (2015).
6. Millrine, D. & Kishimoto, T. A Brighter Side to Thalidomide: Its Potential Use in Immunological Disorders. *Trends in Molecular Medicine* vol. 23 348–361 (2017).
7. Huang, J. Can Drug Repositioning Work as a Systematical Business Model? *ACS Medicinal Chemistry Letters* vol. 11 1074–1075 (2020).
8. Oprea, T. I. & Overington, J. P. Computational and practical aspects of drug repositioning. *Assay Drug Dev. Technol.* 13, 299–306 (2015).
9. Hurle, M. R. *et al.* Computational Drug Repositioning: From Data to Therapeutics. *Clin. Pharmacol. Ther.* 93, 335–341 (2013).
10. Iorio, F., Rittman, T., Ge, H., Menden, M. & Saez-Rodriguez, J. Transcriptional data: A new gateway to drug repositioning? *Drug Discovery Today* vol. 18 350–357 (2013).
11. Low, Z. Y., Farouk, I. A. & Lal, S. K. Drug repositioning: New approaches and future prospects for life-debilitating diseases and the COVID-19 pandemic outbreak. *Viruses* vol. 12 (2020).
12. LINCS Program. NIH LINCS Program. https://lincsproject.org/ (2019).
13. National Center for Biotechnology Information. Home - GEO - NCBI. https://www.ncbi.nlm.nih.gov/geo/ (2015).
14. ArrayExpress. ArrayExpress EMBL-EBI. *ArrayExpress Archive of Functional Genomics Data* https://www.ebi.ac.uk/arrayexpress/ (2015).
15. Kitchen, D. B., Decornez, H., Furr, J. R. & Bajorath, J. Docking and scoring in virtual screening for drug discovery: Methods and applications. *Nature Reviews Drug Discovery* vol. 3 935–949 (2004).
16. Kharkar, P. S., Warrier, S. & Gaud, R. S. Reverse docking: A powerful tool for drug repositioning and drug rescue. *Future Medicinal Chemistry* vol. 6 333–342 (2014).
17. Pagadala, N. S., Syed, K. & Tuszynski, J. Software for molecular docking: a review. *Biophysical Reviews* vol. 9 91–102 (2017).
18. Sanseau, P. *et al.* Use of genome-wide association studies for drug repositioning. *Nature Biotechnology* vol. 30 317–320 (2012).
19. ZY, W. & HY, Z. Rational drug repositioning by medical genetics. *Nat. Biotechnol.* 31, 1080–1082 (2013).
20. Willyard, C. Expanded human gene tally reignites debate. *Nature* vol. 558 354–355 (2018).

21. Smith, S. B., Dampier, W., Tozeren, A., Brown, J. R. & Magid-Slav, M. Identification of common biological pathways and drug targets across multiple respiratory viruses based on human host gene expression analysis. *PLoS One* 7, (2012).
22. Iorio, F., Saez-Rodriguez, J. & Bernardo, D. di. Network based elucidation of drug response: From modulators to targets. *BMC Systems Biology* vol. 7 1–9 (2013).
23. Greene, C. S. & Voight, B. F. Pathway and network-based strategies to translate genetic discoveries into effective therapies. *Human Molecular Genetics* vol. 25 R94–R98 (2016).
24. Molina, D. M. *et al.* Monitoring drug target engagement in cells and tissues using the cellular thermal shift assay. *Science (80-.).* 341, 84–87 (2013).
25. Haymond, A., Davis, J. B. & Espina, V. Proteomics for cancer drug design. *Expert Rev. Proteomics* 16, 647–664 (2019).
26. Sloane, D. A. *et al.* Drug-resistant aurora a mutants for cellular target validation of the small molecule kinase inhibitors MLN8054 and MLN8237. *ACS Chem. Biol.* 5, 563–576 (2010).
27. Barretina, J. *et al.* The Cancer Cell Line Encyclopedia enables predictive modelling of anticancer drug sensitivity. *Nature* 483, 603–607 (2012).
28. Weinstein, J. N. Drug discovery: Cell lines battle cancer. *Nature* vol. 483 544–545 (2012).
29. Issa, N. T., Byers, S. W. & Dakshanamurthy, S. Big data: The next frontier for innovation in therapeutics and healthcare. *Expert Review of Clinical Pharmacology* vol. 7 293–298 (2014).
30. Denny, J. C. *et al.* Systematic comparison of phenome-wide association study of electronic medical record data and genome-wide association study data. *Nat. Biotechnol.* 31, 1102–1110 (2013).
31. Ashburn, T. T. & Thor, K. B. Drug repositioning: Identifying and developing new uses for existing drugs. *Nature Reviews Drug Discovery* vol. 3 673–683 (2004).
32. Jensen, P. B., Jensen, L. J. & Brunak, S. Mining electronic health records: Towards better research applications and clinical care. *Nature Reviews Genetics* vol. 13 395–405 (2012).
33. Home - Clinical Data Publication - clinicaldata.ema.europa.eu . https://clinicaldata.ema.europa.eu/web/cdp/home.
34. Frail, D. E. *et al.* Pioneering government-sponsored drug repositioning collaborations: Progress and learning. *Nature Reviews Drug Discovery* vol. 14 833–841 (2015).
35. Innovation, C. National Center for Advancing Translational Sciences. *Sci. York* 3, 8–9 (2004).
36. Talevi, A. & Bellera, C. L. Challenges and opportunities with drug repurposing: finding strategies to find alternative uses of therapeutics. *Expert Opinion on Drug Discovery* vol. 15 397–401 (2020).
37. Sternitzke, C. Drug repurposing and the prior art patents of competitors. *Drug Discovery Today* vol. 19 1841–1847 (2014).
38. Breckenridge, A. & Jacob, R. Overcoming the legal and regulatory barriers to drug repurposing. *Nature Reviews Drug Discovery* vol. 18 1–2 (2018).
39. Pantziarka, P. Scientific advice-is drug repurposing missing a trick? *Nature Reviews Clinical Oncology* vol. 14 455–456 (2017).

CHAPTER 2

Type 2 Diabetes

Type 2 diabetes (T2DM) is a chronic condition characterized by dysregulation of carbohydrate, lipid, and protein metabolism and results from impaired insulin secretion, insulin resistance, or a combination of both. Of the three major types of diabetes, T2DM is far more common (accounting for more than 90% of all cases) than either type 1 diabetes mellitus (T1DM) or gestational diabetes. T2DM incidence has risen in lockstep with the obesity pandemic during the last half-century[1]. Increasing adiposity, as reflected by higher body mass index levels (BMI), is a key risk factor for T2DM[2] (Figure 2.1). In fact, obesity causes immune cell alterations in adipose tissue that impair insulin sensitivity[3,4]. Both these conditions are crucial drivers in the development of the disease and they have been linked to microvascular (i.e. retinopathy, nephropathy, and neuropathy) and macrovascular complications (i.e. cardiovascular comorbidities).

Figure 2.1 | **Association between BMI and T2DM**

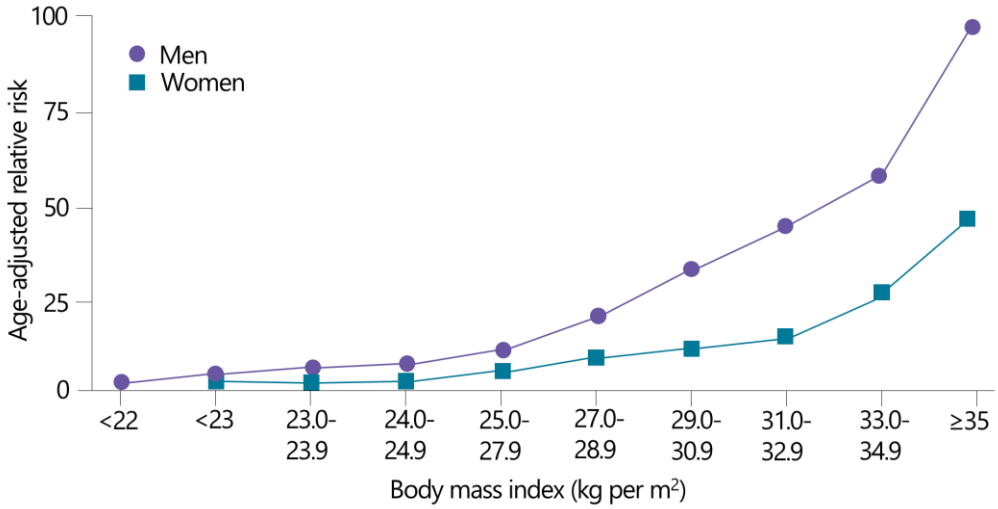

Moreover, a poor diet, a lack of physical exercise, and older age are all noteworthy risk factors. As a consequence, multifactor risk reduction strategies are needed to normalize blood glucose levels, lipid profiles, and blood pressure to prevent or minimize these acute and long-term comorbidities. Hence, T2DM should be viewed as a heterogeneous and chronic disorder with various pathophysiological abnormalities, variable susceptibility to complications, and different clinical responses to treatment intervention. In the end, a real "cure" for T2DM will necessitate the understanding of its molecular etiology as well as efficient obesity-fighting treatments.

Because of the rapidly escalating prevalence of T2DM, there is an urgent need for new preventive and therapeutic approaches to treat this disease.

2.1 Epidemiology

Globalization has led to significant changes in the human environment, as well as in human behavior and lifestyle, which have resulted in an unprecedented increase in the rate of patients with obesity and T2DM[5]. According to the International Diabetes Federation (IDF), 463 million individuals worldwide are currently living with T2DM[6], and this number is expected to rise to 702 million by 2045, as represented in Figure 2.2. However, these IDF estimates are likely an underestimation[7]: the inaccuracy is due to lack of data from many countries, not only poor ones.

Figure 2.2 | **Estimated number of adults with diabetes (in millions)**

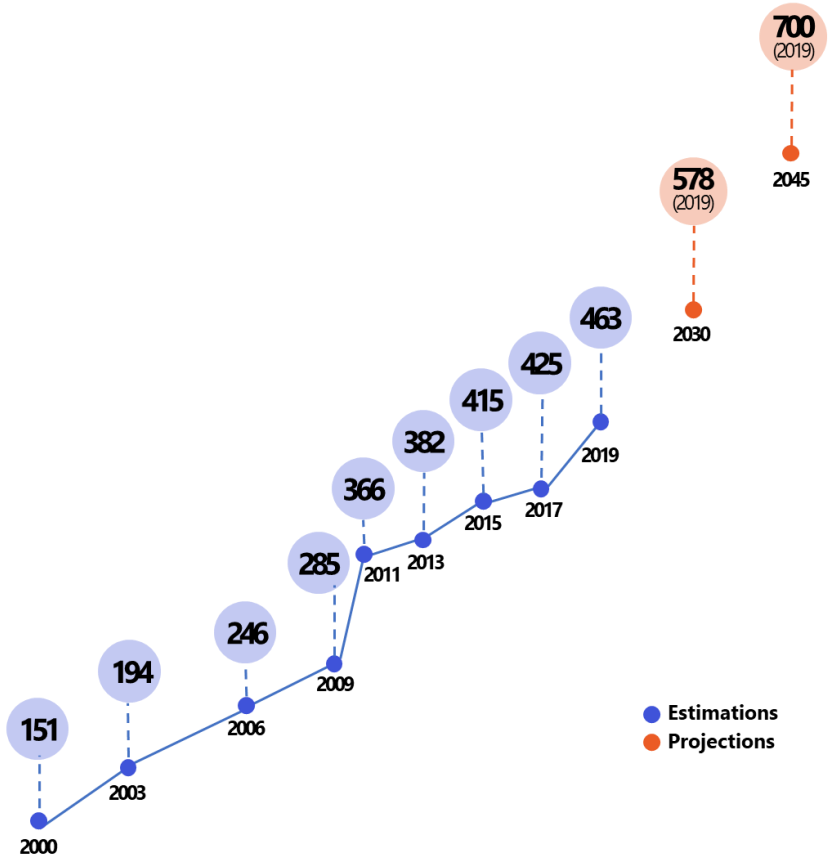

Furthermore, this chronic condition, which was the sixth biggest cause of disability in 2015[8], exerts significant socio-economic constraints on individuals and costs to the global health economy an estimated $825 billion[9], putting a huge burden on healthcare systems.

T2DM incidence and prevalence vary according to the geographic region, with more than 80% of patients living in low-to-middle-income areas, although diabetes prevalence has increased in all countries since 1980[10]. China and India are severely impacted by this condition, as the prevalence of

T2DM has risen dramatically despite the low prevalence of obesity[11]. This increased propensity to T2DM could be explained by the fact that Asians have a higher percentage of body fat mass, more abdominal obesity, and less muscle mass given the same BMI[12]. Furthermore, an additional 318 million people have a preclinical condition of impaired glucose regulation, although T2DM can be prevented or delayed with rigorous lifestyle interventions (weight loss and exercise) alone. Epidemiological studies have improved our understanding of the behavioral, lifestyle, and biological risk factors for T2DM, as represented in Box 2.1.

Box 2.1 | **Risk factors for T2DM**

- Older age
- Non-white ancestry
- Family history of T2DM
- Genetic factors
- Components of the metabolic syndrome (increased waist circumference, increased blood pressure, increased plasma triglyceride levels, and low plasma high-density lipoprotein (HDL) cholesterol levels and small dense low-density lipoprotein (LDL) cholesterol particles
- Overweight or obese (body mass index (BMI of ≥25kg per m^2)
- Abdominal or central obesity (independent of BMI)
- Polycystic ovary syndrome
- History of atherosclerotic cardiovascular disease
- Unhealthy dietary factors (regular consumption of sugary beverages and red meats, and low consumption of whole grains and other fiber-rich foods)
- Cigarette smoking
- Sedentary lifestyle
- History of gestational diabetes or delivery of newborns > 4kg in weight
- Presence of acanthosis nigricans (hyperpigmentation of the skin)
- Some medications
- Short and long sleep duration and rotating shift work
- Psychosocial and economic factors

Although genetics has a crucial role in the development of T2DM[13], the current diabetes pandemic cannot be explained solely by unique genetic changes, but rather by the obesity epidemic[14]. As a consequence, today, the average age of onset is dropping, and diabetes is frequently be detected in youngsters while, until two decades ago, T2DM was commonly observed in adults and elderly. Obesity is associated with an increase in insulin resistance as a result of body composition changes (less muscle in favor of more adipose tissues), a reduction in "sugar burning" ability, and a gradual decrease in physical activity.

Further to that, certain dietary components, such as higher intake of whole grains, green leafy vegetables, nuts, and coffee, are linked to a lower risk of T2DM, regardless of body weight; while higher intake of refined grains, red and processed meat, and sugar-sweetened beverages; and moderate intake of alcohol are strongly associated with higher diabetes risk[15]. Recent pieces of

evidence suggest also that there is a link between T2DM and the intestinal microbiota[16,17].

Physical inactivity is a major behavioral risk factor, and both aerobic and resistance exercise can help[18]. Sedentary behavior, like watching too much television, has been linked to an increased risk[19]. Short (about five hours per night) and long (about nine hours per night) sleep lengths, as well as rotating shift employment, are all linked to an elevated risk[20].

Furthermore, regardless of body weight or other risk variables, cigarette smoking is a major risk factor for developing T2DM[11].

In conclusion, up to 90% of T2DM cases may be avoided by eating a balanced diet, maintaining a BMI of 25 kg per m^2, exercising for at least 30 minutes each day, avoiding smoking, and consuming alcohol in moderation[21,22].

2.2 Pathophysiology

T2DM is a multifactorial disease involving genetic and environmental factors. The relative risk of developing T2DM is 2-3 times higher when a sibling suffers from this disease, but this value markedly increased (up to 30) when two siblings have T2DM[23]. Moreover, genetic factors exert their effect following exposure to an obesogenic environment characterized by sedentary behavior and excessive sugar and fat consumption: lifestyle aspects that are usually shared by family members. It has been indeed challenging to pinpoint which genes are responsible for a complicated polygenic disorder like T2DM. More than 100 common variations of glycemic genetic characteristics for T2DM have been identified by GWASs[24,25]. Some of single-nucleotide polymorphism (SNP) that are reported to have a strong association with T2DM are *TCF7L2, SLC30A8, FTO, CDKAL1, CDKN2A, CDKN2B, HHEX, IGF2BP2, GCKR,* and others. However, these genetic variants only account for 10-20% of the overall risk. In fact, the majority of non-diabetic people carries risk variants for T2DM, and the average frequency of a T2DM-associated risk allele is 54%[26]. Moreover, estimation of genetic architecture suggests that both rare and common variants contribute to the genetic variation and indicates that rarer variants tend to have larger effects on T2DM risk[27].

2.2.1 β-cells in T2DM

The definition of overt T2DM is characterized by blood glucose levels equal to or higher than 7 mmol/L during fasting and a two hours post glucose tolerance test level equal to or higher than 11 mmol/L[28]. According to the literature, T2DM clinical manifestations are consequences of impaired β-cell functions. However, the exact mechanisms of the development of this chronic condition are still undefined[29].

In the prediabetic phase, islet β-cells are capable of maintaining normoglycemia and metabolic

homeostasis following the development of insulin resistance by boosting insulin production and/or its release. Small increases in blood glucose levels (like those seen in obese normal glucose-tolerant people) as well as other variables, such as elevated levels of free fatty acids (FFAs), are likely to play a role in this chronic adaptation[30]. In addition, people who suffer from T2DM are also characterized by a severely compromised incretin hormones (GLP-1 and GIP) system, which fails to stimulate insulin release[31], and the incretin defect is not reversed by reducing the plasma glucose concentration [32]. Over time, the islet β-cells ability to secrete insulin declines, and they may undergo apoptosis[33] or dysregulated autophagy[34] as a result of a variety of stressors, including increased insulin demand, oxidative, endoplasmic, reticulum, dyslipidemic, amyloid, and inflammatory stress[35,36]. Investigation on post-mortem tissues from patients with T2DM[37] demonstrated that the β-cell mass is reduced by 30–40%, compared to the non-diabetic one (Figure 2.3). However, in obese individuals who are not diabetic, β-cell mass is expanded (in some proportion to the degree of weight excess), but their β-cell function is comparable to individuals with a normal BMI. Furthermore, insulin resistance promotes a relative preponderance of α-cells over β-cells[30], which might be due to a process of dedifferentiation and subsequent redifferentiation, leading also to the gradual loss of β-cell mass. It has been reported that the decline in islet β-cell function can begin an average of 12 years before T2DM diagnosis.

Figure 2.3 | **Schematic representation of the relationship between β-cell mass and β-cell function**

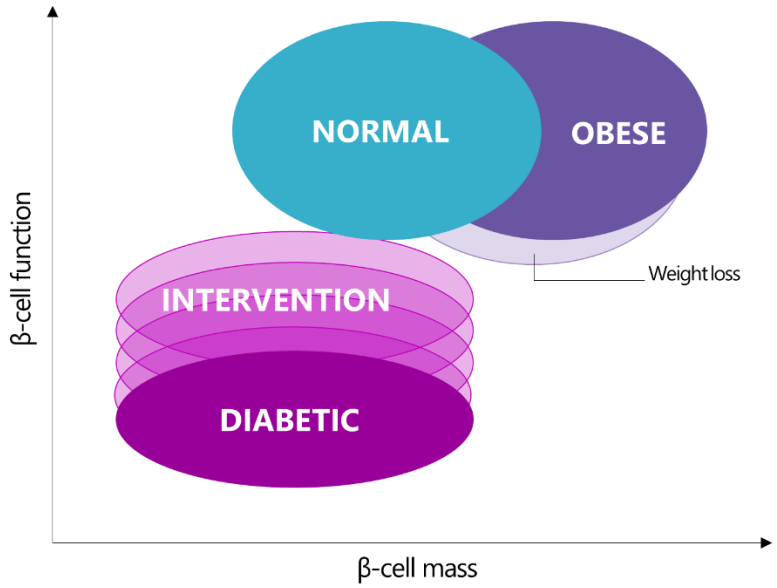

2.2.2 Role of insulin

It has been firmly established that T2DM is caused by the dysfunctional function of the pancreas and peripheral insulin resistance. The capacity of β-cells to produce insulin is harmed by chronic high

glucose levels, which increases hyperglycemia and led to T2DM. As a consequence, peripheral tissues adapt to rely on the catabolism of intracellularly stored macromolecules (i.e. fat and proteins) to create the required ATP, resulting in weight loss, excessive eating, and lethargy. Interestingly, insulin levels are higher in overweight T2DM patients than in normal-weight T2DM patients[38], indicating that the damage of islet β-cell is more severe in the latter group and that peripheral tissue insulin resistance plays a bigger role in the disease phenotype in overweight T2DM patients. Chang *et al.* demonstrated that BMI is linked to the degree of insulin resistance in Korean patients, even in the non-obese range[39]. Furthermore, weight loss in obese T2DM patients and obese T2DM-free individuals is correlated to a decrease in insulin resistance[40], suggesting that insulin resistance is strongly correlated to BMI.

Insulin resistance is usually associated with increased serine phosphorylation of insulin receptor substrates (IRSs)[41,42]. This phenomenon can be caused by a variety of factors, including ectopic lipid accumulation, mitochondrial dysfunction, endoplasmic reticulum (ER) stress, and inflammation.

Ectopic lipid accumulation in muscle and in the liver induces insulin resistance by increasing tissue diacylglycerol (DAG) levels. This effect appeared to be mediated by Protein Kinase C (PKC) activation which phosphorylates serine residues in IRS proteins, thereby inhibiting insulin signaling[43].

Mitochondrial dysfunction has been observed in several tissues like liver, muscle, adipose tissue, and even the brain[44]. The altered mitochondrial function is due to both a reduction in density and impaired functioning in the oxidative phosphorylation system[45]. However, the effects of the impaired functioning may vary by tissue site. In adipocytes, it is correlated with decreased adiponectin levels[46], a potent insulin-sensitizing, while in other tissues, is linked to increase levels of reactive oxygen species (ROS)[47], which activate redox-sensitive serine kinases to phosphorylate IRS proteins and produce insulin resistance.

The ER is where secreted and integral membrane proteins are synthesized and folded. Increases in ROS production and glycation of proteins, exert a tremendous load on ER for conventional refolding of misfolded/unfolded and nascent proteins that perturbs ER homeostasis resulting in apoptotic cell death[48].

Insulin resistance is known to be exacerbated by systemic inflammation. In fact, pro-inflammatory cytokines induce insulin resistance by activating downstream kinases, which can contribute to the phosphorylation of serine residues in IRS proteins[49]. Moreover, they stimulate the production of suppressors of cytokine signaling (SOCS), which block the action of IRSs[50]. Another key element of

insulin resistance is macrophage infiltration in white adipose tissue, which stimulates lipolysis and gluconeogenesis[51].

2.2.3 Diabetic comorbidities

Complications of diabetes, both micro and macro-vascular, tend to occur together since they are closely related to the severity of hyperglycemia[52]. Moreover, hypertension, which is twice likely to have in diabetic patients, markedly increases the risk and accelerates the course of cardiac disease, peripheral vascular disease, stroke, retinopathy, and nephropathy[53].

High blood sugar levels promote the activation of six major pathways, including enhanced polyol pathway flux, increased formation of advanced glycation end products (AGEs), increased AGE receptor expression, activation of PKC isoforms, enhanced hexosamine flux, and increased intracellular reactive oxygen species[54,55]. These biochemical and molecular mechanisms result in the expression of pro-inflammatory genes that persist even after the glycemia is normalized and that affect not only the cardiovascular system, but also skeletal muscle, nervous system (central and peripheral), skin, kidneys, and gastrointestinal tract (GIT).

Additionally, investigations over the last few decades show that some of these diseases emerge during the prediabetic stage, and are therefore potentially implicated in both diabetes pathogenesis and aetiology[56,57]. For example, impaired skeletal muscle metabolism leads to a decreased capacity to oxidize fat and increase fat accumulation, exacerbating the disease phenotype[57].

The most common comorbidity is diabetic neuropathy due to changes in blood vessels and nerves, often leads to ulceration and subsequent limb amputation. Diabetes is the most common cause of non-traumatic amputation of the lower limb. However, cardiovascular complications are the most lethal, responsible for between 50-80% of deaths in people with diabetes.

2.3 Antidiabetic medications

Despite novel drugs have been developed, no definitive cure is available for T2DM, even with new insight into the pathophysiology. Nevertheless, available treatments (Table 2.1) help patients with diabetes to manage the symptoms to a certain degree.

Furthermore, since no single medication reverses the multiple pathophysiological disturbances, combination therapy has gained widespread acceptance and will continue to grow[58,59]. Microvascular problems are prevented by glycemic management, whereas macrovascular complications are addressed by correcting the classical cardiovascular risk elements that comprise the insulin resistance (metabolic) syndrome.

Central to the successful implementation of treatment has been the check of glycated hemoglobin

HbA1c, which should be reduced as close to normal as possible[60], and more controversially, the self-monitoring of blood glucose. HbA1c value is considered as a hallmark of hyperglycemia and although the link between diabetes complications and plasma glucose levels appears to be a continuous variable, HbA1c major than 6.5% has been established as a threshold for diabetic retinopathy.

Patients with T2DM can be treated with insulin if oral or injectable antidiabetic medications fail to correct HbA1c, although high dosages (>80–100 units per day) are typically necessary.

Table 2.1 | **Characteristics of major classes of currently available antidiabetic agents**

Drugs	Glycaemic efficacy (HbA1c)	Durability	Mechanism of action	Body weight	CV risk factors	CV safety	Side effect
Metformin	↓↓	No	↓↓ HGP	↓	↓	Possibly beneficial	GI and lactic acidosis
TZDs (pioglitazone)	↓↓	Yes	↑↑ Insulin sensitivity ↑↑ β-cell function	↑↑	↓↓	Probably beneficial	Fluid retention Bone fractures
AGIs	↓	Not known	↓ Carbohydrate absorption	Neutral	Neutral	Possibly beneficial	GI
GLP1 receptor agonists	↓↓	Yes	↑↑ Insulin secretion ↓↓ Glucagon secretion	↓↓	↓↓	Not known	Nausea and vomiting
DPP-4 inhibitors	↓	No	↓ Glucagon secretion ↑ Insulin secretion (weak)	Neutral	Neutral	Neutral	None
Insulin	↓↓	Yes	↓ HGP ↑ Glucose uptake in muscle	↑↑	Neutral	Neutral	Hypoglycaemia

↓, decreased; ↑, increased; The number of arrows defines severity. AGIs, α-glucosidase inhibitors; CV, cardiovascular; DPP-IV, dipeptidyl peptidase 4; GI, gastrointestinal; GLP-1, glucagon-like peptide-1; HbA1c, hemoglobin A1c; HGP, hepatic glucose production; SGLT-2, sodium/glucose co-transporter-2; TZDs, thiazolidinediones

2.3.1 Frontline treatment

Metformin (dimethyl biguanide) is a frontline treatment for improving insulin sensitivity with a long history of use around the world[61]. This agent (Figure 2.4) is the most prescribed antidiabetic therapy worldwide so that it is currently on the World Health Organization's (WHO) list of essential medicines[62]. Furthermore, metformin is also the preferred antidiabetic drug since it improvs glycemic profile and reduction in cardiovascular mortality, without the risk of hypoglycemia and/or bodyweight gains that are associated with the use of other antidiabetic drugs.

Figure 2.4 | **Chemical structure of metformin**

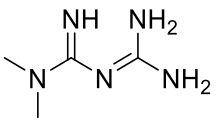

Although metformin has been available for over 60 years the exact mechanism, or mechanisms, of action remain elusive. However, recent findings attribute several actions to its ability to lower blood levels of glucose. For example, inhibition of mitochondrial complex I, activation of AMP-activated

protein kinase (AMPK), inhibition of glycolytic and/or gluconeogenic enzymes and mitochondrial glycerophosphate dehydrogenase[63,64].

Emphasis is now given to the importance of metformin actions within the gut, possibly via alteration of the intestinal microbiota[65].

Gastrointestinal manifestations of abdominal pain, nausea, diarrhea, and vomiting are common adverse effects of metformin that occur in up to 25% of patients[61]. These digestive problems are the leading cause of treatment failure, with 1.2–5% of all patients quitting medication due to these side effects.

2.3.2 Insulin secretagogues

Sulfonylureas are the oldest class of oral antidiabetic medication and despite the large number of anti-diabetic drugs available on the market, only metformin has been used more frequently[66]. Their history is dating back to 1942 when Janbon *et al.* confirmed hypoglycemia in patients treated with some sulfonamides. From these observations and from the fact that the sulfonamide group is a bioisostere of the sulfonylurea moiety[67], carbutamide was synthesized and by the 1960s several sulfonylureas became available on the market (eg, glyburide, glipizide, glimepiride, represented in Figure 2.5).

Figure 2.5 | **Structure of some sulfonylureas**

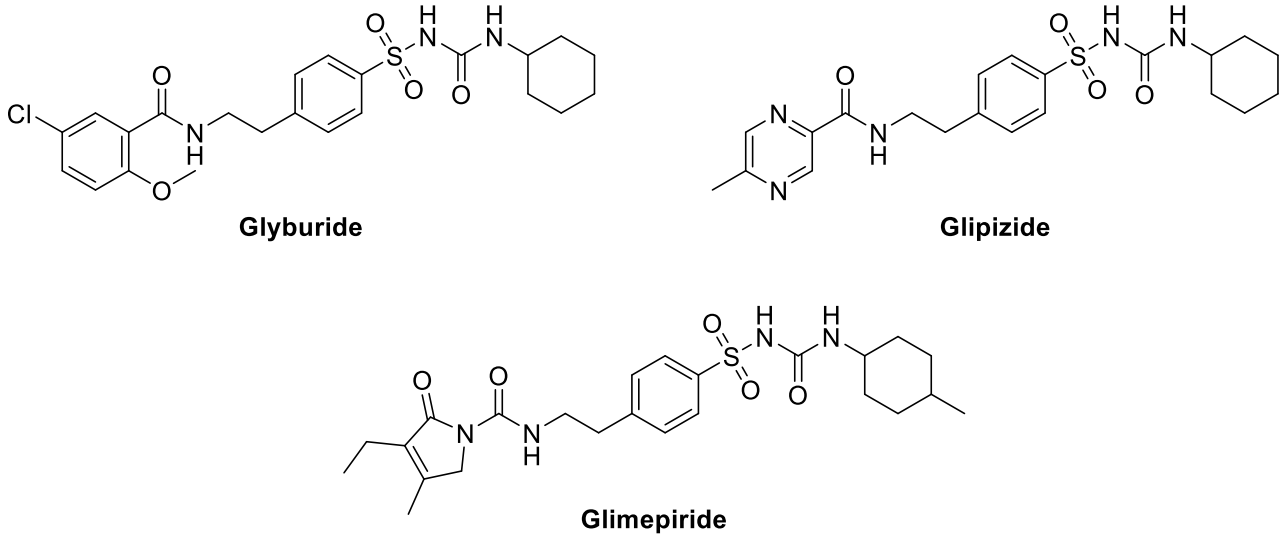

As main effect these compounds increase the plasma insulin concentration despite the serum glucose levels. The mechanism of action involves the inhibition of the sulfonylureas receptor SUR1 on β-pancreatic cells; as a result, the inflow of potassium decrease through the ATP-dependent channel[68]. The β-cell membrane depolarization causes an increased flow of calcium into the intracellular compartment, which leads the exocytosis of insulin.

In addition, sulfonylureas are often characterized by a longer action than their plasm half-life, due to the formation of active metabolites[69].

Regarding the side effects, hypoglycemia is the most common one and it is the major concern associated with sulfonylureas since it may be severe, especially after a missed meal, exercise, or taking sulfonylureas at a high dose.

Similar to sulfonylureas, meglitinide (Figure 2.6) stimulates insulin secretion by the pancreatic β-cells. Since the compounds of this class are derived from benzoic acid, they are classified as non-sulfonylurea insulin secretagogues.

Figure 2.6 | **Meglitinide, the prototype of this drug class**

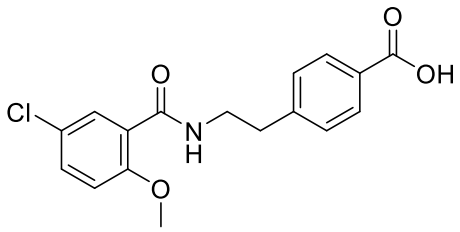

2.3.3 Insulin sensitizers

Thiazolidinediones (TZDs), like pioglitazone and rosiglitazone (Figure 2.7), boost insulin action in skeletal and cardiac muscle, in the liver, and in the adipocytes, beside having a powerful stimulatory effect on β-cells to increase and preserve insulin secretion[70].

Figure 2.7 | **Structures of two well-known thiazolidinediones**

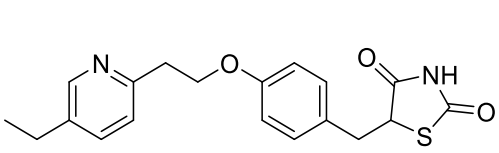

Pioglitazone

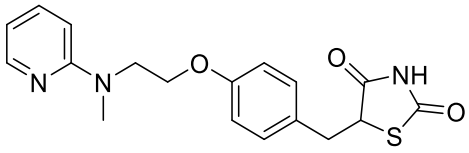

Rosiglitazone

The molecular mechanisms of action of TZDs are partially understood. The antidiabetic effect is exerted by stimulation of several intracellular steps involved in glucose metabolism (GLUT4 glucose transporter, glycogen synthase and pyruvate dehydrogenase); stimulation of peroxisome proliferator-activated receptor-γ (PPAR-γ), a reduction in circulating inflammatory cytokines; and an increase in adiponectin levels[71,72].

The main benefit of TZDs is that they do not cause hypoglycemia when used alone and are not contraindicated in individuals with kidney disease[73]. However, because of concerns about peripheral

edema, fluid retention, and fracture risk in women, their use in older individuals with T2DM may be restricted. Furthermore, pioglitazone is contraindicated in individuals with class III-IV heart failure and should be avoided in elderly adults with congestive heart failure[74].

2.3.4 Targeting intestinal and renal glucose absorption

Alpha-glucosidase inhibitors (AGIs) are a class of drugs particularly useful for reducing the rate of carbohydrate absorption in the intestine and increase meal-stimulated GLP1 secretion[75]. Acarbose and voglibose (Figure 2.8) are the most commonly used drugs of this class, and also the most widely studied. They competitively inhibit enzymes that convert complex non-absorbable carbohydrates into simple absorbable carbohydrates. Moreover, they also minimize glucose fluctuation throughout the day when compared to oral antihyperglycemic medications[76].

Figure 2.8 | **Structures of two well-known AGIs**

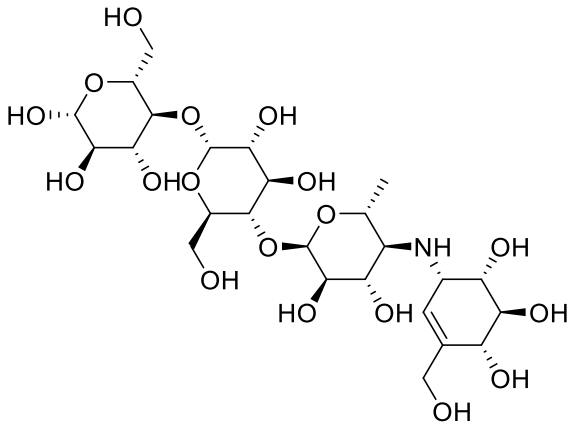

Acarbose

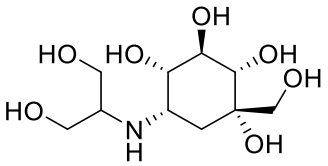

Voglibose

The most prevalent adverse effects of AGIs are gastrointestinal problems. These are caused by bacteria in the colon degrading undigested carbohydrates, resulting in excessive gas production. The most frequent adverse effect is flatulence, which occurs in around 78%. Diarrhea and abdominal pain are other possible effects[77,78].Glucose absorption can be blocked also in the proximal renal tube by inhibiting sodium/glucose co-transporter 2 (SGLT2)[79]. These inhibitors (dapagliflozin, canagliflozin and empagliflozin), shown in Figure 2.9, lower the threshold for glycosuria by lowering the maximum transport capacity or, more likely, by reducing the affinity of the transporter for glucose without causing hypoglycemia[80]. Furthermore, their advantages may also include blood pressure reduction and weight management, since they promote proximal diuresis and calorie leakage into the urine. When the estimated glomerular filtration rate falls to 45–60 mL per minute per 1.73 m^2, the effectiveness of SGLT2 inhibitors is diminished. Moreover, in elderly patients and individuals using

diuretics, adverse effects include vaginal mycotic infections in female patients, balanitis in uncircumcised male patients, urinary tract infections, and volume-related side effects.

Figure 2.9 | **Structure of some SGLT-2 inhibitors**

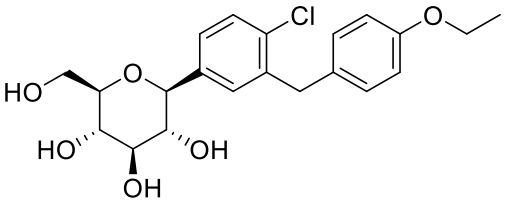

Dapagliflozin

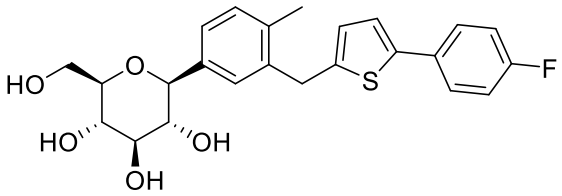

Canagliflozin

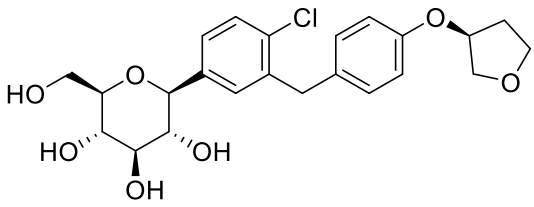

Empagliflozin

2.3.5 GLP-1 modulators

A prominent approach to successfully treat diabetes and to control obesity is to enhance the incretin effects. The glucose dependent insulinotropic polypeptide hormone (GIP) and the glucagon like peptide 1 (GLP-1) are essential players of post-prandial glycemic regulation. These endocrine hormones are released from the gut in response to intraluminal carbohydrates and they are implicated in numerous desirable pancreatic actions, including insulin secretion and gene expression stimulation, increasing β-cell survival, enhancing β-cell glucose sensitivity, and reducing glucagon production[81]. In the metabolically disturbed state, T2DM subjects show reduced activity or desensitization of the GIP-receptors and reduced postprandial circulating level of GLP-1.

Due to their limited half-life, GLP-1 analogues with a considerably longer half-life have been developed. The currently approved GLP-1 receptor (GLP-1R) agonists (Exenatide and Liraglutide) are effective insulinotropic agents and successfully suppress glucagon secretion in a glucose-dependent manner, while induce weight loss.

Another approach for exploit the incretin hormones in the antidiabetic therapy involved the inhibition of dipeptidyl peptidase-4 (DPP-IV), which is the responsible for their degradation. DPP-IV inhibitors (DPP-IVi, Figure 2.10) do not increase but only prolong plasma GLP-1 levels, while they also moderate augment insulin secretion and reduce HbA1c[82].

Figure 2.10 | **Structures of some DPP-IV inhibitors**

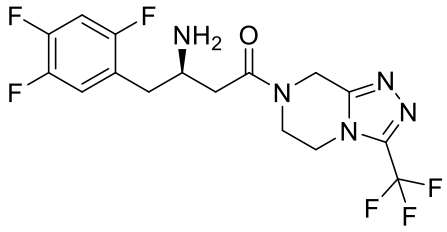

Sitagliptin

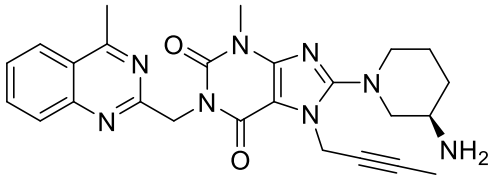

Linagliptin

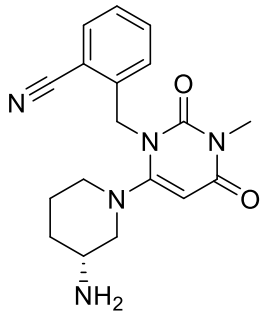

Alogliptin

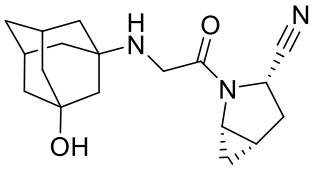

Saxagliptin

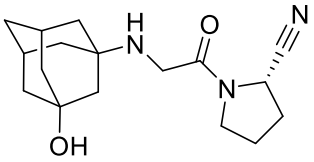

Vildagliptin

Since the functions of DPP-IV and the underlying endocrinology of the incretin system were already known, DPP-IVi were rationally developed based on a known target rather than being developed as a result of observations. This has led to DPP-IVi having an excellent safety profile, with a low incidence of undesired off-target or harmful effects. Furthermore DPP-IVi are not generally associated with drug-drug interactions[82], facilitating the co-formulation with other commonly used antidiabetic agents, which are necessary to treat such a complex pathology.

References

1. Wang, Y. C., McPherson, K., Marsh, T., Gortmaker, S. L. & Brown, M. Health and economic burden of the projected obesity trends in the USA and the UK. The Lancet vol. 378 815–825 (2011).
2. DeFronzo, R. A. et al. Type 2 diabetes mellitus. Nat. Rev. Dis. Prim. 1, (2015).
3. Weisberg, S. P. et al. Obesity is associated with macrophage accumulation in adipose tissue. J. Clin. Invest. 112, 1796–1808 (2003).
4. Xu, H. et al. Chronic inflammation in fat plays a crucial role in the development of obesity-related insulin resistance. J. Clin. Invest. 112, 1821–1830 (2003).
5. Zimmet, P. Z., Magliano, D. J., Herman, W. H. & Shaw, J. E. Diabetes: A 21st century challenge. The Lancet Diabetes and Endocrinology vol. 2 56–64 (2014).
6. International Diabetes Federation. Worldwide toll of diabetes. IDF Diabetes Atlas Ninth edition 2019 9–11 https://www.diabetesatlas.org/en/sections/worldwide-toll-of-diabetes.html (2019).
7. Zimmet, P., Alberti, K. G., Magliano, D. J. & Bennett, P. H. Diabetes mellitus statistics on prevalence and mortality: Facts and fallacies. Nature Reviews Endocrinology vol. 12 616–622 (2016).
8. James, S. L. et al. Global, regional, and national incidence, prevalence, and years lived with disability for 354 diseases and injuries for 195 countries and territories, 1990–2017: a systematic analysis for the Global Burden of Disease Study 2017. Lancet 392, 1789–1858 (2018).

9. Seuring, T., Archangelidi, O. & Suhrcke, M. The Economic Costs of Type 2 Diabetes: A Global Systematic Review. PharmacoEconomics vol. 33 811–831 (2015).
10. Zhou, B. et al. Worldwide trends in diabetes since 1980: a pooled analysis of 751 population-based studies with 4·4 million participants. Lancet 387, 1513–1530 (2016).
11. Hu, F. B. Globalization of diabetes: The role of diet, lifestyle, and genes. in Diabetes Care vol. 34 1249–1257 (Diabetes Care, 2011).
12. Chan, J. C. N. et al. Diabetes in Asia: epidemiology, risk factors, and pathophysiology. JAMA - Journal of the American Medical Association vol. 301 2129–2140 (2009).
13. Barnett, A. H., Eff, C., Leslie, R. D. G. & Pyke, D. A. Diabetes in identical twins - A study of 200 pairs. Diabetologia vol. 20 87–93 (1981).
14. YC, W., K, M., T, M., SL, G. & M, B. Health and economic burden of the projected obesity trends in the USA and the UK. Lancet (London, England) 378, 815–825 (2011).
15. Ley, S. H., Hamdy, O., Mohan, V. & Hu, F. B. Prevention and Management of Type 2 Diabetes: Dietary Components and Nutritional Strategies. Lancet (London, England) 383, 1999 (2014).
16. Larsen, N. et al. Gut microbiota in human adults with type 2 diabetes differs from non-diabetic adults. PLoS One 5, e9085 (2010).
17. Everard, A. & Cani, P. D. Diabetes, obesity and gut microbiota. Best Pract. Res. Clin. Gastroenterol. 27, 73–83 (2013).
18. Grøntved, A., Rimm, E. B., Willett, W. C., Andersen, L. B. & Hu, F. B. A Prospective Study of Weight Training and Risk of Type 2 Diabetes in Men. Arch. Intern. Med. 172, 1306–1312 (2012).
19. Grøntved, A. & Hu, F. B. Television viewing and risk of type 2 diabetes, cardiovascular disease, and all-cause mortality: A meta-analysis. JAMA - Journal of the American Medical Association vol. 305 2448–2455 (2011).
20. FP, C., L, D., P, S. & MA, M. Quantity and quality of sleep and incidence of type 2 diabetes: a systematic review and meta-analysis. Diabetes Care 33, 414–420 (2010).
21. Hu, F. B. et al. Diet, Lifestyle, and the Risk of Type 2 Diabetes Mellitus in Women. N. Engl. J. Med. 345, 790–797 (2001).
22. Sumamo Schellenberg, E., Dryden, D. M., Vandermeer, B., Ha, C. & Korownyk, C. Lifestyle interventions for patients with and at risk for type 2 diabetes: A systematic review and meta-analysis. Annals of Internal Medicine vol. 159 543–551 (2013).
23. Hemminki, K., Li, X., Sundquist, K. & Sundquist, J. Familial risks for type 2 diabetes in Sweden. Diabetes Care 33, 293–297 (2010).
24. Mahajan, A. et al. Fine-mapping type 2 diabetes loci to single-variant resolution using high-density imputation and islet-specific epigenome maps. Nat. Genet. 50, 1505–1513 (2018).
25. Cai, L. et al. Genome-wide association analysis of type 2 diabetes in the EPIC-InterAct study. Sci. Data 7, 1–6 (2020).
26. Morris, A. P. et al. Large-scale association analysis provides insights into the genetic architecture and pathophysiology of type 2 diabetes. Nat. Genet. 44, 981–990 (2012).
27. Xue, A. et al. Genome-wide association analyses identify 143 risk variants and putative regulatory mechanisms for type 2 diabetes. Nat. Commun. 9, 1–14 (2018).
28. World Health Organization (WHO). Classification of diabetes mellitus 2019. (2019).
29. Muoio, D. M. & Newgard, C. B. Mechanisms of disease: Molecular and metabolic mechanisms of insulin resistance and β-cell failure in type 2 diabetes. Nature Reviews Molecular Cell Biology vol. 9 193–205 (2008).
30. Mezza, T. et al. Insulin resistance alters islet morphology in nondiabetic humans. Diabetes 63, 994–1007 (2014).
31. Mari, A. et al. Mechanisms of the Incretin Effect in Subjects with Normal Glucose Tolerance and Patients with Type 2 Diabetes. PLoS One 8, e73154 (2013).
32. Holst, J. J., Knop, F. K., Vilsbøll, T., Krarup, T. & Madsbad, S. Loss of incretin effect is a specific, important, and early characteristic of type 2 diabetes. Diabetes Care vol. 34 S251–S257 (2011).
33. Marchetti, P. et al. The endoplasmic reticulum in pancreatic beta cells of type 2 diabetes patients. Diabetologia 50, 2486–2494 (2007).
34. Masini, M. et al. Autophagy in human type 2 diabetes pancreatic beta cells. Diabetologia 52, 1083–1086

(2009).
35. Boland, B. B., Rhodes, C. J. & Grimsby, J. S. The dynamic plasticity of insulin production in β-cells. Molecular Metabolism vol. 6 958–973 (2017).
36. Cerf, M. E. Beta cell dysfunction and insulin resistance. Frontiers in Endocrinology vol. 4 (2013).
37. Rahier, J., Guiot, Y., Goebbels, R. M., Sempoux, C. & Henquin, J. C. Pancreatic β-cell mass in European subjects with type 2 diabetes. in Diabetes, Obesity and Metabolism vol. 10 32–42 (Diabetes Obes Metab, 2008).
38. Bagdade, J. D., Bierman, E. L. & Porte, D. The significance of basal insulin levels in the evaluation of the insulin response to glucose in diabetic and nondiabetic subjects. J. Clin. Invest. 46, 1549–1557 (1967).
39. Chang, S. A. et al. Body Mass Index Is the Most Important Determining Factor for the Degree of Insulin Resistance in Non-obese Type 2 Diabetic Patients in Korea. Metabolism. 53, 142–146 (2004).
40. Khaodhiar, L., Cummings, S. & Apovian, C. M. Treating diabetes and prediabetes by focusing on obesity management. Current Diabetes Reports vol. 9 348–354 (2009).
41. Copps, K. D. & White, M. F. Regulation of insulin sensitivity by serine/threonine phosphorylation of insulin receptor substrate proteins IRS1 and IRS2. Diabetologia vol. 55 2565–2582 (2012).
42. Bouzakri, K. et al. IRS-1 serine phosphorylation and insulin resistance in skeletal muscle from pancreas transplant recipients. Diabetes 55, 785–791 (2006).
43. Yu, C. et al. Mechanism by which fatty acids inhibit insulin activation of insulin receptor substrate-1 (IRS-1)-associated phosphatidylinositol 3-kinase activity in muscle. J. Biol. Chem. 277, 50230–50236 (2002).
44. Patti, M. E. & Corvera, S. The role of mitochondria in the pathogenesis of type 2 diabetes. Endocrine Reviews vol. 31 364–395 (2010).
45. Ritov, V. B. et al. Deficiency of subsarcolemmal mitochondria in obesity and type 2 diabetes. Diabetes 54, 8–14 (2005).
46. Eun, H. K. et al. Essential role of mitochondrial function in adiponectin synthesis in adipocytes. Diabetes 56, 2973–2981 (2007).
47. Rains, J. L. & Jain, S. K. Oxidative stress, insulin signaling, and diabetes. Free Radical Biology and Medicine vol. 50 567–575 (2011).
48. Pandey, V. K., Mathur, A. & Kakkar, P. Emerging role of Unfolded Protein Response (UPR) mediated proteotoxic apoptosis in diabetes. Life Sciences vol. 216 246–258 (2019).
49. Arkan, M. C. et al. IKK-β links inflammation to obesity-induced insulin resistance. Nat. Med. 11, 191–198 (2005).
50. Lebrun, P. & Van Obberghen, E. SOCS proteins causing trouble in insulin action. in Acta Physiologica vol. 192 29–36 (John Wiley & Sons, Ltd, 2008).
51. Perry, R. J. et al. Hepatic acetyl CoA links adipose tissue inflammation to hepatic insulin resistance and type 2 diabetes. Cell 160, 745–758 (2015).
52. Cade, W. T. Diabetes-related microvascular and macrovascular diseases in the physical therapy setting. Physical Therapy vol. 88 1322–1335 (2008).
53. Epstein, M. & Sowers, J. R. Diabetes mellitus and hypertension. Hypertension vol. 19 403–418 (1992).
54. Brownlee, M. The pathobiology of diabetic complications: A unifying mechanism. in Diabetes vol. 54 1615–1625 (Diabetes, 2005).
55. Giacco, F. & Brownlee, M. Oxidative stress and diabetic complications. Circulation Research vol. 107 1058–1070 (2010).
56. Basu, R. et al. Pathogenesis of prediabetes: Role of the liver in isolated fasting hyperglycemia and combined fasting and postprandial hyperglycemia. J. Clin. Endocrinol. Metab. 98, E409 (2013).
57. Phielix, E. & Mensink, M. Type 2 Diabetes Mellitus and Skeletal Muscle Metabolic Function. Physiol. Behav. 94, 252–258 (2008).
58. Abdul-Ghani, M. A. et al. Initial combination therapy with metformin, pioglitazone and exenatide is more effective than sequential add-on therapy in subjects with new-onset diabetes. Results from the Efficacy and Durability of Initial Combination Therapy for Type 2 Diabetes (EDICT. Diabetes, Obes. Metab. 17, 268–275 (2015).
59. DeFronzo, R. A. et al. Combination of empagliflozin and linagliptin as second-line therapy in subjects with type 2 diabetes inadequately controlled on metformin. Diabetes Care 38, 384–393 (2015).
60. Pozzilli, P. et al. The A1C and ABCD of glycaemia management in type 2 diabetes: A physician's

personalized approach. Diabetes/Metabolism Research and Reviews vol. 26 239–244 (2010).
61. McCreight, L. J., Bailey, C. J. & Pearson, E. R. Metformin and the gastrointestinal tract. Diabetologia vol. 59 426–435 (2016).
62. Ionică, L. N. et al. Metformin alleviates monoamine oxidase-related vascular oxidative stress and endothelial dysfunction in rats with diet-induced obesity. Mol. Cell. Biochem. 476, 4019–4029 (2021).
63. Madiraju, A. K. et al. Metformin suppresses gluconeogenesis by inhibiting mitochondrial glycerophosphate dehydrogenase. Nat. 2014 5107506 510, 542–546 (2014).
64. Ferrannini, E. The Target of Metformin in Type 2 Diabetes. N. Engl. J. Med. 371, 1547–1548 (2014).
65. Foretz, M., Guigas, B. & Viollet, B. Understanding the glucoregulatory mechanisms of metformin in type 2 diabetes mellitus. Nature Reviews Endocrinology vol. 15 569–589 (2019).
66. Sola, D. et al. Sulfonylureas and their use in clinical practice. Archives of Medical Science vol. 11 840–848 (2015).
67. Idrees, D. et al. Implication of sulfonylurea derivatives as prospective inhibitors of human carbonic anhydrase II. Int. J. Biol. Macromol. 115, 961–969 (2018).
68. Panten, U., Schwanstecher, M. & Schwanstecher, C. Sulfonylurea receptors and mechanism of sulfonylurea action. Experimental and Clinical Endocrinology and Diabetes vol. 104 1–9 (1996).
69. Tomlinson, B., Patil, N. G., Fok, M., Chan, P. & Lam, C. W. K. The role of sulfonylureas in the treatment of type 2 diabetes. Expert Opin. Pharmacother. 23, 387–403 (2022).
70. DeFronzo, R. A. From the Triumvirate to the Ominous Octet: A New Paradigm for the Treatment of Type 2 Diabetes Mellitus. Diabetes 58, 773–795 (2009).
71. Hauner, H. The mode of action of thiazolidinediones. Diabetes. Metab. Res. Rev. 18, S10–S15 (2002).
72. Eldor, R., DeFronzo, R. A. & Abdul-Ghani, M. In vivo actions of peroxisome proliferator-activated receptors: Glycemic control, insulin sensitivity, and insulin secretion. Diabetes Care 36, (2013).
73. Wang, W. et al. Efficacy and safety of thiazolidinediones in diabetes patients with renal impairment: A systematic review and meta-analysis. Sci. Rep. 7, 1–11 (2017).
74. Coniff, R. F., Shapiro, J. A., Seaton, T. B. & Bray, G. A. Multicenter, placebo-controlled trial comparing acarbose (BAY g 5421) with placebo, tolbutamide, and tolbutamide-plus-acarbose in non-insulin-dependent diabetes mellitus. Am. J. Med. 98, 443–451 (1995).
75. Van De Laar, F. A. et al. α-Glucosidase inhibitors for patients with type 2 diabetes: Results from a Cochrane systematic review and meta-analysis. Diabetes Care vol. 28 154–163 (2005).
76. Laar, F. A. van de. Alpha-glucosidase inhibitors in the early treatment of type 2 diabetes. Vasc. Health Risk Manag. 4, 1189 (2008).
77. Derosa, G. & Maffioli, P. α-Glucosidase inhibitors and their use in clinical practice. Archives of Medical Science vol. 8 899–906 (2012).
78. Reuser, A. J. J. & Wisselaar, H. A. An evaluation of the potential side-effects of α-glucosidase inhibitors used for the management of diabetes mellitus. Eur. J. Clin. Invest. 24, 19–24 (1994).
79. Hsia, D. S., Grove, O. & Cefalu, W. T. An update on sodium-glucose co-transporter-2 inhibitors for the treatment of diabetes mellitus. Current Opinion in Endocrinology, Diabetes and Obesity vol. 24 73–79 (2017).
80. Ferrannini, E. & Solini, A. SGLT2 inhibition in diabetes mellitus: Rationale and clinical prospects. Nature Reviews Endocrinology vol. 8 495–502 (2012).
81. Artasensi, A., Pedretti, A., Vistoli, G. & Fumagalli, L. Type 2 Diabetes Mellitus: A Review of Multi-Target Drugs. Molecules 25, (2020).
82. Deacon, C. F. Dipeptidyl peptidase 4 inhibitors in the treatment of type 2 diabetes mellitus. Nat. Rev. Endocrinol. 2020 1611 16, 642–653 (2020).

CHAPTER 3

Repurposing drugs to treat T2DM

Despite major investment by pharmaceutical companies in conventional drug discovery pipelines, the development of new drugs has failed to keep up with the increasing incidence of T2DM. Moreover, currently available medications do not address the fundamental cause of hyperglycemia and insulin resistance in peripheral tissues, and patients frequently grow unresponsive to therapy[1,2]. In this context, the promiscuity of the pathophysiological processes in T2DM disease has prompted a re-evaluation of medicines that target these pathways as possible antidiabetic treatments.

In Table 3.1 are shown several significant examples of T2DM drug repositioning, some of which will be discussed below.

Table 3.1 | **Examples of Drug Repurposing for the Treatment of T2DM**

Drug Name or Class	Original use	Proposed mode of action
Amlexanox	Oral aphthous ulcers	Anti-inflammatory
Berberine	Infectious diarrhea	Activates AMPK by inhibiting mitochondrial complex 1
BGP-15	Ischemia–reperfusion injury	PARP inhibitor/HSP72 inducer
Bile acids	Primary biliary cirrhosis	Increases energy expenditure, agonism of FXR and TGR
Diacerein	Osteoarthritis	Improves ER stress and reverses inflammation
Hydroxychloroquine	Malaria, rheumatoid arthritis	Anti-inflammatory
Matrine	Hepatitis B	HSP90/HSP72
Methazolamide	Glaucoma	Suppress hepatic glucose production
MLR-1023	Gastriculcers	Activation of Lyn tyrosine kinase
NEN	Intestinal infection with tapeworm	Mitochondrial uncoupler
Salicylates	Pain and inflammation	NFkB
TUDC	Cholestasis	Alleviates ER stress
Triterpenoids		AMPK, FoxO1

A popular approach involves targeting the inflammatory pathways. The management of inflammation may be an interesting strategy in the prevention and treatment of T2DM since there is

a chronic low-grade inflammation also associated with obesity[3]. Furthermore, this state can promote the development of insulin resistance and impaired glucose tolerance. Clues about the role of inflammation in diabetes can be traced back more than a century when high doses of sodium salicylate were first shown to reduce glycosuria in diabetic patients[4]. However, only 20 years ago salsalate, a prodrug form of salicylic acid that has been used to treat joint pain, was proposed as a possible antidiabetic agent[5]. In 2001 Shoelson and colleagues demonstrated that salsalate has the potential to treat T2DM by inhibiting the NF-κB pathway. Phase III trials demonstrated the value of this strategy: in preliminary proof-of-concept research, 20 obese and non-diabetic adults were given salsalate or a placebo for one month, and the treatment improved glycemia, decreased C-reactive protein levels and boosted adiponectin levels in blood plasma[6].

Repurposing opportunities raised also for Amlexanox, another NF-κB pathway inhibitor commonly utilized as a topical treatment for recurrent aphthous ulcers of the mouth. Amlexanox increases energy expenditure in obese mice *via* promoting thermogenesis, resulting in weight reduction, better insulin sensitivity, and reduced steatosis[7].

Moreover, the anti-inflammatory drug hydroxychloroquine, which is used to treat malaria and rheumatoid arthritis, has been shown to have anti-diabetic benefits in numerous clinical investigations[8–10].

Another example of repurposing could be NEN, the salt form of Niclosamide (5-chloro-salicyl-(2-chloro-4-nitro)anilide), which is an anthelmintic drug approved by the US Food and Drug Administration (FDA) for treating intestinal infections of tapeworms[11]. The mechanism of action of the drug is to uncouple mitochondrial respiration reducing cellular energy efficiency and increasing lipid oxidation. Tao *et al.* proved that, in mice, orally administered NEN enhances energy expenditure and lipid metabolism[12]. It also works to prevent and treat hepatic steatosis and insulin resistance induced by a high-fat diet. Furthermore, in db/db mice, it improves glycemic control and slows disease development.

Several studies have also demonstrated the possibility for matrine to be repurposed[13,14], clinically used as a hepatoprotective drug[15]. Matrine increased glucose tolerance, weight loss, and hepatic steatosis without altering calories intake. In terms of the cellular target, pieces of evidence proved that matrine is able to up-regulate some heat shock proteins (HSPs), which are implicated in hepatosteatosis (the major metabolic defect of non-alcoholic fatty liver disease) and insulin resistance[14].

Potential new T2DM medications have also emerged from the repositioning of bile acid sequestrants

(BASs), agents used to treat primary biliary cirrhosis or cholestasis[16]. In fact, bile acids are endogenous ligands for hepatic farnesoid X receptor (FXR) and Takeda G protein-coupled receptor 5 (TGR-5) which mediate glucose, lipid, and energy metabolism[17]. In 2008 Colesevelam, a second-generation BAS, was approved as adjunct therapy for T2DM and is the only BAS currently approved to treat T2DM[18].

Lastly, MLR-1023, known as Tolimidone when evaluated unsuccessfully by Pfizer for gastric ulcer disease, has been repurposed as a novel oral insulin sensitizer whose actions are mediated by selective activation of Lyn kinase[19]. When Lyn kinase is activated, it directly phosphorylates a tyrosine of insulin receptor substrate-1 (IRS-1), which triggers a chain of events that result in enhanced translocation of glucose transporter type 4, glucose absorption, and glucose utilization[20].

References

1. Brownlee, M. Biochemistry and molecular cell biology of diabetic complications. *Nature* vol. 414 813–820 (2001).
2. Rena, G., Pearson, E. R. & Sakamoto, K. Molecular mechanism of action of metformin: Old or new insights? *Diabetologia* vol. 56 1898–1906 (2013).
3. Donath, M. Y. & Shoelson, S. E. Type 2 diabetes as an inflammatory disease. *Nature Reviews Immunology* vol. 11 98–107 (2011).
4. Kim, J. K. *et al.* Prevention of fat-induced insulin resistance by salicylate. *J. Clin. Invest.* 108, 437–446 (2001).
5. Shoelson, S. E., Lee, J. & Goldfine, A. B. Inflammation and insulin resistance. *Journal of Clinical Investigation* vol. 116 1793–1801 (2006).
6. Donath, M. Y. Targeting inflammation in the treatment of type 2 diabetes: Time to start. *Nature Reviews Drug Discovery* vol. 13 465–476 (2014).
7. Reilly, S. M. *et al.* An inhibitor of the protein kinases TBK1 and IKK-ε improves obesity-related metabolic dysfunctions in mice. *Nat. Med.* 19, 313–321 (2013).
8. Hage, M. P., Badri, M. R. & Azar, S. T. A favorable effect of hydroxychloroquine on glucose and lipid metabolism beyond its anti-inflammatory role. *Therapeutic Advances in Endocrinology and Metabolism* vol. 5 77–85 (2014).
9. Pareek, A. *et al.* Efficacy and safety of hydroxychloroquine in the treatment of type 2 diabetes mellitus: A double blind, randomized comparison with pioglitazone. *Curr. Med. Res. Opin.* 30, 1257–1266 (2014).
10. Mercer, E. *et al.* Hydroxychloroquine improves insulin sensitivity in obese non-diabetic individuals. *Arthritis Res. Ther.* 14, R135 (2012).
11. Park, J. S., Lee, Y. S., Lee, D. H. & Bae, S. H. Repositioning of niclosamide ethanolamine (NEN), an anthelmintic drug, for the treatment of lipotoxicity. *Free Radic. Biol. Med.* 137, 143–157 (2019).
12. Tao, H., Zhang, Y., Zeng, X., Shulman, G. I. & Jin, S. Niclosamide ethanolamine–induced mild mitochondrial uncoupling improves diabetic symptoms in mice. *Nat. Med.* 20, 1263–1269 (2014).
13. Hou, H., Zhang, Q., Dong, H. & Ge, Z. Matrine improves diabetic cardiomyopathy through TGF-β-induced protein kinase RNA-like endoplasmic reticulum kinase signaling pathway. *J. Cell. Biochem.* 120, 13573–13582 (2019).
14. Mahzari, A. *et al.* Repurposing matrine for the treatment of hepatosteatosis and associated disorders in glucose homeostasis in mice. *Acta Pharmacol. Sin.* 39, 1753–1759 (2018).
15. Liu, J., Zhu, M., Shi, R. & Yang, M. Radix Sophorae flavescentis for chronic hepatitis B: A systematic review of randomized trials. *American Journal of Chinese Medicine* vol. 31 337–354 (2003).
16. Turner, N., Zeng, X.-Y., Osborne, B., Rogers, S. & Ye, J.-M. Repurposing Drugs to Target the Diabetes Epidemic. *Trends Pharmacol. Sci.* 37, 379–389 (2016).

17. Ferrell, J. M. & Chiang, J. Y. L. Understanding bile acid signaling in diabetes: From pathophysiology to therapeutic targets. *Diabetes and Metabolism Journal* vol. 43 257–272 (2019).
18. Sedgeman, L. R. *et al.* Intestinal bile acid sequestration improves glucose control by stimulating hepatic miR-182-5p in type 2 diabetes. *Am. J. Physiol. - Gastrointest. Liver Physiol.* 315, G810–G823 (2018).
19. Lee, M. K. *et al.* A novel non-PPARgamma insulin sensitizer: MLR-1023 clinicalproof-of-concept in type 2 diabetes mellitus. *J. Diabetes Complications* 34, 107555 (2020).
20. Müller, G., Schulz, A., Wied, S. & Frick, W. Regulation of lipid raft proteins by glimepiride- and insulin-induced glycosylphosphatidylinositol-specific phospholipase C in rat adipocytes. *Biochem. Pharmacol.* 69, 761–780 (2005).

CHAPTER 4

Polypharmacology approaches in T2DM

The epidemic of diabetes at global level emphasizes the need for urgent therapeutic intervention but, as already mentioned, the treatment of T2DM is challenging, since there is no definitive cure available at the moment. Despite the availability of several diabetes medications, pharmacological monotherapies have proven ineffective in controlling blood glucose levels and other comorbidities. Therefore, therapeutic treatment is frequently done through drug combinations, which operate with many mechanisms of action as shown in Figure 4.1[1].

Combination therapy is a well-established phenomenon caused by an increase in the average lifespan as well as the existence of a significant number of comorbidities in many patients. However, issues associated with this strategy, such as many side effects, toxicity, and undesired drug-drug interactions, may influence this practice. There is also the risk that adverse events are mistakenly interpreted as additional disorders, leading to the prescription of additional drugs, creating a vicious circle. Additionally, doctors must be able to distinguish between "acceptable" and "inappropriate" polypharmacy. The difference between the two stems from the need to prescribe more medicines to a single patient as well as the risk-benefit ratio[2]. Nonetheless, complex combinatorial regimen is one of the leading causes for non-adherence to therapeutic recommendations. This is a serious concern since compliance is a *conditio sine qua non* for improving outcomes for patients with diabetes. However, a piece of evidence suggests that adherence could be improved by fixed-dose combined tablets and individual dose packaging in several settings, but the limits of current data suggest that the degree of these advantages remains unknown[3].

Reducing treatment complexity leads also to potential cost advantages. In fact, the average wholesale price is frequently comparable to or less than the sum of the two components, and also patients have only a single pay for the fixed-combination prescription[4]. These advantages need to be balanced against possible drawbacks. For example, improved glycemic control may increase the risk of hypoglycemia, especially when sulphonylurea-containing combinations are used[5].

Figure 4.1 | **Polypharmacological approaches in T2DM**

ASCVD: Atherosclerotic Cardiovascular Disease, CKD: Chronic Kidney Disease, HF: Heart Failure, i: inhibitor, RA: receptor agonist, SU: sulfonylureas, TZD: thiazolidinediones

The simultaneous modulation of several targets through a polypharmacy approach is a concept included in the definition of polypharmacology. The term is defined as "the design or use of pharmaceutical agents that act on multiple targets or disease pathways". As a result, polypharmacology covers two scenarios: several medicines binding to multiple targets, and a single drug binding to many targets within a network[6].

Multi-target drugs (MTDs) are small molecules rationally designed to be able to modulate disease-relevant targets, promoting the desired therapeutic response and limiting adverse effects.

Box 4.1 provides key features of a good MTD[6].

Box 4.1 | **Desired features in a MTD**

- **Target identification** A new MTD should be directed to networked targets whose connectivity has been proven. This can be done by using system biology and polypharmacological modeling but also by exploiting big data libraries
- **Pharmacokinetic** The physicochemical properties of MTDs are less druglike than single target ones. Early ADME studies should be included in the initial profiling
- **Activity in primary assays** A fundamental prerequisite is that activities against the targets of interest (isolated proteins) are balanced. Ideally, potencies should differ by no more than 1 order of magnitude
- **Selectivity** Hits should be tested for activity against biological target isoforms and closely related proteins to demonstrate the intended selective profile
- **Activity in cellular assays** Activity in these assays should be viewed as the early proof of concept. Different from isolated protein assays, cell-based screening systems maintain molecular−pathway interactions. A superior activity to single-target reference compounds used alone and in combination is required

4.1 Multi-target strategies

Recently, multi-target compound development becomes a more feasible and appealing polypharmacology method. Medicinal chemistry today tends to design MTDs rather than relying on serendipity for their discovery. However, even though various design strategies have been presented and successfully implemented, medicinal chemists have greater hurdles in their discovering and development than single-target medicines.

Multi-target drug design tools that have grown in prominence are *in silico* techniques. Between these methods, fragment-based drug discovery (FBDD) and computational drug discovery are two approaches that are showing promise in terms of speeding up and optimizing drug development. FBDD method identifies fragments that bind modestly to the biological target, and these pieces are then extended or joined together to create high-affinity drug leads. Other well-known *in silico*

methods, such as molecular docking, pharmacophore analysis, quantitative structure-activity relationship (QSAR), machine learning, and their various combinations, have been extensively used as well.

Besides these techniques, screening sets of compounds against several targets like high-throughput screening (HTS) can be exploited as well. HTS allows large, diverse compound sets to be screened against several targets of interest, in parallel.

Although, the knowledge-based approach remains one of the preferred options. This approach, also known as "framework combination," is based on the structure-activity relationship (SAR) knowledge of every target involved. MTDs can be categorized depending on their molecular and pharmacophore architecture, as shown in Figure 4.2.

Figure 4.2 | **Different strategies to design multi-target ligands**

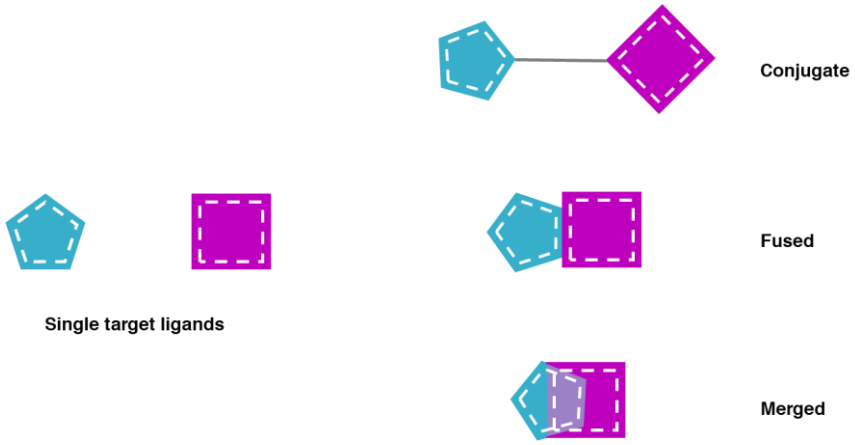

The conjugation of pharmacophores with a linking group, stable or biodegradable, is the simplest method of combining several activities. Such connected pharmacophores have large molecular weights and extensive lipophilicity that provide unfavorable bioavailability or since they are big structures the presence of the linker may significantly hinder the key interactions with target proteins. However, despite the several drawbacks, they are becoming increasingly important in target delivery[7]. When two (or more) separate pharmacophores are combined without a connecting group, fused multiple ligands are formed. These are prone to the same unfavorable properties as conjugate multiple ligands such as large molecular weights and extensive lipophilicity. Furthermore, for some target combinations that strongly differ in the chemotypes of ligands the obtainment of the desired pharmacological profile could be challenging .

The last strategy is to highly integrate different pharmacophores in merged multi-target ligands. This approach can lead to the design of more “drug-like” compounds with low molecular weight and with respect to Lipinski's rule of five[7].

Once the MTDs are established lead optimization is perhaps the phase that required most efforts in the MTD pipeline. At this stage, a balanced activity profile towards the selected targets must be obtained while simultaneously achieved a suitable pharmacokinetic profile[8,9]. Furthermore, preserving low lipophilicity and avoiding significant structural expansion must be a top priority. In this context, rational multitarget optimization strategies may rely on computational models and systematic exploration of the SAR on each individual target.

4.2 Multi-target drugs in T2DM

There are currently no authorized MTDs that can reliably decrease multiple conditions linked to diabetes over the long-term[10]. This situation leads to several medications being prescribed to patients that suffer from this condition. Polypharmacy for metabolic diseases includes lipid-lowering agents, anti-hypertensive agents, anti-diabetic agents, heart failure drugs, and anti-obesity therapies. However, despite all of the progress made so far in diabetes treatment research, the clinical limits of current antidiabetic drugs, whether as monotherapy or in combination, demonstrate the need for new drugs that can effectively halt T2DM and its consequences. A realistic alternative to this therapeutic approach might be to develop molecules with multiple actions. Hence, as already mentioned, MTDs have the potential of facing a multifactorial disease like T2DM.

Investigations of such multi-target drugs have recently been reviewed[1,11] to highlight compounds acting on peroxisome proliferation activated receptors (PPARs), glucagon systems, and incretin, to mention a few, at various stages of development.

4.2.1 PPARs-based therapies

Several attempts have been made to develop drugs that act on multiple PPARs including PPAR α, PPAR γ, and PPAR δ to treat T2DM. Regrettably, these dual-acting PPARs have failed to become approved for treating metabolic diseases due to a not suitable safety profile. Nonetheless, the concept of introducing PPAR activity has been exploited in different multi-target pharmacological approaches[12]. Interesting attempt to identify novel dual PPAR γ/glucokinase (GK) agonists were made by nicotinic acid derivatives (SHP289-03)[13]. *In vivo* studies on this dual target using the T2DM murine model KKA^{y} demonstrated its ability to decrease blood glucose levels, improve glucose tolerance and reduce blood lipid levels.

In recent years, the emerging knowledge about molecular mechanisms that rule the complex pathology of T2DM has led to the discovery of other novel and interesting targets combinations with PPARs to induce a potent anti-diabetic effect; such PPAR agonists are combined with sulfonylurea receptor (SUR)[14], GLP-1R, free fatty acid receptor 1 (FFAR-1, also known as GPR-40, G-protein

coupled receptor 40)[15], and protein tyrosine phosphatase 1B (PTP1B)[16]. Moreover, given the complexity and the multifactorial aspects involved in T2DM, several studies have adopted a multitarget approach in an attempt to normalize blood pressure and lipid metabolism acting simultaneously on PPAR γ and angiotensin II type 1 receptor (AT-1)[17], as antagonists, or soluble epoxide hydrolase (sEH), as inhibitors[18]. Between the latter category of dual modulator, RB394 deserves a particular mention[19]. This sEH inhibitor and PPAR γ agonist prevent in pre-clinical models of the metabolic syndrome pathophysiological features of T2DM and renal injury. Specifically, it effectively reduces the development of hypertension, hyperlipidemia and insulin resistance. Furthermore, RB394 treatment did not alter body weight in SHROB and obese ZSF1 rats.

4.2.2 SGLT-1/SGLT-2 inhibitors

Of particular interest is the development of sotagliflozin (Zynquista™), shown in Figure 4.3. Sotagliflozin is a dual inhibitor of sodium-glucose co-transporter (SGLT), inhibiting both SGLT type 1, which is expressed at high levels in the gastrointestinal tract, and SGLT type 2, which is expressed almost exclusively in the kidneys. This compound aimed at treating both T1DM and T2DM and either as monotherapy or add-on therapy to other antidiabetic agents. However, in 2019, it was approved by EMA as an adjunct to insulin in patients with T1DM with a body mass index ≥ 27 kg/m^2 who have failed to achieve adequate glycemic control despite optimal insulin therapy[20].

Figure 4.3 | **Chemical structure of sotagliflozin**

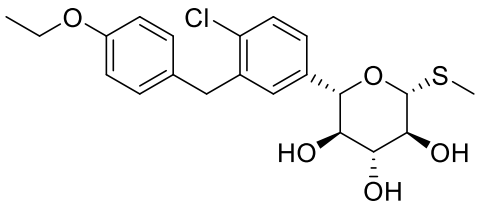

Sotagliflozin has only recently been documented to prevent deaths from cardiovascular causes and hospitalizations for heart failure among patients affected by T2DM[21]. Moreover, it has also been demonstrated to provide beneficial effects on blood pressure and body weight, partially due to the glucosuria as well as the increase in the secretion GLP-1 due to the delayed glucose intestinal absorption[22,23]. Regarding adverse effects, the most frequent ones reported were genital mycotic infections, diabetic ketoacidosis, and diarrhea[24]. Despite this, its dual effect gives it an advantage over selective SGLT-2 inhibitors.

4.2.3 Incretin-based strategies

Prominent therapeutic strategies target the incretin system (Table 4.1), since it is involved in several beneficial pancreatic effects. In fact, the incretin system plays a role in the stimulation of insulin secretion and insulin gene expression, in the promotion of β-cell survival, in the improvement of β cell glucose sensitivity, and decreasing glucagon secretion[25].

Table 4.1 | **List of potential antidiabetic multi-target compounds targeting the incretin system**

	Drug	Company	Stage
GLP-1R/GIPR	LY3298176	Eli Lilly	Phase 2
	NN9709/MAR709/RG7697	Novo Nordisk/Marcadia	Phase 2
	SAR438335	Sanofi	Phase 1
	CPD86	Eli Lilly	Pre-clinical
	ZP-I-98	Zealand	Pre-clinical
	ZP-DI-70	Zealand	Pre-clinical
GLP-1R/GcgR	HM12525A	Hanmi Pharmaceuticals	Phase 2
	MEDI0382	Medimmune	Phase 2
	MK-8521	Merck	Phase 2
	SAR425899	Sanofi	Phase 2
	TT-401	Transition Therapeutics	Phase 2
	JNJ-54728518	Janssen Pharmaceuticals	Phase 1
	NN9277	Novo Nordisk	Phase 1
	MOD-6030/1	Prolor/OPKO Biologics	Phase 1
	ZP2929	Zealand	Phase 1
	VPD-107	Spitfire Pharma	Pre-clinical
GLP-1R/GIPR/GcgR	HM15211	Hanmi Pharmaceuticals	Phase 1
	MAR423	Novo Nordisk/Marcadia	Phase 1

The design focuses on dual drug compounds capable of activating both the endogenous incretins, GLP-1 and GIP. Furthermore, the lack of adverse cardiovascular or cognitive side effects raises interest in incretin-based medications[26]. In addition, published clinical trials on these dual agonists favor beneficial effects of GIP activation in the management of T2DM[27,28]. The design of GLP-1R and glucagon receptor (GcgR) dual-target compounds have been carried out, as well. Glucagon is a hormone produced by pancreatic α-cells that stimulates hepatic glycolysis and gluconeogenesis in the liver, raising plasma glucose levels. It can be used therapeutically as a satiety factor, and it is also able to increase energy expenditure and promote weight loss. Since incretin hormones and glucagon share similar roles, their combined use might have a synergistic impact on diabetes and metabolic disorders. Furthermore, they contain similar N-terminal peptide sequences, allowing for the creation of single-sequence multi-receptor agonists. The research groups of Day *et al.*[29] and Pocai *et al.*[30] were the first to describe peptides that function as dual drugs. They demonstrated in preclinical experiments that therapy with these co-agonists causes better weight and cholesterol reduction in

diet-induced obese (DIO) mice without inducing hyperglycemia or other undesirable effects. Undoubtedly, the peptides' pharmacokinetic profile had to be explored in order to improve their performance, and in addition, co-agonist analogs were rationally developed to have a range of relative activity ratios at GLP-1R and GcgR[31]. Big Pharma companies like Sanofi-Aventis and Eli Lilly have increased their investments in the sector due to the significance of the outcomes obtained with these compounds.

Based on the promising results with GLP-1R/GIPR and GLP-1R/ GcgR dual agonists, further studies have investigated engineered peptides to combine the beneficial effects of triple agonists. Here more than ever, the relative potency of the compound against each receptor is an essential factor to consider. Depending on the intended effects a balanced triagonists or a MTD with an agonism ratio that favors one receptor over the others might be developed. The reduction of body weight by these kinds of triple agonists has been demonstrated to be greater (- 26.6% vs placebo) than the same dose of a GLP-1/GIPR dual agonist (- 15.7% vs placebo) in diet-induced obese mice[32].

Researchers are also working on oxyntomodulin analogues. Oxyntomodulin (OXM) is a gut hormone derived from post-translational modification of pre-proglucagon and its biological effects are attributed to a dual activation of GLP-1R and GcgR[33]. However, similarly to incretins, it is rapidly inactivated by DPP-IV. Therefore, investigations on OXM mimetics aim to improve its half-life. Treatment of T2DM with these compounds resulted in similar glycemic control benefits as specific GLP-1R agonists, and it was also demonstrated positive beneficial actions on glucose homeostasis, β-cell insulin secretion, and body weight[34].

Another rational approach is to combine the inhibition of DPP-IV with another target in order to exhibit a synergistic effect in T2DM treatment. For example some association with melanin concentrating hormone receptor-1 (MCH-1R)[35], angiotensin converting enzyme (ACE)[36], and G protein-coupled receptor-119 (GPR-119)[37] were evaluated.

During this project multi-target modulators of DPP-IV and carbonic anhydrase (CA) were investigated.

References

1. Artasensi, A., Pedretti, A., Vistoli, G. & Fumagalli, L. Type 2 Diabetes Mellitus: A Review of Multi-Target Drugs. *Molecules* 25, 1987 (2020).
2. Dobrică, E.-C. *et al.* Polypharmacy in Type 2 Diabetes Mellitus: Insights from an Internal Medicine Department. *Medicina (B. Aires).* 55, 436 (2019).
3. Settineri, S., Frisone, F., Merlo, E. M., Geraci, D. & Martino, G. Compliance, adherence, concordance, empowerment, and self-management: five words to manifest a relational maladjustment in diabetes. *J. Multidiscip. Healthc.* Volume 12, 299–314 (2019).
4. Bell, D. S. H. Combine and conquer: advantages and disadvantages of fixed-dose combination therapy.

Diabetes, Obes. Metab. 15, 291–300 (2013).
5. Schernthaner, G. Fixed-dose combination therapies in the management of hyperglycaemia in Type 2 diabetes: an opportunity to improve adherence and patient care. *Diabet. Med.* 27, 739–743 (2010).
6. Bolognesi, M. L. Harnessing Polypharmacology with Medicinal Chemistry. *ACS Med. Chem. Lett.* 10, 273–275 (2019).
7. Proschak, E., Stark, H. & Merk, D. Polypharmacology by Design: A Medicinal Chemist's Perspective on Multitargeting Compounds. *J. Med. Chem.* 62, 420–444 (2019).
8. Morphy, R. & Rankovic, Z. Designed Multiple Ligands. An Emerging Drug Discovery Paradigm. *J. Med. Chem.* 48, 6523–6543 (2005).
9. Morphy, R. & Rankovic, Z. The Physicochemical Challenges of Designing Multiple Ligands. *J. Med. Chem.* 49, 4961–4970 (2006).
10. Handelsman, Y. *et al.* American Association of Clinical Endocrinologists Medical Guidelines for Clinical Practice for developing a diabetes mellitus comprehensive care plan. *Endocr. Pract.* 17 Suppl 2, 1–53 (2011).
11. Lillich, F. F., Imig, J. D. & Proschak, E. Multi-Target Approaches in Metabolic Syndrome. *Front. Pharmacol.* 0, 1996 (2021).
12. Ammazzalorso, A., Maccallini, C., Amoia, P. & Amoroso, R. Multitarget PPARγ agonists as innovative modulators of the metabolic syndrome. *European Journal of Medicinal Chemistry* vol. 173 261–273 (2019).
13. Lei, L. *et al.* Antidiabetic potential of a novel dual-target activator of glucokinase and peroxisome proliferator activated receptor-γ. *Metabolism.* 64, 1250–1261 (2015).
14. Ibrahim, M. K. *et al.* Design, synthesis, molecular modeling and anti-hyperglycemic evaluation of novel quinoxaline derivatives as potential PPARγ and SUR agonists. *Bioorganic Med. Chem.* 25, 1496–1513 (2017).
15. Li, Z. *et al.* Design, synthesis, and biological evaluation of novel pan agonists of FFA1, PPARγ and PPARδ. *Eur. J. Med. Chem.* 159, 267–276 (2018).
16. Johnson, T. O., Ermolieff, J. & Jirousek, M. R. Protein tyrosine phosphatase 1B inhibitors for diabetes. *Nature Reviews Drug Discovery* vol. 1 696–709 (2002).
17. Casimiro-Garcia, A. *et al.* Discovery of a series of imidazo[4,5-b]pyridines with dual activity at angiotensin II Type 1 receptor and peroxisome proliferator-activated receptor-γ. *J. Med. Chem.* 54, 4219–4233 (2011).
18. Nocentini, A. *et al.* Discovery of β-Adrenergic Receptors Blocker-Carbonic Anhydrase Inhibitor Hybrids for Multitargeted Antiglaucoma Therapy. *J. Med. Chem.* 61, 5380–5394 (2018).
19. Hye Khan, M. A. *et al.* A novel dual PPAR-γ agonist/sEH inhibitor treats diabetic complications in a rat model of type 2 diabetes. *Diabetologia* 61, 2235–2246 (2018).
20. Markham, A. & Keam, S. J. Sotagliflozin: First Global Approval. *Drugs 2019 799* 79, 1023–1029 (2019).
21. Vallianou, N. G., Christodoulatos, G. S., Kounatidis, D. & Dalamaga, M. Sotagliflozin, a dual SGLT1 and SGLT2 inhibitor: In the heart of the problem. *Metab. Open* 10, 100089 (2021).
22. Cefalo, C. M. A. *et al.* Sotagliflozin, the first dual SGLT inhibitor: Current outlook and perspectives. *Cardiovascular Diabetology* vol. 18 (2019).
23. Bode, D. *et al.* Dual SGLT-1 and SGLT-2 inhibition improves left atrial dysfunction in HFpEF. *Cardiovasc. Diabetol.* 20, (2021).
24. European Medicines Agency. Zynquista | European Medicines Agency. *European Medicines Agency* https://www.ema.europa.eu/en/medicines/human/EPAR/zynquista (2019).
25. Usui, R., Yabe, D. & Seino, Y. Twincretin as a potential therapeutic for the management of type 2 diabetes with obesity. *Journal of Diabetes Investigation* vol. 10 902–905 (2019).
26. Artasensi, A., Pedretti, A., Vistoli, G. & Fumagalli, L. Type 2 Diabetes Mellitus: A Review of Multi-Target Drugs. *Molecules* 25, (2020).
27. Frias, J. P. *et al.* The Sustained Effects of a Dual GIP/GLP-1 Receptor Agonist, NNC0090-2746, in Patients with Type 2 Diabetes. *Cell Metab.* 26, 343-352.e2 (2017).
28. Frias, J. P. *et al.* Efficacy and safety of LY3298176, a novel dual GIP and GLP-1 receptor agonist, in patients with type 2 diabetes: a randomised, placebo-controlled and active comparator-controlled phase 2 trial. *Lancet* 392, 2180–2193 (2018).

29. Day, J. W. *et al.* A new glucagon and GLP-1 co-agonist eliminates obesity in rodents. *Nat. Chem. Biol.* 5, 749–757 (2009).
30. Pocai, A. *et al.* Glucagon-like peptide 1/glucagon receptor dual agonism reverses obesity in mice. *Diabetes* 58, 2258–66 (2009).
31. Day, J. W. *et al.* Optimization of co-agonism at GLP-1 and glucagon receptors to safely maximize weight reduction in DIO-rodents. *Biopolymers* 98, 443–450 (2012).
32. Finan, B. *et al.* A rationally designed monomeric peptide triagonist corrects obesity and diabetes in rodents. *Nat. Med.* 21, 27–36 (2015).
33. Shankar, S. S. *et al.* Native oxyntomodulin has significant glucoregulatory effects independent of weight loss in obese humans with and without type 2 diabetes. *Diabetes* 67, 1105–1112 (2018).
34. Bhat, V. K., Kerr, B. D., Flatt, P. R. & Gault, V. A. A novel GIP-oxyntomodulin hybrid peptide acting through GIP, glucagon and GLP-1 receptors exhibits weight reducing and anti-diabetic properties. *Biochem. Pharmacol.* 85, 1655–1662 (2013).
35. Gattrell, W. T., Sambrook Smith, C. P. & Smith, A. J. An example of designed multiple ligands spanning protein classes: Dual MCH-1R antagonists/DPPIV inhibitors. *Bioorganic Med. Chem. Lett.* 22, 2464–2469 (2012).
36. Sattigeri, J. A. *et al.* Approaches towards the development of chimeric DPP4/ACE inhibitors for treating metabolic syndrome. *Bioorganic Med. Chem. Lett.* 27, 2313–2318 (2017).
37. Li, G. *et al.* The optimization of xanthine derivatives leading to HBK001 hydrochloride as a potent dual ligand targeting DPP-IV and GPR119. *Eur. J. Med. Chem.* 188, 112017 (2020).

CHAPTER 5

Dipeptidyl peptidase-IV

Dipeptidyl peptidase-IV (DPP-IV, Figure 5.1) was first reported in 1966 as glycyl-prolyl-β-naphthylamidase[1] and successively named dipeptidyl peptidase-IV, post-proline dipeptidyl aminopeptidase, and X-Pro dipeptidyl aminopeptidase. The current name recommended by the Enzyme Commission is dipeptidyl-peptidase IV. DPP-IV is an integral membrane protein and it belongs to the prolyl oligopeptidase family, which also includes the structurally homologous enzymes DPP-II, DPP-VIII, DPP-IX, and fibroblast activation protein (FAP)[2].

Figure 5.1 | **3D structure of DPP-IV**

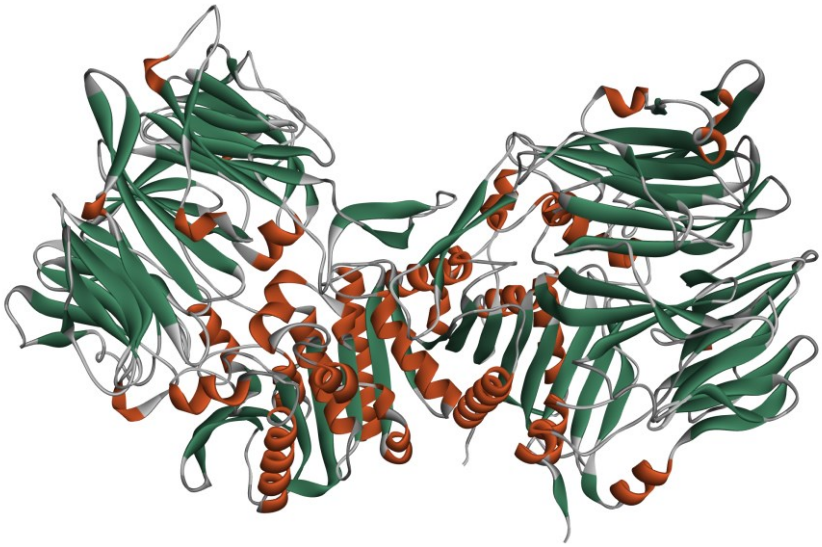

DPP-IV is widespread distributed and its expression involves innumerable tissues including intestinal and renal brush border membranes, vascular endothelium, liver and pancreas, glandular epithelial cells, and cells of the immune system (where it is also known as the T-cell differentiation antigen, CD26)[3]. Since this enzyme is a single-pass type II integral transmembrane glycoprotein, it holds the carboxy-terminus outside the membrane and a short N-terminal in the cytoplasmic area. A soluble form of the enzyme was also found in plasma[4,5] which derived from the cleavage of the extracellular domain.

Crystal structure of DPP-IV in complex with several small molecule inhibitors and substrates have been published[6–8]. The just mentioned data helped to investigate the structure and domain organization of DPP-IV. The DPP-IV monomer is composed of a six-residue-long N-terminal cytoplasmic tail followed by a 22-residue-long transmembrane α-helix and by the extracellular

domain, which is divided into an eight-bladed β-propeller (residues Arg54-Asn497) and a C-terminal α/β-hydrolase domain (residues Gln508-Pro766), which contains the catalytic domain. Furthermore, in native conditions, DPP-IV monomers are associated to form homodimers.

5.1 Substrate access to the active site

DPP-IV exerts its enzymatic action by cleaving from the penultimate position of its substrates. Bioactive peptides may reach the active site in two possible ways: through an opening in the propeller domain or via a side opening formed at the interface of the β-propeller and hydrolase domains[3] (Figure 5.2).

Figure 5.2 | **Surface representation of the two possible ways to access the active site of DPP-IV**

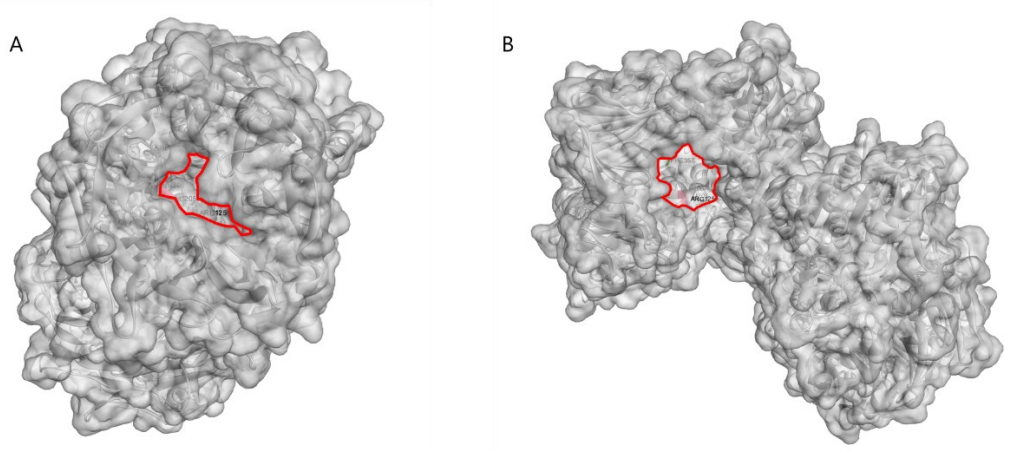

The tunnel of the β-propeller domain is generated by an unusual eightfold repeat of blades, each one is made up of four-strand antiparallel β-sheets. The funnel's lower face has a diameter of approximately 15 Å, and it lies opposite to the hydrolase domain[6]. At the interface of the propeller domain and the hydrolase domain, a bigger side entrance (21 Å) connects the propeller opening to a larger side gate. Large peptides or helical substrates may be able to enter the active site through this side opening.

Once the peptide has reached the active site, its N-termini is recognized and anchored with an hydrogen bond by the negative charges of Glu205 and Glu206. These residues of glutamates are located on a short α-helix, which protrudes from the β-propeller domain and points toward the binding site. The catalytic domain adopts an α/β–hydrolase fold conformation and contains the catalytic triad composed by residues Ser630, Asp708, and His740, which are located within the last 140 residues of the C-terminal region. The Ser630 is located in the sequence Gly-Trp-Ser-Tyr-Gly[7], which corresponds to the serine proteases's common motif, namely Gly-X-Ser-X-Gly. Furthermore, the binding site (Figure 5.3) includes also an oxyanion hole (Tyr631, Tyr547), an hydrophobic S1

pocket (Tyr631, Val656, Trp659, Tyr662, Tyr666, and Val711), and residues of Arg125, Asn710, Glu205, and Glu206[8].

Figure 5.3 | **Binding site of DPP-IV**

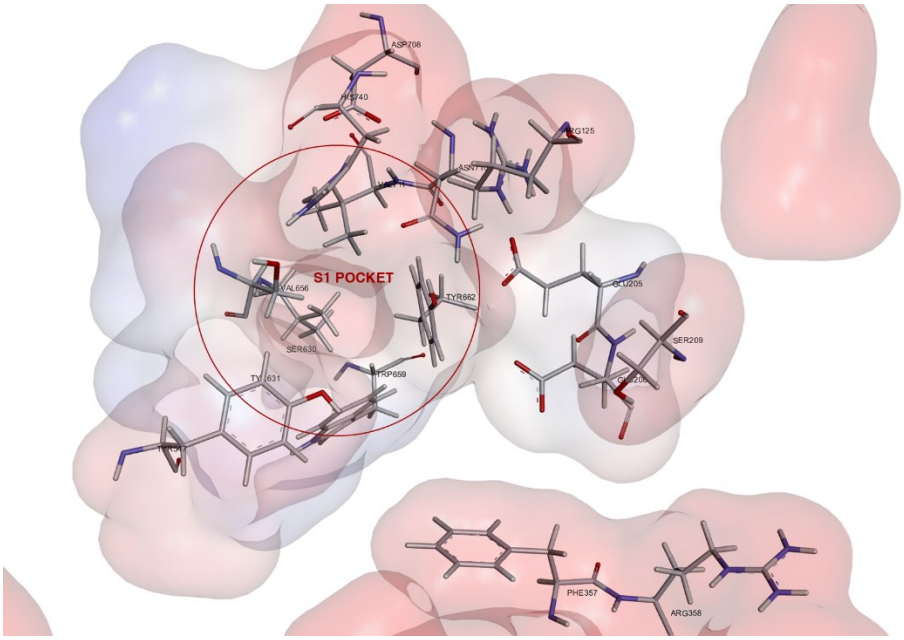

5.2 Substrate specificity

DPP-IV specifically releases a dipeptide from its substrates' N-termini when a proline or alanine is in the penultimate position, as do other members of the family[9]. However, peptides containing other residues (i.e. glycine, serine, valine) in this position can be cleaved, albeit more slowly[10–12]. Nevertheless, the enzyme is unable to cleave substrates with proline in antepenultimate position, namely $P_{1'}$, as represented in Figure 5.4[13].

Figure 5.4 | **Substrate specificity of DPP-IV**

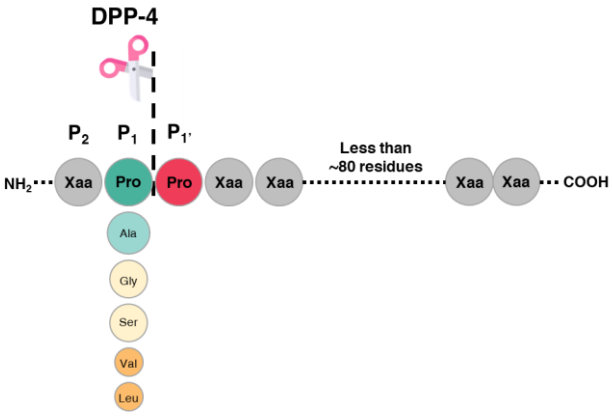

Neuropeptides such as neuropeptide Y, circulating peptide hormones like peptide YY, GLP-1, and -2, gastric inhibitory peptides, and paracrine chemokines like CCL5 (RANTES) are among the

physiological peptides recognized by DPP-IV[14](Table 5.1). In addition, its spectrum of actions goes beyond its proteolytic role since DPP-IV has been identified to impact also in physiological processes such as cell-extracellular matrix contact, cell migration, and proliferation, either alone or in conjunction with its enzymatic activity. All of these lead to its major functional role in immunology, autoimmunity, HIV, and cancer[13].

Furthermore, as already mentioned in the previous chapters, DPP-IV plays an important role in maintaining glucose homeostasis since it is responsible for the inactivation of the incretin hormones, GIP and GLP-1.

Table 5.1 | **Biological effects of DPP-IV on several substrates**

Substrates		Biological effect
Hormones	GLP-1	Inactivation
	GLP-2	Inactivation
	GIP	Inactivation
	Glucagon	Inactivation
	GHRH	Inactivation
	PACAP	Inactivation
	Peptide YY	Change in receptor preference
Vasoactive peptides	Bradykinin	Change in receptor preference
	VIP	Inactivation
	BNP	Change in receptor preference or inactivation
Neuropeptides	NPY	Change in receptor preference
	β-casmorphins	Inactivation
	Endomorphins	Change in receptor preference
	Substance P	Inactivation
Chemokines	CCL3	Enhanced activity
	CCL4	Change in receptor preference
	CCL5	Change in receptor preference
	CCL11	Inactivation
	CCL22	Change in receptor preference
	CXCL6	No changes
	CXCL9	Inactivation, CXCR3 antagonist
	CXCL10	Inactivation, CXCR3 antagonist
	CXCL11	Inactivation, CXCR3 antagonist
	CXCL12	Inactivation, CXCR3 antagonist

GHRH, Growth hormone-releasing hormone; PACAP, Pituitary adenylate cyclase-activating polypeptide; VIP, Vasoactive intestinal peptide; BNP, Brain natriuretic peptide; NPY, Neuropeptide Y; CCL, Chemokine (C-C motif) ligand; CXCL, Chemokine (C-X-C motif) ligand

References

1. Hopsu-Havu, V. K. & Glenner, G. G. A new dipeptide naphthylamidase hydrolyzing glycyl-prolyl-β-naphthylamide. *Histochemie* 7, 197–201 (1966).
2. Yazbeck, R., Howarth, G. S. & Abbott, C. A. Dipeptidyl peptidase inhibitors, an emerging drug class for inflammatory disease? *Trends in Pharmacological Sciences* vol. 30 600–607 (2009).
3. Matteucci, E. & Giampietro, O. Dipeptidyl Peptidase-4 (CD26): Knowing the Function before Inhibiting the Enzyme. *Curr. Med. Chem.* 16, 2943–2951 (2009).
4. Iwaki-Egawa, S., Watanabe, Y., Kikuya, Y. & Fujimoto, Y. Dipeptidyl Peptidase IV from Human Serum:

Purification, Characterization, and N-Terminal Amino Acid Sequence. *J. Biochem.* 124, 428–433 (1998).
5. Durinx, C. *et al.* Molecular characterization of dipeptidyl peptidase activity in serum. *Eur. J. Biochem.* 267, 5608–5613 (2000).
6. Devasthale, P. *et al.* Optimization of activity, selectivity, and liability profiles in 5-oxopyrrolopyridine DPP4 inhibitors leading to clinical candidate (Sa)-2-(3-(aminomethyl)-4-(2,4-dichlorophenyl)-2-methyl-5-oxo-5H-pyrrolo[3,4-b] pyridin-6(7H)-yl)-N, N-dimethylacetamide (B. *J. Med. Chem.* 56, 7343–7357 (2013).
7. Sutton, J. M. *et al.* Novel heterocyclic DPP-4 inhibitors for the treatment of type 2 diabetes. *Bioorganic Med. Chem. Lett.* 22, 1464–1468 (2012).
8. Berger, J. P. *et al.* A comparative study of the binding properties, dipeptidyl peptidase-4 (DPP-4) inhibitory activity and glucose-lowering efficacy of the DPP-4 inhibitors alogliptin, linagliptin, saxagliptin, sitagliptin and vildagliptin in mice. *Endocrinol. Diabetes Metab.* 1, e00002 (2018).
9. Aertgeerts, K. *et al.* Crystal structure of human dipeptidyl peptidase IV in complex with a decapeptide reveals details on substrate specificity and tetrahedral intermediate formation. *Protein Sci.* 13, 412–21 (2004).
10. Röhrborn, D., Wronkowitz, N. & Eckel, J. DPP4 in diabetes. *Frontiers in Immunology* vol. 6 386 (2015).
11. Liu, Y., Hu, Y. & Liu, T. Recent Advances in Non-Peptidomimetic Dipeptidyl Peptidase 4 Inhibitors: Medicinal Chemistry and Preclinical Aspects. *Curr. Med. Chem.* 19, 3982–3999 (2012).
12. Baetta, R. & Corsini, A. Pharmacology of dipeptidyl peptidase-4 inhibitors: Similarities and differences. *Drugs* vol. 71 1441–1467 (2011).
13. Bongers, J., Lambros, T., Ahmad, M. & Heimer, E. P. Kinetics of dipeptidyl peptidase IV proteolysis of growth hormone-releasing factor and analogs. *Biochim. Biophys. Acta (BBA)/Protein Struct. Mol.* 1122, 147–153 (1992).
14. Brandt, I., Lambeir, A. M., Maes, M. B., Scharpé, S. & De Meester, I. Peptide substrates of dipeptidyl peptidases. *Advances in Experimental Medicine and Biology* vol. 575 3–18 (2006).
15. De Meester, I., Korom, S., Van Damme, J. & Scharpé, S. CD26, let it cut or cut it down. *Immunology Today* vol. 20 367–375 (1999).
16. Deacon, C. F. Physiology and Pharmacology of DPP-4 in Glucose Homeostasis and the Treatment of Type 2 Diabetes. *Front. Endocrinol. (Lausanne).* 10, 80 (2019).
17. Mulvihill, E. E. & Drucker, D. J. Pharmacology, physiology, and mechanisms of action of dipeptidyl peptidase-4 inhibitors. *Endocrine Reviews* vol. 35 992–1019 (2014).

CHAPTER 6

Carbonic anhydrase

Human carbonic anhydrases (hCAs) are ubiquitous zinc-metalloenzymes, which act as efficient catalysts for the reversible hydration of carbon dioxide to bicarbonate and protons.

An essential feature of these enzymes is the metal ion, which is crucial for the catalytic activity since the apoenzyme is not active[1]. Fifteen different isoforms have been identified and characterized to date. A plethora of studies investigated the different isoforms of the enzyme, their tissue distribution, and consequent physiological roles, showing that although some isoforms (such as CA I and II) are almost ubiquitous, many others exhibit a more limited distribution. The different isoforms can be divided into four categories based on their location: cytosolic, mitochondrial, secreted, and membrane-associated, as reported in Table 6.1. In 2015 Supuran *et al.* published "Carbonic Anhydrases as Biocatalysts", which presented a thorough molecular, biochemical, and pharmacologic characterization of each human CA[2].

Table 6.1 | **Distribution, localization, and catalytic activity of human carbonic anhydrase (hCA) isoforms**

CA isoforms	Catalytic activity (CO_2 hydration)	Subcellular localization	Organ/tissue distribution
CA-I	Low	Cytosol	Erythrocytes, gastrointestinal tract, and eye
CA-II	High	Cytosol	Erythrocytes, eye, gastrointestinal tract, boneosteoclasts, kidney, lung, testis, and brain
CA-III	Very low	Cytosol	Skeletal muscle and adipocytes
CA-IV	Medium	Membrane-bound	Kidney, lung, pancreas, brain capillaries, colon,heart muscle, and eye
CA-VA	Low	Mitochondria	Liver
CA-VB	High	Mitochondria	Heart and skeletal muscle, pancreas, kidney,spinal cord, and gastrointestinal tract
CA-VI	Low	Saliva and milk secretion	Salivary and mammary gland
CA-VII	High	Cytosol	Central nervous system (CNS)
CA-VIII	Acatalytic	Cytosol	CNS
CA-IX	High	Transmembrane	Tumors and gastrointestinal mucosa
CA-X	Acatalytic	Cytosol	CNS
CA-XI	Acatalytic	Cytosol	CNS
CA-XII	Low	Transmembrane	Kidney, intestine, reproductive epithelia, eye,tumors, and CNS
CA-XIII	Low	Cytosol	Kidney, brain, lung, gut, and reproductive tract
CA-XIV	Low	Transmembrane	Kidney, brain, liver, and eye

Protein sequence, active site residues, quaternary structure, expression, and localization all together play a role in the large differences in catalytic efficiency as well as in their physiological functions. For instance, the absence of one or more histidine in the active site leads to a lack of activity. These isoforms refer to the VIII, X, XI ones, also known as CA-related proteins (CARPs)[3].

6.1 Catalytic features

The involvement of CAs in the reversible hydration of CO_2 had been widely investigated to date[4–6]. However, some members of this enzyme superfamily catalyze a variety of additional hydrolytic reactions, including cyanamide hydration and ester hydrolysis, represented in Equation 6.1[7].

Equation 6.1 | **Several reactions catalyzed by members of CA superfamily**

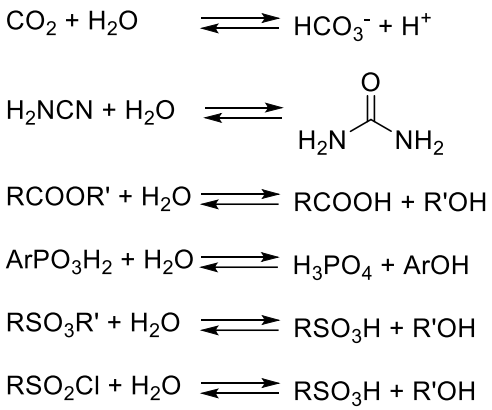

These reactions allow the CAs to play an essential role in pH and CO_2 homeostasis, respiration and transport of CO_2/bicarbonate, electrolyte secretion in many tissues/organs, biosynthetic reactions such as gluconeogenesis, lipogenesis, and ureagenesis in which bicarbonate acts as a substrate for the carboxylation reaction. Moreover, CAs are involved in bone resorption, calcification, and tumorigenicity.

All hCA isoforms have high structural similarities[8]. They feature a 15 Å deep active site cleft, characterized by three histidine residues placed at the bottom of the CA active site (His94, His96, and His119, numbered according to CA-II). The histidine triad coordinate the zinc ion together with a hydroxy group or water molecule, depending on the pH[9]. The catalytically active species is the metal hydroxide species of the enzyme ($E\text{-}Zn^{2+}\text{-}OH^{-}$)[10], which acts as a strong nucleophile (at neutral pH) on the CO_2, leading to the formation of HCO_3^-. The zinc-bound hydroxide is also engaged in an additional hydrogen bond with the hydroxyl moiety of Thr199, which is bridged to the carboxylate group of Glu106, as represented in Figure 6.1. These interactions enhance the nucleophilicity of the hydroxide ion and help the correct orientation of the CO_2 in the hydrophobic pocket of the active site.

Figure 6.1 | **Coordination system of the Zn(II) ion**

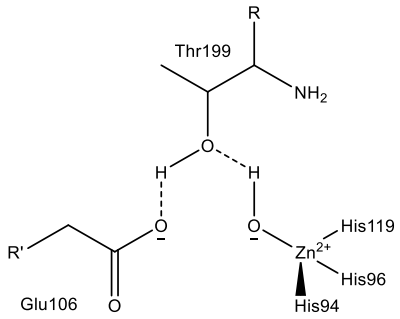

This hydrophobic section is exploited during the catalytic activity since CO_2 is a very poor water soluble molecule. Therefore, CA benefits from the hydrophobic pocket for trapping and orienting CO_2, whereas HCO_3^- and H^+ are hydrophilic (Figure 6.2); thus, they are displaced from the active site by a water molecule, which remained bound to the zinc ion (catalytically inactive form). For the next catalysis cycle, the water molecule must be converted to a hydroxy ion. In order to regenerate the basic form of the metal, a proton transfer reaction from the active site to the environment takes place. This step may be assisted by buffers in the medium or, in the fastest isoforms such as CA-II and CA-IX, is assisted by the proton-shuttle residue His64.

The overall catalysis rate is limited by proton transfer from the zinc ion-bound molecule to the bulk solvent[11].

Figure 6.2 | **CA catalysis mechanism of CO_2 hydration**

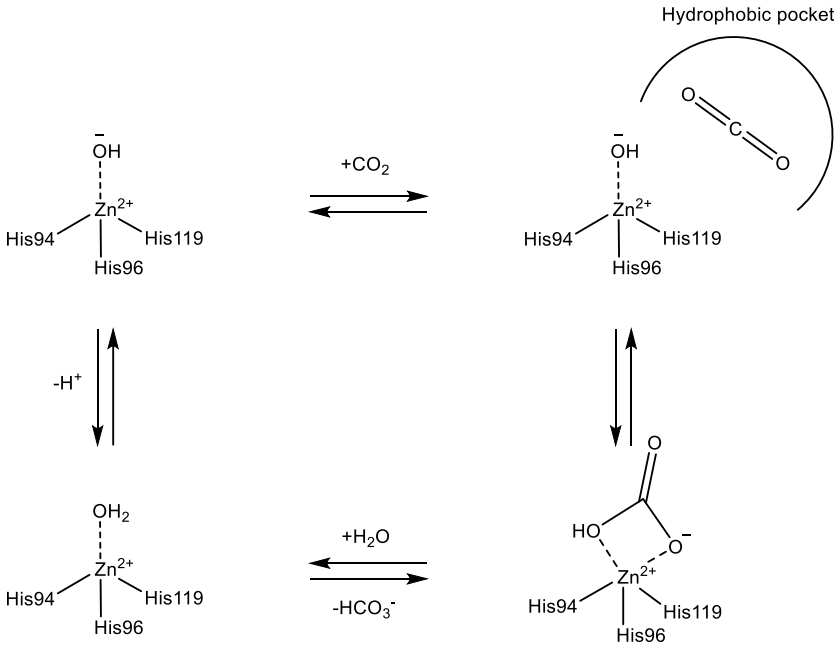

6.2 Carbonic anhydrases as new target for T2DM

6.2.1 Carbonic anhydrase-II

CA-II, represented in Figure 6.3, is the most physiologically relevant isoform and it has been found in several organs/tissues. It shows very high catalytic activity for the conversion (k_{cat} of CO_2 into HCO_3^- and H^+ of 1.40 x 10^6 s^{-1} and k_{cat}/KM of 1.50 x 108 M-1 s-1 at 20°C and pH 7.5) [10,12].

Figure 6.3 | **3D structure of hCA-II (PDB entry code: 3K34)**

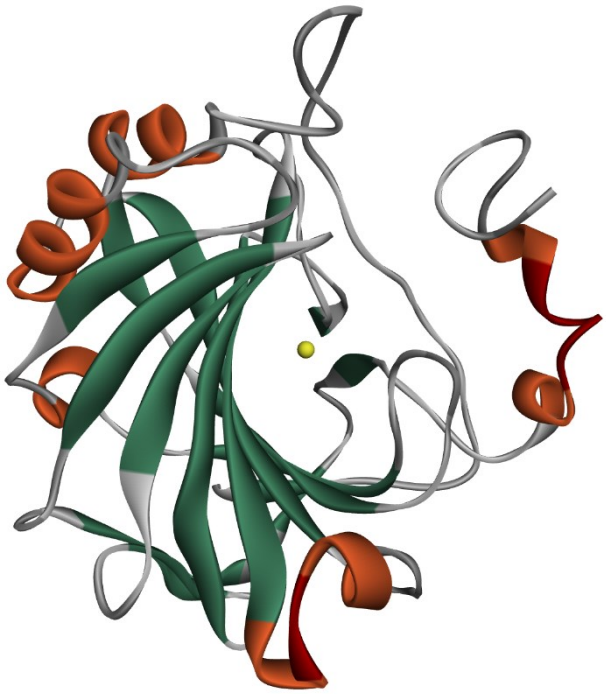

CA-II regulates electrolyte secretion in a variety of tissues, including the bicarbonate-rich aqueous humor in the anterior chamber of the eyes[13,14] and the cerebrospinal fluid (CSF)[15], as well as pH and CO_2 homeostasis throughout the body. Other functions include urine formation and bicarbonate reabsorption in the kidney tubules[15], biosynthetic reactions, such as gluconeogenesis, lipogenesis, ureagenesis[16,17], bone resorption, and calcification[18]. More in detail, CA-II is highly expressed in kidney intercalated cells, proximal tubules, Henle loop, and collecting duct cells, where it regulates bicarbonate transport[19]. Indeed, an autosomal recessive disorder related to CA-II deficiency leads to renal tubular acidosis, osteopetrosis, cerebral calcification, and growth retardation.

Moreover, several studies demonstrated that CA-II interacts with a variety of membrane-bound carriers to regulate the cytoplasmatic pH, such as the sodium/hydrogen exchanger (NHE1)[20] or the sodium bicarbonate cotransporter (NBC1)[21]. Recent investigation shows that NHE1/CA-II metabolon complex is exacerbated in diabetic cardiomyopathy of $ob^{-/-}$ mice, which may lead to perturbation of intracellular pH and Na^+ and Ca^{2+} concentrations, contributing to cardiovascular anomalies.

Moreover, the enhanced NHE1/CA-II metabolon activity was correlated with an increased CA-II expression in hypertrophic and functionally impaired $ob^{-/-}$ mice hearts[22]. Evidence proves also that CA-II is overexpressed in diabetic ischemic human myocardium. Increased myocyte CA-II is associated with NHE1 hyperphosphorylation in diabetic ischemic cardiomyopathy[23]. Up-regulation of CA-II was also found in human atherosclerotic plaques in the major vascular beds at both the transcriptional and protein levels[24].

Isoforms II and V play a significant role in metabolic processes such as gluconeogenesis, fatty acid biosynthesis, and pyrimidine base synthesis[10].

6.2.2 Carbonic anhydrases VA and VB

CA-V is, among all the isoforms, the only one located in the mitochondria. There are two mitochondrial CAs with differing tissue distributions and they are usually refer as CA-VA and CA-VB. The crystal structures of these enzymes are not available to date, although they are closely related to wild-type mouse CA-VA isozyme (wt mCA-VA, PDB entry code: 1DMY), and several mutants are available in protein data bank. Nonetheless, tissue distribution, physiological role, and druggability have been investigated.

hCA-VA is solely expressed in the liver (hepatocytes) while hCA-VB displayed a broad tissue distribution, indeed it is located in the pancreas, kidneys, salivary glands, spinal cord, heart, and skeletal muscle, while it is absent in the liver[25]. Successive investigations located hCA-VA and/or VB also in adipocytes, astrocytes, and neurons[26]. Here, they seem to be involved in the regulation of intramitochondrial calcium levels and neuronal bicarbonate homeostasis[27].

However, the biological significance of the limited expression of CA-VA and the much more widespread expression of CA-VB are not yet understood.

Nonetheless, these isoforms influence many physiological processes, like CO_2 transport, bone resorption gluconeogenesis, production of body fluids, lipogenesis, ureagenesis, and *de novo* synthesis of HCO_3^- within the mitochondrial compartment[28]. Mitocondrial HCO_3^- is essential for pyruvate carboxylase in the gluconeogenic or lipogenic pathways and carbamoyl phosphate synthetase I in the ureagenesis process in the liver. That's because HCO_3^- cannot permeate the inner mitochondria membrane, and no bicarbonate transporter (SLC4A family) is located on this membrane. Therefore, HCO_3^- supplied by CA-VA/VB is thus critical for pyruvate carboxylase to convert pyruvate to oxaloacetate in the mitochondrion (Figure 6.4). Then, the tricarboxylate transporter transports the oxaloacetate to the cytosol, where it is implicated in the synthesis of fatty acids (lipogenesis)[29]. In this cytosolic process, the HCO_3^- used by acetyl-coenzyme A

carboxylase to convert acetyl-CoA into malonyl-CoA is, on the other hand, supplied by the cytosolic CA-II. Moreover, since HCO_3^- is also essential for the first step of oxidative metabolism in the mitochondria, in a recent genetic investigation, CA-VA was found to have a key role in the regulation of reactive oxygen species (ROS) and cell death in pericytes as well, which are early events in the development of diabetes-related cerebrovascular illness.

Furthermore, CA-V is also most likely implicated in the glucose-induced secretion of insulin[30]. There are at least two possible mechanisms by which mitochondrial CAs could participate in the regulation of insulin secretion. In detail, as already mention, CA-V provide HCO_3^- for pyruvate carboxylase, which is abundantly express in the mitochondrial islet cells, and it is important in the pyruvate-malate shuttle, which provides NADPH for normal β-cell functions, like glucose-induced secretion of insulin, as demonstrated by a study of MacDonald *et al.* [31]. Furthermore, the control of mitochondrial calcium concentrations is a second way through which CA-V may be connected to insulin secretion. As observed by Kennedy *et al.* calcium ions have a fundamental role in the energy requirements for exocytosis of insulin from β-cell[32].

In addition, there is clear evidence that the inhibition of both the isoforms VA and VB lead to considerable weight loss[33,34].

Figure 6.4 | **CAs role in the *de novo* lipogenesis**

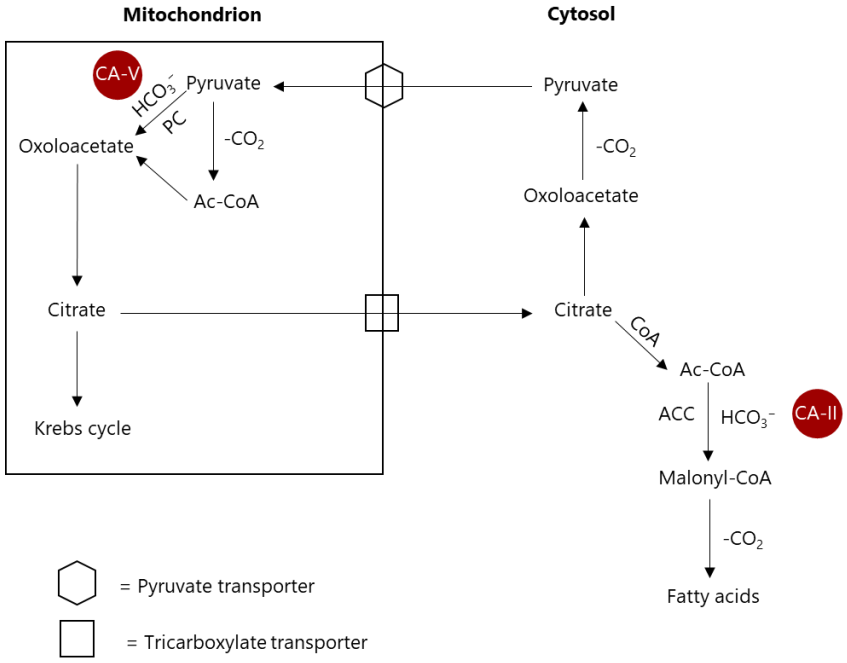

Ac-CoA, Acetyl CoA; ACC, Ac-CoA carboxylase; CoA, Coenzyme A; PC, Pyruvate carboxylase

Thus, to target the CAs, II and V, may provide a unique opportunity to modulate several metabolic pathways, mitigating the development and progression of diabetic comorbidity.

References

1. Supuran, C. T. & De Simone, G. Carbonic Anhydrases: An Overview. Carbon. Anhydrases as Biocatal. From Theory to Med. Ind. Appl. 3–13 (2015) doi:10.1016/B978-0-444-63258-6.00001-9.
2. Supuran, C. T. & De Simone, G. Carbonic Anhydrases as Biocatalysts: From Theory to Medical and Industrial Applications. Carbonic Anhydrases as Biocatalysts: From Theory to Medical and Industrial Applications (Elsevier Inc., 2015). doi:10.1016/C2012-0-13548-1.
3. Aspatwar, A., Tolvanen, M. E. E. & Parkkila, S. Phylogeny and expression of carbonic anhydrase-related proteins. BMC Mol. Biol. 11, (2010).
4. Lionetto, M. G., Caricato, R., Giordano, M. E. & Schettino, T. The complex relationship between metals and carbonic anhydrase: New insights and perspectives. International Journal of Molecular Sciences vol. 17 127 (2016).
5. Boone, C. D., Pinard, M., McKenna, R. & Silverman, D. Catalytic mechanism of α-class carbonic anhydrases: CO2 hydration and proton transfer. Subcell. Biochem. 75, 31–52 (2014).
6. Kim, J. K. et al. Elucidating the role of metal ions in carbonic anhydrase catalysis. Nat. Commun. 11, 1–10 (2020).
7. Mishra, C. B., Tiwari, M. & Supuran, C. T. Progress in the development of human carbonic anhydrase inhibitors and their pharmacological applications: Where are we today? Med. Res. Rev. 40, 2485–2565 (2020).
8. Aggarwal, M., Boone, C. D., Kondeti, B. & McKenna, R. Structural annotation of human carbonic anhydrases. J. Enzyme Inhib. Med. Chem. 28, 267–77 (2013).
9. Kumar, S., Rulhania, S., Jaswal, S. & Monga, V. Recent advances in the medicinal chemistry of carbonic anhydrase inhibitors. European Journal of Medicinal Chemistry vol. 209 112923 (2021).
10. Supuran, C. T. Carbonic anhydrases: Novel therapeutic applications for inhibitors and activators. Nature Reviews Drug Discovery vol. 7 168–181 (2008).
11. Silverman, D. N. & Lindskog, S. The catalytic mechanism of carbonic anhydrase: implications of a rate-limiting protolysis of water. Acc. Chem. Res. 21, 30–36 (1988).
12. Alterio, V., Di Fiore, A., D'Ambrosio, K., Supuran, C. T. & De Simone, G. Multiple binding modes of inhibitors to carbonic anhydrases: How to design specific drugs targeting 15 different isoforms? Chemical Reviews vol. 112 4421–4468 (2012).
13. Kinsey, V. E. & Barany, E. The rate of flow of aqueous humor; derivation of rate of flow and its physiologic significance. Am. J. Ophthalmol. 32 Pt. 2, 189–202 (1949).
14. Supuran, C. T., Capasso, C. & De Simone, G. Carbonic Anhydrase II as Target for Drug Design. in Carbonic Anhydrases as Biocatalysts: From Theory to Medical and Industrial Applications 51–90 (Elsevier, 2015). doi:10.1016/B978-0-444-63258-6.00004-4.
15. Maren, T. H., Conroy, C. W., Wynns, G. C. & Godman, D. R. Renal and cerebrospinal fluid formation pharmacology of a high molecular weight carbonic anhydrase inhibitor. J. Pharmacol. Exp. Ther. 280, 98–104 (1997).
16. Lynch, C. J. et al. Role of hepatic carbonic anhydrase in de nova lipogenesis. Biochem. J. 310, 197–202 (1995).
17. Chegwidden, W. R., Dodgson, S. J. & Spencer, I. M. The roles of carbonic anhydrase in metabolism, cell growth and cancer in animals. EXS 343–63 (2000) doi:10.1007/978-3-0348-8446-4_16.
18. Supuran, C. T. Carbonic anhydrases: novel therapeutic applications for inhibitors and activators. Nat. Rev. Drug Discov. 2008 72 7, 168–181 (2008).
19. Lonnerholm, G., Wistrand, P. J. & Barany, E. Carbonic anhydrase isoenzymes in the rat kidney. Effects of chronic acetazolamide treatment. Acta Physiol. Scand. 126, 51–60 (1986).
20. Li, X., Alvarez, B., Casey, J. R., Reithmeier, R. A. F. & Fliegel, L. Carbonic anhydrase II binds to and enhances activity of the Na+/H+ exchanger. J. Biol. Chem. 277, 36085–36091 (2002).
21. Becker, H. M. & Deitmer, J. W. Carbonic anhydrase II increases the activity of the human electrogenic Na+/HCO3- cotransporter. J. Biol. Chem. 282, 13508–13521 (2007).
22. Jaquenod De Giusti, C. et al. Carbonic anhydrase II/sodium-proton exchanger 1 metabolon complex in cardiomyopathy of ob−/− type 2 diabetic mice. J. Mol. Cell. Cardiol. 136, 53–63 (2019).
23. Torella, D. et al. Carbonic anhydrase activation is associated with worsened pathological remodeling in

human ischemic diabetic cardiomyopathy. J. Am. Heart Assoc. 3, (2014).
24. Oksala, N. et al. Carbonic anhydrases II and XII are up-regulated in osteoclast-like cells in advanced human atherosclerotic plaquesTampere Vascular Study. Ann. Med. 42, 360–370 (2010).
25. Shah, G. N. et al. Mitochondrial carbonic anhydrase CA VB: Differences in tissue distribution and pattern of evolution from chose of CA VA suggest distinct physiological roles. Proc. Natl. Acad. Sci. U. S. A. 97, 1677–1682 (2000).
26. Akdemir, A. & Güzel-Akdemir, Ö. The Structure, Physiological Role, and Potential Medicinal Applications of Carbonic Anhydrase V. in Carbonic Anhydrases as Biocatalysts: From Theory to Medical and Industrial Applications 125–138 (Elsevier, 2015). doi:10.1016/B978-0-444-63258-6.00007-X.
27. Nocentini, A., Donald, W. A. & Supuran, C. T. Human carbonic anhydrases: Tissue distribution, physiological role, and druggability. in Carbonic Anhydrases: Biochemistry and Pharmacology of an Evergreen Pharmaceutical Target 151–185 (Academic Press, 2019). doi:10.1016/B978-0-12-816476-1.00008-3.
28. Akdemir, A. & Güzel-Akdemir, Ö. The Structure, Physiological Role, and Potential Medicinal Applications of Carbonic Anhydrase V. in Carbonic Anhydrases as Biocatalysts: From Theory to Medical and Industrial Applications vol. 64 125–138 (Annu Rev Biochem, 2015).
29. Ismail, I. S. The Role of Carbonic Anhydrase in Hepatic Glucose Production. Curr. Diabetes Rev. 14, 108–112 (2018).
30. Sener, A. et al. Possible role of carbonic anhydrase in rat pancreatic islets: Enzymatic, secretory, metabolic, ionic, and electrical aspects. Am. J. Physiol. - Endocrinol. Metab. 292, (2007).
31. MacDonald, M. J. Feasibility of a mitochondrial pyruvate malate shuttle in pancreatic islets. Further implication of cytosolic NADPH in insulin secretion. J. Biol. Chem. 270, 20051–20058 (1995).
32. Kennedy, E. D. et al. Glucose-stimulated insulin secretion correlates with changes in mitochondrial and cytosolic Ca2+ in aequorin-expressing INS-1 cells. J. Clin. Invest. 98, 2524–2538 (1996).
33. Fiore, A., Supuran, C. & Simone, G. Are Carbonic Anhydrase Inhibitors Suitable for Obtaining Antiobesity Drugs ? Curr. Pharm. Des. 14, 655–660 (2008).
34. Supuran, C. T. Emerging role of carbonic anhydrase inhibitors. Clinical Science vol. 135 1233–1249 (2021).

CHAPTER 7

Aim of the work

Type 2 diabetes mellitus (T2DM) is one of the priority global health problems, which is characterized by dysregulation of carbohydrate, lipid, and protein metabolism and results from impaired insulin secretion, insulin resistance, or a combination of both. The global burden of diabetes had increased significantly since 1990[1], so much that compelled to face this syndrome not only as a major threat to public health but also to its socio-economic development.

The explosion in T2DM prevalence over the past half-century has paralleled that of the obesity epidemic[2]. The two inflammatory diseases are correlated since it has been shown that obesity induces immune cell changes in adipose tissue that affect insulin sensitivity[3,4]. Obesity and insulin resistance are two key drivers in the development of T2DM and are also connected to the development of both microvascular complications (including retinopathy, nephropathy, and neuropathy) and macrovascular complications (such as cardiovascular comorbidities). Other notable risk factors include a poor diet, low physical activity levels, and older age.

Multifactorial risk reduction strategies to normalize blood glucose levels, lipid profile, and blood pressure are required to manage T2DM. Furthermore, medical care is also continuously required together with patient self-management for control of abnormal glucose levels.

Achievement of glycemic control requires a pharmacological approach that has progressed from biguanides and metformin to a wide spectrum of medications that seem to provide a beneficial effect on morbidity and mortality. Despite this, the target treatment goals are still not achieved, so polypharmacological treatment is needed[5]. However, complex treatment regimens may lead to drug-drug interaction and/or poor patient adherence. Thus, novel antidiabetic drug classes capable of simultaneously acting on several levels could be the solution. In the state of metabolic disturbance, like the one affecting the diabetic patient, several major enzymes are abnormally expressed, and they could be interesting targets for drug development. Hence, the conceptualization of multimodal drugs, which could reduce hyperglycemia and concomitantly inhibit the progression of complications, may offer a valuable therapeutic option. The design of these multi-target ligands must focus, of course, on the selection of suitable targets, which must be well characterized and preferably implicated in different pathways of the disease, and on the optimization of the relative potency of the compound towards each interested protein[6].

Keeping in mind what discussed in the previous chapters regarding the classical hurdles and pitfalls of the traditional drug development pipeline and the complexity of the diabetic scenario, a multi-target strategy combined with the repurposing approach have been exploited with the aim to design and to develop new molecules for the treatment of T2DM.

Indeed, the combined strategy could be useful in shorting out the length of time necessary to identify new potential drugs.

In order to select a suitable molecule to be repurposed the research group of Professor Vistoli and Professor Pedretti performed conventional docking simulations (numerous ligands and one target) on two interesting enzymes involved in the diabetic pathology, namely DPP-IV and CA-II.

Given the relevance of the DPP-IV/CAs (II and V) roles in the pathology of T2DM, multi-target ligands able to modulate these enzymes could represent a novel therapeutic approach for antidiabetic treatment. As already mentioned in Chapter 5, DPP-IV inhibitors prolong the half-life of the glucose-dependent insulinotropic polypeptide hormone (GIP) and the glucagon-like peptide 1 (GLP-1), two important regulators of post-prandial glycemic control[7]. On the other hand, CA inhibitors could be useful in the prevention of several common diabetic comorbidities[8], as seen in Chapter 6.2.

During docking simulations, WB-4101 (2-[(2,6-Dimethoxyphenoxyethyl)aminomethyl]-1,4-benzodioxane), an adrenergic ligand in which our laboratory has already prior expertise, results to be an interesting repurposed candidate. As a matter of fact, WB-4101 conveniently fits both the pockets of the two selected enzymes.

However, observing the results from previous computational studies, WB-4101 fails to interact with some key residues in the binding site of each enzyme and in order to strengthen the interactions towards the target enzymes, morphing its structure has been required. The application of morphing allowed the modulation of the activity toward the old and new targets[10,11]. In addition, morphing aid in preserving low lipophilicity and in avoiding significant structural expansion, which both should be a top priority. In this context, rational multitarget optimization strategies relied on computational models and systematic exploration of the SAR on each individual target. Therefore, different WB-4101 derivatives have been designed and synthesized. All compounds were characterized through ^{1}H NMR, ^{13}C NMR and mass spectroscopy analyses. The inhibition activity was investigated on DPP-IV and several isoforms of CA.

Rational drug design for the development of DPP-IV and CAs multi-target inhibitors

To rationalize the dual activity, preliminary repurposing computational studies were performed in order to identify possible candidates able to interact with the binding sites of the interested targets. Between all the compounds of the analyzed database WB-4101, a well-known adrenergic ligand, has been chosen since it conveniently fits into all these enzymes' pockets (Figure 7.1).

Figure 7.1 | **Resolved structure of CA-II (A) and DPP-IV (B) complexed with WB-4101**

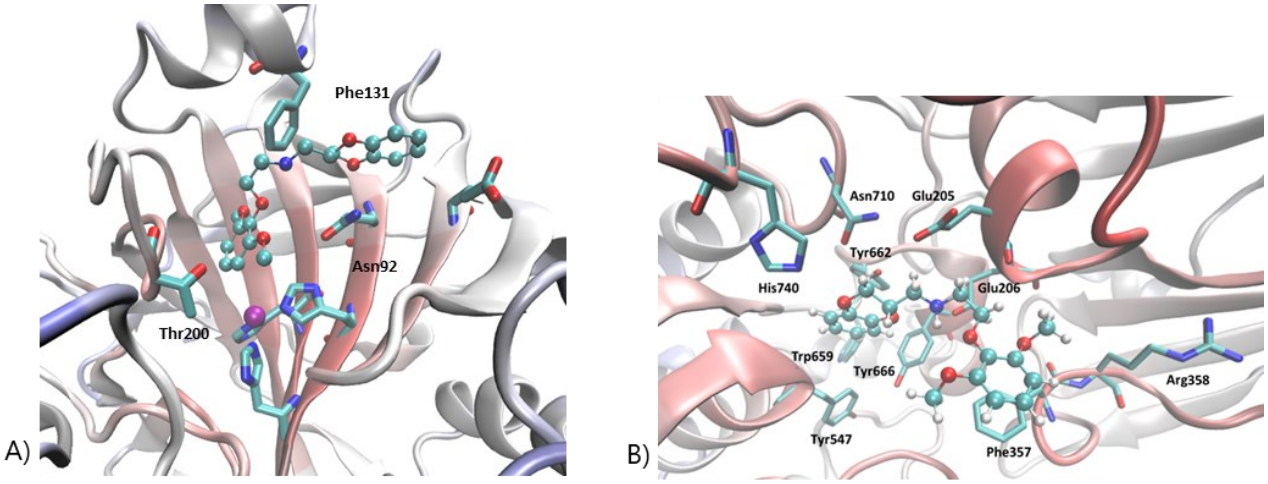

However, WB-4101 fails to stabilize all required interactions. Indeed, it lacks a moiety able to interact with a key arginine residue (Arg358) in the DPP-IV pocket and with the zinc ion of the CAs. In order to strengthen interactions towards the target enzymes, morphing WB-4101 has been mandatory. Therefore, in the design of this novel class of compounds, the structure of the adrenergic ligand has been systematically morphed and the modifications can be organized into three main groups, as represented in Figure 7.2:

- I - Decoration of the 2,6-dimethoxyphenoxy scaffold;
- II - Variations on the secondary amine function;
- III - Deconstruction of the benzodioxane scaffold.

Figure 7.2 | **Morphing approaches applied on the WB-4101 structure**

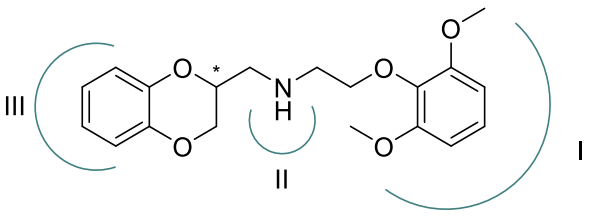

WB-4101

As highlighted in Figure 7.2, WB-4101 is a chiral compound, nevertheless all the synthetic strategies applied are not intended to separate the enantiomers. Only in case of good inhibition activity, an alternative stereoselective synthetic route will be investigated. Therefore, the development of several synthetic schemes allowed the obtainment of the different series of compounds as racemates or diastereomers.

Group I: Decoration of the 2,6-dimethoxyphenoxy scaffold

During the first year, the rational drug design had been focused on morphing the dimethoxy phenoxy ring of WB-4101 while retaining both the benzodioxane scaffold and secondary amine included in the linker. The main changes applied to strengthen the interactions of these compounds towards DPP-IV and CA-II/V have comprised the introduction in para position of the phenoxy ring a sulfonamide function and the elimination of the methoxy groups. The sulfonamide function is a well-known chelating group for the zinc ion of the CAs and can be seen as a valid bioisostere of carboxyl group to interact with Arg358. Furthermore, the position of this moiety was based on previous investigations, which demonstrated that this substitution abrogates or strongly reduces the adrenergic affinity[12]. In order to simplify and speed up the obtainment of the first derivatives, the influence of the methoxy groups was not evaluated in a first step. Several derivatives have been designed and synthesized to evaluate the biological activity of different sulfonamides. As depicted in Figure 7.3, the atom of the sulfonamide group linked to the scaffold has been investigated as well.

Figure 7.3 | **First generation of potential multi-target inhibitors for DPP-IV and CAs**

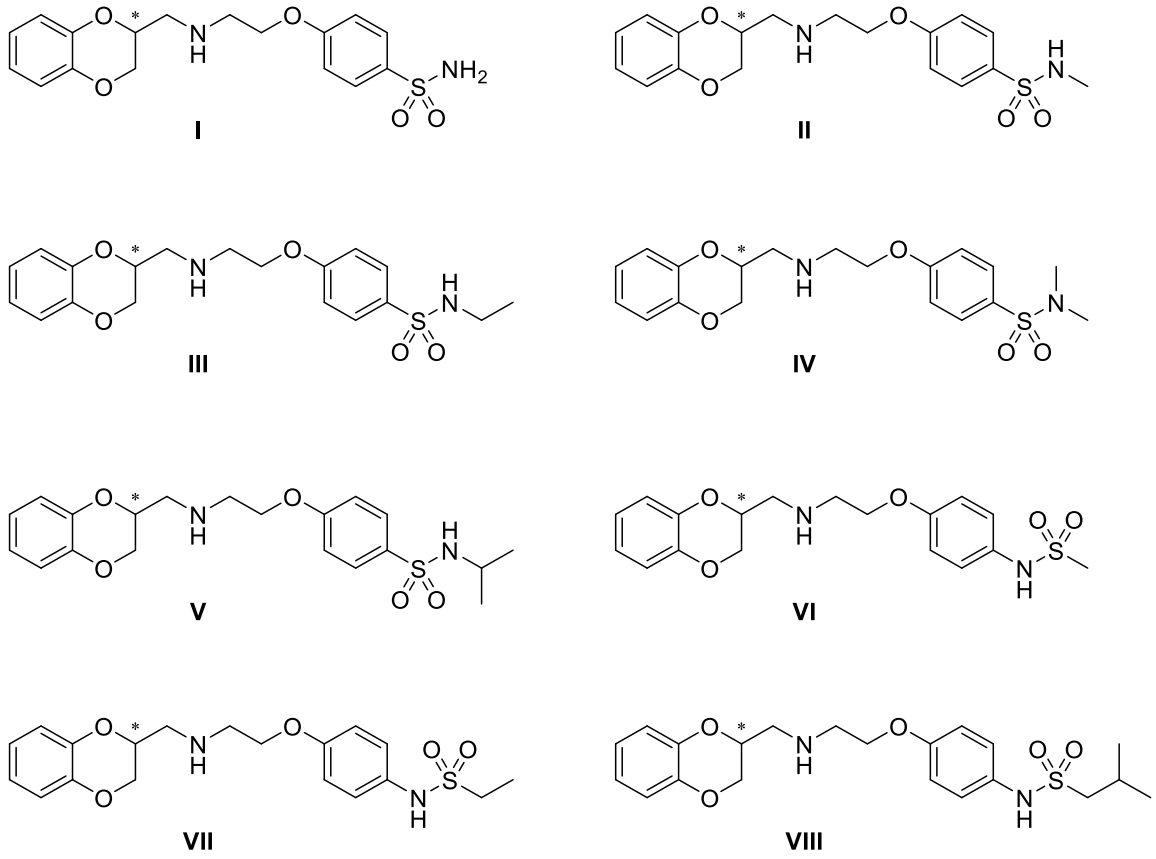

Group II: Variations on the secondary amine function

SAR studies on the first wave of compounds have shown that the primary sulfonamide function is fundamental to inhibit CAs by chelating its zinc ion since even a methyl residue is detrimental. Moreover, the unsatisfactory results on DPP-IV of the compounds carrying the secondary amine in the linker may indicate the key role of the primary amine that is a common feature of commercially available DPP-IV inhibitors (i.e. Sitagliptin, Omarigliptin).

Hence, inspired by the drugs already available on the market, to prove the influence of the primary amine function has been a further goal. Besides the previous considerations, the rational drug design has been focused on the decoration of the phenolic ring, which was not evaluated at first, and it has been considered as well in order to deeply investigate the influence of these functions on the stereo- and electronic features of these compounds. Therefore, a new set of morphed WB-4101 derivatives which are reported in Figure 7.4 have been designed.

Figure 7.4 | **General structure of a second generation of potential multi-target inhibitor for DPP-IV and CAs**

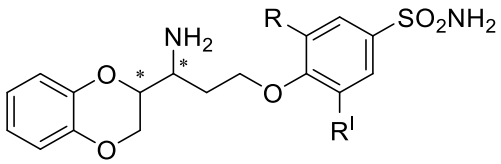

During the second year the health emergency due to the Sars-Cov-2 outbreak limited the laboratory activities and, consequently, some synthetic attempts. In order to have a positive outlook, the lock-down period was approached as a resource to enrich my knowledge. In fact, thanks to the collaboration with the research group of Professor Vistoli and Professor Pedretti, I gained basic computational skills which allowed me to expand the computational studies. In order to continuously rationalize the dual activity, docking simulations were performed to deeply explore the binding mode of this new class of molecules to both CAs and DPP-IV enzymes and to support the design.

As already mentioned, all the derivatives presented in this work are characterized by two chiral centers and since each chiral center may accept R or S stereoisomers, four configurations could be produced. Because of distinct stereoisomers have variable pharmacological, pharmacokinetic, and toxicological features, drug chirality is an important property.

In order to deeply investigate this aspect, molecular docking was performed on each diasteromer for every compounds since the majority of biomolecular interactions are in fact chirally specific. The theory of chiral molecular recognition aims to comprehend shape matching through interactions, like hydrogen bond formation, that occur throughout a successful docking process.

Observing the data, we strengthen the rational behind the design of the second generation, which had been characterized by a primary amine moiety, instead of a secondary one. This function should be able to establish stronger interactions with two residue of Glu in the DPP-IV binding site, namely Glu205 and Glu206, leading to the improvement of the inhibition activity.

Among all the steroisomers's orientations, the poses that achieve the best performance in the binding site of DPP-IV are the RS and SR ones, whose dock score are represented in Figure 7.5.

Figure 7.5 | **Dock score of the derivatives of the second generation**

R	R'	Stereoisomer	Docking score
H	H	RR	-81.9586
		RS	-96.6884
		SS	-86.5239
		SR	-92.6217
H	OMe	RR	-87,6184
		RS	-91,7391
		SS	-92,2660
		SR	-95,7302
OMe	OMe	RR	-76.8424
		RS	-78.9355
		SS	-73.3509
		SR	-85.4533

The computational evaluations suggested that in these compounds the amine moiety is closer to the two aforementioned glutamates residues of the DPP-IV active site, which seems to be crucial. for the biological activity. Figure 7.6 reports the 3D visualization of the best poses of the different primary amine derivatives docked in the binding pocket of DPP-IV. Furthermore, it is interesting to note that the hydrophobic interactions and hydrogen bond are conserved in all compounds.

Figure 7.6 | **Docking studies of the primary amine derivatives with DPP-IV**

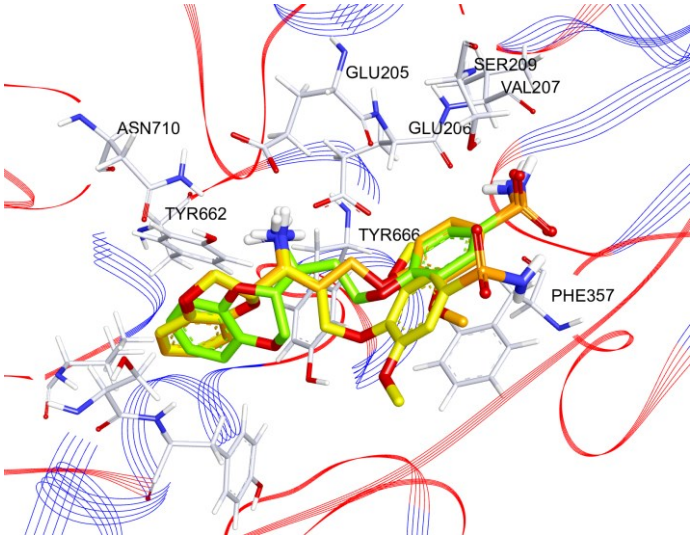

On top of that, the design of this new class of compounds was enriched by the insertion of an azide moiety, inspired by promising docking results. In fact, the compound reported in Figure 7.7 showed interesting docking poses.

Figure 7.7 | **Compound characterized by high dock score**

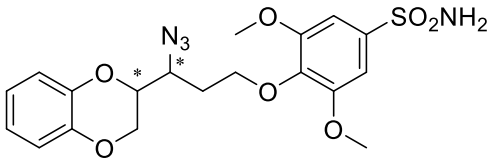

This molecule exhibited a different binding mode from the amine series since the azide group move away from the Glu205 and 206 whilst getting closer to Ser630, a residue of the catalytic triad as shown in Figure 7.8.

In addition, the synthetic pathway developed for the amine derivatives allows convenient access to the compounds bearing the azide function.

Figure 7.8 | **Docking studies of compound XIII with DPP-IV**

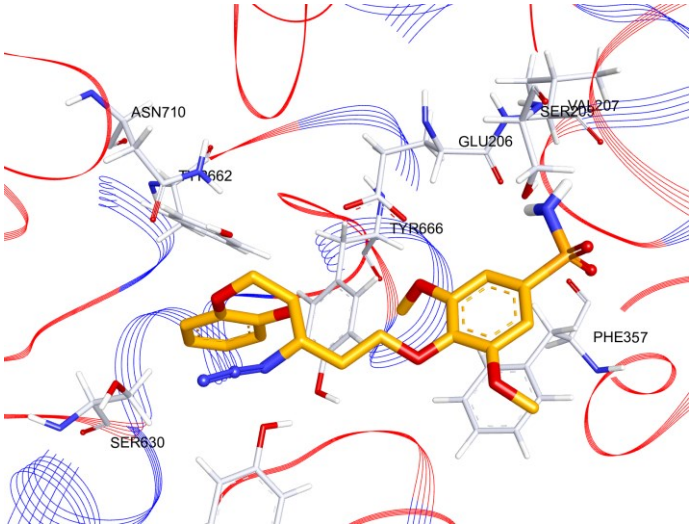

This distinctive binding mode in which the azide moiety is close to Ser630 let us hypothesize a reversible covalent interaction with the enzyme, like the one established by Saxagliptin or other cyanoproline derivatives (Figure 2.10). This theory is supported by the 1,3-dipolar character of the azide motif that let it behave as pseudo nitrenes allowing the formation of a new bond to nitrogen N^1, with loss of molecular nitrogen[13].

Consequently, a new set of morphed WB-4101 derivatives which are depicted in Figure 7.9 have been designed and synthesized.

Figure 7.9 | **Second generation of potential multi-target inhibitors for DPP-IV and CAs**

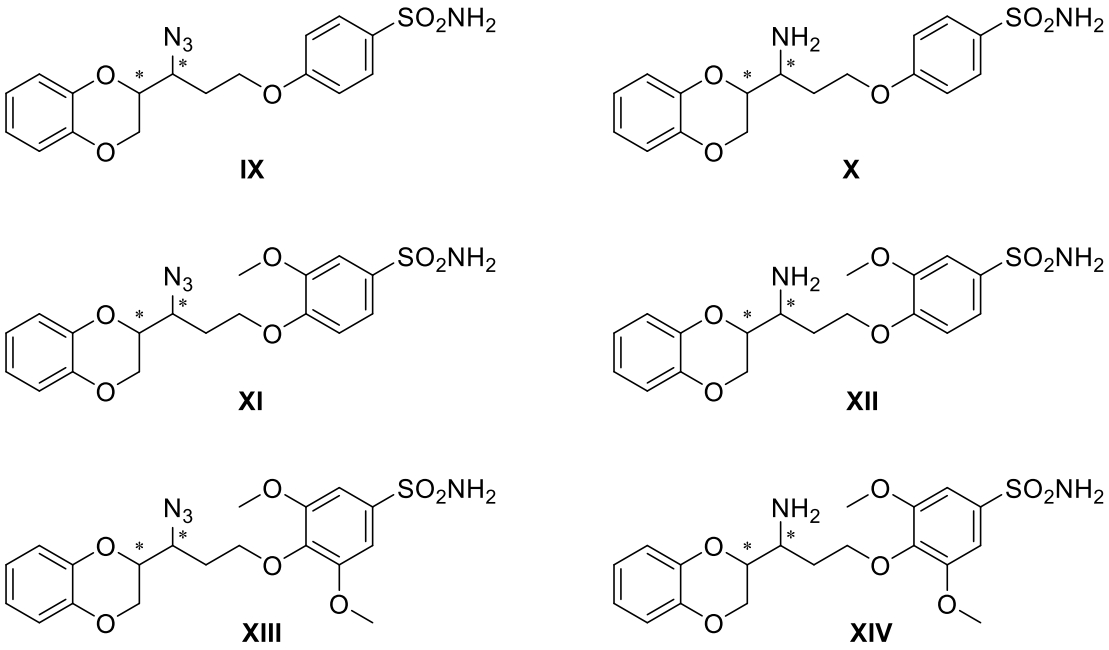

Group III: Deconstruction of the benzodioxane scaffold

Pharmacological investigations on the second generation have confirmed the importance of the primary amine function. Additionally, the dimethoxy groups have resulted in a strongly positive influence on the DPP-IV inhibition while being disadvantageous on the CAs.

The encouraging results invite us to further optimize the structure-activity relationships of these molecules with a view to enhancing the potency while maintaining a suitable selectivity profile.

The next step in the rational drug design, corroborated also by computational simulations, has focused on the investigation of the benzodioxane scaffold.

As a consequence "deconstructed derivatives" have been designed (Figure 7.10) and synthesized to investigate the role of the benzodioxane moiety while maintaining the primary amine/azide function and the primary sulfonamide moiety, which are necessary for the inhibiting activities. In detail, the deconstruction approach have given the opportunity to evaluate how enhancing the flexibility while maintaining the connectivity and spacing influence the biological activity. In theory, this strategy should allow the ligand to explore the receptor's active region more thoroughly, thus improving binding affinity. Before investigating these possibilities, we performed some computational studies on DPP-IV and in order to strengthen the interaction toward the S1 pocket, which is rich in Tyr residues, we decorated the new phenoxy ring with one, two or none methoxy or hydroxy moieties.

Figure 7.10 | **Third generation of potential multi-target inhibitors for DPP-IV and CAs**

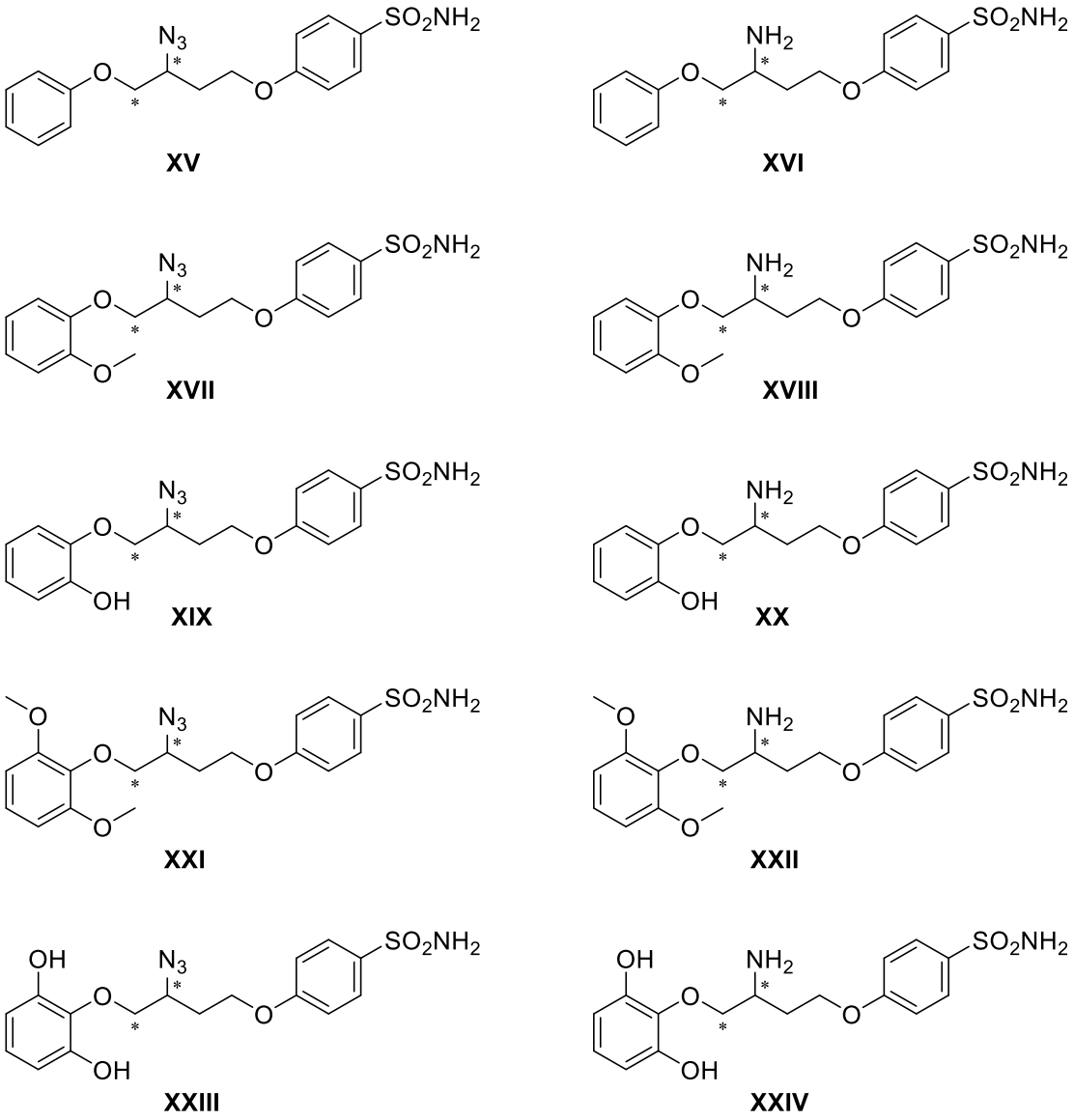

References

1. Saeedi, P. *et al.* Global and regional diabetes prevalence estimates for 2019 and projections for 2030 and 2045: Results from the International Diabetes Federation Diabetes Atlas, 9th edition. *Diabetes Res. Clin. Pract.* 157, (2019).
2. Wang, Y. C., McPherson, K., Marsh, T., Gortmaker, S. L. & Brown, M. Health and economic burden of the projected obesity trends in the USA and the UK. *The Lancet* vol. 378 815–825 (2011).
3. Weisberg, S. P. *et al.* Obesity is associated with macrophage accumulation in adipose tissue. *J. Clin. Invest.* 112, 1796–1808 (2003).
4. Xu, H. *et al.* Chronic inflammation in fat plays a crucial role in the development of obesity-related insulin resistance. *J. Clin. Invest.* 112, 1821–1830 (2003).
5. Artasensi, A., Pedretti, A., Vistoli, G. & Fumagalli, L. Type 2 Diabetes Mellitus: A Review of Multi-Target Drugs. *Molecules* 25, (2020).
6. Morphy, R., Kay, C. & Rankovic, Z. From magic bullets to designed multiple ligands. *Drug Discov. Today* 9, 641–651 (2004).
7. Irwin, N. New perspectives on exploitation of incretin peptides for the treatment of diabetes and related disorders. *World J. Diabetes* 6, 1285 (2015).
8. Supuran, C. T. Carbonic anhydrases: novel therapeutic applications for inhibitors and activators. *Nat.*

Rev. Drug Discov. 2008 72 7, 168–181 (2008).
9. Proschak, E., Stark, H. & Merk, D. Polypharmacology by Design: A Medicinal Chemist's Perspective on Multitargeting Compounds. *J. Med. Chem.* 62, 420–444 (2019).
10. Morphy, R. & Rankovic, Z. Designed Multiple Ligands. An Emerging Drug Discovery Paradigm. *J. Med. Chem.* 48, 6523–6543 (2005).
11. Morphy, R. & Rankovic, Z. The Physicochemical Challenges of Designing Multiple Ligands. *J. Med. Chem.* 49, 4961–4970 (2006).
12. Pallavicini, M. Budriesi, R., Fumagalli, L., Ioan, P., Chiarini, A., Bolchi, C., Ugenti, M. P., Colleoni, S., Gobbi, M. & Valoti, E. WB4101-Related Compounds: New, Subtype-Selective α 1 -Adrenoreceptor Antagonists (or Inverse Agonists?). *J. Med. Chem.* 49, 7140–7149 (2006).
13. Doebelin, C., Schmitt, M., Antheaume, C., Bourguignon, J. J. & Bihel, F. Nucleophilic substitution of azide acting as a pseudo leaving group: One-step synthesis of various aza heterocycles. *J. Org. Chem.* 78, 11335–11341 (2013).

CHAPTER 8

Results and discussions

A multi-target drug strategy has been proposed to manage T2DM through the inhibition of DPP-IV and CAs (II and IV). In detail, repurposing and morphing approaches were applied on WB-4101 in order to develop a new class of compounds. The herein-reported derivatives (Figure 8.1), were designed starting from the chemical structure of WB-4101, whose phenoxy ring, amine moiety, and benzodioxane scaffold were morphed, in turn, giving rise to different generations.

Figure 8.1 | **General molecular structures of different generations of DPP-IV and CAs multi-target compounds**

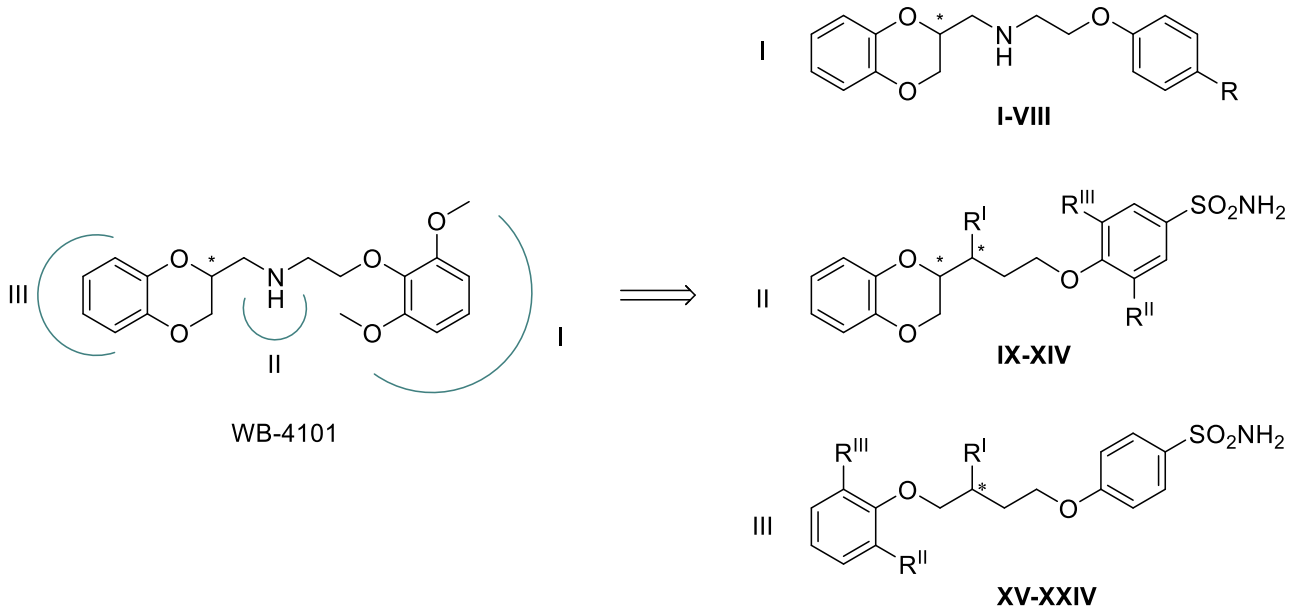

The DPP-IV inhibition activities of the entire sets of compounds were carried out on purified recombinant human DPP-IV using conditions previously optimized[1].

The structure−activity relationships (SAR) can be gathered from the inhibition data reported in Table 8.1 as follow:

i. The first generation of these multi-target ligands do not show a noticeable inhibitor activity for DPP-IV. Indeed, the data reported in Table 8.1 highlight the absence of activity toward this enzyme for all derivatives except compound **VI**, even if its profile is still not satisfactory. It is noteworthy to emphasize that these derivatives share a secondary amine moiety, which seems to be not adequate for the inhibition of DPP-IV since it cannot establish an hydrogen bond with residues Glu205 and Glu206, probably due to the molecules' distance.

Table 8.1 | **Inhibitor activity of compounds I-XXIV on DPP-IV and CAs**

Compound	R	R^{I}	R^{II}	R^{III}	IC_{50} [a] μM	K_i [b] nM					
					DPP-IV	CA-I	CA-II	CA-IV	CA-VA	CA-VB	CA-IX
I	SO_2NH_2	-	-	-	>700	84.9	7.2	290.8	77.9	89.5	20.3
II	SO_2NHMe	-	-	-	>700	>10000	>10000	>10000	>10000	>10000	>10000
III	SO_2NHEt	-	-	-	>700	>10000	>10000	>10000	>10000	>10000	>10000
IV	$SO_2NH(Me)_2$	-	-	-	>700	>10000	>10000	>10000	>10000	>10000	>10000
V	SO_2NH*i* Pr	-	-	-	>700	>10000	>10000	>10000	>10000	>10000	>10000
VI	$NHSO_2Me$	-	-	-	300.2 ± 25.2	>10000	>10000	>10000	>10000	>10000	>10000
VII	$NHSO_2Et$	-	-	-	>700	>10000	>10000	>10000	>10000	>10000	>10000
VIII	$NHSO_2$*i* Bu	-	-	-	326.6 ± 10.4	>10000	>10000	>10000	>10000	>10000	>10000
IX	-	N_3	H	H	669.3 ± 23.5	8705	862.5	4551	658.8	182.8	328.0
X	-	NH_2	H	H	0.0490 ± 0.0045	261.5	36.1	3034	94.1	42.8	132.8
XI	-	N_3	OMe	H	326.6 ± 10.4	971.8	349.7	6144	77.5	386.6	110.6
XII	-	NH_2	OMe	H	57.44 ± 3.2	914.0	842.6	478.3	456.0	409.7	31.1
XIII	-	N_3	OMe	OMe	0.0332 ± 0.0058	6134	4890	4564	89.6	155.0	745.4
XIV	-	NH_2	OMe	OMe	0.0283 ± 0.0035	5960	4310	4840	4346	231.7	954.9
XV	-	N_3	H	H	>700	22.9	4.2	49.0	93.1	56.6	5.8
XVI	-	NH_2	H	H	63.3 ± 5.7	45.2	6.9	693.7	810.4	651.7	89.9
XVII	-	N_3	OMe	H	>700	58.1	7.8	390.3	213.3	337.7	7.3
XVIII	-	NH_2	OMe	H	no trend	226.8	13.2	578.8	894.8	638.8	86.9
XIX	-	N_3	OH	H	>700	7.7	4.9	9.6	151.9	235.8	5.3
XX	-	NH_2	OH	H	507.3 ± 12.5	96.9	9.0	56.2	527.4	766.7	8.6
XXI	-	N_3	OMe	OMe	no trend	7480	71.7	923.0	71.2	55.1	51.5
XXII	-	NH_2	OMe	OMe	no trend	94.3	35.0	626.3	693.3	375.9	64.6
XXIII	-	N_3	OH	OH	no trend	56.5	6.2	92.2	643.8	588.4	80.5
XXIV	-	NH_2	OH	OH	no trend	87.7	9.6	22.5	759.8	414.0	60.1
WB-4101					>700	>10000	>10000	>10000	>10000	>10000	>10000
Sitagliptin					0.0088 ± 0.0011	>10000	>10000	>10000	>10000	>10000	>10000
AAZ					ND	250	12.1	74	63.0	54.0	25.7

[a] Mean from 3 different assays; [b] Mean from 3 different assays by a stopped-flow technique (errors were in the range of ± 5-10 % of the reported values), ND; not determined.

ii. Compounds belonging to the second generation, which are characterized by the presence of a primary amine or an azide moiety, show a different trend of inhibition. In detail, compounds **X**, **XIII,** and **XIV** possess a nanomolar efficacy comparable to the commercially available DPP-IV inhibitor Sitagliptin. This satisfactory efficacy could be explained by the docking poses, in which these derivatives established all the key interactions with the binding site. In fact, among the second generation, almost all compounds which incorporate the primary amine function exhibit low nanomolar inhibition, corroborating the rational design. Moreover, as assumed, a significant role seems to be also played by the substituent on the phenoxy ring since the decoration by the methoxy groups results in a strong positive contribution for the inhibition activity.

iii. Despite the similar docking poses between the prime amine derivatives (Figure 7.6), the unexpected range of activity showed by compound **XII** deserves to be further investigated.

iv. The biological results display that derivative **XIII** has a strong activity on DPP-IV. The docking results of this compound exhibit a distinctive binding mode with the azide moiety close to the Ser630. Due to its 1,3-dipolar character, azide can behave as pseudo nitrenes and allow the formation of a new bond to nitrogen N^1, with loss of molecular nitrogen[2]. Therefore, we propose a reversible covalent interaction with the enzyme, like Saxagliptin or other cyanoproline derivatives.

However, further investigations in this direction are needed to better elucidate the inhibition mechanism.

v. Unpleasantly, the compounds derived by the deconstruction of the benzodioxane scaffold show an unsatisfactory inhibition activity on DPP-IV in contrast with the docking simulations. Although the disappointing potencies, a clear structure activity relationship can be deduced anyway: only compound **XVI** which carries the primary amine function and maintains one oxygen of the deconstructed benzodioxane shows activity even if in the micromolar range. In fact, any other decoration of the aromatic ring previously belonging to the benzodioxane is detrimental for the inhibitor activity.

Furthermore, the CA inhibition profiles of all the compounds were evaluated on several common isoforms, namely hCA-I, II, IV, V (A and B), and IX. In addition, Acetazolamide (**AAZ**) was used as positive control. The choice of these isoforms was based upon their sequence homology, in order to better evaluate the selectivity profile.

An Applied Photophysics stopped-flow instrument was used for assaying the CA catalyzed CO_2 hydration activity[3]. All CA isoforms were recombinant proteins obtained inhouse, as reported[4–7]. Data reported in Table 8.1 show that:

i. Most of the compounds of the first generation demonstrate weak inhibitor effectiveness. Conversely, the primary sulfonamide moiety of compound **I** shows strong inhibitor activity on the physiologically dominant isoform hCA-II (K_i 7.2 nM) with comparable efficacy to that of the AAZ (K_I of 25 nM). Moreover, this compound has also shown a good selectivity profile against hCA-II.

ii. Derivatives of the second series result to be generally more effective against hCAs. Among this generation compound **X**, which bears a primary amine moiety and has no decoration on the phenoxy ring, is able to target hCA-II with selectivity over the cytosolic isozymes (selectivity ratio hCA I/II of 7.24 and hCA IX/II of 3.68) and VB, both in the low nanomolar

range (36.1 and 42.8, respectively). The satisfactory DPP-IV inhibition and the selectivity CAs profile indicate compound **X** as potential lead of this novel class of multi-target ligands.

iii. Compounds **XI** and **XIII** effectively and selectively inhibit the mitochondrial isoform hCA-VA with inhibition constants ranging in the nanomolar range, between 77.5 and 89.6 nM. Both these compounds bear the azide moiety and have at least one methoxy group on the phenoxy ring.

iv. Moreover, dimethoxy derivatives in the second generation are generally less efficacious on hCAs in comparison to the compounds of the same wave leading to the conclusion that this substitution is disadvantageous on the CAs, while being quite influential on the DPP IV inhibition. The reasons behind this behavior might be found in the different electronic property of the sulfonamide moiety, which is now bound to a more electron-rich system, which influences its chelating capability.

v. Results coming from the third generation, namely compounds obtained by the deconstruction of the benzodioxane scaffold, show a general improved activity on hCA-II. In particular, the presence of one or two hydroxy groups do not significantly affect the inhibitor activity on hCA-II. On the contrary, the stepwise changing of the phenolic functions into the corresponding methyl ethers results detrimental for the potency towards hCA-II.

Generally, compounds carrying the azide moiety are more active than the ones with the primary amine, except compound **XXI** that shows a noticeable decrease in activity while remaining in the nanomolar range.

Unfortunately, the deconstruction strategy does not lead to the same positive improvement on both mitochondrial CAs (VA and VB).

However, this third generation shows very interesting selective profile towards also CA-IX. In addition, a study on the more interesting compounds (**XI** and **XIII**) with the aim of identifying the effective loss for adrenergic affinity is in progress.

Stereochemical evaluation

As already mentioned, the strategy applied was to first evaluate the mixture of chiral compounds and only in case of good inhibition activity, a stereoselective synthetic route would have been investigated.

Therefore, the several applied synthetic schemes have allowed the obtainment of the different series of compounds as racemates or diastereomers.

Nevertheless, as reported in chapter 7 the spatial orientation crucially affects the biological activity.

Since compounds of the second generation, in addition to intriguing structures, possess potent biological activity toward both DPP-IV and CAs (II and V) deserve a stereochemical investigation. Indeed, we observed a stereoconvergent behavior of the Reformatsky reaction which has been applied to obtain the β-ketoester (Figure 8.2).

Figure 8.2 | **Generation of diastereomers in the Reformatsky step**

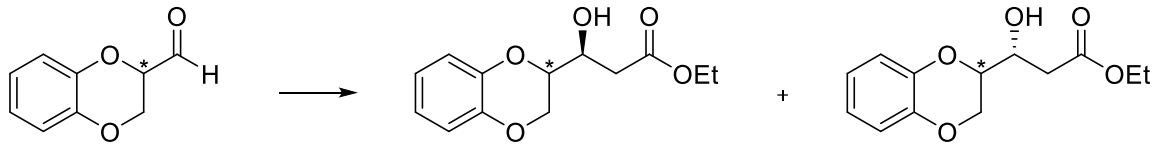

The consequent reduction of the ester moiety to alcohol allowed us to separate the four diastereomers in two enantiomeric mixtures via flash chromatography, with a 70:30 ratio.

Hence, we decided to start the synthetic pathway from enantiomeric pure (R)-1,4-benzodioxan-2-carboxylic acid in order to obtain the two enantiopure 1,3-diols and to assess the configuration of the new chiral center. Diastereomers can be distinguished with ^{1}H-NMR spectroscopy since the corresponding ^{1}H nuclei in both diastereomeric environments have different electronic surroundings, resulting in distinct chemical shifts, as clearly represented in Figure 8.3. Especially, the overlap of the ^{1}H-NMR spectra highlights the different diastereotopic behavior of the protons 2-H and 3'-H. Moreover, Procopiou *et al.*[8] unambiguously obtained the structure of (±)-(1S,2'R)-1-(1,4-benzodioxan)-1,3-propanediol by spectroscopic methods and, in particular, by long-range ^{1}H-^{13}C correlation NMR experiments (HMBC). In addition, their work includes the elucidation of the structure and the relative configuration by X-ray crystallography.

Figure 8.3 | ***^{1}H-NMR spectra (CD_3OD) of the single diastereomers of 1,3 diols***

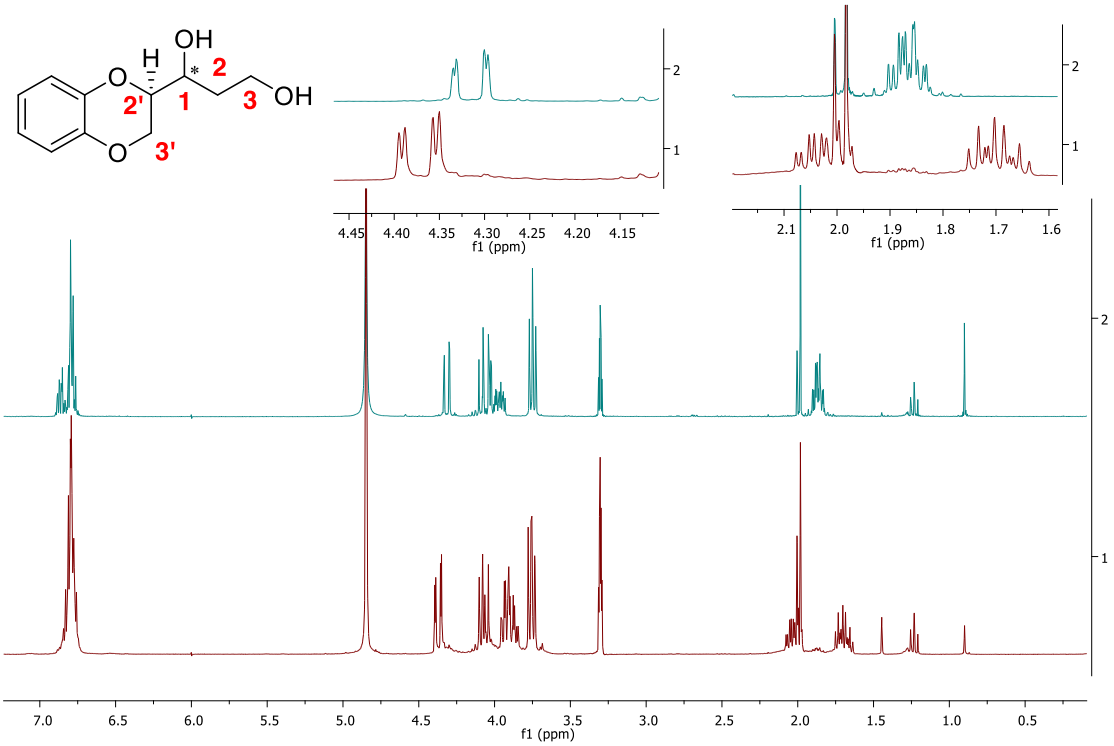

Comparing the data, we were able to identify that the less abundant diastereomers were the one characterized in the aforementioned work, which carries the stereochemistry (1S,2'R)-1-(1,4-benzodioxan)-1,3-propanediol. Therefore, we were also able to determine the absolute configurations of the more abundant one and consequentially the stereoconvergence of the Reformatsky reaction (Figure 8.4).

Figure 8.4 | ***Stereoconvergency of the Reformatsky reaction***

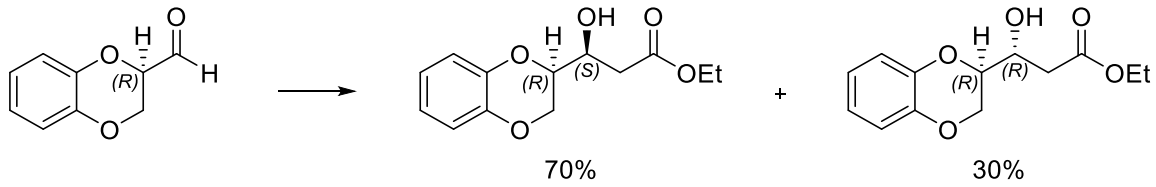

In addition, the docking simulations substantiated the interesting inhibitor activity since the most abundant diastereomers, namely the R,S one and its enantiomer, show the best orientation in the DPP-IV binding site.

Nevertheless, a stereoselective synthetic route will be investigated in order to obtain the most active compounds as pure diastereomers.

References

1. Lammi, C., Zanoni, C., Arnoldi, A. & Vistoli, G. Peptides Derived from Soy and Lupin Protein as Dipeptidyl-

Peptidase IV Inhibitors: In Vitro Biochemical Screening and in Silico Molecular Modeling Study. *J. Agric. Food Chem.* 64, 9601–9606 (2016).

2. Doebelin, C., Schmitt, M., Antheaume, C., Bourguignon, J. J. & Bihel, F. Nucleophilic substitution of azide acting as a pseudo leaving group: One-step synthesis of various aza heterocycles. *J. Org. Chem.* 78, 11335–11341 (2013).
3. Khalifah, R. G. The carbon dioxide hydration activity of carbonic anhydrase. I. Stop-flow kinetic studies on the native human isoenzymes B and C. *J. Biol. Chem.* 246, 2561–73 (1971).
4. Khalifah, R. G. The Carbon Dioxide Hydration Activity of Carbonic Anhydrase. *J. Biol. Chem.* 246, 2561–2573 (1971).
5. Berrino, E. *et al.* Azidothymidine "Clicked" into 1,2,3-Triazoles: First Report on Carbonic Anhydrase–Telomerase Dual-Hybrid Inhibitors. *J. Med. Chem.* 63, 7392–7409 (2020).
6. Berrino, E. *et al.* Synthesis and Evaluation of Carbonic Anhydrase Inhibitors with Carbon Monoxide Releasing Properties for the Management of Rheumatoid Arthritis. *J. Med. Chem.* 62, 7233–7249 (2019).
7. Akgul, O. *et al.* Handling drug-target selectivity: A study on ureido containing Carbonic Anhydrase inhibitors. *Eur. J. Med. Chem.* 212, 113035 (2021).
8. Procopiou, P. A., Cherry, P. C., Deal, M. J. & Lamont, R. B. A reinvestigation of the synthesis of trans-(±)-1,2,3,4,4a,10a-hexahydro [1,4] benzodioxino[2,3-c]pyridine. *J. Chem. Soc., Perkin Trans. 1* 1773–1777 (1994) doi:10.1039/P19940001773.

CHAPTER 9

Conclusions

With the incidence of T2DM steadily growing, new pharmacologic therapies that possess more favorable benefit-risk profiles are needed. Given the relevance of the DPP-IV/CAs (II and V) roles in the pathology of T2DM, multi-target ligands able to modulate these enzymes could represent a novel therapeutic approach for antidiabetic treatment. During my PhD project repositioning of WB-4101 and morphing its structure have been the strategies applied to obtain potent and selective multi-target ligands against DPP-IV and CAs (isoform II and V). Concurrent modulation of DPP-IV and CAs (II and V) could be an interesting option to minimize hyperglycemia while concomitantly inhibiting the progression of comorbidities. Furthermore, preserving low lipophilicity and avoiding significant structural expansion have been a top priority. In this context, rational multitarget optimization strategies have been relied on computational models and systematic exploration of the SAR on each individual target.

The designed sets of molecules, which result from the morphing of the phenoxy ring, the variation of the secondary amine function, and/or from the deconstruction of the benzodioxane scaffold of WB-4101 can be roughly divided in three generations. All the compounds have been synthesized and investigated for their inhibitor activity on the selected targets, namely CA-II, V and DPP-IV and off-targets (CA I, IV, and IX). The first generation of derivatives possess no multitarget modulatory efficacy, despite a remarkable CA-II inhibitor potency showed by compound **I**. The second generation, that exhibit the primary amine or the azide moiety, inhibits DPP-IV at nanomolar concentrations, which are comparable to Sitagliptin. In addition, they show an interesting CA inhibitor profile, enriched by a satisfactory selectivity. Finally, the third generation, derived from deconstruction of the benzodioxane scaffold, demonstrate that enhancing the flexibility of the structure lead to a notably improvement of the potency toward hCA-II while losing the inhibitor activity on the mitochondrial isoforms (VA and VB). Unpleasantly, the deconstruction approach does not ameliorate the inhibitor activity on DPP-IV, rather it leads to unsatisfactory potency values even resulting in a no trend behavior.

On the basis of the structure activity relationship, in order to adequately modulate the selected enzymes a primary amine function closely connected to a rigid substructure, that is in turn joined to a *p*-hydroxybenzensulfonamide portion is a crucial feature.

In addition, identification of potential eutomers within the racemic mixture has been achieved *via* stereochemical investigations, whose results were also corroborated by molecular docking simulations. The performed analyses have allowed to deduce a preliminary stereochemical structure activity relationship, according to which the R,S and S,R diastereomers show the best orientation in the DPP-IV binding site supposedly gaining the best inhibitor activity.

Synthesis and pharmacological evaluation of enantiomerically pure eutomers will be a future goal, that, hopefully, will achieve lower IC50 values .

The satisfactory DPP-IV inhibition and the selectivity CAs profile indicate compound **X** as potential lead of this novel class of multi-target ligands even if the design and synthesis of other new morphed derivatives of WB-4101 will help to further understand the key recognition features of the target enzymes.

This work paved the way for the development of more effective antidiabetic agents acting on both systems in a balanced and powerful manner.

CHAPTER 8

Chemistry

The attempt to develop a single and flexible synthetic scheme for similar derivatives was hampered by substantial substrate-dependent differences in reactivity.

Therefore, sometimes different synthetic schemes had to be followed for the obtainment of several compounds.

First-generation

Synthesis of intermediate 5

Derivatives **I-VIII** have the benzodioxane moiety as a common feature and its synthesis started, as shown in Scheme 1, from commercially available ethyl acrylate (**1**), which was treated with bromine to give 2,3-dibromopropionic ethyl ester (**2**). The benzodioxane ethyl ester (**3**) was obtained from the condensation of **2** with catechol. Then, the reduction of the ester led to the obtainment of the hydroxyl function (**4**), which was mesylated to give intermediate **5**.

Scheme 1 | **Synthesis of intermediate 5**

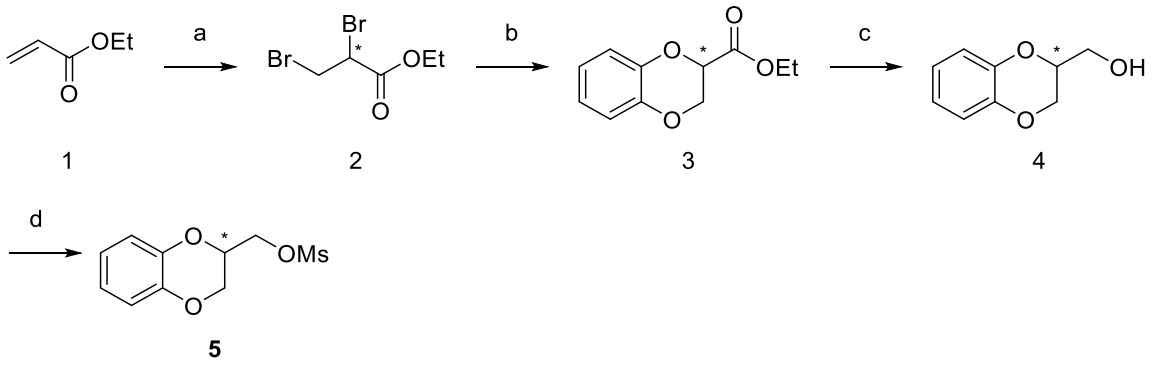

Reagents and conditions: (a) Br_2, DCM, reflux, (b) catechol, K_2CO_3, acetone, reflux, (c) $LiAlH_4$, THF, 0°C, (d) MsCl, TEA DCM.

Synthesis of compounds I-V

The procedure for the obtainment of compounds **I-V** (Scheme 2) started from the reaction between commercially available phenol (**6**) and 1-bromo-2-chloroethane that led to 2-chloroethoxybenzene

(**7**), which underwent an acylation in *para* position with chlorosulfonic acid (**8**). Afterwards the nucleophilic substitution with different amines gave the sulfonamide moiety (**9**). These compounds were treated with sodium azide to obtain compounds **10** and then reduced using hydrazine (**11**). The subsequent condensation with intermediate **5** and the treatment with diethyl ether hydrochloride gave derivatives **I-V**.

Scheme 2 | **General synthetic procedure for compounds I-V**

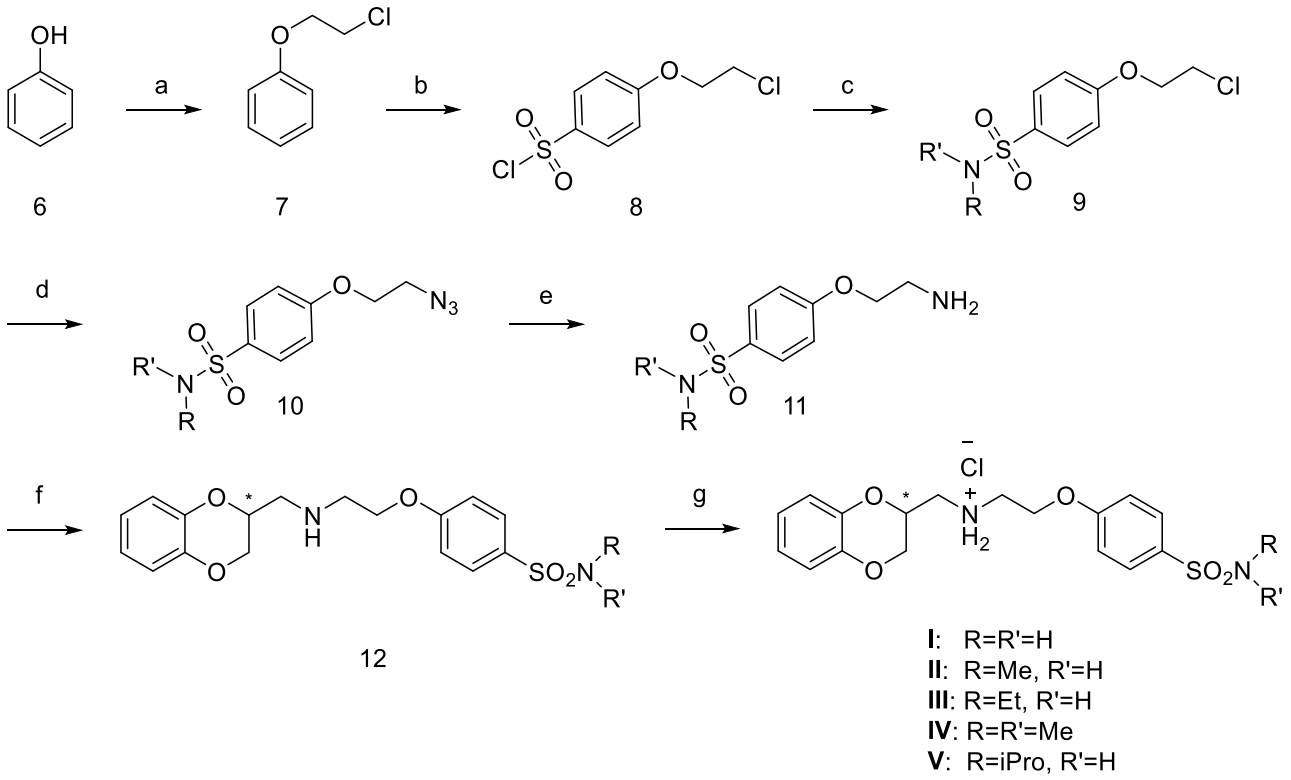

Reagents and conditions: (a) 1-bromo-2-chloroethane, TBAB, NaOH, DCM, RT, (b) chlorosulfonic acid, DCM, -10°C (c) HNRR', THF, 0°C, (d) NaN_3, KI, DMF/H_2O 3:1, 90°C, (e) $NH_2NH_2 \cdot H_2O$, PdO, MeOH, reflux, (f) 2-(R,S)-mesyloxymethyl-1,4-benzodioxane (**5**), TEA, IPA, reflux, (g) diethyl ether hydrochloride, 0°C.

Synthesis of compound VI

The obtainment of compound **VI**, shown in Scheme 3, started from the protection of the amino group of commercially available *p*-aminophenol (**13**) with di-tert-butyl dicarbonate (**14**). The hydroxyl moiety underwent subsequently a hydroxyalkoxylation by ethylene carbonate (**15**). Then, the amino group was deprotected using methanol hydrochloride (**16**) and the mesylation of both amino and hydroxyl groups gave derivative **17**. The conversion of mesyloxy moiety in azide achieved compound **18**, which was subsequently reduced by hydrazine hydrate. The obtained amine function

(**19**) was then condensed with intermediated **5** to give **20**, that was converted in the hydrochloride derivative leading desired compound **VI**.

Scheme 3 | **Synthesis of compound VI**

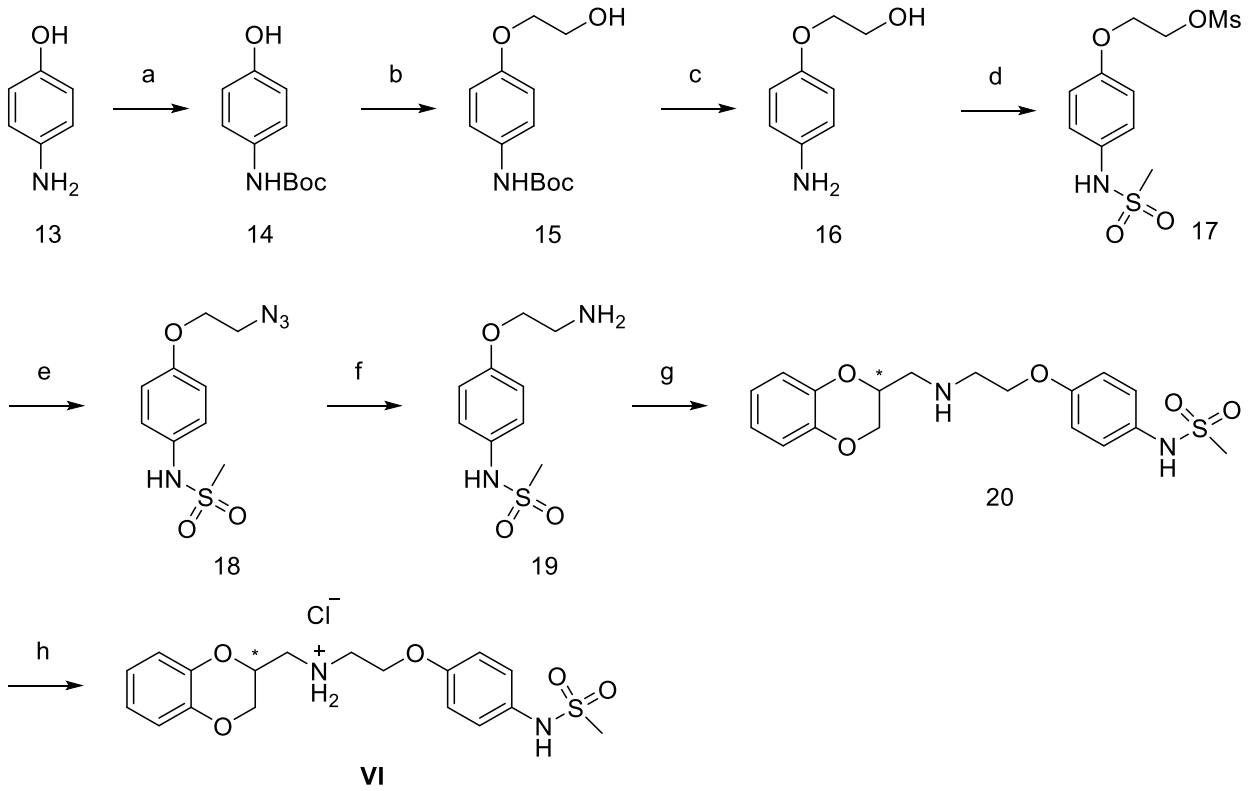

Reagents and conditions: (a) Boc_2O, THF, 0°C, (b) ethylene carbonate, K_2CO_3, DMF, reflux, (c) MeOH·HCl, 50°C, (d) MsCl, TEA, DCM, 0°C, (e) NaN_3, KI, DMF/H_2O 3:1, 90°C, (f) $NH_2NH_2 \cdot H_2O$, PdO, MeOH, reflux, (g) **5**, TEA, IPA, reflux, (h) diethyl ether hydrochloride, 0°C.

Synthesis of compounds VII-VIII

The synthetic pathway to obtain compounds **VII-VIII**, shown in Scheme 4, started from t-butyl 4-(2-hydroxyethoxy) phenylcarbamate (**15**) which was already described for the synthesis of compound VI. The hydroxyl function was mesylated (**21**) and subsequently substituted by sodium azide (**22**). The deprotection of the amine function (**23**) was achieved by treatment with methanol hydrochloride. Then through reaction with ethane- or isobutene-sulfonyl chloride the sulfonamide moiety (**24**) was obtained. The azide function was then reduced with hydrazine giving the amine moiety (**25**), which was condensed with 2-(R,S)-mesyloxymethyl-1,4-benzodioxane (**5**) giving derivative **26**. The treatment with diethyl ether hydrochloride accomplished compounds **VII-VIII**.

Scheme 4 | **General synthetic procedure for compounds VII-VIII**

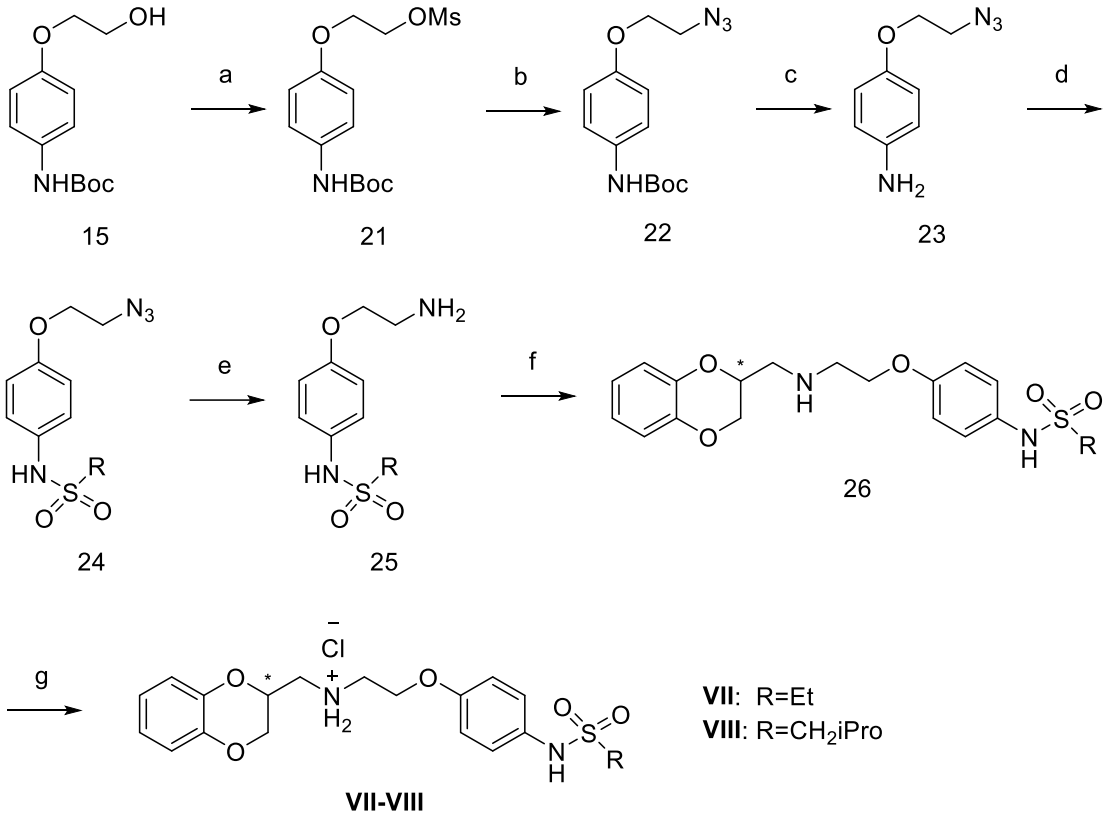

Reagents and conditions: (a) MsCl, TEA, DCM, 0°C, (b) NaN_3, KI, DMF/H_2O 3:1, 90°C, (c) MeOH·HCl, 50°C, (d) RSO_2Cl, TEA, DCM, 0°C, (e) $NH_2NH_2 \cdot H_2O$, PdO, MeOH, reflux, (f) **5**, TEA, IPA, reflux, (g) diethyl ether hydrochloride, 0°C.

Second generation

Synthesis of scaffold 29

The obtainment of scaffold **29**, shown in Scheme 5, started from commercially available sulfonamide (**27**) whose amine function was converted into a hydroxy one (**28**),*via* Sandmeyer reaction. Consequently, **29** was prepared from 4-hydroxybenzenesulphonamide by the protection of the sulfonamide moiety as N-sulfonylformamidine.

Scheme 5 | **Synthesis of scaffold 29**

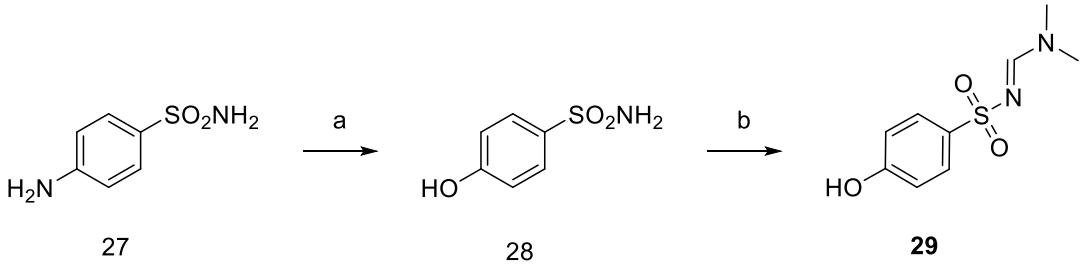

27 28 **29**

Reagents and conditions: (a) $NaNO_2$, H_2SO_4, water, reflux, (b) DMF-DMA, DMF, RT.

Synthesis of scaffold 32

The synthetic strategy to achieve scaffold **32** is shown in Scheme 6. Regioselective monobromination of 4-hydroxybenzenesulfonamide (**28**) gave compound **30** which was treated with sodium methoxide and CuI at reflux to obtain **31**. Consequently, **32** was achieved *via* protection of the sulfonamide group with N,N-dimethylformamide dimethyl acetal.

Scheme 6 | **Synthesis of scaffold 32**

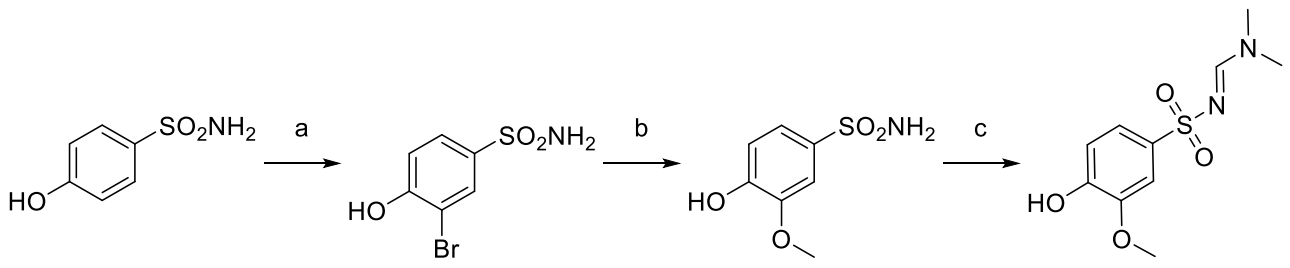

28 30 31 **32**

Reagents and conditions: (a) NBS, DMF, 0°C, (b) Na, CuI, MeOH, reflux, (c) DMF-DMA, DMF, RT.

Synthesis of scaffold 35

The obtainment of scaffold **35**, shown in Scheme 7, started from **28** which underwent *ortho*-dibromination. The treatment of intermediate **33** with sodium methoxide and CuI at reflux led to the obtainment of **34**. The protection of the sulfonamide moiety as N-sulfonylformamidine accomplished scaffold **35**.

Scheme 7 | **Synthesis of scaffold 35**

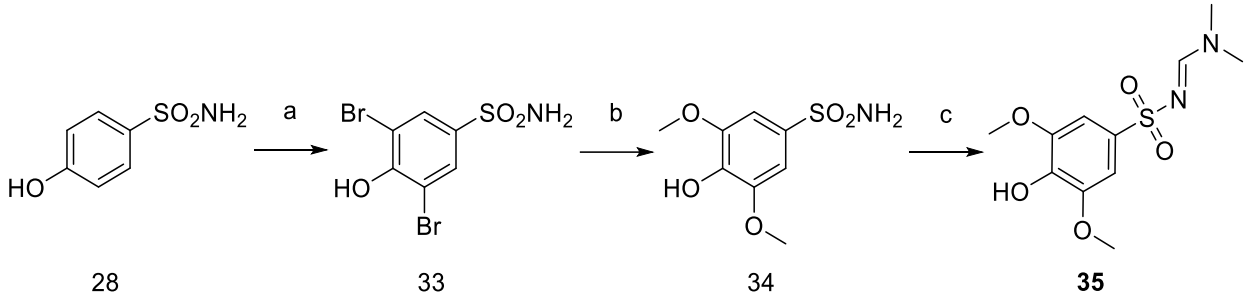

Reagents and conditions: (a) Br_2, DCM/EtOH, RT, (b) Na, CuI, MeOH, reflux, (b) DMF-DMA, DMF, RT.

Synthesis of compounds IX-XIV

As reported in Scheme 8, all the compounds of the second wave can be obtained from benzodioxane ethyl ester (**3**), whose ester function was hydrolyzed to afford the carboxylic acid (**36**). The treatment of 1,4-benzodioxan-2-carboxylic acid with N,O-dimethylhydroxylamine, preceded by the conversion into the corresponding acyl chloride, led to the obtainment of the Weinreb amide (**37**), which was reduced and transformed in **38**. The aldehydic function underwent Reformatsky reaction with ethyl bromoacetate, accomplishing the β-hydroxy ester (**39**). The reduction of the ester moiety afforded the primary alcohol (**40**), which was protected with trityl chloride (**41**). After the Mitsunobu reaction, which produced the azide derivative (**42**), the deprotection of trityl ether was achieved *via* treatment with Amberlyst 15 (**43**). The hydroxyl moiety was mesylated (**44**) and then condensed with different *p*-hydroxybenzenesulfonamidine (scaffold **29**, **32,** or **35**) to give compounds **45**. The deprotection of the sulfonamide moiety led to the obtainment of compounds **IX, XI, XIII,** and the subsequent reduction of the azide moiety accomplished compounds **X, XII,** and **XIV**.

Scheme 8 | **General synthetic procedure for compounds of the second generation**

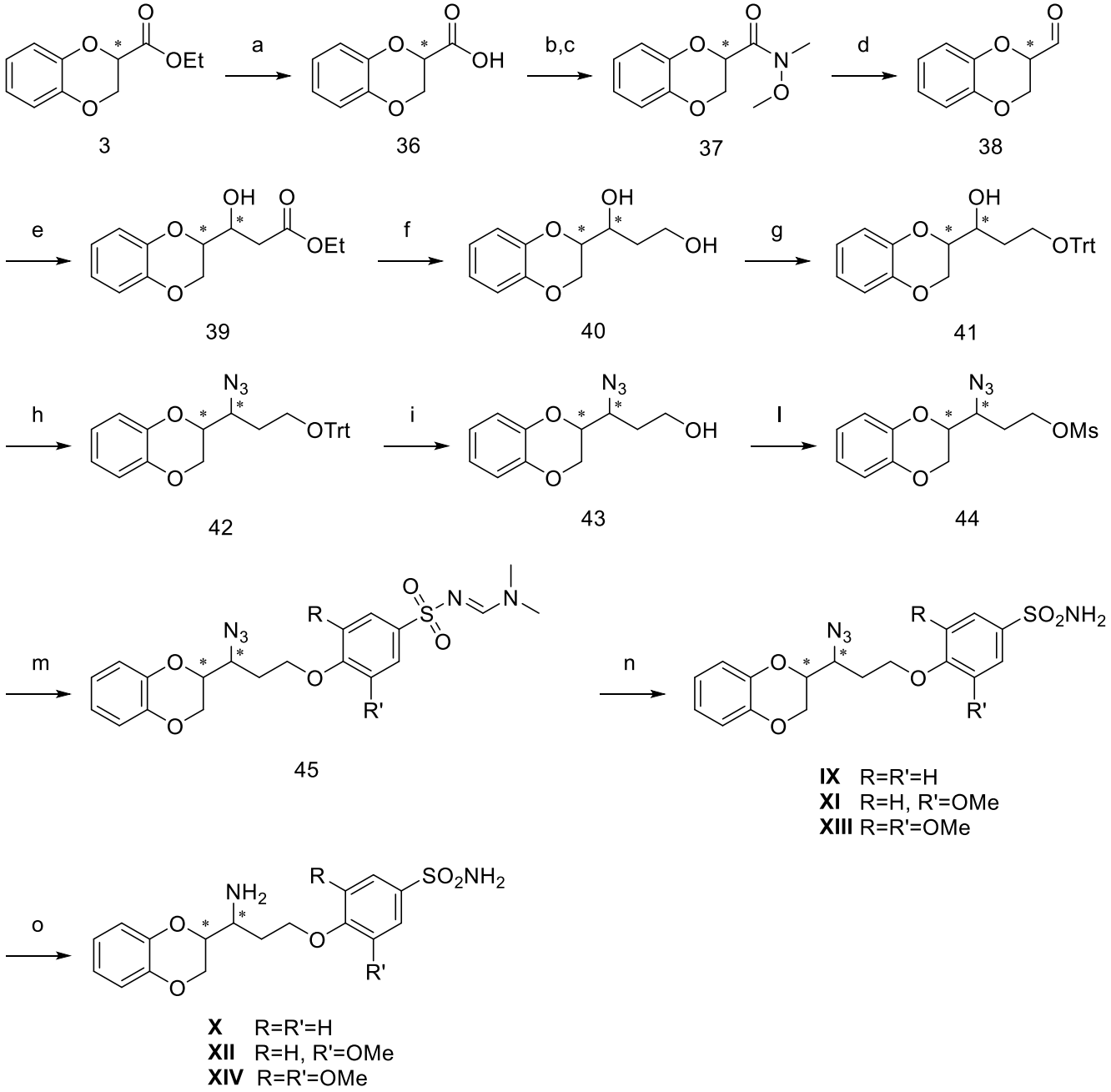

Reagents and conditions: (a) NaOH, MeOH, reflux, (b) $SOCl_2$, DCM, reflux, (c) N,O-dimethylhydroxylamine, DCM, RT, (d) $LiAlH_4$, THF, -20°C, (e) Zn, TBDMSiCl, Ethyl Bromoacetate, THF, reflux, (f) $LiAlH_4$, THF, -10°C, (g) TrtCl, TEA, DCM, RT, (h) PPh_3, DEAD, DPPA, THF, RT, (i) Amberlyst 15, DCM, MeOH, reflux, (l) MsCl, TEA, DCM, RT, (m) K_2CO_3, scaffold **29**, **32** or **35**, DMF, 90°C, (n) $NH_2NH_2 \cdot H_2O$, MeOH, RT, (o) $NH_2NH_2 \cdot H_2O$, PdO, MeOH, reflux.

Third-generation

Synthesis of scaffold 48

2-methoxyethoxymethyloxyphenol (**48**) is a common intermediate for the obtainment of compounds **XIX** and **XX**, whose synthesis is represented in Scheme 10. The preparation started from commercially available 2-hydroxybenzaldehyde (**46**) by MEM protection of the phenolic moiety (**47**). Subsequently, Baeyer–Villiger oxidation of the aldehydic function was performed and the hydrolysis of the resulting formyl group led to **48**.

Scheme 9 | **Synthesis of scaffold 48**

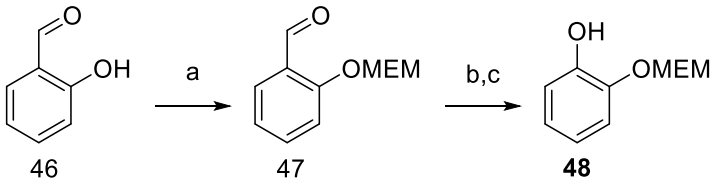

46 47 **48**

Reagents and conditions: (a) DIPEA, MEMCl, DCM, RT; (b) *m*-CPBA, DCM, RT; (c) 2 M KOH, MeOH, RT.

Synthesis of scaffold 52

2,6-dimethoxyethoxymethyloxy phenol (**52**) was synthesized starting from resorcinol (**49**) which firstly underwent halogenation by bromine (**50**). Then, the phenol groups of the 2-bromo- resorcinol **50** were protected as methoxyethoxymethyl ethers (**51**) and the subsequent reaction, which converted the halogen into a hydroxy moiety *via* metalation with *n*-butyl lithium gave compound **52**.

Scheme 10 | **Synthesis of scaffold 52**

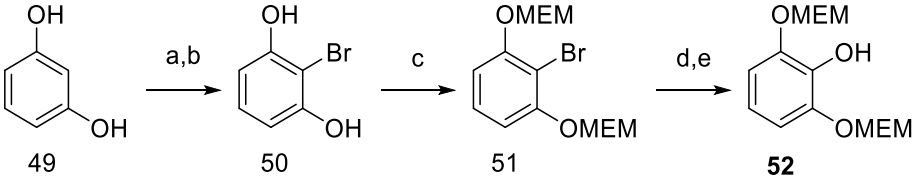

49 50 51 **52**

Reagents and conditions: (a) Br_2, $CHCl_3$, reflux; (b) Na_2SO_3, NaOH, MeOH, H_2O, RT; (c) DIPEA, MEMCl, DCM, RT; (d) *n*-BuLi, THF, -78°C; then $B(OMe)_3$; (e) oxone, $NaHCO_3$, acetone, H_2O, RT

Synthesis of compounds XV-XXIV

The preparation of derivatives of the third wave (**XV-XXIV**) shared as common key the epoxy intermediate **56**, whose synthetic route is depicted in Scheme 11. Mesylation of commercially available 3-buten-1-ol (**53**), gave compound **54**. Coupling of the resulting derivative with **29** (**55**) followed by epoxidation of the olefinic function in the presence of *m*-CPBA provided intermediate **56**. Epoxide ring opening to afford derivatives **57** were achieved by treatment with an excess of different phenols (i.e. phenol, guaiacol, **48**, 2,6-dimethoxyphenol, **52**). The resulting hydroxy group was then mesylated (**58**) and subsequently treated with sodium azide (**59**). Reaction with hydrazine hydrate led to the cleavage of the sulfonamide protecting group, resulting directly in **XV, XVII,** and **XXI** derivatives. A different strategy was applied for the MEM-protected compounds that were treated in acidic media in order to cleavage all the protective groups (**XVII** and **XXIII**). The subsequent reduction of the azide moiety accomplished compounds **XVI**, **XVIII**, **XX**, **XXII**, and **XXIV**.

Scheme 11 | **General synthetic procedure for compounds of the third generation**

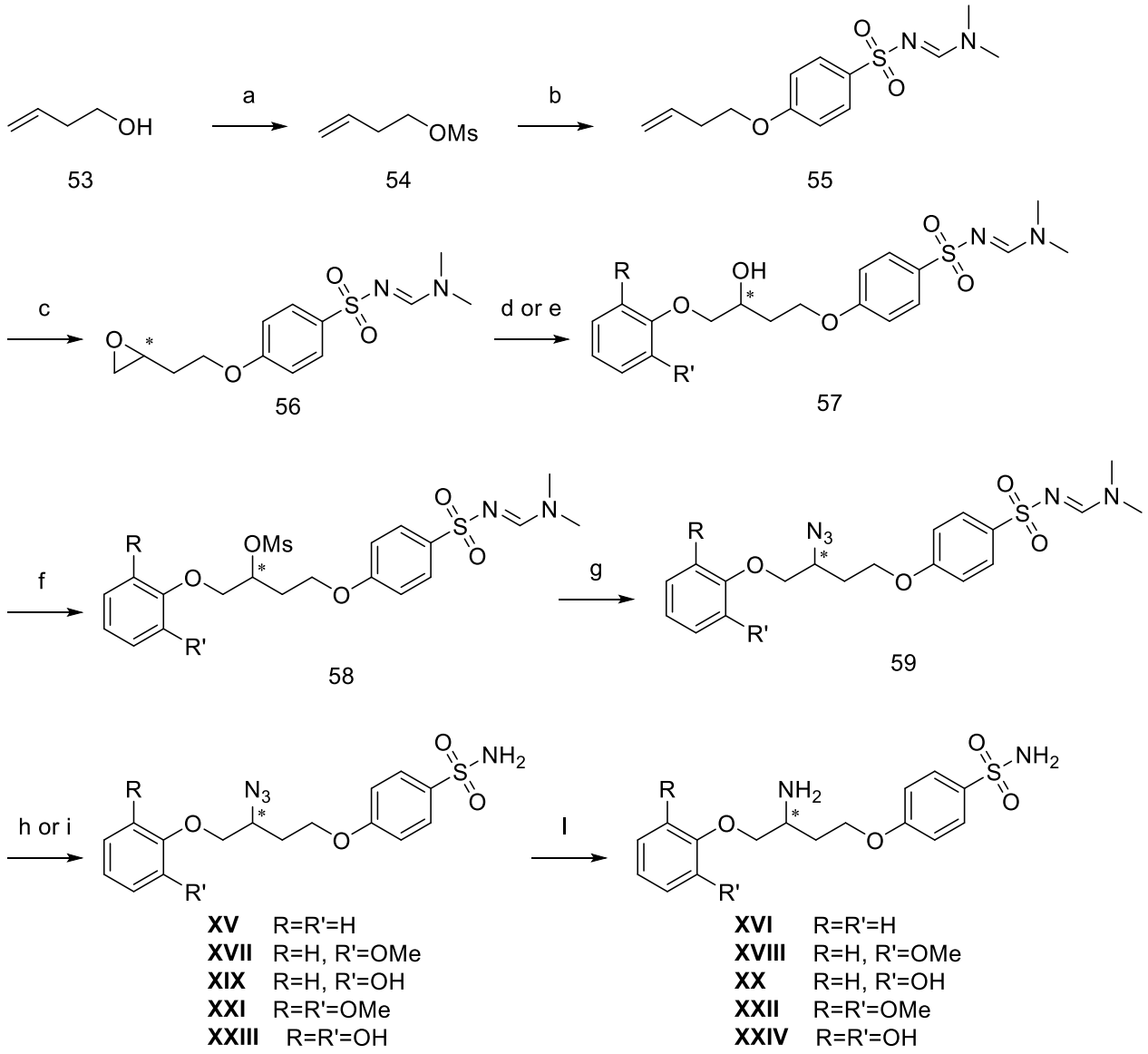

Reagents and conditions: (a) MsCl, TEA, DCM, RT; (b) K_2CO_3, **29**, DMF, 60°C; (c) *m*-CPBA,·DCM, RT; (d) K_2CO_3, phenols, DMF, 60°C; (e) phenols, $PdCl_2$, TBAB, K_2CO_3, H_2O, 60°C; (f) MsCl, TEA, DCM, RT; (g) NaN_3, DMF, H_2O, reflux, (h) $NH_2NH_2{\cdot}H_2O$, MeOH, RT; (i) HCl, MeOH, reflux (l) Pd/C, H_2, MeOH, RT.

CHAPTER 10

Materials and methods

Chemistry

All the reagents and the solvents were used without purification or distillation, after purchasing from commercial sources (Merck, Fluorochem, and TCI). Silica gel matrix, having fluorescent indicator 254 nm, was used both in TLC (thin-layer chromatography, on aluminum foils), and in flash chromatography (particle size 40–63 µm, Merck) on a Biotage instrument. The visualization was with UV light at 254 nm (λ). Varian (Palo Alto, CA, USA) Mercury 300 NMR spectrometer/Oxford Narrow Bore superconducting magnet operating at 300 MHz was used for all ^{1}H-NMR spectra.^{13}C-NMR spectra were acquired at 75 MHz. We reported all chemical shifts (δ) in ppm, relative to residual solvent as internal standard. The following abbreviations refer to signal multiplicity: s = singlet, d = doublet, dd = doublet of doublets, t = triplet, q = quadruplet,dq = doublet of quadruplets, m = multiplet, bs = broad singlet.

Mass analysis

Each compound was dissolved in methanol to obtain a stock solution at a concentration of 1 mg/mL and then further diluted 1:25 with CH_3CN/H_2O/HCOOH 50:50:0.1 (% v/v) before the direct infusion into the mass spectrometer. High-resolution mass spectra were acquired with an LTQ Orbitrap XL mass spectrometer (Thermo Scientific, Milan, Italy) equipped with an ESI source. Source parameters for the positive ion mode were set as follows: spray voltage 4.0 kV, capillary temperature 275 °C, sheath gas 10 a.u., capillary voltage 42 V, tube lens offset 90 V; for the negative ion mode: spray voltage -3.5 kV, capillary temperature 275 °C, sheath gas 10 a.u., capillary voltage -33 V, tube lens offset 180 V. Full MS spectra were acquired in profile mode by the FT analyzer in a scan range of m/z 120–800, using a resolution of 30,000 FWHM at *m/z* 400. The software Xcalibur 4.0 was used for instrument control and spectra analysis.

Computational methods

The crystal of human DPP-IV was retrieved from RCSB PDB (entry code: 1x70)[1] in complex with ligand 715 (Sitagliptin) and the crystal of human CA-II was likewise retrieved from RCSB PDB (entry code: 3k34)[2] in complex with ligand SUA (a benzensulfonamide inhibitor). Since DPP-IV is a homodimer, the best chain has been evaluated, choosing the one with the lower number of outliers and the best

fitting in according to section 6 "Fit of the model and data" of the PDB report.

Both the crystal were then prepared adding eventual missing residues and checking alternative conformations of the side chains, chirality, trans-peptide bond and ring interaction. Hydrogen atoms were added to all crystal structures according to physiological pH, and they underwent to an energy minimization using NAMD2[3], CHARMM22 as force field and constraints on the backbone atoms. In order to prevent the binding site collapse, the respective ligand was inserted into their crystal structure. Moreover, for CA-II, the Zn^{2+} ion was re-introduced into the structure by overlapping it with the PDB downloaded structure.

Both binding sites was calculated by re-docking, and the bound ligands were removed from the structure for docking experiments. The docking simulations were performed by PLANTS focusing the search on a 10.0 Å radius sphere around the bound ligands. The conformational profile of the considered ligands was explored by Monte Carlo procedures as described elsewhere[4]. For each ligand, 10 poses were generated and scored by the ChemPLP score with a speed equal to 1. The complexes were finally minimized by keeping fixed all atoms outside a 10 Å radius sphere around the bound ligand.

In vitro measurement of the DPP-IV inhibitor activity

The *in vitro* experiments were carried out in a half volume 96 well solid plate (white) using conditions previously optimized[5]. Each reaction system (50 µL) was prepared containing 1 × assay buffer [20 mM Tris-HCl, pH 8.0, containing 100 mM NaCl, and 1 mM EDTA]; compounds at the final range of concentration of 10^{-10}–10^{-2} M, Sitagliptin at 1.0 µM (positive control), or vehicle (C, H_2O); and purified human recombinant DPP-IV enzyme. Subsequently, the mixed reagents were transferred in each well of the plate and the reaction was started by adding 50 µL of substrate solution (5 mM H-Gly-Pro-7-amido-4-methylcoumarin (AMC)) to each well and incubated at 37°C for 30 minutes. Fluorescence signals were collected using the Synergy H1 fluorescent plate reader from Biotek (ex./em. wavelengths 360/465 nm).

In vitro measurement of the CA inhibitor activity

An Applied Photophysics stopped-flow instrument was used for assaying the CA catalyzed CO_2 hydration activity[6]. Phenol red (at a concentration of 0.2 mM) was used as an indicator, working at the absorbance maximum of 557 nm, with 20 mM Hepes (pH 7.4) as buffer and 20 mM Na_2SO_4 for maintaining constant ionic strength, following the initial rates of the CA-catalyzed CO_2 hydration reaction for a period of 10-100 s. The CO_2 concentrations ranged from 1.7 to 17 mM for the

determination of the kinetic parameters and inhibition constants. For each inhibitor, at least six traces of the initial 5-10% of the reaction were used for determining the initial velocity. The uncatalyzed rates were determined in the same manner and subtracted from the total observed rates. Stock solutions of the inhibitor (0.1 mM) were prepared in distilled-deionized water and dilutions up to 0.01 nM were done thereafter with the assay buffer. Inhibitor and enzyme solutions were preincubated together for 15 min at room temperature prior to the assay, to allow for the formation of the E-I complex. The inhibition constants were obtained by non-linear least-squares methods using PRISM 3 and the Cheng-Prusoff equation as reported earlier and represent the mean from at least three different determinations. All CA isoforms were recombinant proteins obtained inhouse, as reported earlier[7–10].

References

1. Kim, D. et al. (2R)-4-Oxo-4-[3-(trifluoromethyl)-5,6-dihydro[1,2,4]triazolo[4,3-a] pyrazin-7(8H)-yl]-1-(2,4,5-trifluorophenyl)butan-2-amine: A potent, orally active dipeptidyl peptidase IV inhibitor for the treatment of type 2 diabetes. J. Med. Chem. 48, 141–151 (2005).
2. Behnke, C. A. et al. Atomic resolution studies of carbonic anhydrase II. Acta Crystallogr. D. Biol. Crystallogr. 66, 616–27 (2010).
3. Phillips, J. C. et al. Scalable molecular dynamics with NAMD. Journal of Computational Chemistry vol. 26 1781–1802 (2005).
4. Vistoli, G., Mazzolari, A., Testa, B. & Pedretti, A. Binding Space Concept: A New Approach To Enhance the Reliability of Docking Scores and Its Application to Predicting Butyrylcholinesterase Hydrolytic Activity. J. Chem. Inf. Model. 57, 1691–1702 (2017).
5. Lammi, C., Zanoni, C., Arnoldi, A. & Vistoli, G. Peptides Derived from Soy and Lupin Protein as Dipeptidyl-Peptidase IV Inhibitors: In Vitro Biochemical Screening and in Silico Molecular Modeling Study. J. Agric. Food Chem. 64, 9601–9606 (2016).
6. Khalifah, R. G. The carbon dioxide hydration activity of carbonic anhydrase. I. Stop-flow kinetic studies on the native human isoenzymes B and C. J. Biol. Chem. 246, 2561–73 (1971).
7. Khalifah, R. G. The Carbon Dioxide Hydration Activity of Carbonic Anhydrase. J. Biol. Chem. 246, 2561–2573 (1971).
8. Berrino, E. et al. Azidothymidine "Clicked" into 1,2,3-Triazoles: First Report on Carbonic Anhydrase–Telomerase Dual-Hybrid Inhibitors. J. Med. Chem. 63, 7392–7409 (2020).
9. Berrino, E. et al. Synthesis and Evaluation of Carbonic Anhydrase Inhibitors with Carbon Monoxide Releasing Properties for the Management of Rheumatoid Arthritis. J. Med. Chem. 62, 7233–7249 (2019).
10. Akgul, O. et al. Handling drug-target selectivity: A study on ureido containing Carbonic Anhydrase inhibitors. Eur. J. Med. Chem. 212, 113035 (2021).

CHAPTER 11

Experimental

Starting materials and solvents were purchased from commercial suppliers and were used without further purification. Reaction conditions and yields were not optimized;

^{1}H and ^{13}C NMR spectra were acquired on a Varian 300 Mercury NMR spectrometer operating at 300 MHz for ^{1}H NMR, and 75 MHz for ^{13}C NMR; the chemical shifts are reported in ppm. Signal multiplicity is used according to the following abbreviations: s= singlet, d= doublet, dd= doublet of doublets, t = triplet, td= triplet of doublets, q = quadruplet, m = multiplet, sept= septuplet, and bs= broad singlet;

Melting points were measured either on a Büchi Melting Point B-540 apparatus or a TA Instruments Q20 DSC system;

TLCs were performed on standard analytical silica gel layers (thickness 0.20 mm; Macherey-Nagel ALUGRAM SIL G/UV254);

Chromatographic purifications were performed, in normal phase, using Biotage instruments (Isolera or SP1) over different Biotage SNAP Ultra flash chromatography cartridges, filled with Merck Silica Gel 60 (0.040-0.063 μm).

The final compounds purity was assessed on LTQ Orbitrap XL mass spectrometer (Thermo Scientific, Milan, Italy) equipped with an ESI source.

Abbreviations used: DCM: dichloromethane; DMF: dimethylformamide; DMSO: dimethylsulfoxide; MEM-Cl: 2-methoxyethoxymethyl chloride; mp: melting point; MW: molecular weight; $LiAlH_4$: lithium aluminum hydride; NBS: N-bromosuccinimide; RT: room temperature; TBAB: tetrabutylammonium bromide; TEA: triethylamine; THF: tetrahydrofuran.

Ethyl 2,3-dibromopropionate

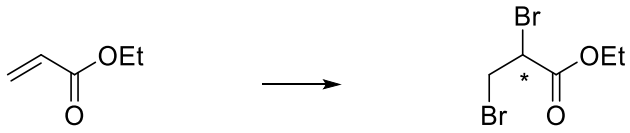

Chemical Formula:$C_5H_8O_2$
MW: 100,12

Chemical Formula:$C_5H_8Br_2O_2$
MW: 259,93

Bromine (7.11 mL, 183.38 mmol) was added dropwise to a solution of methyl acrylate (18.36 g, 183.38 mmol) in dichloromethane (200 mL) under reflux. The resulting reaction mixture was stirred at reflux for 30 min. Afterward, the mixture was brought to room temperature, then sequentially quenched with aqueous 10% solution of $Na_2S_2O_5$. The organic layer was then dried over anhydrous sodium sulfate, filtered and the solvent was evaporated in vacuo affording the desired product (47.41 g, 182.39 mmol) as a colorless oil.

Yield = 99.5%

^{1}H NMR ($CDCl_3$): δ 4.42 (dd, *J* = 11.4, 4.4 Hz), 4.30 (q, *J* = 7.1 Hz, 2H), 3.93 (dd, *J* = 11.4, 9.9 Hz, 1H), 3.67 (dd, *J* = 9.9, 4.4 Hz, 1H), 1.33 (t, *J* = 7.1 Hz, 3H).

Ethyl-1,4-benzodioxan-2-carboxylate

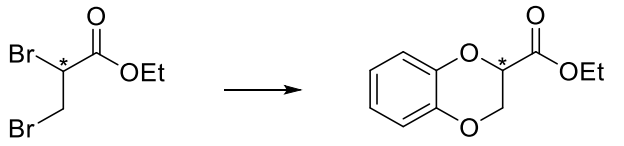

Chemical Formula:$C_5H_8Br_2O_2$ MW: 259,93

Chemical Formula:$C_{11}H_{12}O_4$ MW: 208,21

K_2CO_3 (34.93 g, 252.77 mmol) was added to a solution of catechol (9.28 g, 84.26 mmol) in 120 mL di acetone. After the mixture was stirred at room temperature for 30 minutes, ethyl 2,3-dibromopropionate (21.90 g, 84.26 mmol) was added dropwise. Afterward, the reaction was stirred at reflux until TLC indicated the disappearance of starting material[1]. The solution was concentrated in vacuo and the resulting residue was then diluted with ethyl acetate and then washed with water and brine. The organic phase was dried over anhydrous sodium sulfate and the solvent was evaporated in vacuo affording 16.29 g (78.24 mmol) of the desired product.

Yield = 92.8%

^{1}H NMR ($CDCl_3$): δ 7.04 – 6.99 (m, 1H), 6.92 – 6.85 (m, 3H), 4.82 (t, *J* = 3.9 Hz), 4.39 (d, *J* = 3.9 Hz, 2H), 4.28 (q, *J* = 7.2 Hz, 2H), 1.29 (t, *J* = 7.2 Hz, 3H).

[1] Cyclohexane/ethyl acetate 7:3. R_f starting material = 0.5; R_f product = 0.9.

2-hydroxymethyl-1,4-benzodioxane

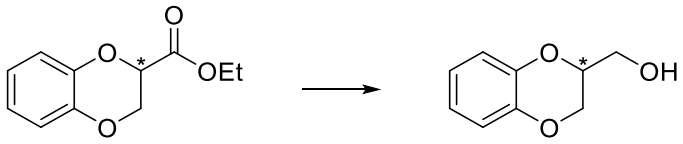

Chemical Formula:$C_{11}H_{12}O_4$
MW: 208,21

Chemical Formula:$C_9H_{10}O_3$
MW: 166,18

Under nitrogen atmosphere, a solution of ethyl-1,4-benzodioxan-2-carboxylate (5.07 g, 24.35 mmol) in 100 mL of dry tetrahydrofuran was added dropwise to an ice-cooled suspension of 1.95 g of $LiAlH_4$ (51.38 mmol) in 68.5 mL of anhydrous tetrahydrofuran. The reaction mixture was stirred at room temperature until TLC[2] indicated the disappearance of starting material. Afterward, the excess of $LiAlH_4$ was quenched by slowly adding water dropwise. The resulting suspension was filtered through a Celite pad and the solvent was evaporated under vacuum. The resulting crude was diluted with dichloromethane, washed with 10% aqueous solution of HCl, and then with 10% aqueous solution of NaOH. The organic phase was dried over anhydrous sodium sulfate and filtered. The solvent was evaporated in vacuo, providing the pure product as a white solid (2.43 g, 14.62 mmol).

Yield: 60.0%

m.p. *89 °C*

^{1}H NMR ($CDCl_3$): δ 6.86 (m, 4H), 4.3 (m, 2H), 4.11 (m, 1H), 3.88 (m, 2H), 1.94 (s, 1H).

[2] Cyclohexane/ethyl acetate 7:3. R_f starting material = 0.9; R_f product = 0.5.

2-mesyloxymethyl-1,4-benzodioxane

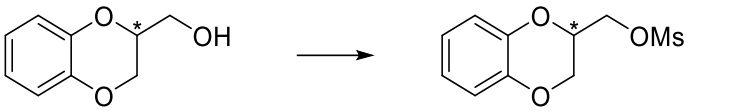

Chemical Formula:$C_9H_{10}O_3$
MW: 166,18

Chemical Formula:$C_{10}H_{12}O_5S$
MW: 244,26

2-hydroxymethyl-1,4-benzodioxane (2.43 g, 14.62 mmol) was dissolved in dichloromethane (20 mL), triethylamine (2.24 mL, 16.08 mmol) was added, and after the reaction mixture was cooled down to 0°C mesyl chloride (1.24 mL, 16.08 mmol) was added dropwise. The solution was stirred at room temperature until TLC[3] indicated the disappearance of starting material. The reaction mixture was washed with 10% aqueous solution of HCl and then with brine. The organic phase was dried over anhydrous sodium sulfate and filtered and the solvent was evaporated in vacuo, providing the pure product as 3.11 g of a white solid (12.73 mmol).

Yield = 87.1%

m.p. *59°C*

^{1}H NMR ($CDCl_3$): δ 6.89 (m, 4H), 4.55 – 4.43 (m, 3H), 4.32 (dd, *J* = 11.7, 1.8 Hz, 1H), 4.17 (dd, *J* = 11.7, 5.6 Hz, 1H), 3.09 (s, 3H).

[3] Cyclohexane/ethyl acetate 7:3. R_f starting material = 0.5; R_f product = 0.9.

2-chloroethoxybenzene

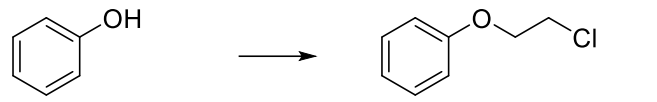

Chemical Formula:C_6H_6O MW: 94,11

Chemical Formula:C_8H_9ClO MW: 156,61

TBAB (685.0 g, 2.13 mmol) was added to a stirred solution of 2.00 g of phenol (21.25 mmol) in dichloromethane (40 mL) and NaOH 2.5N (85 mL). After 30 minutes, 1-bromo-2-chloroethane (7.1 mL, 85.90 mmol) was added dropwise and the resulting mixture was stirred for 48 h at room temperature[4]. Afterward, the phases were separated and the organic one was sequentially washed brine, dried over anhydrous sodium sulfate, filtered, and concentrated under reduced pressure, affording a crude that was purified through silica gel flash chromatography (cyclohexane/ethyl acetate 8:2). The pure product was isolated as a colorless oil (1.58 g, 10.09 mmol).

Yield = 47.5%

^{1}H NMR ($CDCl_3$): δ 7.36 – 7.24 (m, 2H), 7.02 – 6.89 (m, 3H), 4.24 (t, *J* = 5.9 Hz, 2H), 3.82 (t, *J* = 5.9 Hz, 2H).

[4] Cyclohexane/ethyl acetate 7:3. R_f starting material = 0.7; R_f product = 0.6.

4-(2-chloroethoxy)benzenesulfonyl chloride

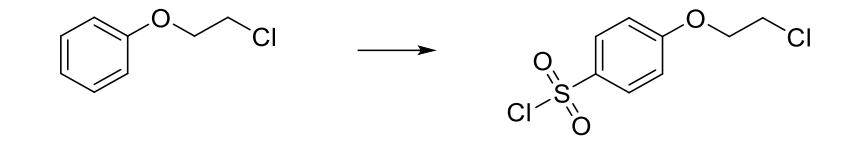

Chemical Formula:C_8H_9ClO
MW: 156,61

Chemical Formula:$C_8H_8Cl_2O_3S$
MW: 255,11

3.00 g of 2-chloroethoxybenzene (19.16 mmol) was dissolved in 50 mL of dichloromethane and after the solution was cooled to -10°C, chlorosulfonic acid (2.55 mL, 38.32 mmol) was added dropwise. The resulting reaction was stirred at -10°C for 2 hours and another hour at room temperature. Afterward, the reaction mixture was quenched with ice, extracted with dichloromethane and the organic phase was dried over anhydrous sodium sulfate and filtered. The solvent was evaporated in vacuo, providing 3.44 g (13.48 mmol) of the desired product as a pink oil.

Yield = 70.4%

^{1}H NMR ($CDCl_3$): δ 7.99 (d, *J* = 9.1 Hz, 2H), 7.07 (d, *J* = 9.1 Hz, 2H), 4.34 (t, *J* = 5.7 Hz, 2H), 3.86 (t, *J* = 5.7 Hz, 2H).

4-(2-chloroethoxy)benzenesulfonamide

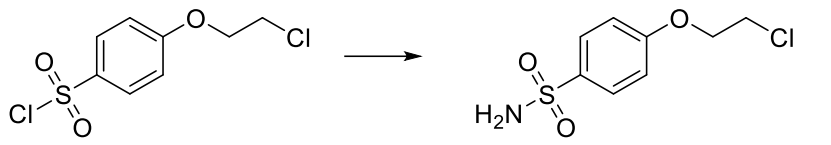

Chemical Formula:$C_8H_8Cl_2O_3S$
MW: 255,11

Chemical Formula:$C_8H_{10}ClNO_3S$
MW: 235,68

Gaseous ammonia was bubbled in an ice-cooled solution of 4-(2-chloroethoxy)benzenesulfonyl chloride (850 mg, 3.33 mmol) in 20 mL of dichloromethane until saturation. The reaction mixture was stirred for 45 minutes. Afterward, ammonium chloride was removed by filtration, dichloromethane was evaporated under vacuum in order to obtain the pure product as a white solid (730 mg, 3.12 mmol).

Yield = 94.0%

m.p. *115°C*

^{1}H NMR ($CDCl_3$): δ 7.88 (d, *J* = 9.0 Hz, 2H), 7.00 (d, *J* = 9.0 Hz, 2H), 4.75 (s, 2H), 4.29 (t, *J* = 5.8 Hz, 2H), 3.84 (t, *J* = 5.8 Hz, 2H).

4-(2-azidoethoxy)benzenesulfonamide

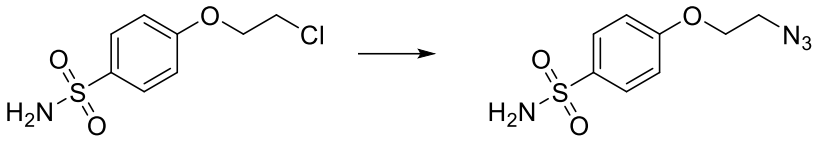

Chemical Formula:$C_8H_{10}ClNO_3S$
MW: 235,68

Chemical Formula:$C_8H_{10}N_4O_3S$
MW: 242,25

Sodium azide (2.03 g, 31.22 mmol) and KI (52 mg, 0.31 mmol) were added to a solution of 4-(2-Chloroethoxy)benzenesulfonamide (736 mg, 3.12 mmol) in DMF (10 mL) and water (3 mL). Then, the mixture was refluxed, under stirring, until TLC[5] indicated the disappearance of starting material. Afterward, the mixture was diluted with water and extracted with diethyl ether. The organic phase was dried over anhydrous sodium sulfate, filtered, and evaporated in vacuo, affording 685.0 mg (2.83 mmol) of the pure product as a colorless oil.

Yield = 91.0%

^{1}H NMR ($CDCl_3$): δ 7.88 (d, *J* = 9.0 Hz, 2H), 7.01 (d, *J* = 9.0 Hz, 2H), 4.90 (s, 2H), 4.21 (t, *J* = 5.9 Hz, 2H), 3.65 (t, *J* = 5.9 Hz, 2H).

[5] Dichloromethane/methanol 95:5. R_f starting material = 0.45; R_f product = 0.5.

4-(2-aminoethoxy)benzenesulfonamide

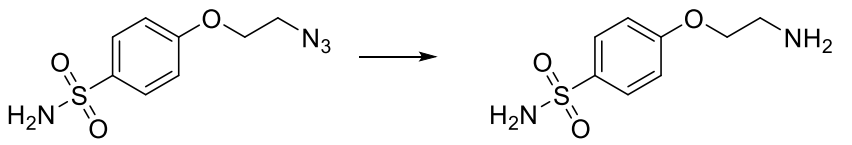

Chemical Formula:$C_8H_{10}N_4O_3S$
MW: 242,25

Chemical Formula:$C_8H_{12}N_2O_3S$
MW: 216,26

Palladium(II) oxide (34.28 mg, 0.28 mmol) and hydrazine hydrate (1.38 mL, 28.30 mmol) were added to a solution of 4-(2-azidoethoxy)benzenesulfonamide (685 mg, 2.83 mmol) in methanol (25 mL). Then, the mixture was refluxed, under stirring, until TLC[6] indicated the disappearance of starting material. Afterward, the catalyst was removed by filtration, and methanol was evaporated in vacuo. The resulting crude was dissolved in ethyl acetate and the organic phase was extracted with 10% aqueous solution of HCl. After being basified to pH 10 with 10M solution of KOH, the aqueous layer was further extracted with ethyl acetate. The organic phase was dried over anhydrous sodium sulfate, filtered, and evaporated in vacuo, affording 410 mg (1.91 mmol) of the pure product as a white solid.

Yield = 68.0%

m.p. *139°C*

^{1}H NMR (CD_3OD): δ 7.83 (d, *J* = 9.0 Hz, 2H), 7.07 (d, *J* = 9.0 Hz, 2H), 4.08 (t, *J* = 5.3 Hz, 2H), 3.03 (t, *J* = 5.3 Hz, 2H).

[6] Dichloromethane/methanol 90:10 + 1% aq. NH_3 Rf starting material = 0.7, Rf product = 0.21.

[((2-(4-sulfonamidephenoxy)ethyl)amino)-methyl]-1,4-benzodioxane

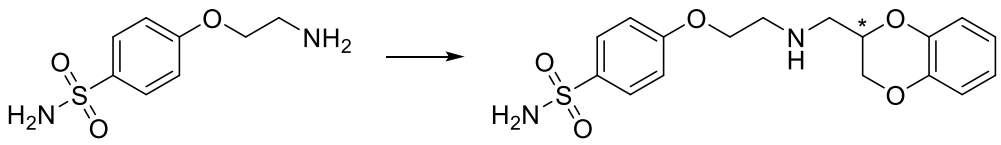

Chemical Formula:$C_8H_{12}N_2O_3S$
MW: 216,26

Chemical Formula:$C_{17}H_{20}N_2O_5S$
MW: 364,42

4-(2-aminoethoxy)benzenesulfonamide (414 mg, 1.91 mmol) and 2-mesyloxymethyl-1,4-benzodioxane (425 mg, 1.74 mmol) were dissolved in 20 mL of 2-propanol. Triethylamine (0.24 mL, 1.74 mmol) was added to the solution and the resulting mixture was refluxed, under stirring, until TLC[7] indicated the disappearance of starting material. Afterward, the solvent was evaporated in vacuo, the crude was dissolved in ethyl acetate and filtered. The filtrate was washed with 10% aqueous solution of $NaHCO_3$ and water. The organic phase was dried over anhydrous sodium sulfate, filtered, and evaporated in vacuo, affording a yellow oil. Flash chromatography (dichloromethane/methanol 95:5 + 0.5% aq. NH_3) was performed in order to obtain 67 mg (0.18 mmol) of the pure product as light yellow oil.

Yield = 10.3%

^{1}H NMR ($CDCl_3$): δ 7.86 (d, *J* = 8.9 Hz, 2H), 6.98 (d, *J* = 8.9 Hz, 2H), 6.90 – 6.81 (m, 4H), 4.78 (s, 2H), 4.32 – 4.24 (m, 2H), 4.14 (t, *J* = 5.1 Hz, 2H), 4.04 (dd, *J* = 11.6, 7.6 Hz, 1H), 3.10 (t, *J* = 5.1 Hz, 2H), 2.98 (dd, *J* = 8.8, 5.7 Hz, 2H).

[7]Dichloromethane/methanol 95:5 + 0.5% NH_3. R_f starting material = 0.15; R_f product = 0.32.

Compound I

[((2-(4-sulfonamidephenoxy)ethyl)amino)-methyl]-1,4-benzodioxane hydrochloride

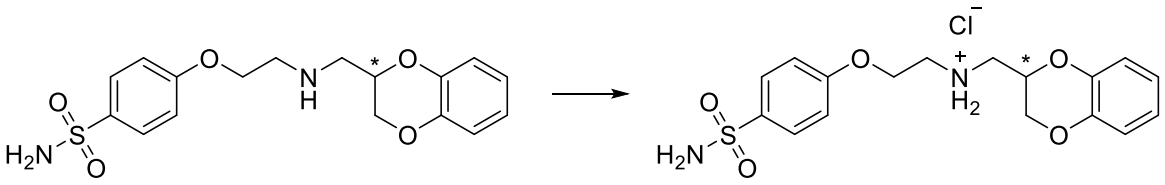

Chemical Formula:$C_{17}H_{20}N_2O_5S$
MW: 364,42

Chemical Formula:$C_{17}H_{21}ClN_2O_5S$
MW: 400,87

A solution of [((2-(4-sulfonamidephenoxy)ethyl)amino)-methyl]-1,4-benzodioxane (67 mg, 0.18 mmol) in 2.5 mL of hydrogen chloride solution 2.0 M in diethyl ether was stirred overnight. The reaction mixture was diluted with ethyl ether, the solid was filtered and washed with cooled ethyl ether to obtain the desired product as a pale yellow solid (35.57 mg, 0.09 mmol).

Yield = 50.0%

m.p. *232°C (*decomposition)

HRMS: *m/z* 365.1165 ($[M+H]^+$

^{1}H NMR (CD_3OD): δ 7.87 (d, *J* = 8.5 Hz, 2H), 7.14 (d, *J* = 8.5 Hz, 2H), 7.00 – 6.80 (m, 4H), 4.63 (ddt, *J* = 9.4, 6.4, 2.3 Hz, 1H), 4.41 (t, *J* = 4.9 Hz, 2H), 4.35 (dd, *J* = 11.6, 2.3 Hz, 1H), 4.06 (dd, *J* = 11.6, 6.4 Hz, 1H), 3.62 (t, *J* = 4.9 Hz, 2H), 3.56 – 3.37 (m, 2H).

^{13}C NMR (CD_3OD): δ 160.51, 127.95, 121.94, 121.69, 117.14, 117.03, 114.33, 69.09, 64.74, 63.11.

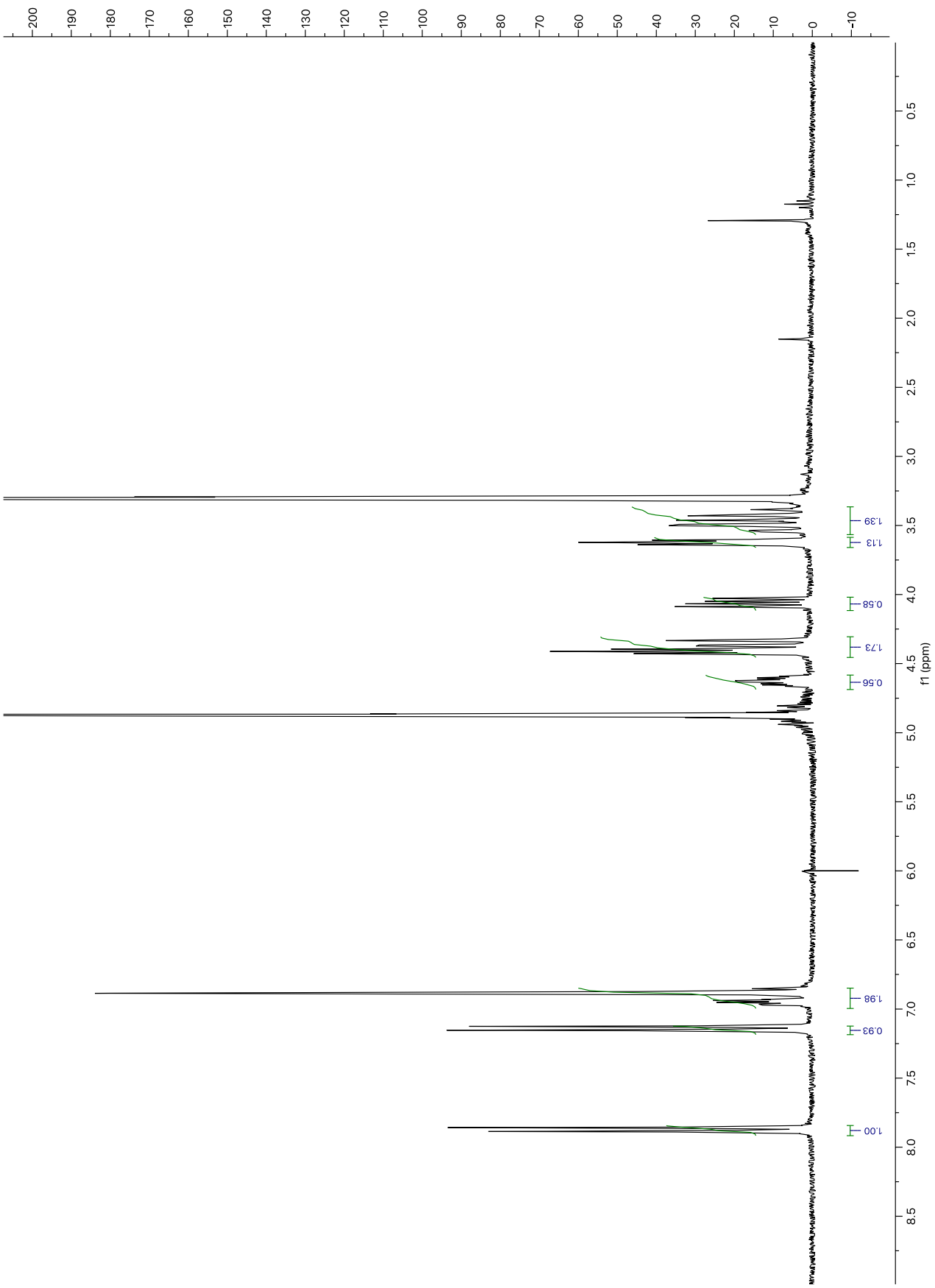
f1 (ppm)
1.39
1.13
0.58
1.73
0.56
1.98
0.93
1.00

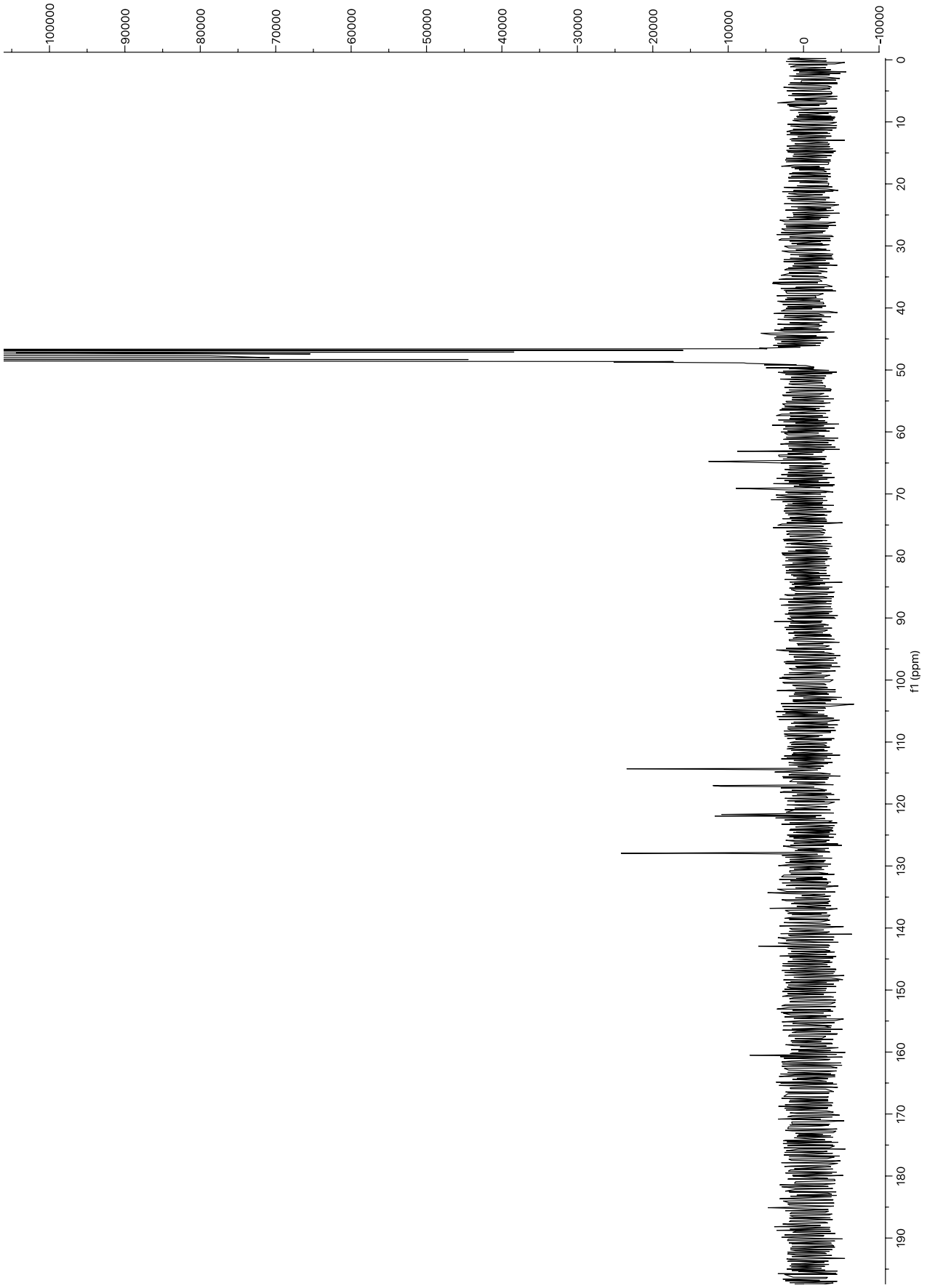
100000
90000
80000
70000
60000
50000
40000
30000
20000
10000
0
-10000
0
10
20
30
40
50
60
70
80
90
100
110
120
130
140
150
160
170
180
190
f1 (ppm)

4-(2-chloroethoxy)-N-methylbenzenesulfonamide

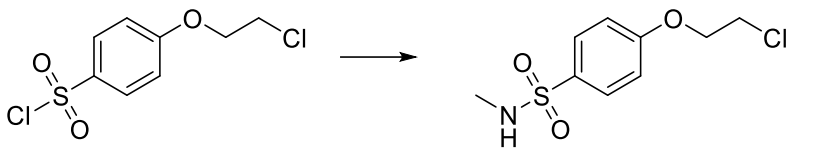

Chemical Formula:$C_8H_8Cl_2O_3S$
MW: 255,11

Chemical Formula:$C_9H_{12}ClNO_3S$
MW: 249,71

Methylamine solution 2.0 M in tetrahydrofuran (10 mL, 20.00 mmol) was added to an ice-cooled solution of 4-(2-chloroethoxy)benzenesulfonyl chloride (500 mg, 1.96 mmol) in tetrahydrofuran (2mL).

Afterward, the solid was removed by filtration, the solvent was evaporated under vacuum in order to obtain the pure product as a yellow oil (449 mg, 1.80 mmol).

Yield = 91.8%

^{1}H NMR ($CDCl_3$): δ 7.81 (d, *J* = 8.8 Hz, 2H), 7.01 (d, *J* = 8.8 Hz, 2H), 4.29 (t, *J* = 5.8 Hz, 2H), 3.84 (t, *J* = 5.8 Hz, 2H), 2.65 (s, 3H).

4-(2-azidoethoxy)-N-methylbenzenesulfonamide

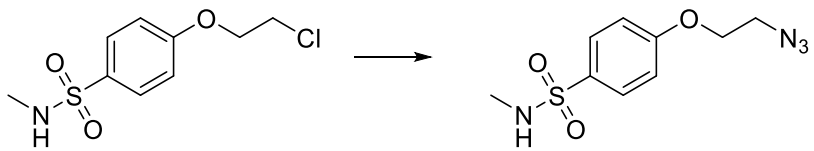

Chemical Formula:$C_9H_{12}ClNO_3S$
MW: 249,71

Chemical Formula:$C_9H_{12}N_4O_3S$
MW: 256,28

Sodium azide (1.14 g, 17.53 mmol) and KI (30 mg, 0.18 mmol) were added to a solution of 4-(2-chloroethoxy)-N-methylbenzenesulfonamide (440 mg, 1.76 mmol) in DMF (6 mL) and water (2 mL). Then, the mixture was refluxed, under stirring, until TLC[8] indicated the disappearance of starting material.

Afterward, the mixture was diluted with water and extracted with diethyl ether. The organic phase was dried over anhydrous sodium sulfate, filtered, and evaporated in vacuo, affording 451 mg (1.76 mmol) of the pure product as a pale yellow oil.

Yield = 100%.

^{1}H NMR ($CDCl_3$): δ 7.78 (d, *J* = 8.9 Hz, 2H), 6.98 (d, *J* = 8.9 Hz, 2H), 4.19 (t, *J* = 6.2 Hz, 2H), 3.62 (t, *J* = 6.2 Hz, 2H), 2.61 (s, 3H).

[8] Dichloromethane/methanol 95:5. R_f starting material = 0.5; R_f product = 0.55.

4-(2-aminoethoxy)-N-methylbenzenesulfonamide

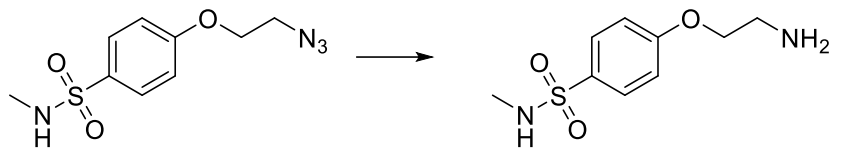

Chemical Formula:$C_9H_{12}N_4O_3S$
MW: 256,28

Chemical Formula:$C_9H_{14}N_2O_3S$
MW: 230,28

Palladium (II) oxide (21.54 mg, 0.18 mmol) and hydrazine hydrate (0.86 mL, 17.60 mmol) were added to a solution of 4-(2-azidoethoxy)-N-methylbenzenesulfonamide (451 mg, 1.76 mmol) in methanol (6 mL).

Then, the mixture was refluxed, under stirring, until TLC[9] indicated the disappearance of starting material. Afterward, the catalyst was removed by filtration, and methanol was evaporated in vacuo. The resulting crude was dissolved in ethyl acetate and the organic phase was extracted with 10% aqueous solution of HCl. After being basified to pH 10 with 10M solution of KOH, the aqueous layer was further extracted with ethyl acetate. The organic phase was dried over anhydrous sodium sulfate, filtered, and evaporated in vacuo, affording 170 mg (0.74 mmol) of the pure product as an orange oil.

Yield = 42.0%

^{1}H NMR (CD_3OD): δ 7.83 (d, *J* = 9.0 Hz, 2H), 7.07 (d, *J* = 9.0 Hz, 2H), 4.08 (t, *J* = 5.3 Hz, 2H), 3.03 (t, *J* = 5.3 Hz, 2H), 2.50 (s, 3H).

[9]Dichloromethane/methanol 90:10 + 1% aq. NH_3. R_f starting material = 0.65; R_f product = 0.15.

[((2-(4-methylsulfonamidephenoxy)ethyl)amino)-methyl]-1,4-benzodioxane

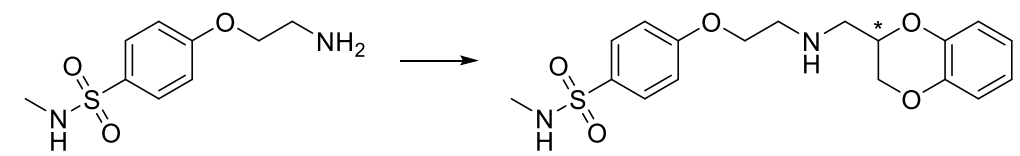

Chemical Formula:$C_9H_{14}N_2O_3S$
MW: 230,28

Chemical Formula:$C_{18}H_{22}N_2O_5S$
MW: 378,44

4-(2-aminoethoxy)-N-methylbenzenesulfonammide (170 mg, 0.74 mmol) and 2-mesyloxymethyl-1,4-benzodioxane (164 mg, 0.67 mmol) were dissolved in 7 mL of 2-propanol. Triethylamine (0.093 mL, 0.67 mmol) was added to the solution and the resulting mixture was refluxed, under stirring, until TLC[10] indicated the disappearance of starting material. Afterward, the solvent was evaporated in vacuo, the crude was dissolved in dichloromethane, and was washed with 10% aqueous solution of $NaHCO_3$ and water. The organic phase was dried over anhydrous sodium sulfate, filtered, and evaporated in vacuo, affording a yellow oil. Flash chromatography (dichloromethane/methanol 90:10 + 1% aq. NH_3) was performed in order to obtain 66 mg (0.17 mmol) of the pure product as a light yellow oil.

Yield = 22.9%

^{1}H NMR ($CDCl_3$): δ 7.78 (d, *J* = 8.9 Hz, 2H), 6.98 (d, *J* = 8.9 Hz, 2H), 6.90 – 6.79 (m, 4H), 5.05 (s, 1H), 4.32 – 4.24 (m, 2H), 4.14 (t, *J* = 5.1 Hz, 2H), 4.04 (dd, *J* = 11.6, 7.6 Hz, 1H), 3.10 (t, *J* = 5.1 Hz, 2H), 2.98 (dd, *J* = 8.8, 5.7 Hz, 2H), 2.59 (s, 3H).

[10]Dichloromethane/methanol 95:5 + 1% aq. NH_3. R_f starting material = 0.25; R_f product = 0.40.

Compound II

[((2-(4-methylsulfonamidephenoxy)ethyl)amino)-methyl]-1,4-benzodioxane hydrochloride

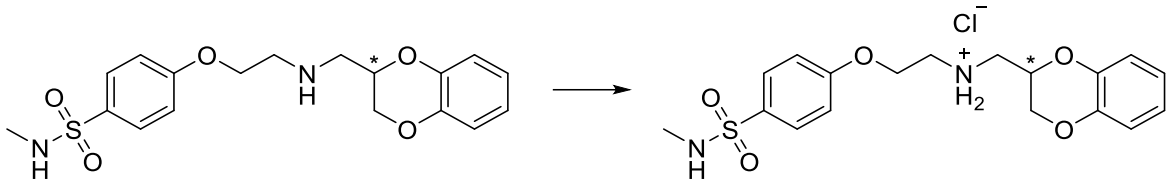

Chemical Formula:$C_{18}H_{22}N_2O_5S$
MW: 378,44

Chemical Formula:$C_{18}H_{23}ClN_2O_5S$
MW: 414,90

A solution of [((2-(4-Methylsulfonamidephenoxy)ethyl)amino)-methyl]-1,4-benzodioxane (66 mg, 0.17 mmol) in 2 mL of hydrogen chloride solution 2.0 M in diethyl ether was stirred overnight. The reaction mixture was diluted with ethyl ether, the solid was filtered and washed with cooled ethyl ether to obtain the desired product as a pale yellow solid (20.24 mg, 0.05 mmol).

Yield = 29.4%

m.p. *161°C*

HRMS: *m/z* 379.1318 ($[M+H]^+$

^{1}H NMR (CD_3OD): δ 7.80 (d, *J* = 8.9 Hz, 2H), 7.18 (d, *J* = 8.9 Hz, 2H), 6.99 – 6.83 (m, 4H), 4.64 (m, 1H), 4.41 (t, *J* = 4.9 Hz, 2H), 4.35 (dd, *J* = 11.6, 2.4 Hz, 1H), 4.06 (dd, *J* = 11.6, 6.4 Hz, 1H), 3.62 (t, *J* = 4.9 Hz, 2H), 3.58 – 3.36 (m, 2H), 2.50 (s, 3H).

^{13}C NMR (CD_3OD): δ 160.93, 142.94, 141.59, 132.03, 129.02, 121.90, 121.66, 117.17, 117.02, 114.60, 69.10, 64.77, 63.17, 27.77.

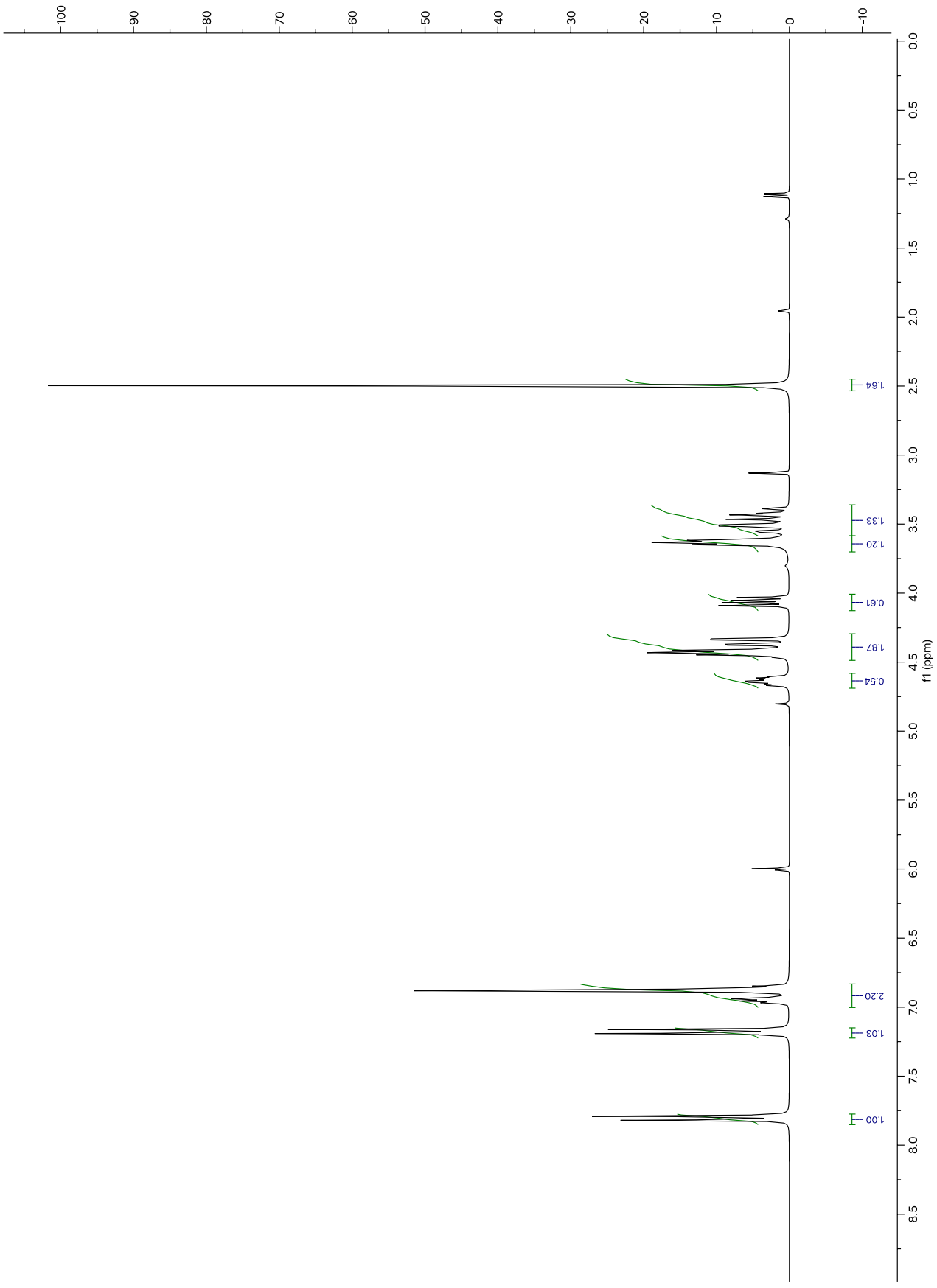
1.64
1.33
1.20
0.61
1.87
0.54
2.20
1.03
1.00
f1 (ppm)

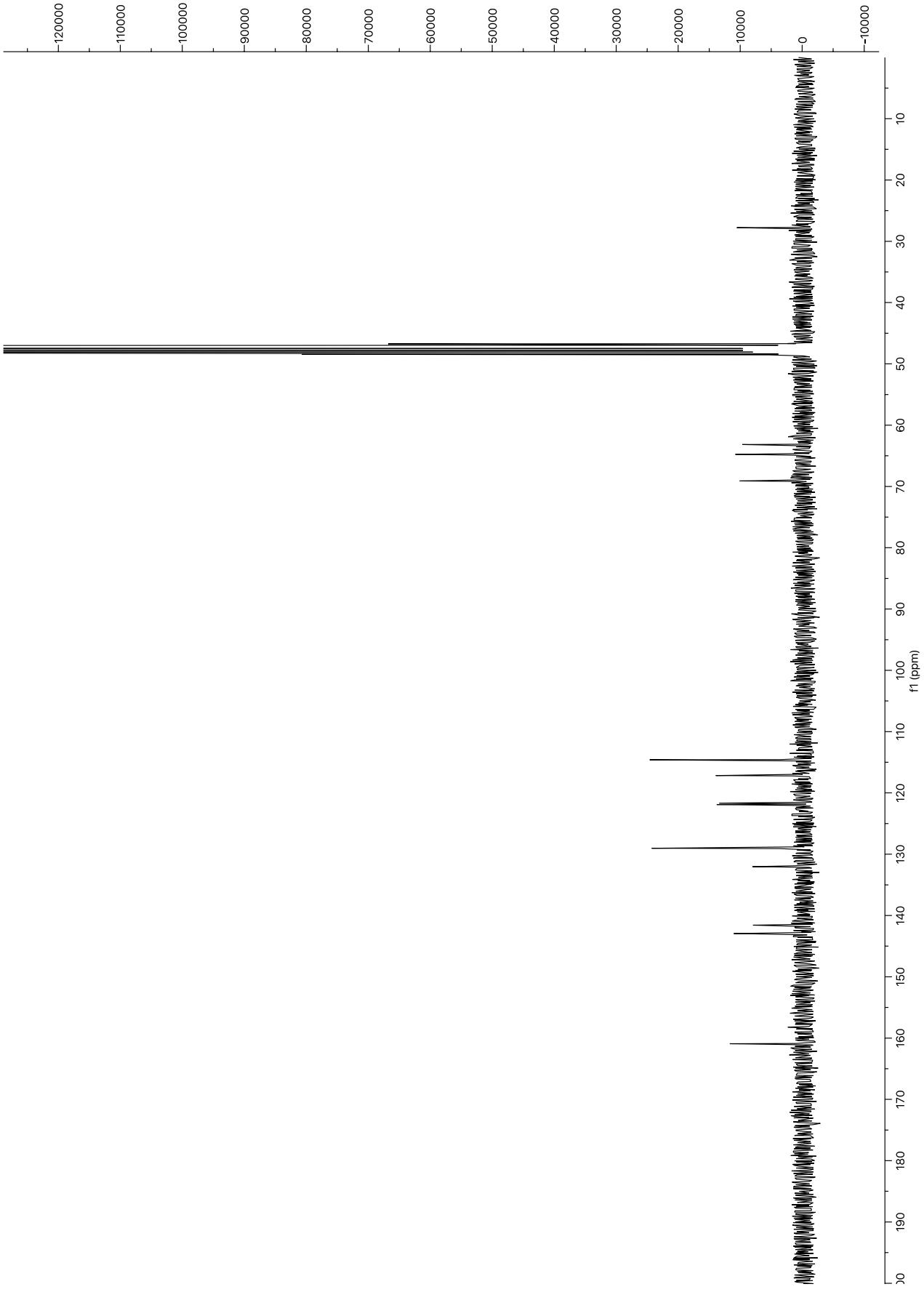
120000
110000
100000
90000
80000
70000
60000
50000
40000
30000
20000
10000
0
-10000
10
20
30
40
50
60
70
80
90
100
110
120
130
140
150
160
170
180
190
200
f1 (ppm)

4-(2-chloroethoxy)-N-ethylbenzenesulfonamide

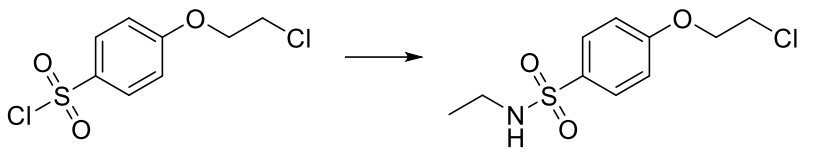

Chemical Formula:$C_8H_8Cl_2O_3S$
MW: 255,11

Chemical Formula:$C_{10}H_{14}ClNO_3S$
MW: 263,74

Ethylamine solution 2.0 M in tetrahydrofuran (9 mL, 18.00 mmol) was added to an ice-cooled solution of 4-(2-Chloroethoxy)benzenesulfonyl chloride (458 mg, 1.8 mmol) in tetrahydrofuran (0.5 mL). Afterward, the solid was removed by filtration, the solvent was evaporated under vacuum in order to obtain the pure product as orangish oil (474 mg, 1.8 mmol).

Yield = 100%

^{1}H NMR ($CDCl_3$): δ 7.81 (d, *J* = 8.9 Hz, 2H), 7.00 (d, *J* = 8.9 Hz, 2H), 4.29 (t, *J* = 5.8 Hz, 2H), 3.84 (t, *J* = 5.7 Hz, 2H), 2.99 (q, *J* = 7.2 Hz, 2H), 1.10 (t, *J* = 7.2 Hz, 3H).

4-(2-azidoethoxy)-N-ethylbenzenesulfonamide

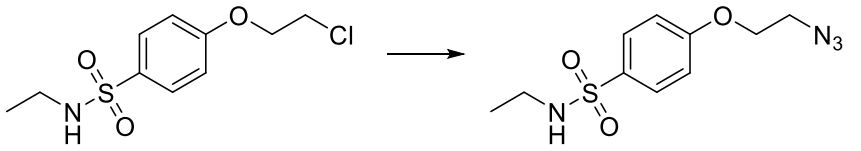

Chemical Formula:$C_{10}H_{14}ClNO_3S$
MW: 263,74

Chemical Formula:$C_{10}H_{14}N_4O_3S$
MW: 270,31

Sodium azide (1.17 g, 18.00 mmol) and KI (30 mg, 0.18 mmol) were added to a solution of 4-(2-Chloroethoxy)-N-methylbenzenesulfonamide (474 mg, 1.80 mmol) in DMF (5 mL) and water (2 mL). Then, the mixture was refluxed, under stirring, until TLC[11] indicated the disappearance of starting material.

Afterward, the mixture was diluted with water and extracted with diethyl ether. The organic phase was dried over anhydrous sodium sulfate, filtered, and evaporated in vacuo, affording 486 mg (1.80 mmol) of the pure product as a pale yellow oil.

Yield = 100%

^{1}H NMR ($CDCl_3$): δ 7.81 (d, *J* = 8.7 Hz, 2H), 7.00 (d, *J* = 8.7 Hz, 2H), 4.20 (t, *J* = 6.2 Hz, 2H), 3.64 (t, *J* = 6.2 Hz, 2H), 2.95 (q, *J* = 7.1 Hz, 2H), 1.10 (t, *J* = 7.1 Hz, 3H).

[11]Dichloromethane/methanol 99:1. R_f starting material = 0.3; R_f product = 0.32.

4-(2-aminoethoxy)-N-ethylbenzenesulfonamide

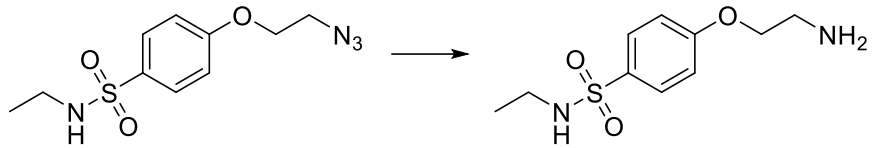

Chemical Formula:$C_{10}H_{14}N_4O_3S$
MW: 270,31

Chemical Formula:$C_{10}H_{16}N_2O_3S$
MW: 244,31

Palladium(II) oxide (22.04 mg, 0.18 mmol) and hydrazine hydrate (0.88 mL, 18.00 mmol) were added to a solution of 4-(2-azidoethoxy)-N-ethylbenzenesulfonamide (486 mg, 1.80 mmol) in methanol (15 mL).

Then, the mixture was refluxed, under stirring, until TLC[12] indicated the disappearance of starting material. Afterward, the catalyst was removed by filtration, and methanol was evaporated in vacuo. The resulting crude was dissolved in ethyl acetate and the organic phase was extracted with 10% aqueous solution of HCl. After being basified to pH 10 with 10M solution of KOH, the aqueous layer was further extracted with ethyl acetate. The organic phase was dried over anhydrous sodium sulfate, filtered, and evaporated in vacuo, affording 428 mg (1.75 mmol) of the pure product as orange oil.

Yield = 97.3%

^{1}H NMR (CD_3OD): δ 7.76 (d, *J* = 8.9 Hz, 2H), 7.09 (d, *J* = 8.9 Hz, 2H), 4.08 (t, *J* = 5.3 Hz, 2H), 3.02 (t, *J* = 5.3 Hz, 2H), 2.85 (q, *J* = 7.1 Hz, 2H), 1.04 (t, *J* = 7.1 Hz, 3H).

[12]Dichloromethane/methanol 95:5 + 1% aq. NH_3. R_f starting material = 0.7; R_f product = 0.22.

[((2-(4-ethylsulfonamidephenoxy)ethyl)amino)-methyl]-1,4-benzodioxane

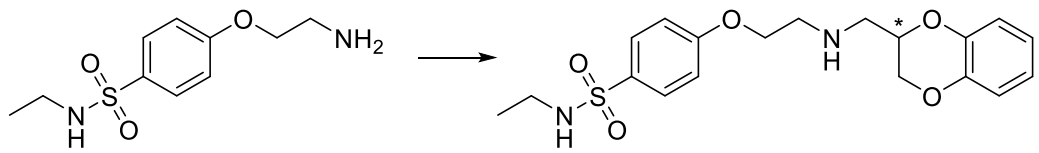

Chemical Formula:$C_{10}H_{16}N_2O_3S$
MW: 244,31

Chemical Formula:$C_{19}H_{24}N_2O_5S$
MW: 392,47

4-(2-aminoethoxy)-N-ethylbenzenesulfonammide (428 mg, 1.75 mmol) and 2-mesyloxymethyl-1,4-benzodioxane (389 mg, 1.59 mmol) were dissolved in 18 mL of 2-propanol. Triethylamine (0.22 mL, 1.59 mmol) was added to the solution and the resulting mixture was refluxed, under stirring, until TLC[13] indicated the disappearance of starting material. Afterward, the solvent was evaporated in vacuo, the crude was dissolved in dichloromethane, and was washed with 10% aqueous solution of $NaHCO_3$ and water. The organic phase was dried over anhydrous sodium sulfate, filtered, and evaporated in vacuo, affording a yellow oil. Flash chromatography (dichloromethane/methanol 97:3 + 0.5% aq. NH_3) was performed in order to obtain 124 mg (0.32 mmol) of the pure product as orange oil.

Yield =18%

^{1}H NMR ($CDCl_3$): δ 7.79 (d, *J* = 8.9 Hz, 2H), 6.98 (d, *J* = 8.9 Hz, 2H), 6.87 (m, 4H), 4.32 – 4.24 (m, 2H), 4.14 (t, *J* = 5.1 Hz, 2H), 4.04 (dd, *J* = 11.6, 7.6 Hz, 1H), 3.10 (t, *J* = 5.1 Hz, 2H), 3.06 – 2.90 (m, 4H), 1.10 (t, *J* = 7.2 Hz, 3H).

[13] Dichloromethane/methanol 95:5 + 0.5% aq. NH_3. R_f starting material = 0.22; R_f product = 0.50.

Compound III

[((2-(4-ethylsulfonamidephenoxy)ethyl)amino)-methyl]-1,4-benzodioxane hydrochloride

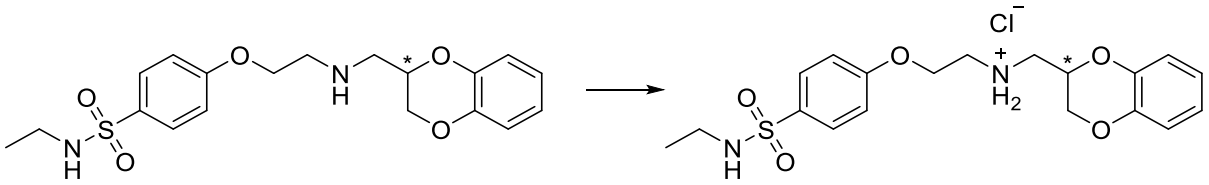

Chemical Formula: $C_{19}H_{24}N_2O_5S$
MW: 392,47

Chemical Formula: $C_{19}H_{25}ClN_2O_5S$
MW: 428,93

A solution of [((2-(4-Ethylsulfonamidephenoxy)ethyl)amino)-methyl]-1,4-benzodioxane (124 mg, 0.32 mmol) in 4 mL of hydrogen chloride solution 2.0 M in diethyl ether was stirred overnight. The reaction mixture was diluted with ethyl ether, the solid was filtered and washed with cooled ethyl ether to obtain the desired product as a pale yellow solid (65.58 mg, 0.15 mmol).

Yield = 46.9%

m.p. *167°C*

HRMS: *m/z* 393.1473 $([M+H]^+$

^{1}H NMR (CD_3OD): δ 7.81 (d, *J* = 8.9 Hz, 2H), 7.17 (d, *J* = 8.9 Hz, 2H), 7.02 – 6.82 (m, 4H), 4.64 (m, 1H), 4.41 (t, *J* = 4.9 Hz, 2H), 4.35 (dd, *J* = 11.6, 2.4 Hz, 1H), 4.06 (dd, *J* = 11.6, 6.4 Hz, 1H), 3.62 (t, *J* = 4.9 Hz, 2H), 3.58 – 3.36 (m, 2H), 2.86 (q, *J* = 7.1 Hz, 2H), 1.05 (t, *J* = 7.1 Hz, 3H).

^{13}C NMR (CD_3OD): δ 160.89, 142.93, 141.62, 133.20, 128.83, 121.87, 121.66, 117.23, 116.99, 114.64, 69.11, 64.81, 63.20, 37.58, 13.81.

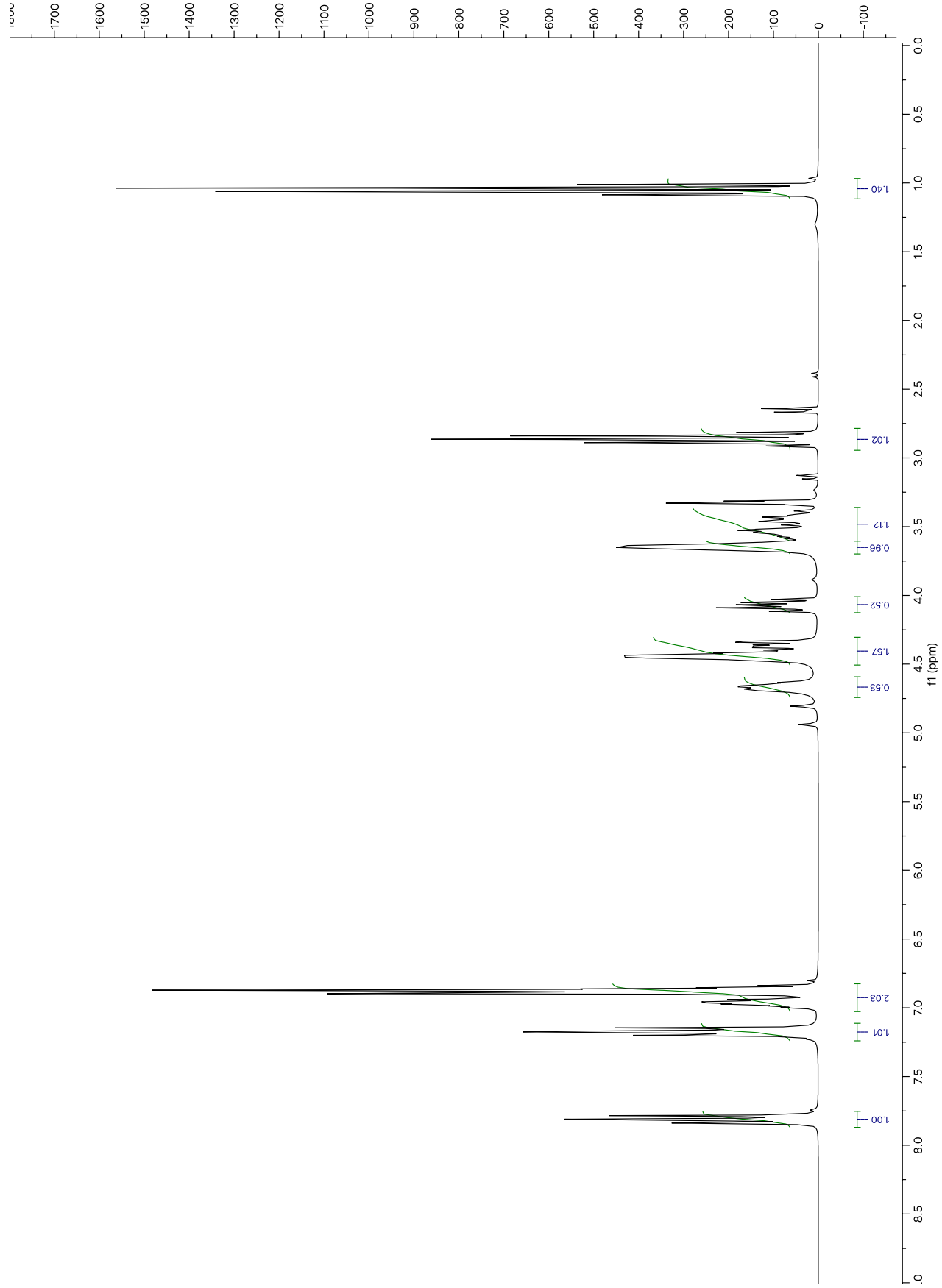
1.40
1.02
1.12
0.96
0.52
1.57
0.53
2.03
1.01
1.00
f1 (ppm)

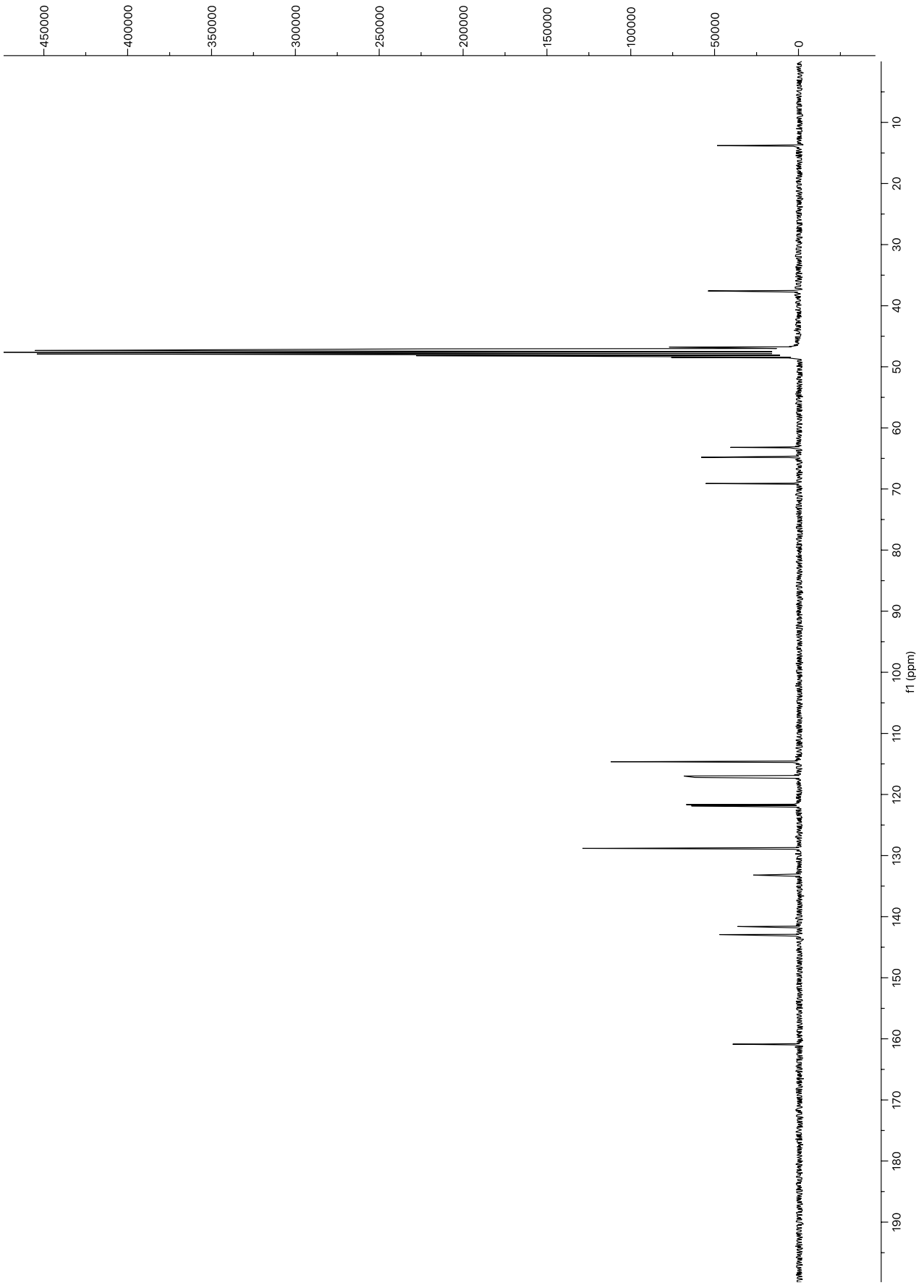
450000
400000
350000
300000
250000
200000
150000
100000
50000
0
10
20
30
40
50
60
70
80
90
100
110
120
130
140
150
160
170
180
190
f1 (ppm)

4-(2-chloroethoxy)-N,N-dimethylbenzenesulfonamide

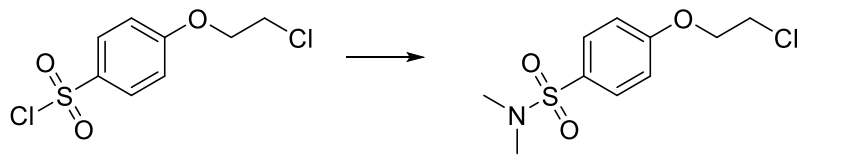

Chemical Formula:$C_8H_8Cl_2O_3S$
MW: 255,11

Chemical Formula:$C_{10}H_{14}ClNO_3S$
MW: 263,74

Dimethylamine solution 2.0 M in tetrahydrofuran (9 mL, 18.00 mmol) was added to an ice-cooled solution of 4-(2-chloroethoxy)benzenesulfonyl chloride (458 mg, .1.80 mmol) in tetrahydrofuran (0.5 mL).

Afterward, the solid was removed by filtration, the solvent was evaporated under vacuum in order to obtain the pure product as a pale yellow oil (396 mg, 1.50 mmol).

Yield = 83.4%

^{1}H NMR ($CDCl_3$): δ 7.73 (d, *J* = 8.9 Hz, 2H), 7.02 (d, *J* = 8.9 Hz, 2H), 4.30 (t, *J* = 5.7 Hz, 2H), 3.85 (t, *J* = 5.7 Hz, 2H), 2.68 (s, 6H).

4-(2-azidoethoxy)-N,N-dimethylbenzenesulfonamide

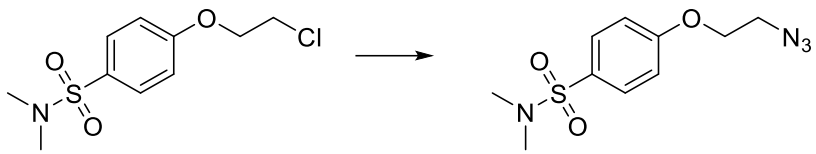

Chemical Formula:$C_{10}H_{14}ClNO_3S$
MW: 263,74

Chemical Formula:$C_{10}H_{14}N_4O_3S$
MW: 270,31

Sodium azide (975 mg, 15.00 mmol) and KI (25 mg, 0.15 mmol) were added to a solution of 4-(2-chloroethoxy)-N,N-dimethylbenzenesulfonamide (396 mg, 1.50 mmol) in DMF (5 mL) and water (2 mL). Then, the mixture was refluxed, under stirring, until TLC[14] indicated the disappearance of starting material.

Afterward, the mixture was diluted with water and extracted with diethyl ether. The organic phase was dried over anhydrous sodium sulfate, filtered, and evaporated in vacuo, affording 290 mg (1.07 mmol) of the pure product as a pale yellow oil.

Yield = 72.0%

^{1}H NMR ($CDCl_3$): δ 7.72 (d, *J* = 8.9 Hz, 2H), 7.03 (d, *J* = 8.9 Hz, 2H), 4.21 (t, *J* = 5.7 Hz, 2H), 3.64 (t, *J* = 5.7 Hz, 2H), 2.68 (s, 6H).

[14] Dichloromethane/methanol 99:1. R_f starting material = 0.70; R_f product = 0.70.

4-(2-aminoethoxy)-N,N-dimethylbenzenesulfonamide

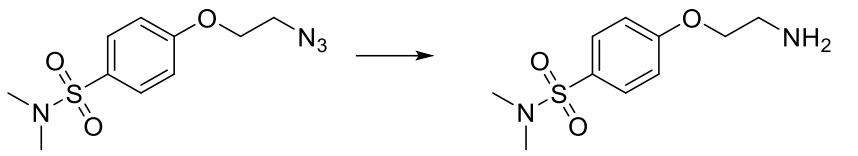

Chemical Formula:$C_{10}H_{14}N_4O_3S$
MW: 270,31

Chemical Formula:$C_{10}H_{16}N_2O_3S$
MW: 244,31

Palladium(II) oxide (13.47 mg, 0.11 mmol) and hydrazine hydrate (0.52 mL, 10.70 mmol) were added to a solution of 4-(2-azidoethoxy)-N,N-dimethylbenzenesulfonamide (290 mg, 1.07 mmol) in methanol (9 mL).

Then, the mixture was refluxed, under stirring, until TLC[15] indicated the disappearance of starting material. Afterward, the catalyst was removed by filtration, and methanol was evaporated in vacuo. The resulting crude was dissolved in ethyl acetate and the organic phase was extracted with 10% aqueous solution of HCl. After being basified to pH 10 with 10M solution of KOH, the aqueous layer was further extracted with ethyl acetate. The organic phase was dried over anhydrous sodium sulfate, filtered, and evaporated in vacuo, affording 261 mg (1.07 mmol) of the pure product as a pale yellow solid.

Yield = 100%

m.p. *69°C*

^{1}H NMR (CD_3OD): δ 7.71 (d, *J* = 8.9 Hz, 2H), 7.15 (d, *J* = 8.9 Hz, 2H), 4.10 (t, *J* = 5.3 Hz, 2H), 3.03 (t, *J* = 5.3 Hz, 2H), 2.64 (s, 6H).

[15]Dichloromethane/methanol 90:10 + 1% aq. NH_3. R_f starting material = 0.8; R_f product = 0.22.

[((2-(4-dimethylsulfonamidephenoxy)ethyl)amino)-methyl]-1,4-benzodioxane

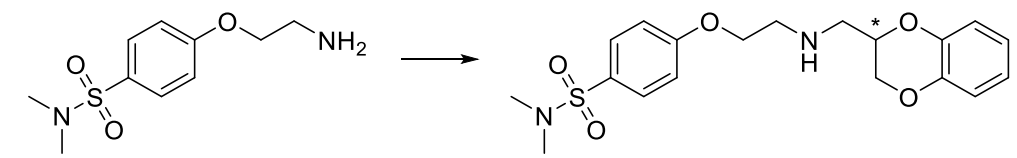

Chemical Formula:$C_{10}H_{16}N_2O_3S$
MW: 244,31

Chemical Formula:$C_{19}H_{24}N_2O_5S$
MW: 392,47

4-(2-aminoethoxy)-N,N-dimethylbenzenesulfonammide (261 mg, 1.07 mmol) and 2-mesyloxymethyl-1,4-benzodioxane (238 mg, 0,97 mmol) were dissolved in 10 mL of 2-propanol. Triethylamine (0.13 mL, 0.97 mmol) was added to the solution and the resulting mixture was refluxed, under stirring, until TLC[16] indicated the disappearance of starting material. Afterward, the solvent was evaporated in vacuo, the crude was dissolved in dichloromethane, and was washed with 10% aqueous solution of $NaHCO_3$ and water. The organic phase was dried over anhydrous sodium sulfate, filtered, and evaporated in vacuo, affording an orangish oil. Flash chromatography (dichloromethane/methanol 97:3 + 0.5% aq. NH_3) was performed in order to obtain 96 mg (0.24 mmol) of the pure product as an orange oil.

Yield = 22.4%

^{1}H NMR ($CDCl_3$): δ 7.71 (d, *J* = 8.9 Hz, 2H), 7.01 (d, *J* = 8.9 Hz, 2H), 6.91 – 6.80 (m, 4H), 4.36 – 4.24 (m, 2H), 4.14 (t, *J* = 5.1 Hz, 2H), 4.04 (dd, *J* = 11.6, 7.6 Hz, 1H), 3.10 (t, *J* = 5.1 Hz, 2H), 2.98 (dd, *J* = 8.8, 5.7 Hz, 2H), 2.68 (s, 6H).

[16]Dichloromethane/methanol 95:5 + 0.5% aq. NH_3. R_f starting material = 0.22; R_f product = 0.61.

Compound IV

[((2-(4-dimethylsulfonamidephenoxy)ethyl)amino)-methyl]-1,4-benzodioxane hydrochloride

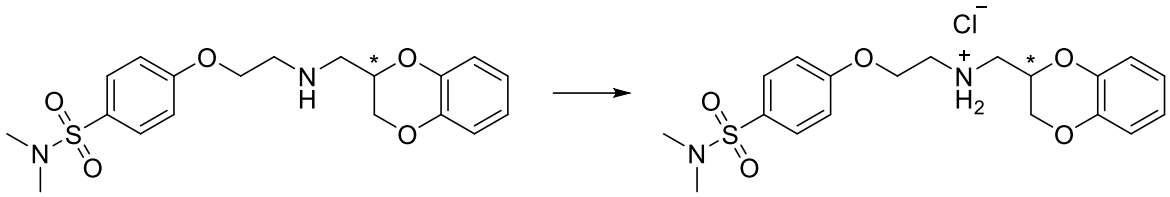

Chemical Formula: $C_{19}H_{24}N_2O_5S$
MW: 392,47

Chemical Formula: $C_{19}H_{25}ClN_2O_5S$
MW: 428,93

A solution of [((2-(4-Ethylsulfonamidephenoxy)ethyl)amino)-methyl]-1,4-benzodioxane (96 mg, 0.24 mmol) in 3 mL of hydrogen chloride solution 2.0 M in diethyl ether was stirred overnight. The reaction mixture was diluted with ethyl ether, the solid was filtered and washed with cooled ethyl ether to obtain the desired product as a pale yellow solid (79.94 mg, 0.19 mmol).

Yield = 79.2%

m.p. *177°C*

HRMS: *m/z* 393.1475 $([M+H]^+$

^{1}H NMR (CD_3OD): δ 7.76 (d, *J* = 8.9 Hz, 2H), 7.22 (d, *J* = 8.9 Hz, 2H), 7.01 – 6.81 (m, 4H), 4.62 (m, 1H), 4.41 (t, *J* = 4.9 Hz, 2H), 4.35 (dd, *J* = 11.6, 2.3 Hz, 1H), 4.06 (dd, *J* = 11.6, 6.4 Hz, 1H), 3.64 (t, *J* = 4.9 Hz, 2H), 3.57 – 3.37 (m, 2H), 2.65 (s, 6H).

^{13}C NMR (CD_3OD): δ 161.28, 142.94, 141.58, 129.78, 127.94, 121.91, 121.67, 117.16, 117.02, 114.68, 9.11, 64.77, 63.20, 36.87.

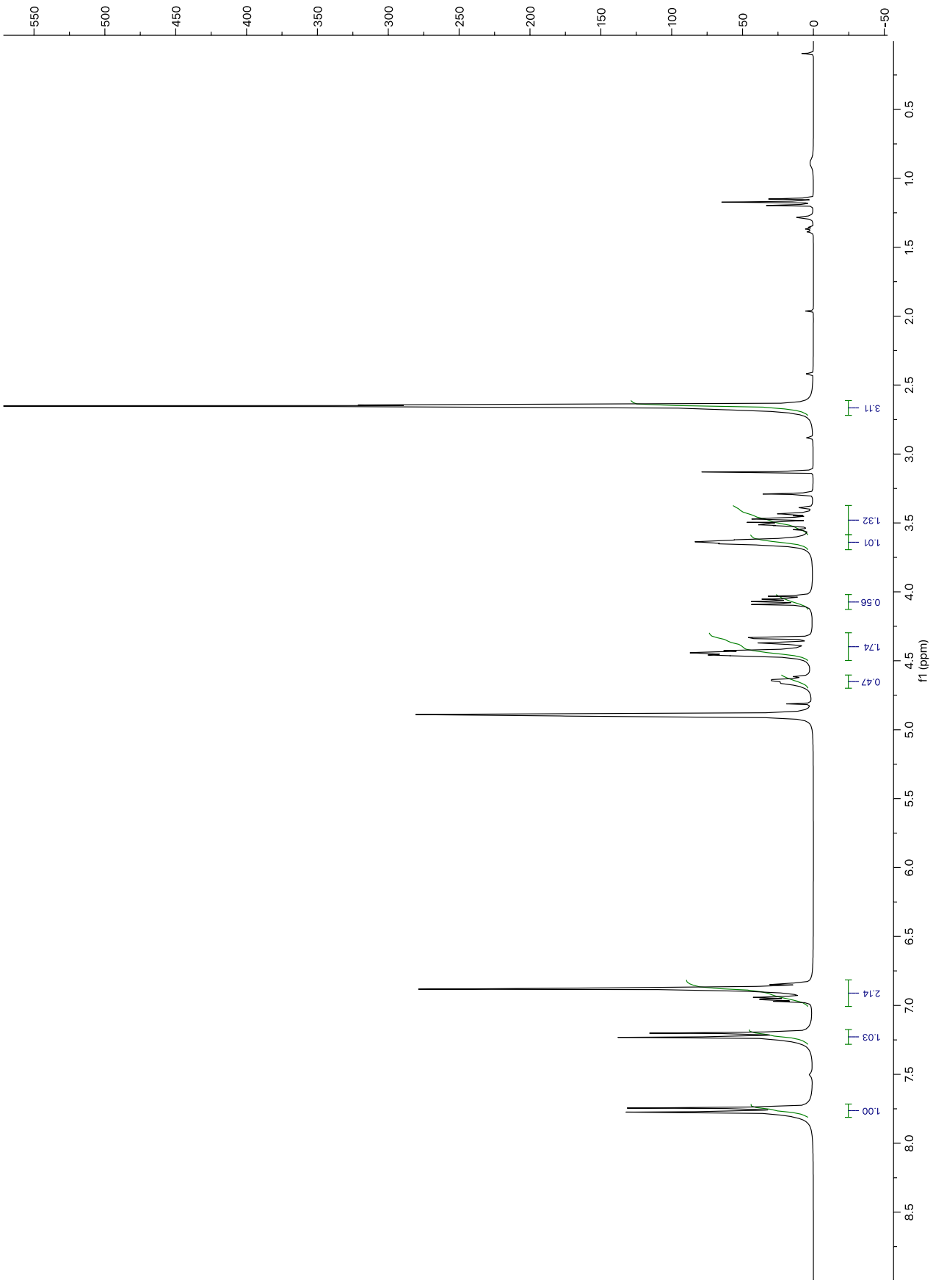
550
500
450
400
350
300
250
200
150
100
50
0
-50
0.5
1.0
1.5
2.0
2.5
3.0
3.5
4.0
4.5
5.0
5.5
6.0
6.5
7.0
7.5
8.0
8.5
f1 (ppm)
3.11
1.32
1.01
0.56
1.74
0.47
2.14
1.03
1.00

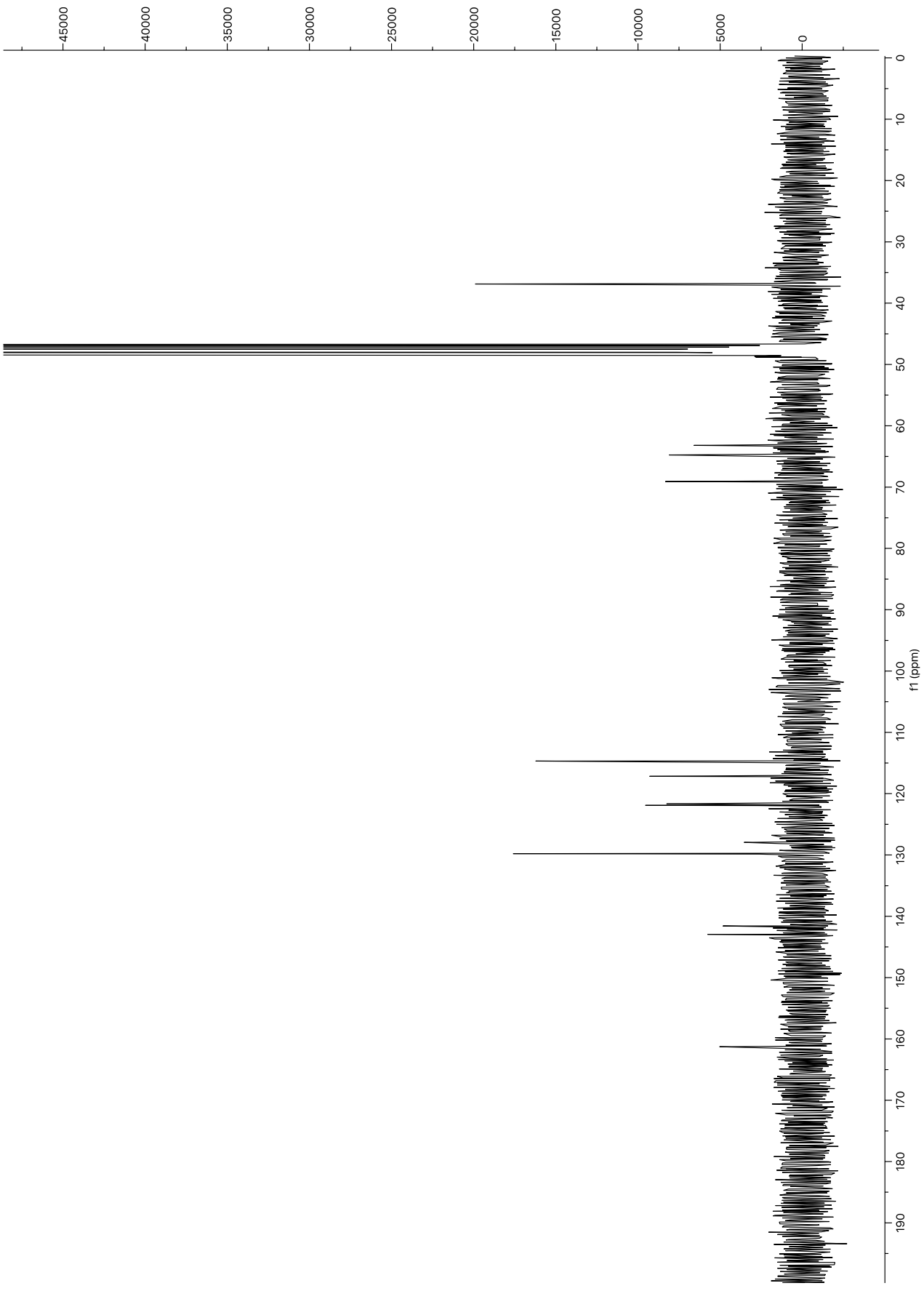
45000
40000
35000
30000
25000
20000
15000
10000
5000
0
0
10
20
30
40
50
60
70
80
90
100
110
120
130
140
150
160
170
180
190
f1 (ppm)

4-(2-chloroethoxy)-N-isopropylbenzenesulfonamide

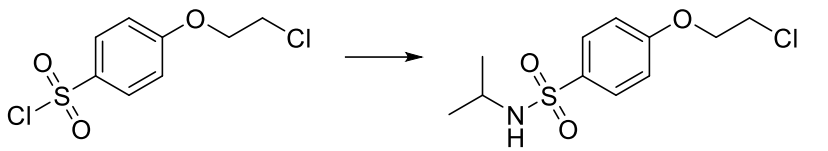

Chemical Formula:$C_8H_8Cl_2O_3S$
MW: 255,11

Chemical Formula:$C_{11}H_{16}ClNO_3S$
MW: 277,76

Isopropylamine (0.63 mL, 7.41 mmol) was added to an ice-cooled solution of 4-(2-chloroethoxy)benzenesulfonyl chloride (860 mg, 3.37 mmol) in dichloromethane (20 mL). Afterward, the solid was removed by filtration, the solvent was evaporated under vacuum in order to obtain the pure product as a pale yellow oil (936 mg, 3.37 mmol).

Yield = 100%

^{1}H NMR ($CDCl_3$): δ 7.82 (d, *J* = 8.9 Hz, 2H), 6.98 (d, *J* = 8.9 Hz, 2H), 4.28 (t, *J* = 5.7 Hz, 2H), 3.84 (t, *J* = 5.7 Hz, 2H), 3.42 (sep, *J* = 6.6 Hz, 1H), 1.06 (d, *J* = 6.6 Hz, 6H).

4-(2-azidoethoxy)-N-isopropylbenzenesulfonamide

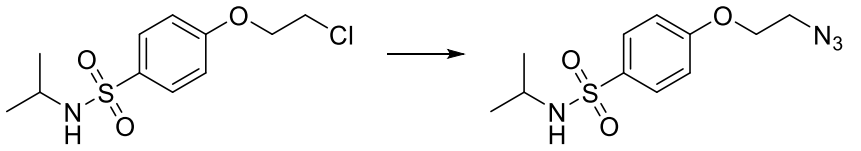

Chemical Formula:$C_{11}H_{16}ClNO_3S$
MW: 277,76

Chemical Formula:$C_{11}H_{16}N_4O_3S$
MW: 284,33

Sodium azide (2.19 g, 33.7 mmol) and KI (56 mg, 0.34 mmol) were added to a solution of 4-(2-chloroethoxy)-N-isopropylbenzenesulfonamide (936 mg, 3.37 mmol) in DMF (10 mL) and water (2 mL). Then, the mixture was refluxed, under stirring, until TLC[17] indicated the disappearance of starting material.

Afterward, the mixture was diluted with water and extracted with diethyl ether. The organic phase was dried over anhydrous sodium sulfate, filtered, and evaporated in vacuo, affording 841 mg (2.96 mmol) of the pure product as a pale yellow oil.

Yield = 88.0%

^{1}H NMR ($CDCl_3$): δ 7.82 (d, *J* = 8.9 Hz, 2H), 6.99 (d, *J* = 8.9 Hz, 2H), 4.19 (t, *J* = 5.7 Hz, 2H), 3.64 (t, *J* = 5.7 Hz, 2H), 3.43 (sep, *J* = 6.6 Hz, 1H), 1.07 (d, *J* = 6.6 Hz, 6H).

[17]Dichloromethane/methanol 99:1. R_f starting material = 0.4; R_f product = 0.4.

4-(2-aminoethoxy)-N-isopropylbenzenesulfonamide

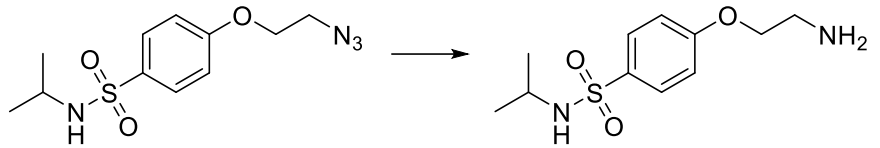

Chemical Formula:$C_{11}H_{16}N_4O_3S$
MW: 284,33

Chemical Formula:$C_{11}H_{18}N_2O_3S$
MW: 258,34

Palladium(II) oxide (36.73 mg, 0.30 mmol) and hydrazine hydrate (1.44 mL, 29.60 mmol) were added to a solution of 4-(2-azidoethoxy)-N-isopropylbenzenesulfonamide (841 mg, 2.96 mmol) in methanol (25 mL).

Then, the mixture was refluxed, under stirring, until TLC[18] indicated the disappearance of starting material. Afterward, the catalyst was removed by filtration, and methanol was evaporated in vacuo. The resulting crude was dissolved in ethyl acetate and the organic phase was extracted with 10% aqueous solution of HCl. After being basified to pH 10 with 10M solution of KOH, the aqueous layer was further extracted with ethyl acetate. The organic phase was dried over anhydrous sodium sulfate, filtered and evaporated in vacuo, affording 718 mg (2.78 mmol) of the pure product as a pale yellow solid.

Yield = 94.0%

m.p. *119°C*

^{1}H NMR (CD_3OD): δ 7.78 (d, *J* = 8.9 Hz, 2H), 7.09 (d, *J* = 8.9 Hz, 2H), 4.08 (t, *J* = 5.3 Hz, 2H), 3.02 (t, *J* = 5.3 Hz, 2H), 3.30 (sep, *J* = 6.6 Hz, 1H), 1.00 (d, *J* = 6.6 Hz, 6H).

[18] Dichloromethane/methanol 90:10 + 1% aq. NH_3. R_f starting material = 0.52; R_f product = 0.13.

[((2-(4-isopropylsulfonamidephenoxy)ethyl)amino)-methyl]-1,4-benzodioxane

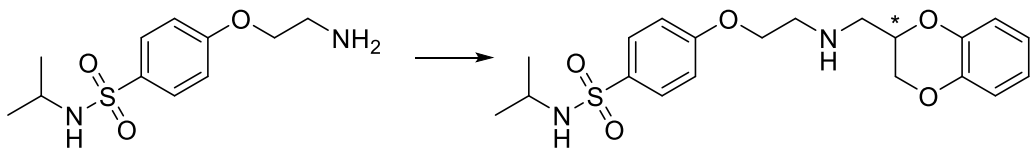

Chemical Formula:$C_{11}H_{18}N_2O_3S$
MW: 258,34

Chemical Formula:$C_{20}H_{26}N_2O_5S$
MW: 406,50

4-(2-aminoethoxy)-N-ispropylbenzenesulfonammide (718 mg, 2.78 mmol) and 2-mesyloxymethyl-1,4-benzodioxane (617 mg, 2.53 mmol) were dissolved in 30 mL of 2-propanol. Triethylamine (0.35 mL, 2.53 mmol) was added to the solution and the resulting mixture was refluxed, under stirring, until TLC[19] indicated the disappearance of starting material. Afterward, the solvent was evaporated in vacuo, the crude was dissolved in dichloromethane and was washed with 10% aqueous solution of $NaHCO_3$ and water. The organic phase was dried over anhydrous sodium sulfate, filtered, and evaporated in vacuo, affording an orangish oil. Flash chromatography (dichloromethane/methanol 97:3 + 0.5% aq. NH_3) was performed in order to obtain 30 mg (0.07 mmol) of the pure product as a pale yellow oil.

Yield = 2.5%

^{1}H NMR ($CDCl_3$): δ 7.80 (d, *J* = 8.9 Hz, 2H), 6.98 (d, *J* = 8.9 Hz, 2H), 6.91 – 6.80 (m, 4H), 4.36 – 4.24 (m, 2H), 4.14 (t, *J* = 5.1 Hz, 2H), 4.04 (dd, *J* = 11.6, 7.6 Hz, 1H), 3.43 (sep, *J* = 6.6 Hz, 1H), 3.10 (t, *J* = 5.1 Hz, 2H), 2.98 (dd, *J* = 8.8, 5.7 Hz, 2H), 1.07 (d, *J* = 6.6 Hz, 6H).

[19] dichloromethane/methanol 95:5 + 0.5% aq. NH_3. R_f starting material = 0.27; R_f product = 0.60.

Compound V

[((2-(4-isopropyllsulfonamidephenoxy)ethyl)amino)-methyl]-1,4-benzodioxane hydrochloride

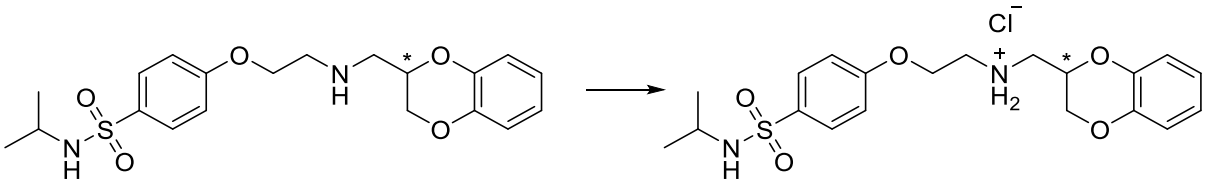

Chemical Formula: $C_{20}H_{26}N_2O_5S$
MW: 406,50

Chemical Formula: $C_{20}H_{27}ClN_2O_5S$
MW: 442,96

A solution of [((2-(4-isopropylsulfonamidephenoxy)ethyl)amino)-methyl]-1,4-benzodioxane (30 mg, 0.07 mmol) in 2,5 mL of hydrogen chloride solution 2.0 M in diethyl ether was stirred overnight. The reaction mixture was diluted with ethyl ether, the solid was filtered and washed with cooled ethyl ether to obtain the desired product as a pale yellow solid (18.95 mg, 0.04 mmol).

Yield = 57.1%

m.p. 169°C

HRMS: *m/z* 407.1639 ($[M+H]^+$

^{1}H NMR (CD_3OD): δ 7.83 (d, *J* = 8.9 Hz, 2H), 7.16 (d, *J* = 8.9 Hz, 2H), 7.00 – 6.83 (m, 4H), 4.63 (m, 1H), 4.41 (t, *J* = 4.9 Hz, 2H), 4.35 (dd, *J* = 11.6, 2.3 Hz, 1H), 4.06 (dd, *J* = 11.6, 6.4 Hz, 1H), 3.64 (t, *J* = 4.9 Hz, 2H), 3.57 – 3.37 (m, 2H), 3.30 (sep, *J* = 6.6 Hz, 1H), 1.01 (d, *J* = 6.6 Hz, 6H).
^{13}C NMR (CD_3OD): δ 160.74, 142.94, 141.58, 134.69, 128.75, 121.92, 121.67, 117.15, 117.02, 114.49, 69.10, 64.75, 63.13, 45.43, 22.31.

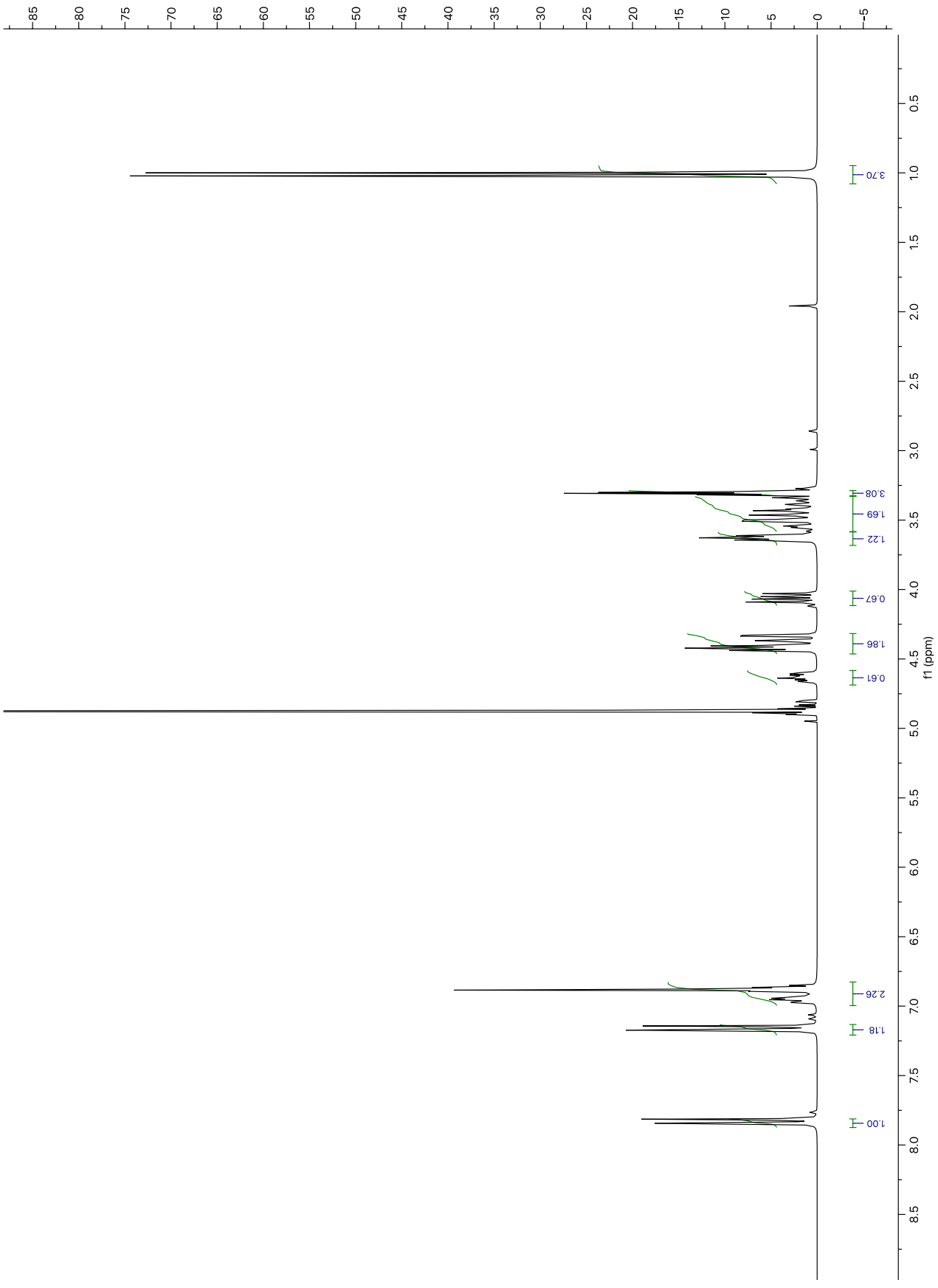
3.70
3.08
1.69
1.22
0.67
1.86
0.61
2.26
1.18
1.00
f1 (ppm)

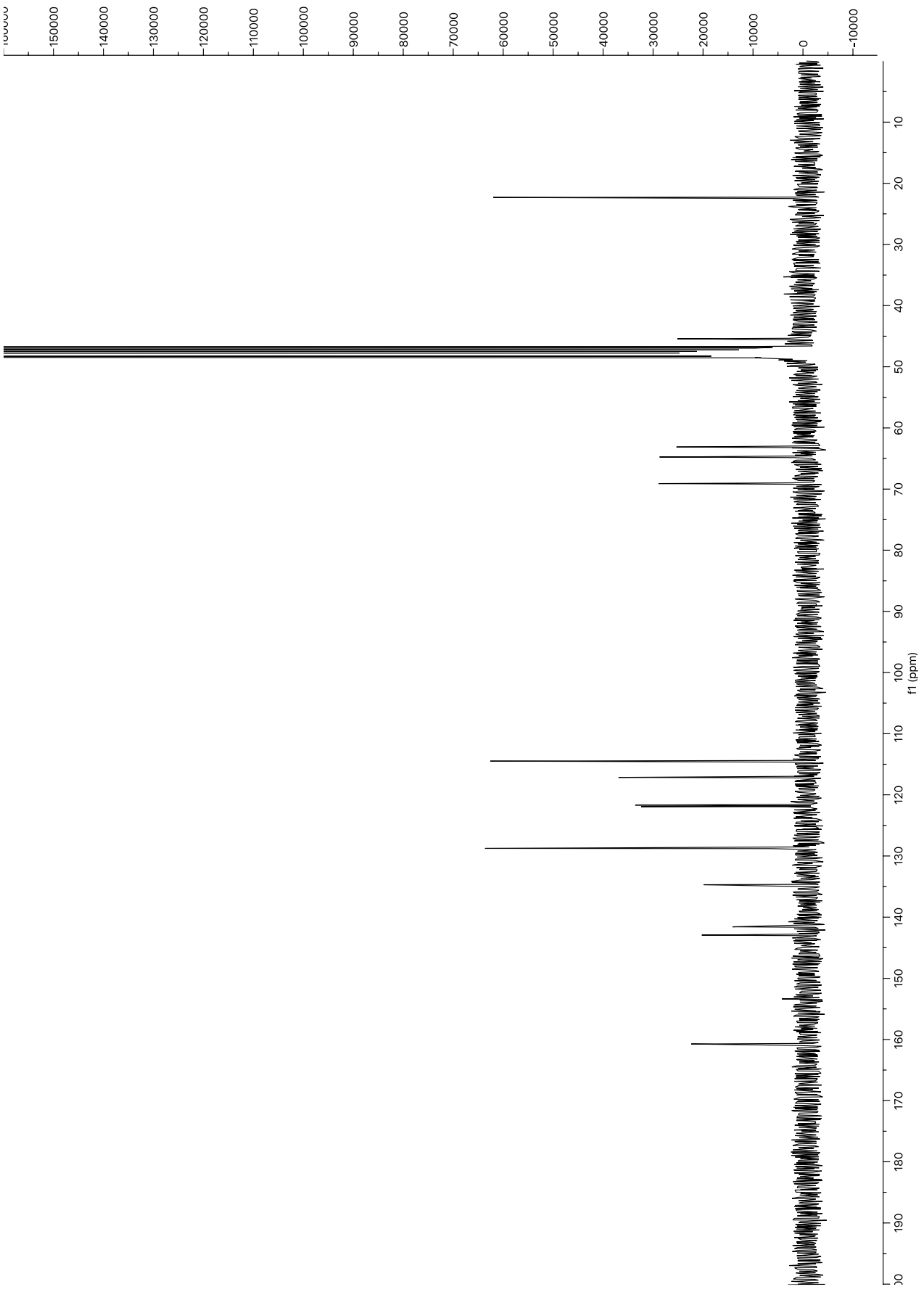
150000
140000
130000
120000
110000
100000
90000
80000
70000
60000
50000
40000
30000
20000
10000
0
-10000
10
20
30
40
50
60
70
80
90
100
110
120
130
140
150
160
170
180
190
f1 (ppm)

tert-butyl (4-hydroxyphenyl)carbamate

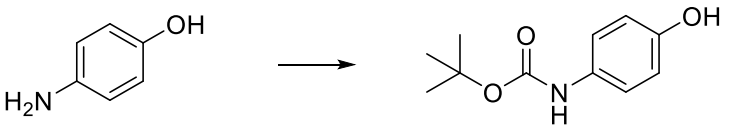

Chemical Formula:C_6H_7NO
MW: 109,13

Chemical Formula:$C_{11}H_{15}NO_3$
MW: 209,25

p-aminophenol (5.0 g, 45.82 mmol) was added to an ice-cooled solution of Boc_2O (11.0 g, 50.40 mmol) in tetrahydrofuran (50 mL). The reaction mixture was stirred for 12 hours at 0°C until TLC[20] indicated the disappearance of starting material. Afterward, the solvent was evaporated in vacuo and the crude was dissolved in ethyl acetate. The organic phase was washed with water and dried over anhydrous sodium sulfate, filtered, and evaporated in vacuo, affording 9.59 g (45.82 mmol) of the pure product as a white solid.

Yield = 100%

m.p. *145°C*

^{1}H NMR ($CDCl_3$): δ 7.18 (d, *J* = 8.8 Hz, 2H), 6.74 (d, *J* = 8.8 Hz, 2H), 6.32 (s, 1H), 1.50 (s, 9H).

[20] Cyclohexane/Ethyl acetate7:3. Rf starting material = 0.5, Rf product = 0.86.

tert-butyl (4-hydroxyethoxy)phenyl)carbamate

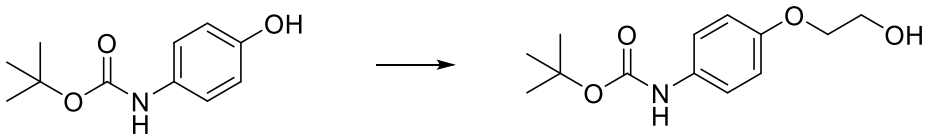

Chemical Formula:$C_{11}H_{15}NO_3$
MW: 209,25

Chemical Formula:$C_{13}H_{19}NO_4$
MW: 253,30

Ethylene carbonate (5.26 g, 59.73 mmol) and K_2CO_3 (8.26 g, 59.77 mmol) were added to a solution of tert-butyl (4-hydroxyphenyl)carbamate (5.0 g, 23.89 mmol) in 50 mL of DMF. The reaction mixture was stirred at reflux overnight[21]. Afterward, the solvent was evaporated in vacuo and the crude was dissolved in ethyl acetate. The organic phase was washed with 10% aqueous solution of NaOH, brine and then dried over anhydrous sodium sulfate, filtered, and evaporated in vacuo, affording a brownish oil. Flash chromatography (cyclohexane/ethyl acetate 8:2) was performed in order to obtain 3.27 g (12.93 mmol) of the pure product as a brown oil.

Yield = 54.1%

^{1}H NMR ($CDCl_3$): δ 7.18 (d, *J* = 8.9 Hz, 2H), 6.90 (d, *J* = 8.9 Hz, 2H), 4.05 (t, *J* = 4.5 Hz, 2H), 3.93 (t, *J* = 4.5 Hz, 2H), 2.75 (s, 1H), 1.50 (s, 9H).

[21] Cyclohexane/ethyl acetate 6:4. R_f starting material = 0.7; R_f product = 0.8.

2-(4-aminophenoxy)ethanol hydrochloride

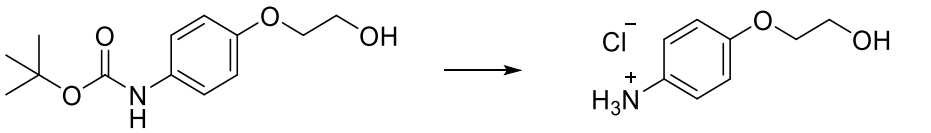

Chemical Formula:$C_{13}H_{19}NO_4$
MW: 253,30

Chemical Formula:$C_8H_{12}ClNO_2$
MW: 189,64

A solution of *tert*-butyl (4-hydroxyethoxy)phenyl)carbamate (610 mg, 2.41 mmol) in 5 mL of hydrogen chloride solution 2.0 M in methanol was stirred at reflux until TLC[22] indicated the disappearance of starting material. Afterward, the solvent was evaporated in vacuo affording 369 mg (1.94 mmol) of the desired product as a white solid.

Yield = 81%

m.p. *72°C*

^{1}H NMR (CD_3OD): δ 7.33 (d, *J* = 9.1 Hz, 2H), 7.11 (d, *J* = 9.1 Hz, 2H), 4.05 (t, *J* = 4.5 Hz, 2H), 3.93 (t, *J* = 4.5 Hz, 2H), 2.75 (s, 1H).

[22] Cyclohexane/Ethyl acetate6:4. R_f starting material = 0.8; R_f product = 0.

2-(4-methylsulfonamide)phenoxy)ethyl methanesulfonate

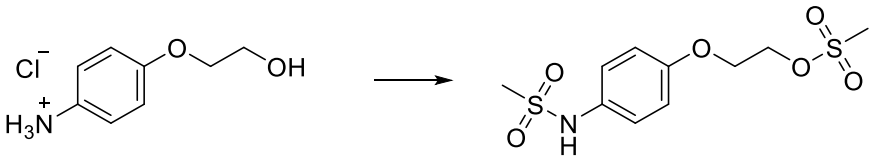

Chemical Formula:$C_8H_{12}ClNO_2$
MW: 189,64

Chemical Formula:$C_{10}H_{15}NO_6S_2$
MW: 309,35

Triethylamine (0.27 mL, 1.97 mmol) was added to a solution of 2-(4-aminophenoxy)ethanol (369 mg, 1.94 mmol) in dichloromethane (10 mL), and the reaction solution was stirred for 20 minutes. Then, triethylamine (0.55 mL, 3.94 mmol) and mesyl chloride (0.31 mL, 3.94 mmol) were added dropwise to the ice-cooled reaction solution. The mixture was stirred at room temperature until TLC[23] indicated the disappearance of starting material. Afterward, the reaction was diluted with dichloromethane and the organic phase was washed with 10% aqueous solution of HCl and then with brine. The organic phase was dried over anhydrous sodium sulfate and filtered and the solvent was evaporated in vacuo, providing the pure product as 402 mg of a white solid (1.30 mmol).

Yield = 53.3%

m.p. *137°C*

^{1}H NMR ($CDCl_3$): δ 7.21 (d, *J* = 7.9 Hz, 2H), 6.91 (d, *J* = 7.9 Hz, 2H), 4.57 (t, *J* = 3.6 Hz, 2H), 4.24 (t, *J* = 3.6 Hz, 2H), 3.10 (s, 3H), 2.96 (s, 3H).

[23] Dichloromethane/methanol 95:5 + 1% aq. NH_3. R_f starting material = 0.1; R_f product = 0.7

N-(4-(2-azidoethoxy)phenyl)methanesulfonamide

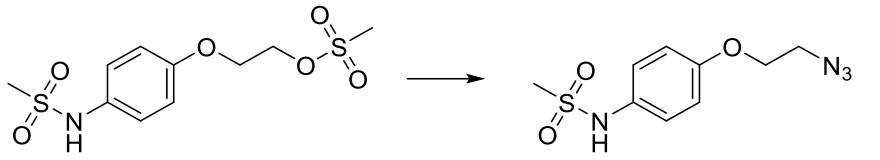

Chemical Formula:$C_{10}H_{15}NO_6S_2$
MW: 309,35

Chemical Formula:$C_9H_{12}N_4O_3S$
MW: 256,28

Sodium azide (832 mg, 12.80 mmol) was added to a solution of 2-(4-methylsulfonamide)phenoxy)ethyl methanesulfonate (396 mg, 1.28 mmol) in DMF (26 mL) and water (9 mL). Then, the mixture was refluxed, under stirring, until TLC[24] indicated the disappearance of starting material.

Afterward, the mixture was diluted with water and extracted with diethyl ether. The organic phase was dried over anhydrous sodium sulfate, filtered, and evaporated in vacuo, affording 219 mg (0.86 mmol) of the pure product as an orangish oil.

Yield = 67.2%

^{1}H NMR ($CDCl_3$): δ 7.22 (d, *J* = 8.9 Hz, 2H), 6.90 (d, *J* = 8.9 Hz, 2H), 4.13 (t, *J* = 5.0 Hz, 2H), 3.60 (t, *J* = 5.0 Hz, 2H), 2.91 (s, 3H).

[24] Dichloromethane/methanol 99:1 R_f starting material = 0.5; R_f product = 0.8

N-(4-(2-aminoethoxy)phenyl)methanesulfonamide

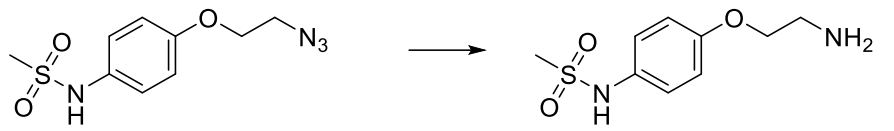

Chemical Formula:$C_9H_{12}N_4O_3S$
MW: 256,28

Chemical Formula:$C_9H_{14}N_2O_3S$
MW: 230,28

Palladium(II) oxide (13.47 mg, 0.11 mmol) and hydrazine hydrate (0.53 mL, 10.9 mmol) were added to a solution of N-(4-(2-azidoethoxy)phenyl)methanesulfonamide (841 mg, 2.96 mmol) in methanol (9 mL).

Then, the mixture was refluxed, under stirring, until TLC[25] indicated the disappearance of starting material. Afterward, the catalyst was removed by filtration, and methanol was evaporated in vacuo, affording 238 mg (1.03 mmol) of the pure product as a pale yellow solid.

Yield = 95.0%

^{1}H NMR (CD_3OD): δ 7.19 (d, *J* = 8.9 Hz, 2H), 6.94 (d, *J* = 8.9 Hz, 2H), 4.00 (t, *J* = 5.3 Hz, 2H), 3.01 (t, *J* = 5.3 Hz, 2H), 2.87 (s, 3H).

[25] Dichloromethane/methanol 90:10 + 1% aq. NH_3 R_f starting material = 0.62; R_f product = 0.09

[((2-(4-methylsulfonylamidephenoxy)ethyl)amino)-methyl]-1,4-benzodioxane

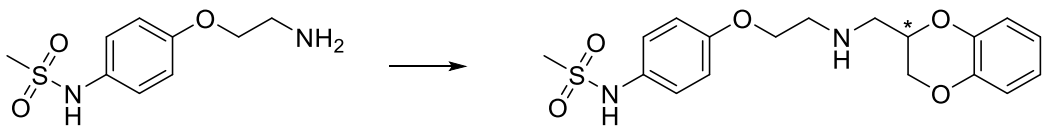

Chemical Formula:$C_9H_{14}N_2O_3S$
MW: 230,28

Chemical Formula:$C_{18}H_{22}N_2O_5S$
MW: 378,44

N-(4-(2-aminoethoxy)phenyl)methanesulfonamide (238 mg, 1.03 mmol) and 2-mesyloxymethyl-1,4-benzodioxane (229 mg, 0.94 mmol) were dissolved in 10 mL of 2-propanol. Triethylamine (0.13 mL, 0.94 mmol) was added to the solution and the resulting mixture was refluxed, under stirring, until TLC[26] indicated the disappearance of starting material. Afterward, the solvent was evaporated in vacuo, the crude was dissolved in dichloromethane and was washed with 10% aqueous solution of $NaHCO_3$ and water. The organic phase was dried over anhydrous sodium sulfate, filtered, and evaporated in vacuo, affording an orangish oil. Flash chromatography (dichloromethane/methanol 98:2 + 0.5% aq. NH_3) was performed in order to obtain 61 mg (0.16 mmol) of the pure product as a pale yellow oil.

Yield = 15.5%

^{1}H NMR ($CDCl_3$): δ 7.18 (d, *J* = 8.9 Hz, 2H), 6.97 – 6.80 (m, 6H), 4.41 – 4.25 (m, 2H), 4.12 – 4.00 (m, 3H), 3.11 – 3.05 (m, 2H), 3.03 – 2.92 (m, 5H).

[26]Dichloromethane/methanol 95:5 + 0.5% aq. NH_3 R_f starting material = 0.19; R_f product = 0.44.

Compound VI

[((2-(4-methylsulfonylamidephenoxy)ethyl)amino)-methyl]-1,4-benzodioxane hydrochloride

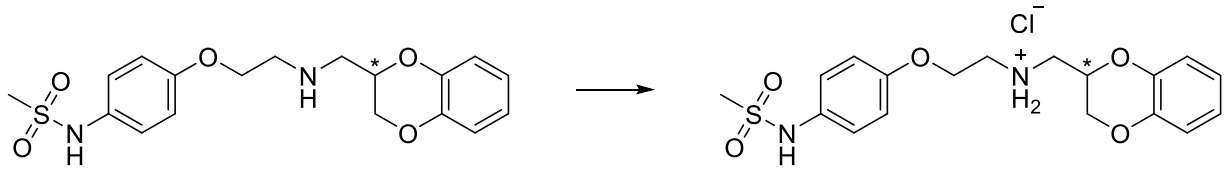

Chemical Formula: $C_{18}H_{22}N_2O_5S$
MW: 378,44

Chemical Formula: $C_{18}H_{23}ClN_2O_5S$
MW: 414,90

A solution of [((2-(4-methylsulfonylamidephenoxy)ethyl)amino)-methyl]-1,4-benzodioxane (61 mg, 0.16 mmol) in 2 mL of hydrogen chloride solution 2.0 M in diethyl ether was stirred overnight. The reaction mixture was diluted with ethyl ether, the solid was filtered and washed with cooled ethyl ether to obtain the desired product as a pale yellow solid (42.4 mg, 0.10 mmol).

Yield = 62.5%

m.p. 200°C (**decomposition**)

HRMS: *m/z* 379.1319 ($[M+H]^+$

^{1}H NMR (CD_3OD): δ 7.23 (d, *J* = 8.9 Hz, 2H), 7.06 – 6.83 (m, 6H), 4.63 (m, 1H), 4.40 – 4.29 (m, 3H), 4.06 (dd, *J* = 11.6, 6.4 Hz, 1H), 3.58 (t, *J* = 5.0 Hz, 2H), 3.55 – 3.34 (m, 2H), 2.89 (s, 3H).
^{13}C NMR (CD_3OD): δ 155.55, 142.93, 141.59, 131.74, 123.56, 121.90, 121.67, 117.17, 117.01, 115.08, 69.09, 64.77, 63.02, 37.39.

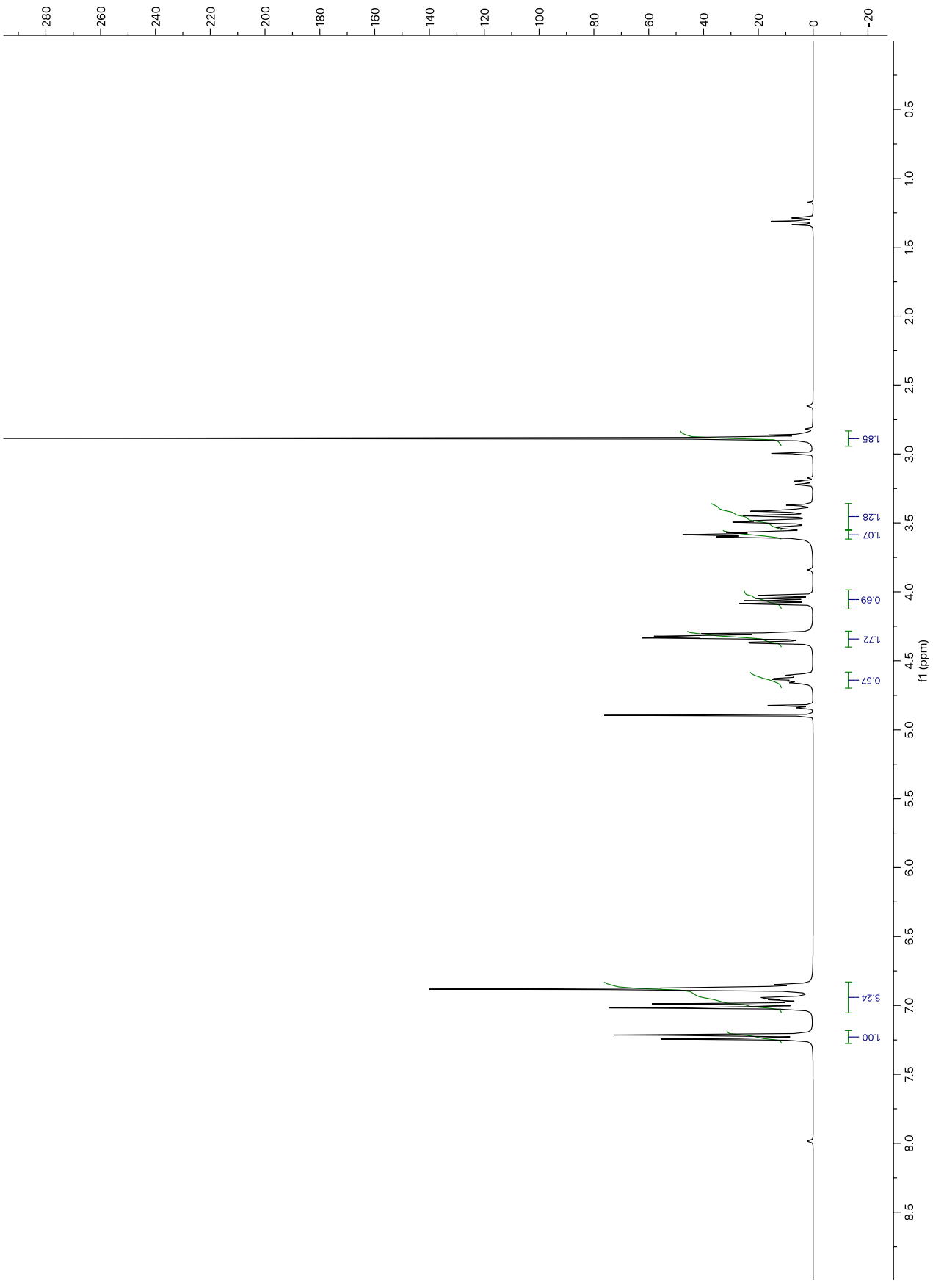
f1 (ppm)
1.85
1.28
1.07
0.69
1.72
0.57
3.24
1.00

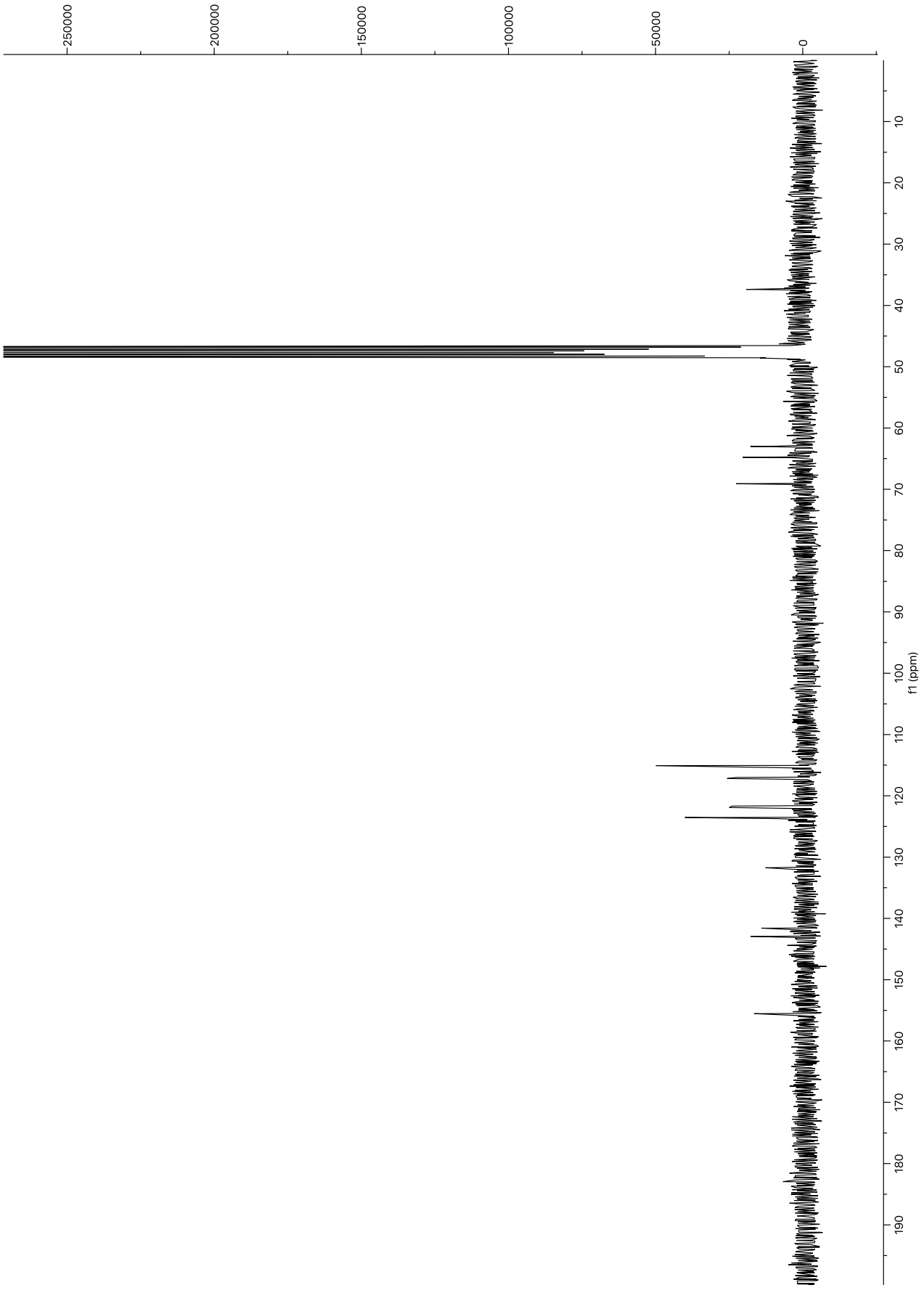
250000
200000
150000
100000
50000
0
10
20
30
40
50
60
70
80
90
100
110
120
130
140
150
160
170
180
190
f1 (ppm)

2-(4-((*tert*-butoxycarbonyl)amino)phenoxy)ethyl methanesulfonate

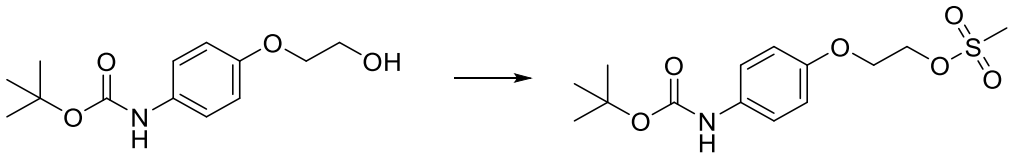

Tert-butyl (4-hydroxyethoxy)phenyl)carbamate (1.0 g, 3.95 mmol) was dissolved in dichloromethane (10 mL), triethylamine (0.66 mL, 4.74 mmol) was added, and after the reaction mixture was cooled down to 0°C mesyl chloride (0.37 mL, 4.74 mmol) was added dropwise. The solution was stirred at room temperature until TLC[27] indicated the disappearance of starting material. The reaction mixture was washed with 10% aqueous solution of HCl and then with brine. The organic phase was dried over anhydrous sodium sulfate and filtered and the solvent was evaporated in vacuo, providing the pure product as 1.31 g of a yellow oil (3.95 mmol).

Yield = 100%

m.p. *125°C*

^{1}H NMR ($CDCl_3$): δ 7.18 (d, *J* = 8.9 Hz, 2H), 6.90 (d, *J* = 8.9 Hz, 2H), 4.57 (t, *J* = 3.6 Hz, 2H), 4.24 (t, *J* = 3.6 Hz, 2H), 3.10 (s, 3H), 1.50 (s, 9H).

[27] Cyclohexane/ethyl acetate 6:4. R_f starting material = 0.8; R_f product = 0.8.

tert-butyl (4-(2-azidoethoxy)phenyl)carbamate

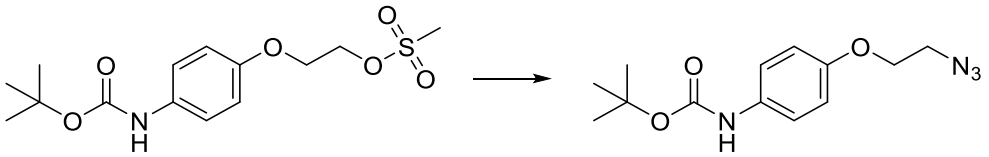

Chemical Formula:$C_{14}H_{21}NO_6S$
MW: 331,38

Chemical Formula:$C_{13}H_{18}N_4O_3$
MW: 278,31

Sodium azide (592 mg, 9.10 mmol) was added to a solution of 2-(4-((*tert*-butoxycarbonyl)amino)phenoxy)ethyl methanesulfonate (300 mg, 0.91 mmol) in DMF (18 mL) and water (6 mL). Then, the mixture was refluxed, under stirring, until TLC[28] indicated the disappearance of starting material.

Afterward, the mixture was diluted with water and extracted with diethyl ether. The organic phase was dried over anhydrous sodium sulfate, filtered, and evaporated in vacuo, affording 238 mg (0.85 mmol) of the pure product as an orangish oil.

Yield = 94.0%

^{1}H NMR ($CDCl_3$): δ 7.28 (d, *J* = 9.0 Hz, 2H), 6.86 (d, *J* = 9.0 Hz, 2H), 6.36 (s, 1H), 4.12 (t, *J* = 5.0 Hz, 2H), 3.58 (t, *J* = 5.0 Hz, 2H), 1.51 (s, 9H).

[28]Dichloromethane/methanol 99:1 R_f starting material = 0.34; R_f product = 0.7.

4-(2-azidoethoxy)aniline

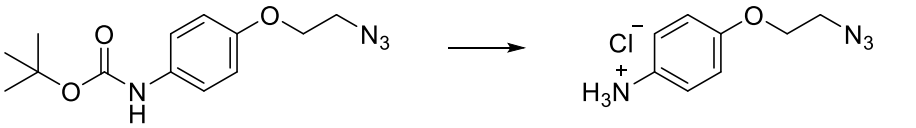

Chemical Formula: $C_{13}H_{18}N_4O_3$
MW: 278,31

Chemical Formula: $C_8H_{11}ClN_4O$
MW: 214,65

A solution of *tert*-butyl (4-(2-azidoethoxy)phenyl)carbamate (768 mg, 2.76 mmol) in 5.3 mL of hydrogen chloride solution 2.0 M in methanol was stirred at reflux until TLC[29] indicated the disappearance of starting material. Afterward, the solvent was evaporated in vacuo affording 491.83 mg (2.74 mmol) of the desired product as a white solid.

Yield = 99.4%

m.p. *72°C*

^{1}H NMR (CD_3OD): δ 7.33 (d, *J* = 9.1 Hz, 2H), 7.11 (d, *J* = 9.1 Hz, 2H), 4.21 (t, *J* = 5.0 Hz, 2H), 3.62 (t, *J* = 5.0 Hz, 2H).

[29] Cyclohexane/ethyl acetate 6:4 R_f starting material = 0.8; R_f product = 0.

N-(4-(2-azidoethoxy)phenyl)ethansulfonamide

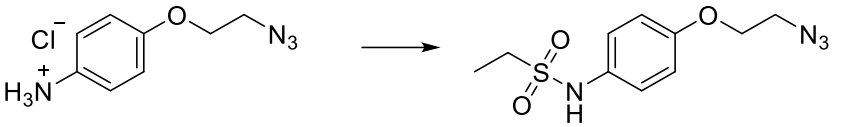

Chemical Formula:$C_8H_{11}ClN_4O$
MW: 214,65

Chemical Formula:$C_{10}H_{14}N_4O_3S$
MW: 270,31

Triethylamine (0.36 mL, 2.56 mmol) was added to a solution of 4-(2-azidoethoxy)aniline (369 mg, 1.94 mmol) in dichloromethane (10 mL), and the reaction solution was stirred for 20 minutes. Then, triethylamine (0.39 mL, 2.82 mmol) and ethanesulfonyl chloride (0.27 mL, 2.82 mmol) were added dropwise to the ice-cooled reaction solution. The mixture was stirred at room temperature until TLC[30] indicated the disappearance of starting material. Afterward, the reaction was diluted with dichloromethane and the organic phase was washed with 10% aqueous solution of HCl and then with brine. The organic phase was dried over anhydrous sodium sulfate and filtered and the solvent was evaporated in vacuo, providing the pure product as 590 mg of a red oil (2.18 mmol).

Yield = 71.0%

^{1}H NMR ($CDCl_3$): δ 7.20 (d, *J* = 8.9 Hz, 2H), 6.89 (d, *J* = 8.9 Hz, 2H), 6.51 (s, 1H), 4.13 (t, *J* = 4.9 Hz, 2H), 3.59 (t, *J* = 4.9 Hz, 2H), 3.06 (q, *J* = 7.4 Hz, 2H), 1.37 (t, *J* = 7.4 Hz, 3H).

[30]Dichloromethane/methanol 97:3 + 1% aq. NH_3. R_f starting material = 0.77; R_f product = 0.55.

N-(4-(2-aminoethoxy)phenyl)ethansulfonamide

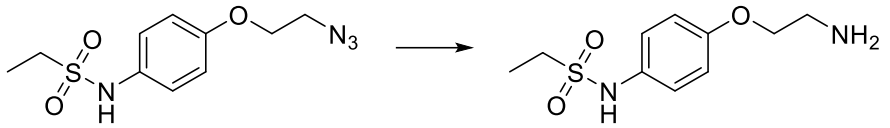

Chemical Formula:$C_{10}H_{14}N_4O_3S$
MW: 270,31

Chemical Formula:$C_{10}H_{16}N_2O_3S$
MW: 244,31

Palladium (II) oxide (26.93 mg, 0.22 mmol) and hydrazine hydrate (1.05 mL, 21.50 mmol) were added to a solution of N-(4-(2-azidoethoxy)phenyl)ethansulfonamide (580 mg, 2.15 mmol) in methanol (18 mL).

Then, the mixture was refluxed, under stirring, until TLC[31] indicated the disappearance of starting material. Afterward, the catalyst was removed by filtration, and methanol was evaporated in vacuo, affording 527 mg (2.15 mmol) of the pure product as a yellow oil.

Yield = 100%

^{1}H NMR (CD_3OD): δ 7.19 (d, *J* = 8.2 Hz, 2H), 6.93 (d, *J* = 8.2 Hz, 2H), 4.82 (s, 1H), 4.00 (t, *J* = 5.3 Hz, 2H), 3.05 – 2.95 (m, 4H), 1.30 (t, *J* = 7.4 Hz, 3H).

[31]Dichloromethane/methanol 90:10 + 1% aq. NH_3. R_f starting material = 0.58; R_f product = 0.16.

[((2-(4-ethylsulfonylamidephenoxy)ethyl)amino)-methyl]-1,4-benzodioxane

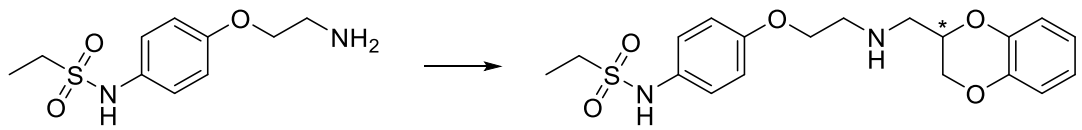

Chemical Formula:$C_{10}H_{16}N_2O_3S$
MW: 244,31

Chemical Formula:$C_{19}H_{24}N_2O_5S$
MW: 392,47

N-(4-(2-aminoethoxy)phenyl)ethansulfonamide (525 mg, 2.15 mmol) and 2-mesyloxymethyl-1,4-benzodioxane (477 mg, 1.95 mmol) were dissolved in 20 mL of 2-propanol. Triethylamine (0.27 mL, 1.95 mmol) was added to the solution and the resulting mixture was refluxed, under stirring, until TLC[32] indicated the disappearance of starting material. Afterward, the solvent was evaporated in vacuo, the crude was dissolved in dichloromethane dichloromethane in order to remove by filtration unreacted N-(4-(2-aminoethoxy)phenyl)ethansulfonamide. The organic phase was washed with 10% aqueous solution of $NaHCO_3$ and water and dried over anhydrous sodium sulfate, filtered, and evaporated in vacuo, affording an orangish oil. Flash chromatography (dichloromethane/methanol 95:5 + 0.5% aq. NH_3) was performed in order to obtain 114.0 mg (0.29 mmol) of the pure product as a pale yellow oil.

Yield = 13.5%

^{1}H NMR ($CDCl_3$): δ 7.17 (d, *J* = 8.9 Hz, 2H), 6.95 – 6.76 (m, 6H), 6.40 (s, 1H), 4.37 – 4.25 (m, 2H), 4.11 – 3.98 (m, 3H), 3.17 – 2.87 (m, 6H), 1.37 (t, *J* = 7.4 Hz, 3H).

[32] Dichloromethane/methanol 90:10 + 1% aq. NH_3. R_f starting material = 0.16, R_f product = 0.42.

Compound VII

[((2-(4-ethylsulfonylamidephenoxy)ethyl)amino)-methyl]-1,4-benzodioxane hydrochloride

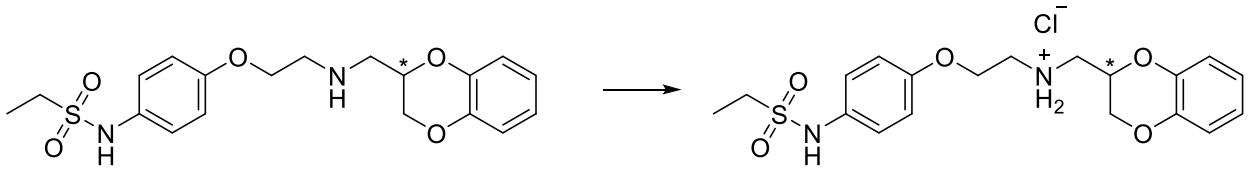

Chemical Formula:$C_{19}H_{24}N_2O_5S$
MW: 392,47

Chemical Formula:$C_{19}H_{25}ClN_2O_5S$
MW: 428,93

A solution of [((2-(4-ethylsulfonylamidephenoxy)ethyl)amino)-methyl]-1,4-benzodioxane (114 mg, 0.29 mmol) in 4 mL of hydrogen chloride solution 2.0 M in diethyl ether was stirred overnight. The reaction mixture was diluted with ethyl ether, the solid was filtered and washed with cooled ethyl ether to obtain the desired product as a pale yellow solid (21.6 mg, 0.05 mmol).

Yield = 17.2%

m.p. *192°C (*decomposition)

HRMS: *m/z* 393.1473 ($[M+H]^+$

^{1}H NMR (CD_3OD): δ 7.21 (d, *J* = 8.9 Hz, 2H), 7.02 – 6.81 (m, 6H), 4.62 (ddt, *J* = 9.5, 6.5, 2.8 Hz), 4.37 – 4.28 (m, 3H), 4.05 (dd, *J* = 11.6, 6.5 Hz, 1H), 3.58 (t, *J* = 5.0 Hz, 2H), 3.53 – 3.35 (m, 2H), 3.01 (q, *J* = 7.4 Hz, 2H), 1.30 (t, *J* = 7.4 Hz, 3H).

^{13}C NMR (CD_3OD): δ 155.26, 142.93, 141.59, 131.79, 123.00, 121.90, 121.66, 117.16, 117.01, 115.07, 69.08, 64.76, 63.01, 44.69, 6.96.

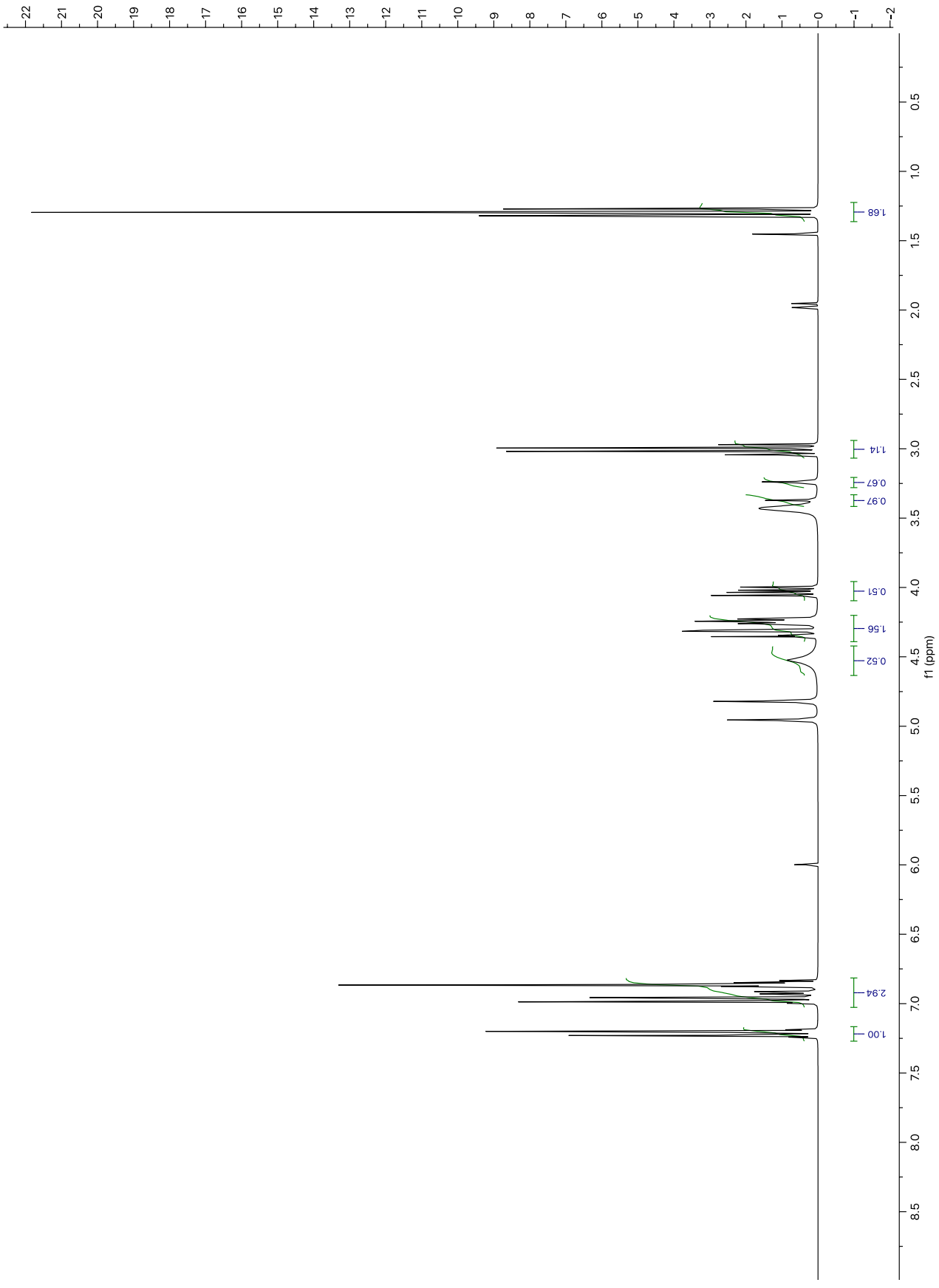
1.68
1.14
0.67
0.97
0.51
1.56
0.52
2.94
1.00
f1 (ppm)

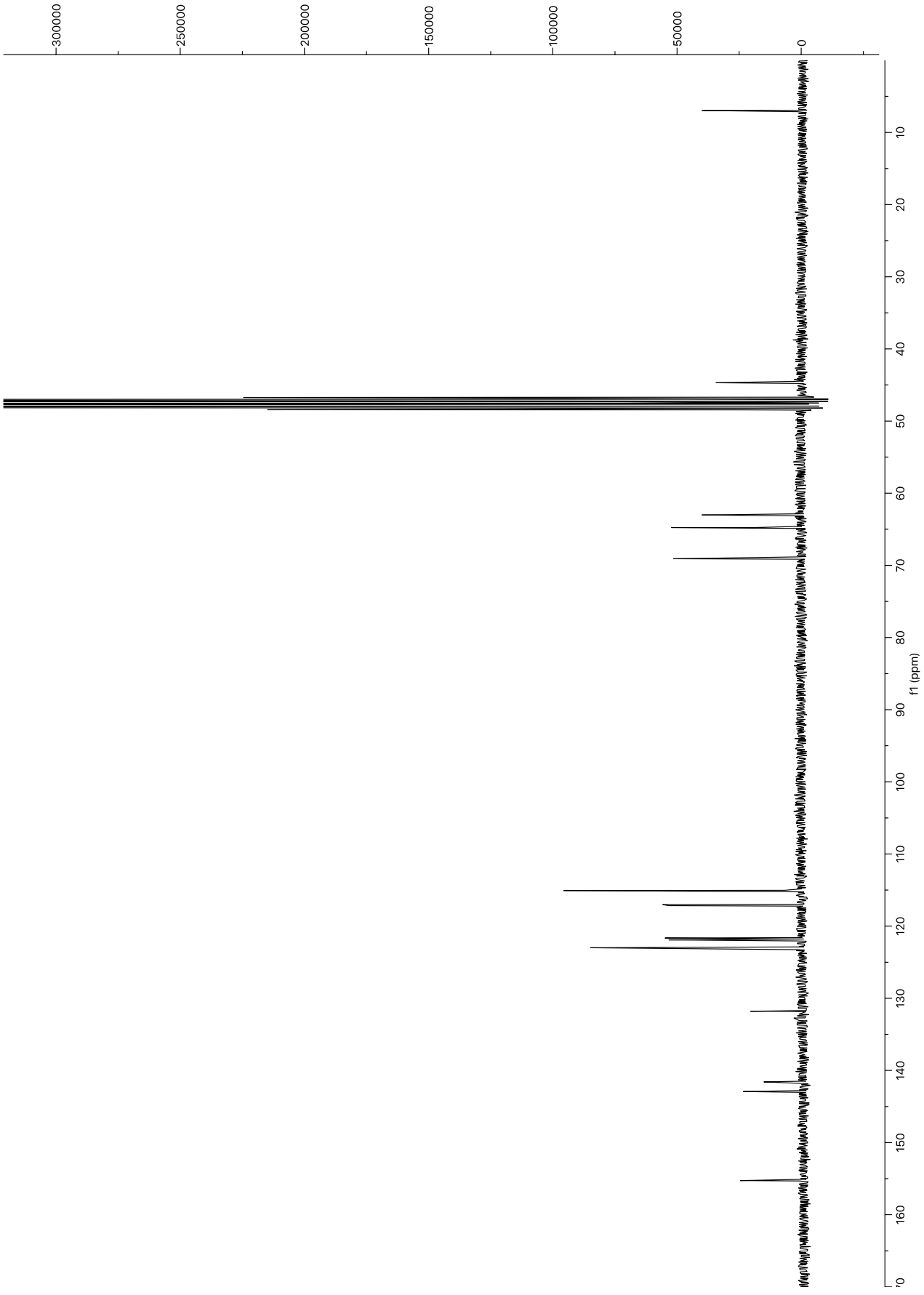
300000
250000
200000
150000
100000
50000
0
10
20
30
40
50
60
70
80
90
100
110
120
130
140
150
160
f1 (ppm)

N-(4-(2-azidoethoxy)phenyl)-2-methylpropan-1-sulfonamide

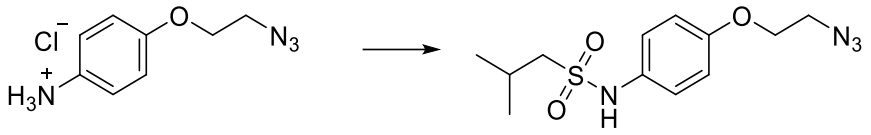

Chemical Formula:$C_8H_{11}ClN_4O$
MW: 214,65

Chemical Formula:$C_{12}H_{18}N_4O_3S$
MW: 298,36

Triethylamine (0.38 mL, 2.76 mmol) was added to a solution of 4-(2-azidoethoxy)aniline (593 mg, 3.33 mmol) in dichloromethane (10 mL), and the reaction solution was stirred for 20 minutes. Then, triethylamine (0.42 mL, 3.04 mmol) and isobutanesulfonyl chloride (0.4 mL, 3.04 mmol) were added dropwise to the ice-cooled reaction solution. The mixture was stirred at room temperature until TLC[33] indicated the disappearance of starting material. Afterward, the reaction was diluted with dichloromethane and the organic phase was washed with 10% aqueous solution of HCl and then with brine. The organic phase was dried over anhydrous sodium sulfate and filtered and the solvent was evaporated in vacuo, providing the pure product as 679 mg of a brown oil (2.28 mmol).

Yield = 68.5%

^{1}H NMR ($CDCl_3$): δ 7.19 (d, *J* = 8.9 Hz, 2H), 6.90 (d, *J* = 8.9 Hz, 2H), 6.50 (s, 1H), 4.14 (t, *J* = 4.9 Hz, 2H), 3.60 (t, *J* = 4.9 Hz, 2H), 2.92 (d, *J* = 6.7 Hz, 2H), 2.27 (m, 1H), 1.08 (d, *J* = 6.7 Hz, 6H).

[33]Dichloromethane/methanol 97:3 + 1% aq. NH_3. R_f starting material = 0.77, R_f product = 0.67.

N-(4-(2-aminoethoxy)phenyl)-2-methylpropan-1-sulfonamide

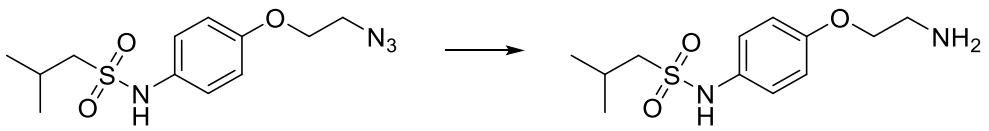

Chemical Formula:$C_{12}H_{18}N_4O_3S$
MW: 298,36

Chemical Formula:$C_{12}H_{20}N_2O_3S$
MW: 272,36

Palladium (II) oxide (28.16 mg, 0.23 mmol) and hydrazine hydrate (1.11 mL, 22.80 mmol) were added to a solution of N-(4-(2-azidoethoxy)phenyl)ethansulfonamide (679 mg, 2.28 mmol) in methanol (18 mL).

Then, the mixture was refluxed, under stirring, until TLC[34] indicated the disappearance of starting material. Afterward, the catalyst was removed by filtration, and methanol was evaporated in vacuo, affording 621 mg (2.28 mmol) of the pure product as an orange oil.

Yield = 100%

^{1}H NMR (CD_3OD): δ 7.17 (d, *J* = 8.5 Hz, 2H), 6.93 (d, *J* = 8.5 Hz, 2H), 4.00 (t, *J* = 5.3 Hz, 2H), 3.02 (t, *J* = 5.3 Hz, 2H), 2.87 (d, *J* = 6.7 Hz, 2H), 2.20 (m, 1H), 1.04 (d, *J* = 6.7 Hz, 6H).

[34]Dichloromethane/methanol 90:10 + 0.5% aq. NH_3. R_f starting material = 0.74, R_f product = 0.32.

[((2-(4-isobuthylsulfanilaminophenoxy)ethyl)amino)-methyl]-1,4-benzodioxane

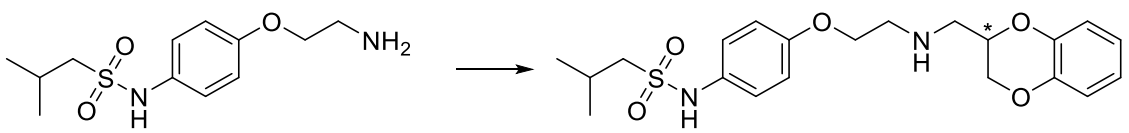

Chemical Formula:$C_{12}H_{20}N_2O_3S$
MW: 272,36

Chemical Formula:$C_{21}H_{28}N_2O_5S$
MW: 420,52

N-(4-(2-aminoethoxy)phenyl)-2-methylpropan-1-sulfonamide (658 mg, 2.42 mmol) and 2-mesyloxymethyl-1,4-benzodioxane (445 mg, 1.82 mmol) were dissolved in 20 mL of 2-propanol. Triethylamine (0.25 mL, 1.82 mmol) was added to the solution and the resulting mixture was refluxed, under stirring, until TLC[35] indicated the disappearance of starting material. Afterward, the solvent was evaporated in vacuo, the crude was dissolved in dichloromethane in order to remove by filtration unreacted N-(4-(2-aminoethoxy)phenyl)-2-methylpropan-1-sulfonamide. The organic phase was washed with 10% aqueous solution of $NaHCO_3$ and water and dried over anhydrous sodium sulfate, filtered, and evaporated in vacuo, affording an orangish oil. Flash chromatography (dichloromethane/methanol 97:3 + 0.5% aq. NH_3) was performed in order to obtain 150 mg (0.36 mmol) of the pure product as a pale yellow oil.

Yield = 14.9%

^{1}H NMR ($CDCl_3$): δ 7.16 (d, *J* = 8.9 Hz, 2H), 6.95 – 6.8 (m, 6H), 6.38 (s, 1H), δ 4.35 – 4.24 (m, 2H), 4.16 – 4.01 (m, 3H), 3.07 (t, *J* = 5.2 Hz, 2H), 3.02 – 2.84 (m, 4H), 2.28 (m, 1H), 1.08 (d, *J* = 6.8 Hz, 6H).

[35] Dichloromethane/methanol 90:10 + 0.5% aq. NH_3. R_f starting material = 0.32, R_f product = 0.44.

Compound VIII

[((2-(4-isobuthylsulfanilaminophenoxy)ethyl)amino)-methyl]-1,4-benzodioxane hydrochloride

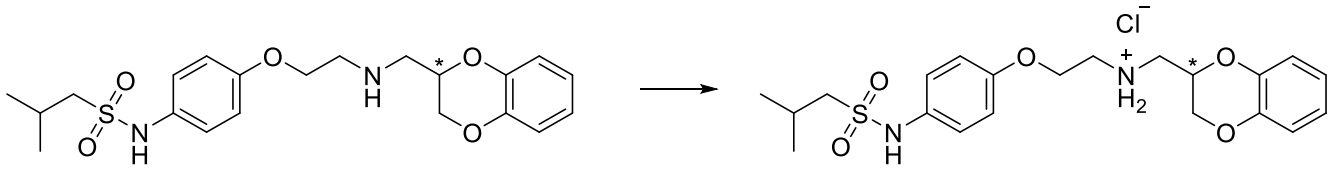

Chemical Formula:$C_{21}H_{28}N_2O_5S$
MW: 420,52

Chemical Formula:$C_{21}H_{29}ClN_2O_5S$
MW: 456,98

A solution of [((2-(4-isobuthylsulfanilaminophenoxy)ethyl)amino)-methyl]-1,4-benzodioxane (150 mg, 0.36 mmol) in 4.5 mL of hydrogen chloride solution 2.0 M in diethyl ether was stirred overnight. The reaction mixture was diluted with ethyl ether, the solid was filtered and washed with cooled ethyl ether to obtain the desired product as a pale yellow solid (165 mg, 0.36 mmol).

Yield = 100%

m.p. 206°C (**decomposition**)

HRMS: *m/z* 421.1785 ($[M+H]^+$

^{1}H NMR (CD_3OD): δ 7.21 (d, *J* = 8.9 Hz, 2H), 7.05 – 6.83 (m, 6H), δ 4.64 (ddt, *J* = 9.4, 6.5, 3.0 Hz, 1H), 4.37 – 4.27 (m, 3H), 4.06 (dd, *J* = 11.6, 6.5 Hz, 1H), 3.59 (t, *J* = 5.0 Hz, 2H), 3.56 – 3.37 (m, 2H), 2.89 (d, *J* = 6.4 Hz, 2H), 2.20 (m, 1H), 1.04 (d, *J* = 6.7 Hz, 6H).

^{13}C NMR (CD_3OD): δ 155.30, 142.93, 141.62, 131.75, 125.90, 122.98, 121.86, 121.65, 117.20, 116.99, 115.10, 69.09, 64.79, 63.03, 57.98, 24.53, 21.34.

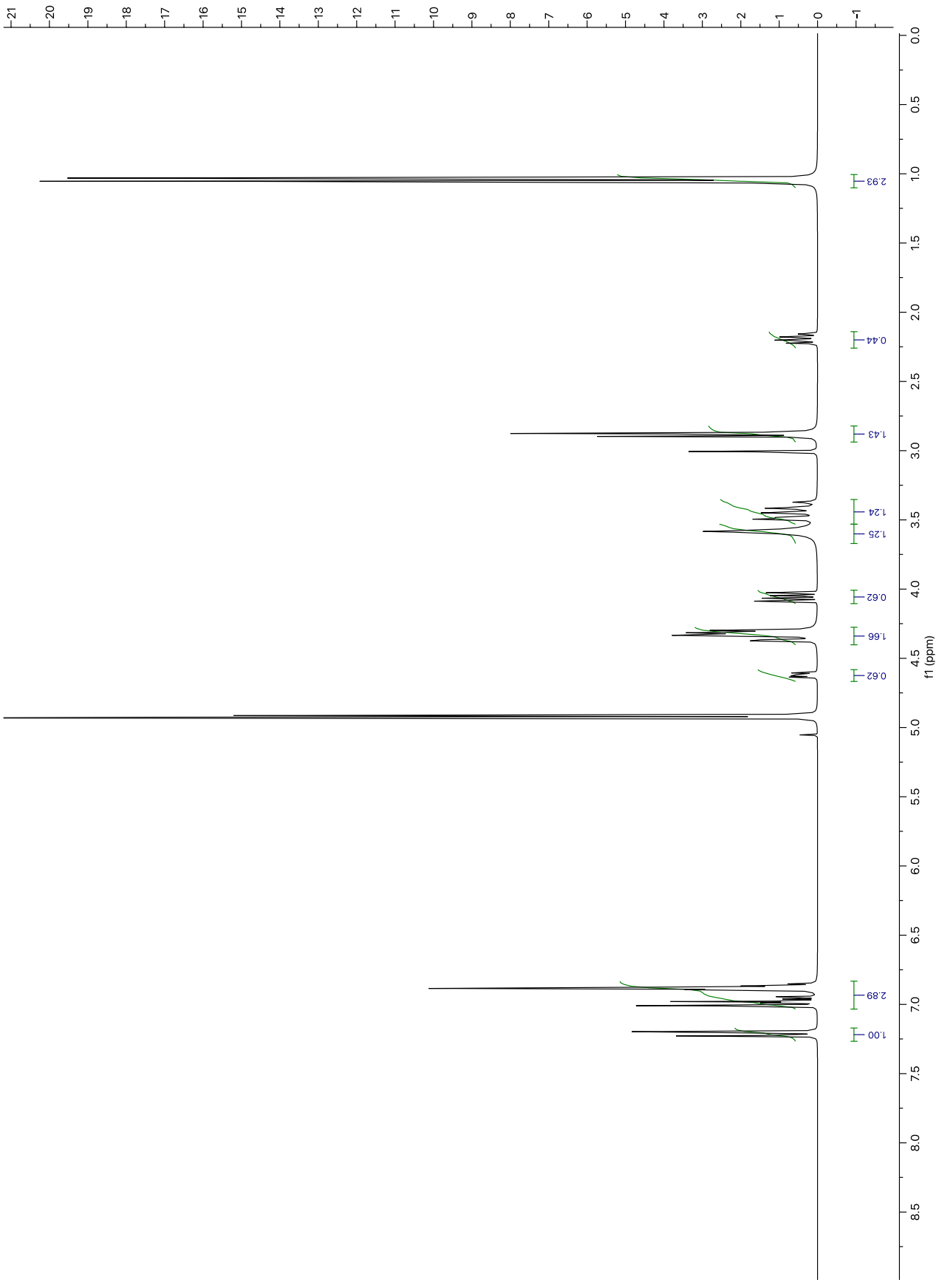
2.93
0.44
1.43
1.24
1.25
0.62
1.66
0.62
2.89
1.00
f1 (ppm)

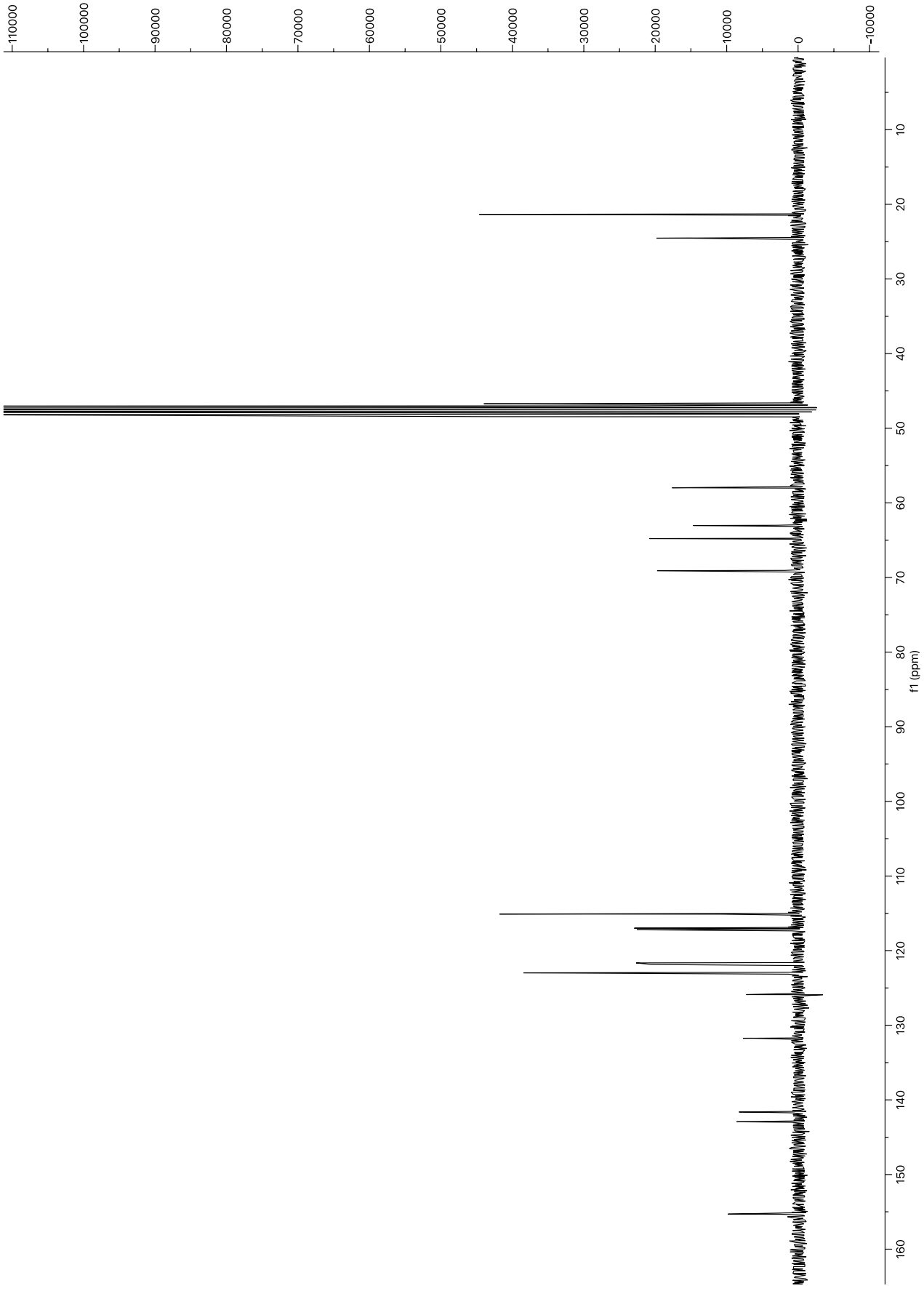
110000
100000
90000
80000
70000
60000
50000
40000
30000
20000
10000
0
-10000
10
20
30
40
50
60
70
80
90
100
110
120
130
140
150
160
f1 (ppm)

1,4-benzodioxan-2-carboxylic acid

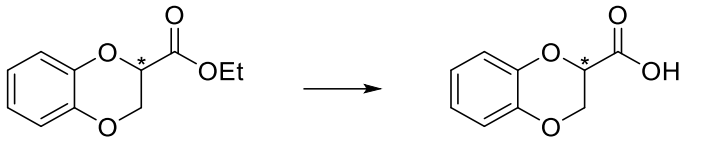

Chemical Formula:$C_{11}H_{12}O_4$
MW: 208,21

Chemical Formula:$C_9H_8O_4$
MW: 180,16

42 mL of NaOH 2.5M was added to a solution of ethyl-1,4-benzodioxan-2-carboxylate (14.0 g, 67.24 mmol) in methanol (56 mL). Afterward, the mixture was stirred at reflux until TLC[36] indicated the disappearance of starting material. Methanol was then evaporated under reduced pressure, and the residue acidified with diluted hydrochloric acid and extracted with dichloromethane. The organic layers were washed with brine, dried over anhydrous sodium sulfate. After evaporating to dryness under reduced pressure the pure product was obtained as a white solid (11.52 g, 63.94 mmol).

Yield: *95.1%*

m.p. *115°C*

^{1}H NMR ($CDCl_3$): δ 7.05-6.86 (m, 4H), 4.95-4.87 (m, 1H), 4.46-4.39 (dd, *J*=4.2, 0.6 Hz, 2H).

[36] Cyclohexane/ethyl acetate 7:3 + 1% formic acid. R_f starting material: 0.65, R_f product: 0.23.

N-methoxy-N-methyl-1,4-benzodioxan-2-carboxamide

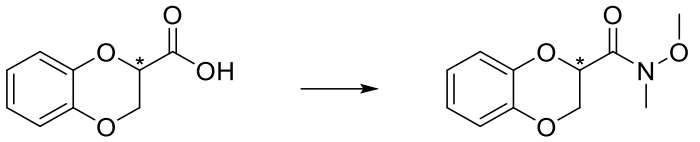

Chemical Formula:$C_9H_8O_4$
MW: 180,16

Chemical Formula:$C_{11}H_{13}NO_4$
MW: 223,23

Thionyl chloride (3.26 mL, 44.74 mmol) was added dropwise to an ice-cooled solution of 1,4-benzodioxan-2-carboxylic acid (4.03 g, 22.37) in 40 mL of dichloromethane. The mixture was stirred at reflux until NMR[37] indicated the disappearance of starting material. Afterward, the solvent was evaporated in vacuo, the crude was dissolved in 30 mL dichloromethane and cooled down to 0°C. Then N-dimethylhydroxylamine hydrochloride (3.27 g, 33.56 mmol) was slowly added in small amounts to the mixture and the reaction was stirred until TLC[38] indicated the disappearance of starting material. Afterward, the reaction was diluted with additional dichloromethane, washed three times with 10% aqueous solution of $NaHCO_3$ and brine, dried over Na_2SO_4, filtered. The solvent was then evaporated in vacuo, providing the pure product as a yellow solid (4.69 g, 21.00 mmol).

Yield: *93.9%*

m.p. *87°C*

^{1}H NMR ($CDCl_3$): δ 7.04-6.81 (m, 4H), 5.12-4.98 (m, 1H), 4.44 (dd, *J*=11.4, 2.5 Hz, 1H), 4.26 (dd, *J*=11.4, 7 Hz, 1H), 3.8 (s, 3H), 3.27 (s, 3H).

[37] ^{1}H NMR ($CDCl_3$): δ 7.07-6.86 (m, 4H), 5.10 (m, 1H), 4.75 (dd, *J*=11.8, 2.8 Hz, 1H), 4.34 (dd, *J*=11.8, 2.8 Hz, 1H)
[38] Cyclohexane/ethyl acetate 7:3 + 1% formic acid. R_f starting material: 0.23, R_f product: 0.5.

1,4-benzodioxan-2-carboxyaldehyde

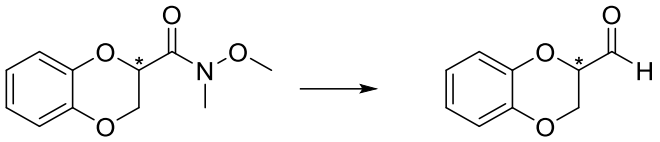

Chemical Formula:$C_{11}H_{13}NO_4$
MW: 223,23

Chemical Formula:$C_9H_8O_3$
MW: 164,16

Under nitrogen atmosphere, a solution of N-methoxy-N-methyl-1,4-benzodioxan-2-carboxamide (2 g, 8.46 mmol) in 32 mL of tetrahydrofuran was added dropwise to a suspension of 425 mg of $LiAlH_4$ (11.20 mmol) in tetrahydrofuran (8 mL) cool down to -20°C. The reaction mixture was stirred at the same temperature until TLC[39] indicated the disappearance of starting material. Afterward, the excess of $LiAlH_4$ was quenched by slowly adding 10% aqueous solution of HCl and diluted with dichloromethane. After the separation of the phases, the aqueous layer was further extracted with dichloromethane. The reunited organic phases were washed with brine, dried over anhydrous sodium sulfate, and filtered. The solvent was evaporated in vacuo, providing the pure product as a yellow oil (1.38 g, 8.46 mmol).

The neat product quickly degraded at room temperature but was stable for several days if dissolved in dichloromethane (ca. 20% w/v).

Yield: *100.0%*

^{1}H NMR ($CDCl_3$): δ 9.77 (s, 1H), 7.09-6.78 (m, 4H), 4.69-4.56 (m, 1H), 4.35 (dd, *J*=4.5, 1.0 Hz, 2H).

[39] Cyclohexane/ethyl acetate 7:3. R_f starting material: 0.5, R_f product: 0.55.

Ethyl 3-(1,4-benzodioxan)-3-hydroxypropanoate

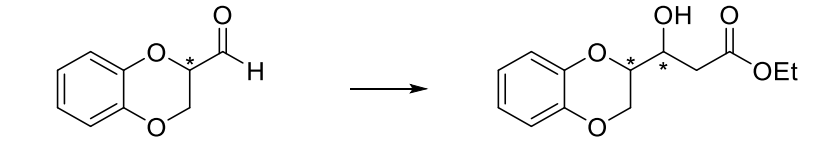

Chemical Formula:$C_9H_8O_3$
MW: 164,16

Chemical Formula:$C_{13}H_{16}O_5$
MW: 252,27

Under nitrogen atmosphere, 1.21 g of zinc (18.52 mmol) and 209 mg of TBDMSiCl (1.39 mmol) were suspended in 12 mL of tetrahydrofuran. The mixture was stirred at 50°C for 40 minutes. Then, a solution of 1.52 g of 1,4-benzodioxan-2-carboxyaldehyde (9.26 mmol) and 1.54 mL of ethyl bromoacetate (13.89 mmol) in 24 mL of tetrahydrofuran was added dropwise to the suspension. The reaction mixture was stirred at 50°C until TLC[40] indicated the disappearance of starting material. Afterward, the solution was diluted with ethyl acetate and the organic layer was sequentially washed with 10% aqueous solution of HCl, 10% aqueous solution of $NaHCO_3$, saturated solution of Na_2SO_3, and finally with brine. The organic phase was dried over anhydrous sodium sulfate, filtered and the solvent was evaporated in vacuo, providing the pure product as a yellow oil (2.08, 8.24 mmol).

Yield: *89.0%*

^{1}H NMR ($CDCl_3$): δ 6.99-6.71 (m,4H), 4.42 (dd, *J*=11.3, 2.2 Hz,1H), 4.27-4.00(m, 4H), 2.89 (dd, *J*=17.0, 2.8 Hz), 1H), 2.62 (dd, *J*=17.0, 8.6 Hz, 1Hz), 1.29 (t, *J*=7.2 Hz, 3H).

[40] Cyclohexane/ethyl acetate 8:2. R_f starting material: 0.31, R_f product: 0.53.

1-(1,4-benzodioxan)-1,3-propanediol

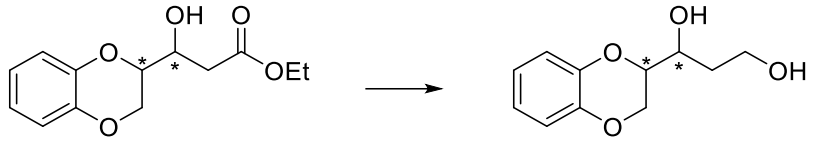

Chemical Formula:$C_{13}H_{16}O_5$
MW: 252,27

Chemical Formula:$C_{11}H_{14}O_4$
MW: 210,23

Under nitrogen atmosphere, a solution of ethyl 3-(1,4-benzodioxan)-3-hydroxypropanoate (1.59 g, 6.30 mmol) in 20 mL of tetrahydrofuran was added dropwise to a suspension of 298 mg of $LiAlH_4$ (7.87 mmol) in tetrahydrofuran (5 mL) cooled down to -10°C. The reaction mixture was stirred at the same temperature until TLC[41] indicated the disappearance of starting material. Afterward, the excess of $LiAlH_4$ was quenched by slowly adding 10% aqueous solution of HCl and diluted with dichloromethane. After the separation of the phases, the aqueous layer was further extracted with dichloromethane. The reunited organic phases were washed with brine, dried over anhydrous sodium sulfate, and filtered. The solvent was evaporated in vacuo, affording a yellow oil. Flash chromatography (cyclohexane/ethyl acetate 1:1) was performed in order to obtain 630 mg (2.99 mmol) of the two pure diastereomers as a white solid.

Yield: *47.5%*

m.p. 61°C

^{1}H NMR (CD_3OD): δ 6.93-6.65 (m, 4H), 4.37 (dd, *J*=11.3, 2.1 Hz, 1H), 4.07, *J*=11.3, 6.9 Hz, 1H), 4.00-3.82 (m, 2H), 3.76 (dd, *J*=7.5, 5.7 Hz, 2H), 2.12-1.94(m, 1H), 1.78-1.61(m, 1H).

^{1}H NMR (CD_3OD): δ 6.91-6.74 (m, 4H), 4.32 (dd, *J*=10.4, 1.1 Hz, 1H), 4.13-3.92 (m, 3H), 3.75 (t, *J*=6.3, 2H), 1.93-1.81(m, 2H).

[41] Cyclohexane/ethyl acetate 1:1. R_f starting material: 0.76, R_f product: 0.36, 0,34.

1-(1,4-benzodioxan)-3-trityloxy-1-propanol

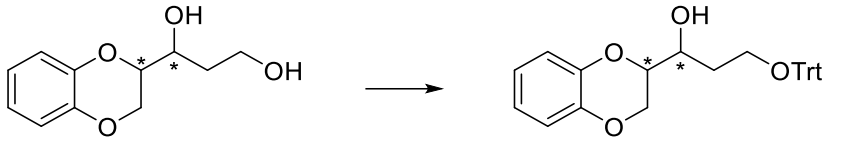

Chemical Formula:$C_{11}H_{14}O_4$
MW: 210,23

Chemical Formula:$C_{30}H_{28}O_4$
MW: 452,55

Triethylamine (0.50 mL, 3.52 mmol) was added dropwise to an ice-cooled solution of 673 mg of 1-(1,4-benzodioxan)-1,3-propanediol (3.20 mmol) was dissolved in 10 mL of dichloromethane. The reaction mixture was warmed to room temperature, then a solution of trityl chloride (981 g, 3.52 mmol) in 15 mL of dichloromethane was added dropwise to the solution. Then, the mixture was stirred, until TLC[42] indicated the disappearance of starting material.

Afterward, the mixture was diluted with dichloromethane, and the organic phase was washed with brine, dried over anhydrous sodium sulfate, filtered, and evaporated in vacuo, affording 1.39 g (3.07 mmol) of the pure product as a brown oil.

Yield: *95.9%*

^{1}H NMR (CD_3OD): δ 7.48-7.03 (m, 15H), 6.92-6.72 (m,4H), 4.34 (dd, *J*=11.3, 2.1 Hz, 1H), 4.08 (dd, *J*=11.3, 6.6 Hz, 1H), 4.02-3.83(m, 2H), 3.37-3.20 (m,2H), 2.20-2.03 (m, 1H), 1.76 (m, 1H).

[42] Cyclohexane/ethyl acetate 1:1. R_f starting material: 0.36, R_f product: 0.92.

1-azido-1-(1,4-benzodioxan)-3-trityloxypropane

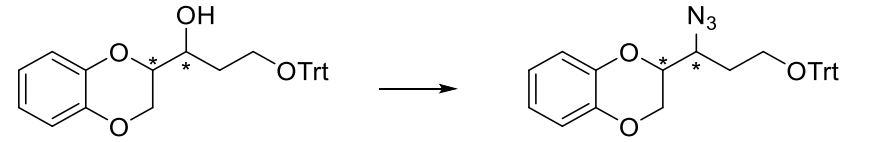

Chemical Formula:$C_{30}H_{28}O_4$
MW: 452,55

Chemical Formula:$C_{30}H_{27}N_3O_3$
MW: 477,56

Nitrogen was bubbled in a solution of 1-(1,4-benzodioxan)-3-trityloxy-1-propanol (1.23 g, 2.83 mmol) in 22 mL of dry toluene for 15 minutes. Then, triphenyl phosphine (816 mg, 3.11 mmol) and diethyl azodicarboxylate solution 40 wt. % in toluene (2.57 mL, 5.66 mmol) were added to the ice-cooled solution. After the reaction mixture was stirred at 0°C for an hour, 1.22 mL of DPPA (5.66 mmol) was added dropwise. The reaction mixture was warmed to room temperature and stirred until TLC[43] indicated the disappearance of starting material. Afterward, the solvent was evaporated in vacuo, affording an orangish oil. Flash chromatography (cyclohexane/ethyl acetate 9:1) was performed in order to obtain 430 mg (0.90 mmol) of the pure product as a white oil.

Yield: *31.8%*

^{1}H NMR (CD_3OD): δ 7.56-7.09(m, 15H), 6.94-6.72 (m,4H), 4.30 (d, *J*=9.1 Hz, 1H), 4.21-4.01 (m, 2 Hz), 3,88-3,72 (m, 1H), 2.14-1.94 (m, 1H), 1,94-1,75 (m, 1H).

[43] Cyclohexane/ethyl acetate 9:1. R_f starting material: 0.23, R_f product: 0.67.

3-azido-3-(1,4-benzodioxan)-1-propanol

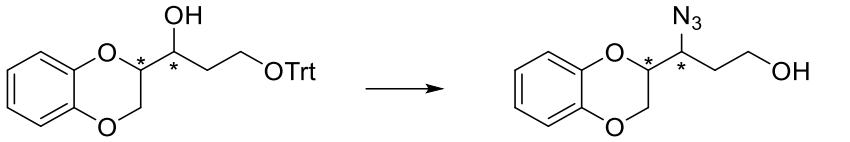

Chemical Formula:$C_{30}H_{28}O_4$
MW: 452,55

Chemical Formula:$C_{11}H_{13}N_3O_3$
MW: 235,24

600 mg of Amberlyst 15 was added to a solution of 1-azido-1-(1,4-benzodioxan)-3-trityloxypropane (450 mg, 0.99 mmol) in 19 mL of methanol and 8 mL of dichloromethane. Then, the mixture was stirred at reflux until TLC[44] indicated the disappearance of starting material. Afterward, the solvent was evaporated in vacuo, affording a grey oil. Flash chromatography (cyclohexane/ethyl acetate 7:3) was performed in order to obtain 96 mg (0.41 mmol) of the pure product as an orange oil.

Yield: *41.4%*

^{1}H NMR (CD_3OD): δ 6.88-6.69 (m, 4H), 4.27 (dd, *J*=11.2, 2.2 Hz, 1H), 4.23-4.13 (m, 1H), 4.07 (dd, *J*=11.2, 7.1 Hz, 1H), 3.81-3.58 (m, 3H), 1.98-1.85 (m, 2H).

[44] Cyclohexane/ethyl acetate 9:1. R_f starting material: 0.67, R_f product: 0.17.

1-azido-1-(1,4-benzodioxan)-propylmethanesulfonate

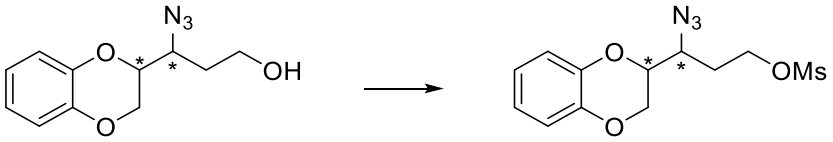

Chemical Formula:$C_{11}H_{13}N_3O_3$
MW: 235,24

Chemical Formula:$C_{12}H_{15}N_3O_5S$
MW: 313,33

3-azido-3-(1,4-benzodioxan)-1-propanol (300 mg, 1.43 mmol) was dissolved in dichloromethane (12 mL), triethylamine (0.20 mL, 1.68 mmol) was added, and after the reaction mixture was cooled down to 0°C mesyl chloride (0.13 mL, 1.68 mmol) was added dropwise. The solution was stirred at room temperature until TLC[45] indicated the disappearance of starting material. The reaction mixture was washed with 10% aqueous solution of HCl and then with brine. The organic phase was dried over anhydrous sodium sulfate and filtered and the solvent was evaporated in vacuo, providing the pure product as 413 mg of a yellow oil (1.32 mmol).

Yield: *92.3%*

^{1}H NMR (CD_3OD): 6.96-6.76 (m, 4H), 4.42 (dd, *J*=7.1, 5.0 Hz, 2H), 4.37-4.18 (m, 2H), 4.13 (dd, *J*=11.3, 6.8 Hz, 1H), 3.83-3.68 (m, 1H), 3.10 (s, 3H), 2.24-1.97 (m, 2H).

[45] Dichloromethane/methanol 95:5. R_f starting material = 0.40; R_f product = 0.78.

4-hydroxybenzensulfonamide

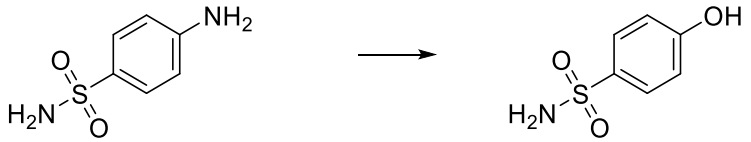

Chemical Formula:$C_6H_8N_2O_2S$
MW: 172,20

Chemical Formula:$C_6H_7NO_3S$
MW: 173,19

At 0°C, 5 g of sulfanilamide (29 mmol) was dissolved in water (40 mL) and concentrated sulfuric acid (20 mL). Then, a solution of sodium nitrite (2g, 29 mmol) in 20 mL of water was added dropwise, and the reaction was stirred at reflux until the evolution of nitrogen ceased.

The mixture was cooled down to room temperature and was kept overnight at 4°C. Afterward, the crystals of 4-hydroxybenzensulfonamide (3.78 g, 21.83 mmol) were collected by filtration.

Yield: *75.28%*

m.p. *175°C*

^{1}H NMR ($CDCl_3$): δ 7.73 (d, *J*=8.8 Hz, 2H), 6.87 (d, *J*=8.8 Hz, 2H).

N,N-dimethylaminomethylene-4-hydroxybenzenesulfonamide

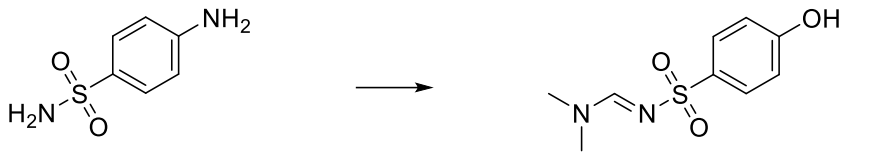

Chemical Formula:$C_6H_8N_2O_2S$
MW: 172,20

Chemical Formula:$C_9H_{12}N_2O_3S$
MW: 228,27

N,N-dimethylformamide dimethyl acetal (3.87 mL, 29.12 mmol) was added to a solution of 4-hydroxybenzenesulfonamide (4.20 g, 24.27 mmol) in DMF (4 mL) at 0°C and that was stirred for 2 hours at RT. The reaction mixture was treated with ethyl acetate, and the obtained white solid was filtered to afford the titled compound (5.21 g, 22.82 mmol).

Yield: 94.0%

m.p. *178°C*

^{1}H NMR (CD_3OD): δ 8.12 (s)

N,N-dimethylaminomethylene-4-(3-azido-3-(1,4-benzodioxan)-propoxy)benzenesulfonamide

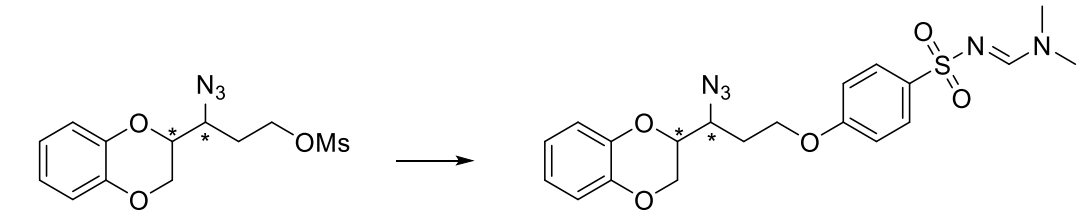

Chemical Formula:$C_{12}H_{15}N_3O_5S$
MW: 313,33

Chemical Formula:$C_{20}H_{23}N_5O_5S$
MW: 445,49

N,N-dimethylaminomethylene-4-hydroxybenzenesulfonamide (18 mg, 0.077mmol) was treated with 12 mg K_2CO_3 (0.080 mmol) in 0.5 mL DMF and the suspension was stirred at rt for 30 minutes under a nitrogen atmosphere. Then a solution of 1-azido-1-(1,4-benzodioxan)-propylmethanesulfonate (22 mg, 0.07 mmol) in DMF (1 mL) was added dropwise and the reaction was stirred at 40°C until starting material was consumed (TLC monitoring)[46].

The reaction mixture was quenched with cold water and the precipitate formed was collected by filtration, dried under vacuo to afford 25 mg (0.056 mmol).

Yield: 80.2%

m.p. *178°C*

^{1}H NMR ($CDCl_3$): δ 8.12 (s, 1H), 7.83 (d, *J*=8.8 Hz, 2H), 6.99-6.82 (m, 6H), 4.25 (m, 5H), 3.83 (m, 1H), 3.12 (s, 2H), 3.01 (s, 2H), 2.20 (m, 2H).

[46] Dichloromethane/methanol 98:2. R_f starting material = 0.71; R_f product = 0.56.

Compound IX

4-(3-azido-3-(1,4-benzodioxan)propoxy)benzenesulfonamide

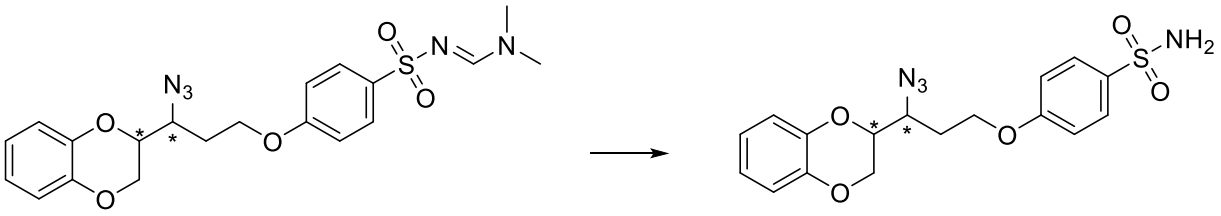

Chemical Formula:$C_{20}H_{23}N_5O_5S$
MW: 445,49

Chemical Formula:$C_{17}H_{18}N_4O_5S$
MW: 390,41

Hydrazine monohydrate (0.52 µL, 1.09 mmol) was added at room temperature to a stirred mixture of 52 mg of N,N-dimethylaminomethylene-4-(3-azido-3-(1,4-benzodioxan)-propoxy)benzene sulfonamide (0.109 mmol) in methanol (1.5 mL). The reaction mixture was stirred until starting material was consumed (TLC monitoring)[47]. Then the solvent was removed in order to obtain 45 mg of the pure product (0.109 mmol) as a pale yellow solid.

Yield: 100%

m.p. 107°C

HRMS: *m/z* 389.0923 ($[M+H]^-$

^{1}H NMR (CD_3OD): δ 7.93-7.79 (d, *J*=9.0 Hz, 2H), 7.15-7.05 (d, *J*=9.0 Hz, 2 H), 7.15-7.05 (m, 4H), 4.61-4.25 (m, 5H), 3.91-3.67 (m, 1H), 2.51-2.35 (m, 1H), 2.37-2.22 (m,1H).

^{13}C NMR (CD_3OD): δ 161.52, 143.27, 142.63, 135.63, 127.85, 121.35, 121.29, 116.87, 116.79, 116.69, 114.23, 75.63, 65.07, 64.46, 58.35, 29.31.

[47] Dichloromethane/methanol 98:2. R_f starting material = 0.56; R_f product = 0.44.

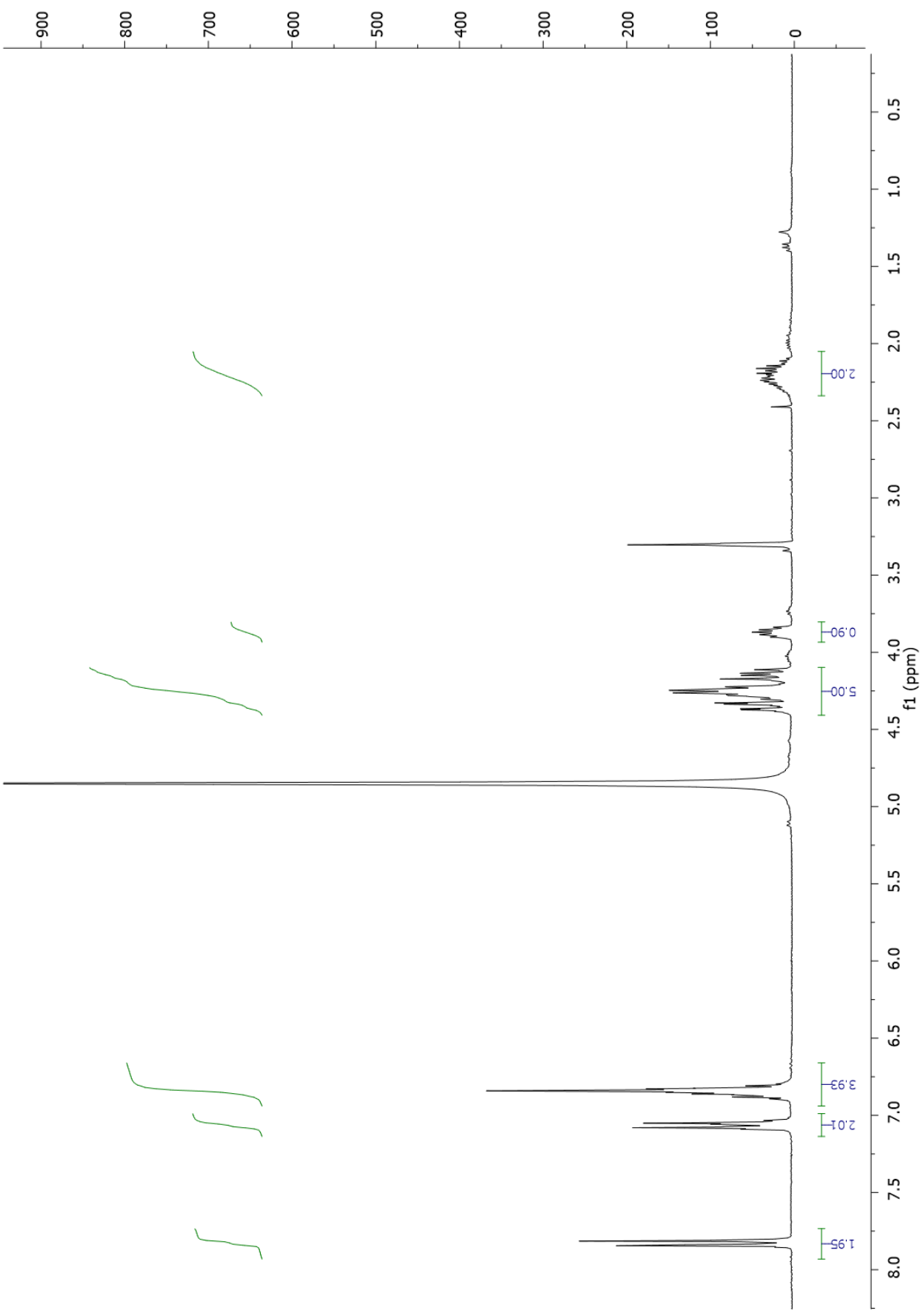
900
800
700
600
500
400
300
200
100
0
0.5
1.0
1.5
2.0
2.5
3.0
3.5
4.0
4.5
5.0
5.5
6.0
6.5
7.0
7.5
8.0
f1 (ppm)
2.00
0.90
5.00
3.93
2.01
1.95

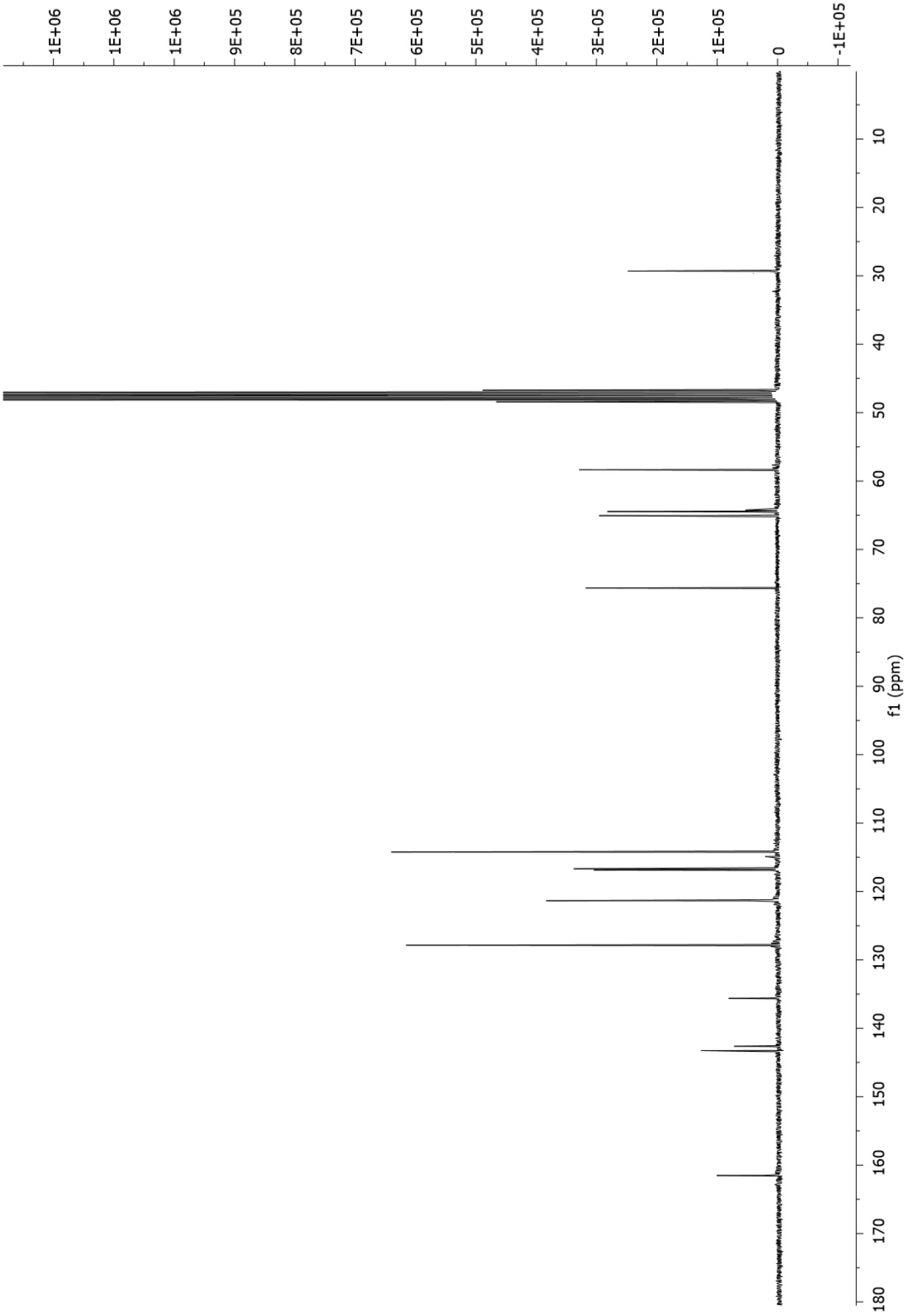
1E+06
1E+06
1E+06
9E+05
8E+05
7E+05
6E+05
5E+05
4E+05
3E+05
2E+05
1E+05
0
-1E+05
10
20
30
40
50
60
70
80
90
100
110
120
130
140
150
160
170
180
f1 (ppm)

Compound X

4-(3-amino-3-(1,4-benzodioxan)propoxy)benzenesulfonamide

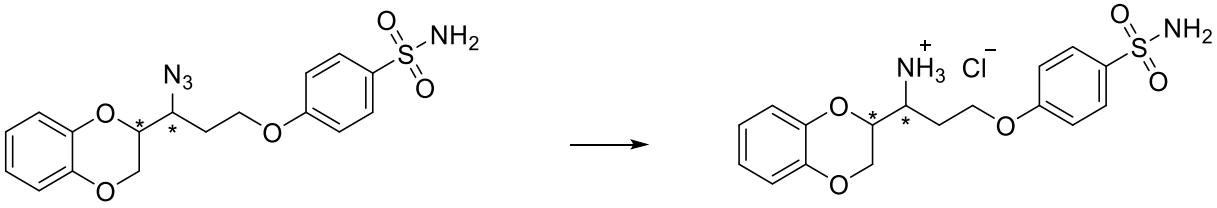

Chemical Formula:$C_{17}H_{18}N_4O_5S$
MW: 390,41

Chemical Formula:$C_{17}H_{21}ClN_2O_5S$
MW: 400,87

To a solution of 178 mg of 4-(3-azido-3-(1,4-benzodioxan)propoxy)benzenesulfonamide (0.45 mmol) in methanol (4 mL) was added 36 mg of Pd/C 5%. The mixture was then vigorously shaken under hydrogen atmosphere at room temperature until starting material was consumed (TLC monitoring)[48]. After filtering on a diatomaceous earth pad (Celite®), the solvent was evaporated under reduced pressure to obtain 115 mg of crude, which was dissolved in 2 mL of hydrogen chloride solution 2.0 M in diethyl ether and stirred overnight. The reaction mixture was diluted with ethyl ether, the solid was filtered and washed with cooled ethyl ether to obtain the desired product as a pale yellow solid (90 mg, 0.22 mmol).

Yield: 49.9%

m.p. *172°C*

HRMS: *m/z* 365.1166 ($[M+H]^+$

^{1}H NMR (CD_3OD): δ 7.85 (d, *J*=8.9 Hz, 2H), 7.10 (d, *J*=8.9 Hz, 2H), 7-04-6.77 (m, 4H), 4.59-4.38 (m, 2H), 4.38-4.23 (m, 2H), 4.23-4.03 (m, 1H), 3.86-3.65 (m, 1H), 2.49-2.36 (m, 1H), 2.36-2.18 (m, 1H).

^{13}C NMR (CD_3OD): δ 161.02, 143.08, 141.94, 127.85, 121.93, 121.57, 117.10, 116.88, 114.27, 72.39, 64.42, 63.91, 49.34, 28.78.

[48] Dichloromethane/methanol 99:1 + 1% NH_3. R_f starting material = 0.27; R_f product = 0.09.

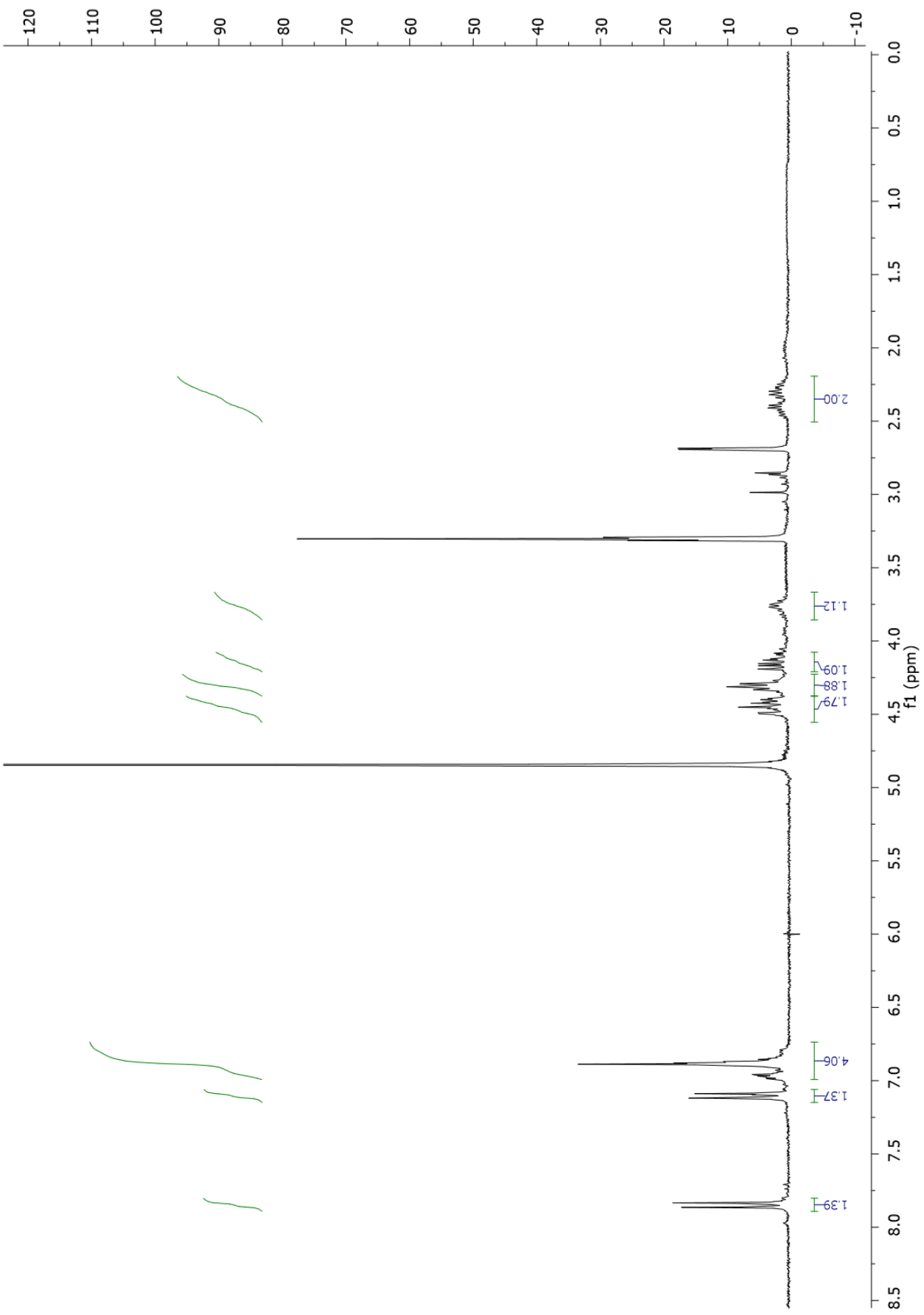
f1 (ppm)
2.00
1.12
1.09
1.88
1.79
4.06
1.37
1.39

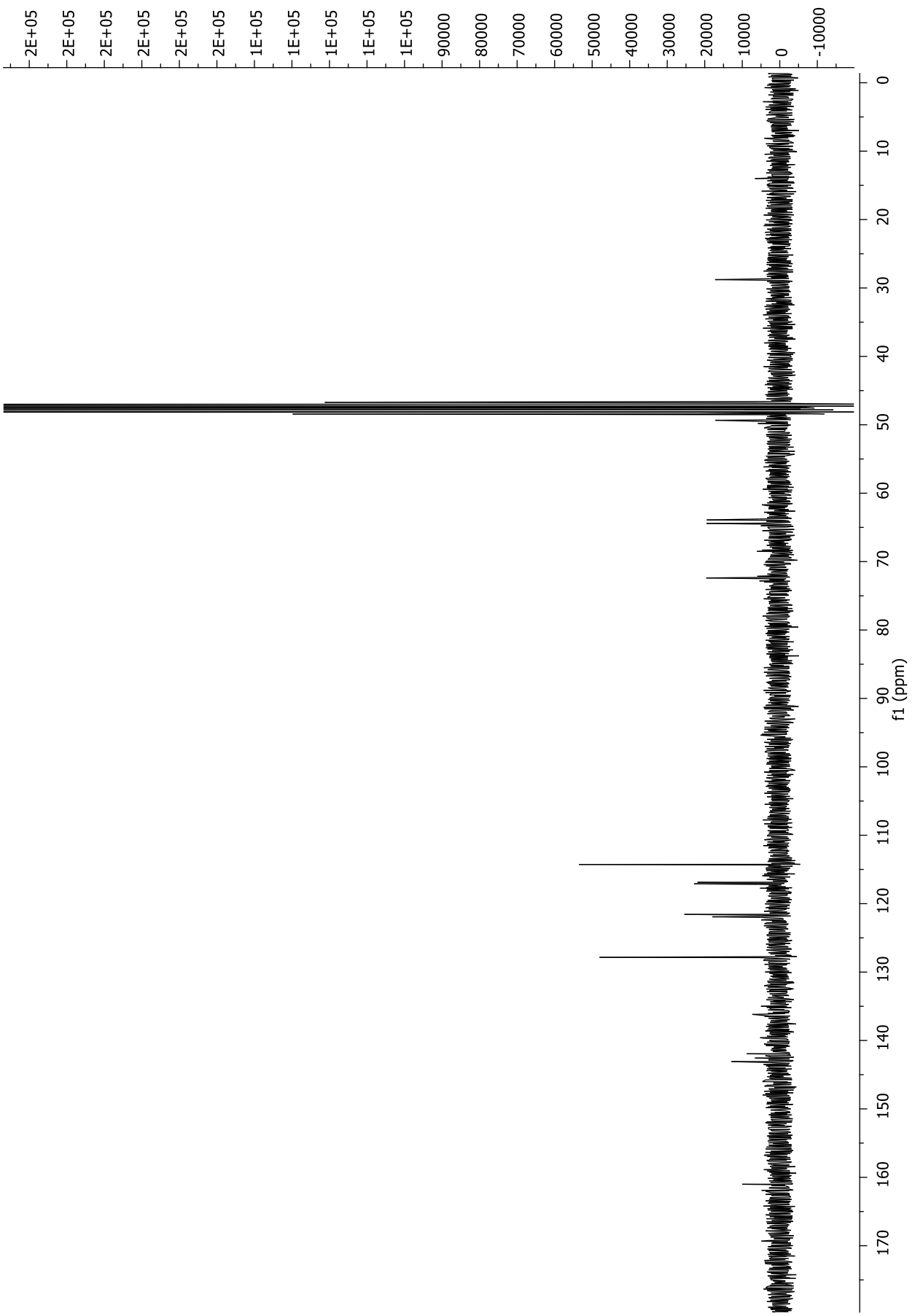
2E+05
2E+05
2E+05
2E+05
2E+05
2E+05
1E+05
1E+05
1E+05
1E+05
1E+05
90000
80000
70000
60000
50000
40000
30000
20000
10000
0
-10000
0
10
20
30
40
50
60
70
80
90
100
110
120
130
140
150
160
170
f1 (ppm)

3-bromo-4-hydroxybenzensulfonamide

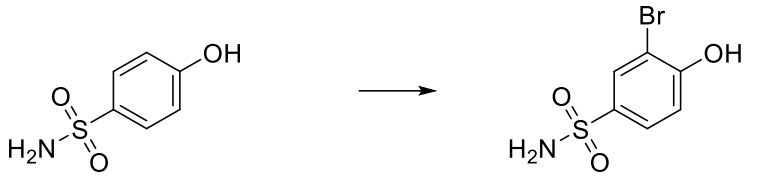

Chemical Formula:$C_6H_7NO_3S$
MW: 173,19

Chemical Formula:$C_6H_6BrNO_3S$
MW: 252,08

To a stirred solution of 2 g of 4-hydroxybenzenesulfonamide (11.55 mmol) in tetrahydrofuran (10 mL) was added NBS (2.06 gr, 11.55 mmol) at -20°C. The reaction mixture was stirred at the same temperature until TLC[49] indicated the disappearance of starting material. After that, the reaction mixture was evaporated under reduced pressure and the crude product was diluted with ethyl acetate. The organic phase was washed with 10% aqueous solution of $NaHCO_3$ brine, dried over Na_2SO_4, and filtered. The solvent was then evaporated in vacuo, providing a green oil. Flash chromatography (cyclohexane/ethyl acetate 1:1) was performed in order to obtain 972 mg (3.85 mmol) of the pure product as a white oil.

Yield: 33.4%

m.p. 161°C

^{1}H NMR ($CDCl_3$): δ 7.99 (d, *J*=2.3 Hz, 1H), 7.69 (dd, *J*=8.6, 2.3 Hz, 1H), 6.97 (d, 8.6 Hz, 1H).

[49] Cyclohexane/ethyl acetate 3:7. R_f starting material: 0.67, R_f product: 0.70.

3-methoxy-4-hydroxybenzensulfonamide

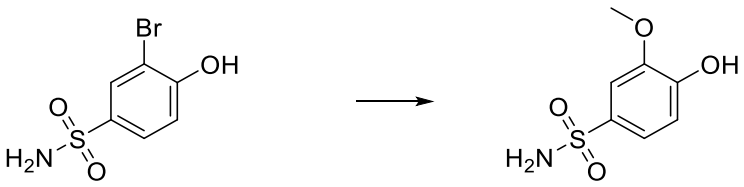

Chemical Formula:$C_6H_6BrNO_3S$
MW: 252,08

Chemical Formula:$C_7H_9NO_4S$
MW: 203,21

Under nitrogen atmosphere, 3-bromo-4-hydroxybenzensulfonamide (270 mg, 1.07 mmol) and CuI (815 g, 4.28 mmol) were dissolved in 10 mL of a solution of sodium methoxide. The mixture was stirred at reflux for 18 hours checking the progress of the reaction via TLC[50].

Afterward, the mixture was cooled down to room temperature and it was acidified with diluted hydrochloric acid and extracted with ethyl acetate. The organic layers were washed with brine and dried over anhydrous sodium sulfate. After evaporating to dryness under reduced pressure 215 mg of crude was obtained. Flash chromatography (cyclohexane/ethyl acetate 6:4) was performed in order to obtain 160 mg (0.78 mmol) of the pure product as a white solid.

Yield: 73.7%

m.p. 103°C

^{1}H NMR ($CDCl_3$): δ 7.42 (d, *J*=2.2, 1H), 7.37 (dd, *J*=8.3, 2.2 Hz, 1H), 6.89 (d=, *J*=8.3 Hz, 1H), 3.78 (s, 3H).

[50] Cyclohexane/ethyl acetate 7:3. R_f starting material: 0.70, R_f product: 0.52.

N,N-dimethylaminomethylene-3-methoxy-4-hydroxybenzensulfonamide

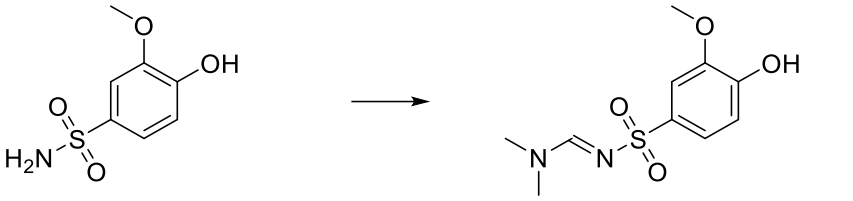

Chemical Formula: $C_7H_9NO_4S$
MW: 203,21

Chemical Formula: $C_{10}H_{14}N_2O_4S$
MW: 258,29

N,N-dimethylformamide diethyl acetal (0.12 mL, 0.94 mmol) was added to a solution of 3-methoxy-4-hydroxybenzensulfonamide (160 mg, 0.78 mmol) in DMF (1 mL) at 0°C and that was stirred for 2 hours at RT, checking the progress of the reaction via TLC [51]. The reaction mixture was treated with ethyl acetate, and the obtained solid was filtered to afford the titled compound as a white solid (223 mg, 0.86 mmol).

Yield: 92.0%

m.p. 108°C

^{1}H NMR ($CDCl_3$): δ 8.12 (s, 1H), 7.47 (dd, *J*=7.5, 1.4 Hz, 1H), 7.41 (d, *J*=1.3 Hz, 1H), 7.04 (d, *J*=7.5 Hz, 1H), 3.78 (s, 3H), 3.10 (s, 3H), 2.88 (s,3H).

[51] Dichloromethane/methanol 95:5. R_f starting material: 0.37; R_f product: 0.59.

N,N-dimethylaminomethylene-3-methoxy-4-(3-azido-3-(1,4-benzodioxan)propoxy)benzenesulfonamide

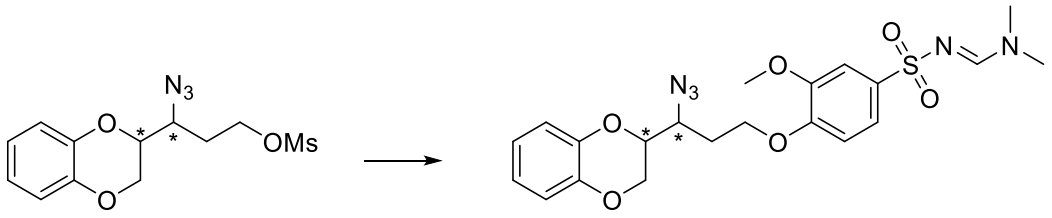

Chemical Formula:$C_{12}H_{15}N_3O_5S$
MW: 313,33

Chemical Formula:$C_{21}H_{25}N_5O_6S$
MW: 475,52

N,N-dimethylaminomethylene-3-methoxy-4-hydroxybenzensulfonamide (45 mg, 0.17 mmol) was treated with 25 mg K_2CO_3 (0.18 mmol) in 0.5 mL DMF and the suspension was stirred at rt for 30 minutes under a nitrogen atmosphere. Then a solution of 1-azido-1-(1,4-benzodioxan)-propylmethanesulfonate (50 mg, 0.16 mmol) in DMF (1.5 mL) was added dropwise and the reaction was stirred at 40°C until starting material was consumed (TLC monitoring)[52].

The reaction mixture was quenched with cold water and the white precipitate formed was collected by filtration, dried under vacuo to afford 52 mg (0.11 mmol).

Yield: 68.7 %

m.p. 180°C

^{1}H NMR (CD_3OD): δ 8.16 (s, 1H), 7.11 (s, 2H), 6.96-6.70 (m, 4H), 4.43 3.97 (m, 5H), 3.87-3.74 (m, 1H), 3.83-3.68 (m, 6H), 3.17 (s, 3H), 3.00 (s, 3H), 2.28-2.02 (m, 1H), 2.00-1.77 (m, 1H).

[52] Dichloromethane/methanol 98:2. R_f starting material = 0.98; R_f product = 0.51.

Compound XI

3-methoxy-4-(3-azido-3-(1,4-benzodioxan)propoxy)benzenesulfonamide

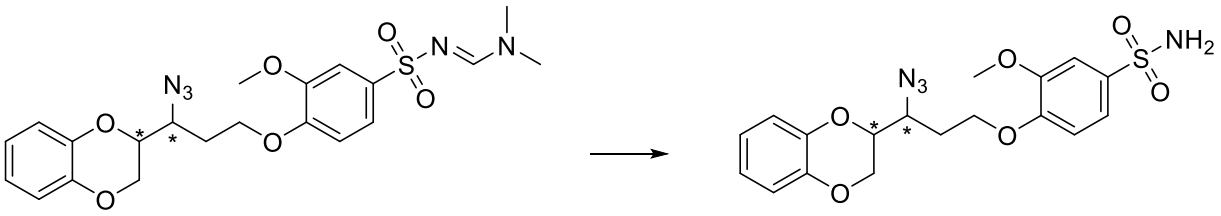

Chemical Formula:$C_{21}H_{25}N_5O_6S$
MW: 475,52

Chemical Formula:$C_{18}H_{20}N_4O_6S$
MW: 420,44

Hydrazine monohydrate (0.17 mL, 3.58 mmol) was added at room temperature to a stirred mixture of N,N-dimethylaminomethylene-3-methoxy-4-(3-azido-3-(1,4-benzodioxan)propoxy)benzene. sulfonamide (181 mg, 0.36 mmol) in methanol (4 mL). The reaction mixture was stirred until starting material was consumed (TLC monitoring)[53]. Then the solvent was removed in order to obtain 161 mg of the pure product (0.35 mmol) as an pale yellow solid.

Yield: 92%

m.p. 114°C

HRMS: *m/z* 419.1027 ([M+H]$^-$

^{1}H NMR (CD_3OD): δ 7.48 (dd, *J*=8.4, 2.2 Hz, 1H), 7.42 (d, *J*=2.1 Hz, 1H), 7.08 (dd, *J*=8.4, 3.5 Hz, 1H), 6.90-6.76 (m, 4H), 4.43-4.32 (m, 1H), 4.31-4.14 (m, 4H), 3.97-3.87 (m, 1H), 3.81 (s, *J*=8.7 Hz, 3H), 2.36-2.21 (m, 1H), 2.20-2.07 (m, 1H).

^{13}C NMR (CD_3OD): δ 153.23, 143.39, 143.24, 138.90, 121.07, 116.90, 116.57, 103.23, 75.55, 70.11, 65.56, 55.43, 49.06, 32.46.

[53] Dichloromethane/methanol 98:2. R_f starting material = 0.51; R_f product = 0.37.

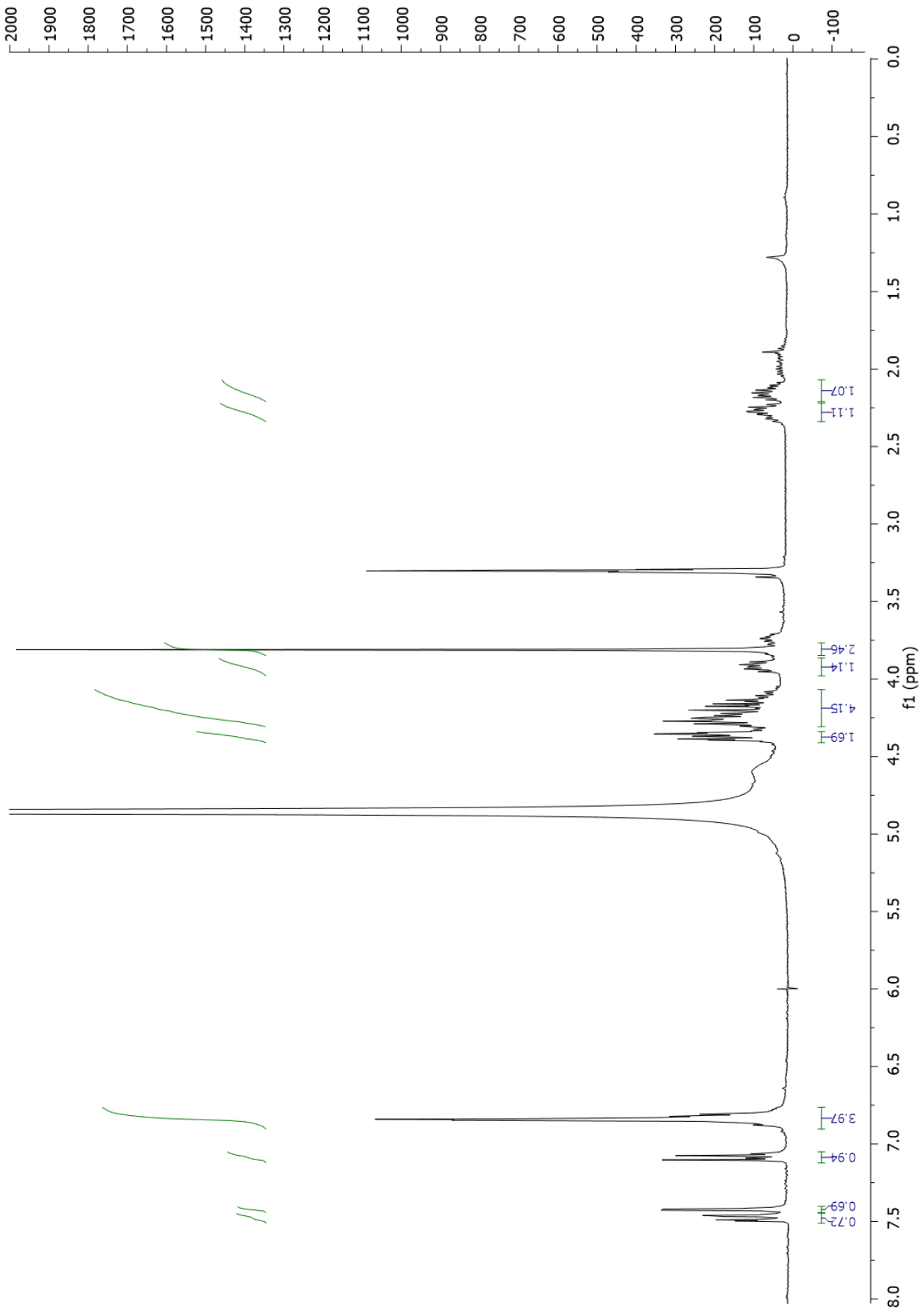
f1 (ppm)
1.07
1.11
2.46
1.14
4.15
1.69
3.97
0.94
0.72
0.69

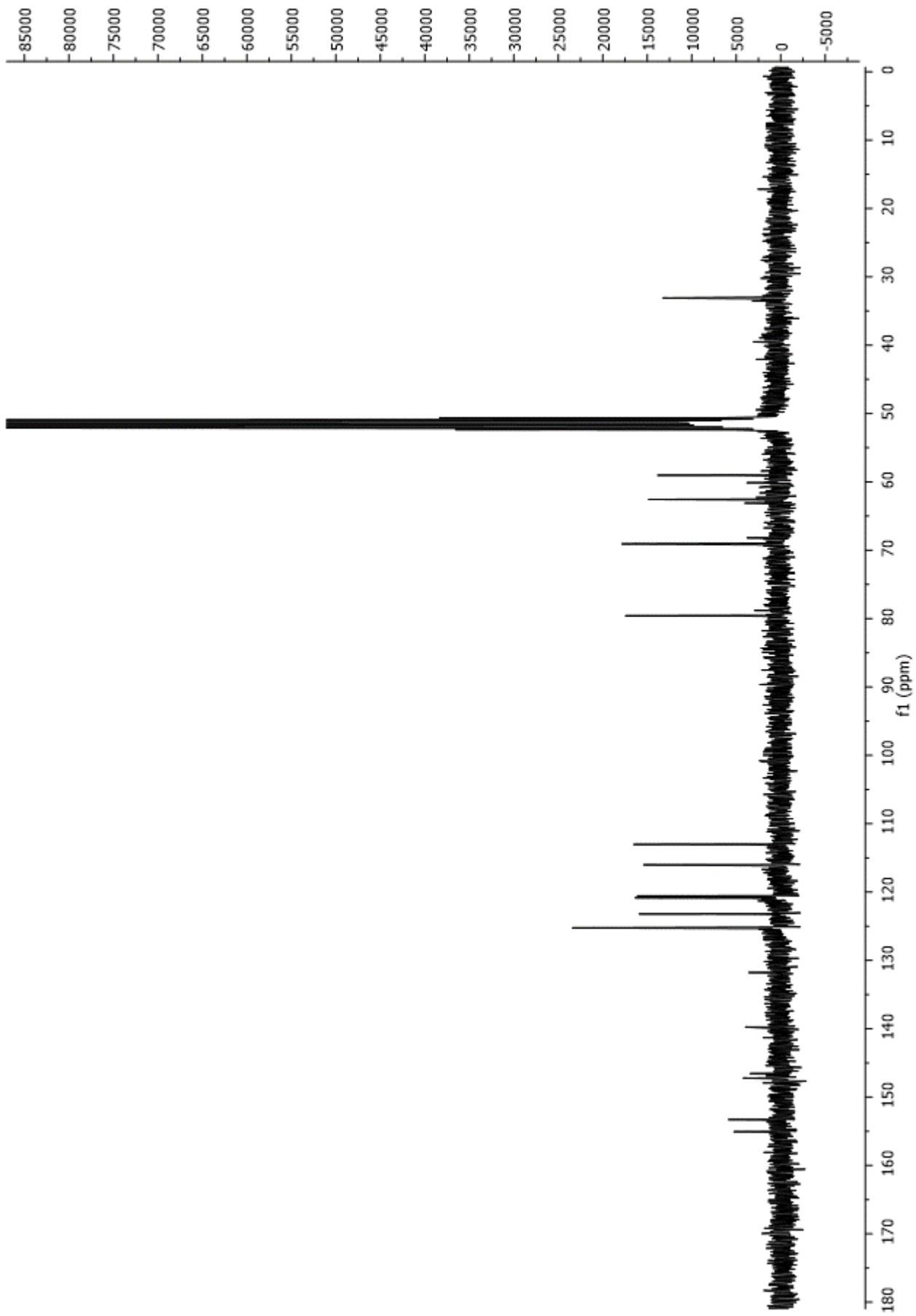
85000
80000
75000
70000
65000
60000
55000
50000
45000
40000
35000
30000
25000
20000
15000
10000
5000
0
-5000
0
10
20
30
40
50
60
70
80
90
100
110
120
130
140
150
160
170
180
f1 (ppm)

Compound XII

3-methoxy-4-(3-amino-3-(1,4-benzodioxan)propoxy)benzenesulfonamide

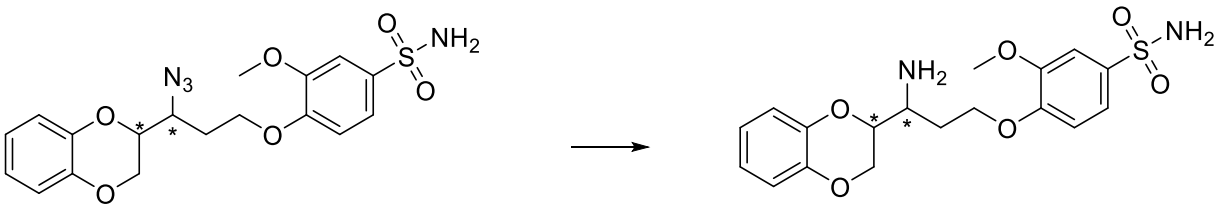

Chemical Formula:$C_{18}H_{20}N_4O_6S$
MW: 420,44

Chemical Formula:$C_{18}H_{22}N_2O_6S$
MW: 394,44

To a solution of 62 mg of 3-methoxy-4-(3-azido-3-(1,4-benzodioxan)propoxy)benzene sulfonamide (0.13 mmol) in methanol (1.5 mL) was added 63 µL of hydrazine hydrate (1.3 mmol), and PdO (16 mg, 0.13 mmol). The mixture was then heated at reflux until starting material was consumed (TLC monitoring)[54]. After that, the solvent was evaporated under reduced pressure to obtain 41 mg of the pure product (0.10 mmol) as a pinkish solid.

Yield: 80.0%

m.p. 125°C

HRMS: *m/z* 395.1271 ($[M+H]^+$

^{1}H NMR (CD_3OD): 7.48 (dd, *J*=8.4, 2.2 Hz, 1H), 7.42 (d, *J*=2.2 Hz, 1H), 7.08 (d, *J*=8.4 Hz, 1H), 6.87-6.75 (m, 4H), 4.40 (d, *J*=9.2 Hz, 1H), 4.33-4.19 (m, 2H), 4.16-4.03 (m, 2H), 3.82 (s, 3H), 2.25-2.10 (m, 1H), 2.09-1.91 (m, 1H).

^{13}C NMR (CD_3OD): δ 151.77, 148.26, 147.33, 139.67, 121.58, 120.84, 117.85, 117.46, 115.91, 110.73, 79.54, 67.60, 66.98, 56.78, 48.64, 32.48.

[54] Dichloromethane/methanol 98:2 + 1% NH_3. R_f starting material = 0.75; R_f product = 0.12.

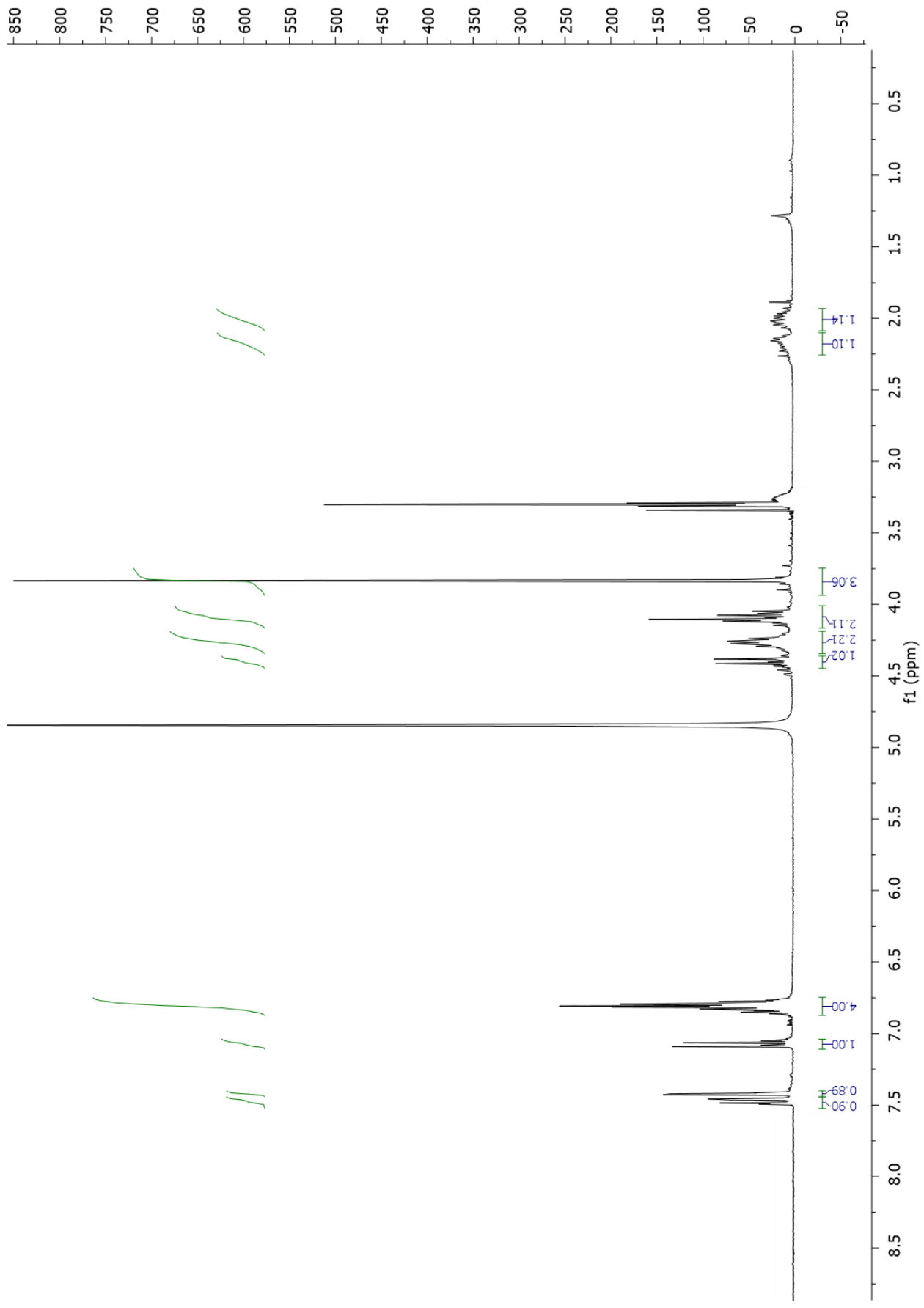
850
800
750
700
650
600
550
500
450
400
350
300
250
200
150
100
50
0
-50
0.5
1.0
1.5
2.0
2.5
3.0
3.5
4.0
4.5
5.0
5.5
6.0
6.5
7.0
7.5
8.0
8.5
f1 (ppm)
1.14
1.10
3.06
2.11
2.21
1.02
4.00
1.00
0.89
0.90

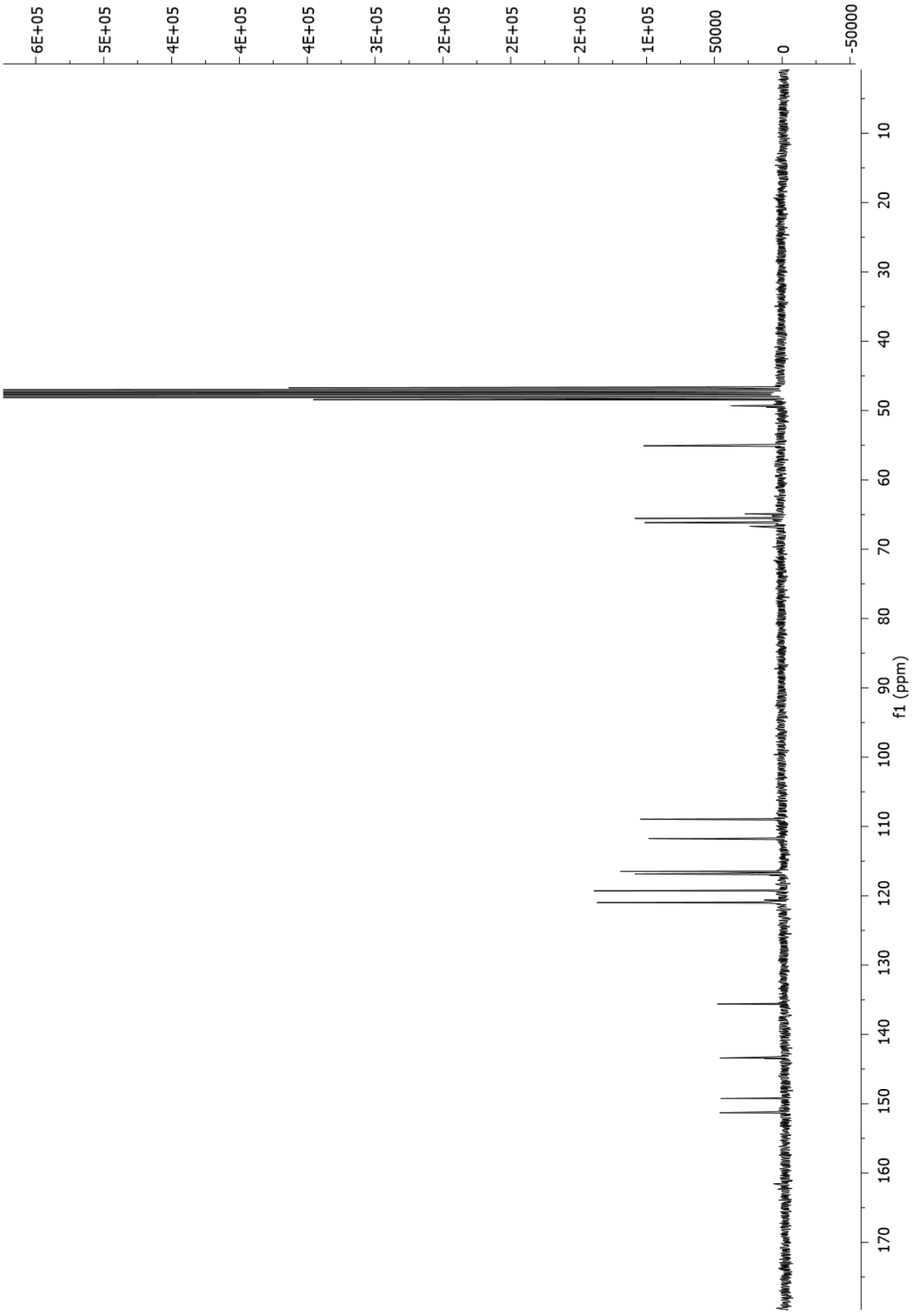
6E+05
5E+05
4E+05
4E+05
4E+05
3E+05
2E+05
2E+05
2E+05
1E+05
50000
0
-50000
10
20
30
40
50
60
70
80
90
100
110
120
130
140
150
160
170
f1 (ppm)

3,5-dibromo-4-hydroxybenzensulfonamide

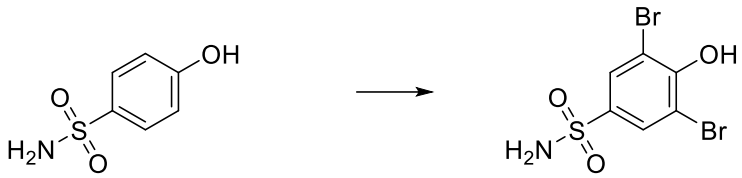

Chemical Formula:$C_6H_7NO_3S$
MW: 173,19

Chemical Formula:$C_6H_5Br_2NO_3S$
MW: 330,98

A solution of bromine (1.47 mL, 28.87 mmol) in 12 mL of dichloromethane and methanol in a mixing ratio of 1:1 was added dropwise to an ice-cooled solution of 2 g of 4-hydroxybenzensulfonamide (11.55 mmol) dissolved in the same solvent mixture. Then, the reaction mixture was stirred at room temperature until TLC[55] indicated the disappearance of starting material. The solid was filtered and washed with dichloromethane in order to obtain the desired product as a white solid (3.28 g, 9.93 mmol).

Yield: 85.9%

m.p. *228°C*

^{1}H NMR ($CDCl_3$): δ 7.97 (s, 2H).

[55] Cyclohexane/ethyl acetate 7:3. R_f starting material: 0.69, R_f product: 0.86.

3,5-dimethoxy-4-hydroxybenzensulfonamide

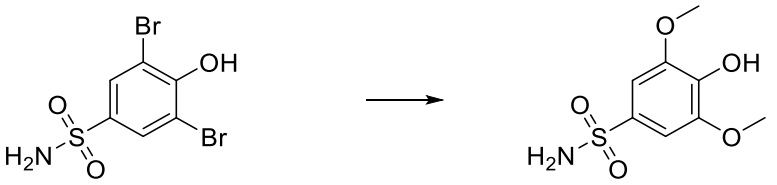

Chemical Formula: $C_6H_5Br_2NO_3S$
MW: 330,98

Chemical Formula: $C_8H_{11}NO_5S$
MW: 233,24

Under nitrogen atmosphere, 3,5-dibromo-4-hydroxybenzensulfonamide (2.04 g, 6.16 mmol) and CuI (4.70 g, 2.64 mmol) were dissolved in 20 mL of a solution of sodium methoxide. The mixture was stirred at reflux for 18 hours checking the progress of the reaction via TLC[56].

Afterward, the mixture was cooled down to room temperature and it was acidified with diluted hydrochloric acid and extracted with ethyl acetate. The organic layers were washed with brine and dried over anhydrous sodium sulfate. After evaporating to dryness under reduced pressure 934 mg of crude was obtained. Flash chromatography (cyclohexane/ethyl acetate 6:4) was performed in order to obtain 160 mg (0.68 mmol) of the pure product as a white solid.

Yield: 25.76%

m.p. 165°C

^{1}H NMR ($CDCl_3$): δ 7.18 (s, 2H), 3.90 (s, 6H).

[56] Cyclohexane/ethyl acetate 7:3. R_f starting material: 0.74, R_f product: 0.26

N,N-dimethylaminomethylene-3,5-dimethoxy-4-hydroxybenzen sulfonamide

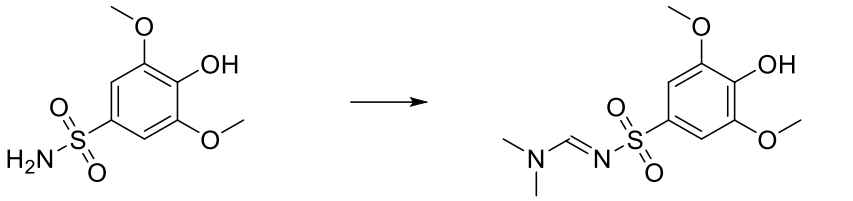

N,N-dimethylformamide diethyl acetal (0,93 mL, 6,96 mmol) was added to a solution of 3,5-dimethoxy-4-hydroxybenzensulfonamide (1 g, 4.28 mmol) in DMF (2 mL) at 0°C and that was stirred for 2 hours at RT, checking the progress of the reaction via TLC [57]. The reaction mixture was treated with ethyl acetate, and the obtained solid was filtered to afford the titled compound as a white solid (1.13 g, 3,94 mmol).

Yield: 92.0%

m.p. 171°C

^{1}H NMR ($CDCl_3$): δ 8.12 (s, 1H), 6.96 (s, 2H), 3.78 (s, 6H), 3.10 (s, 3H), 2.88 (s,3H).

[57] Dichloromethane/methanol 95:5. R_f starting material: 0.37; R_f product: 0.59.

N,N-dimethylaminomethylene-3,5-dimethoxy-4-(3-azido-3-(1,4-benzodioxan)propoxy)benzenesulfonamide

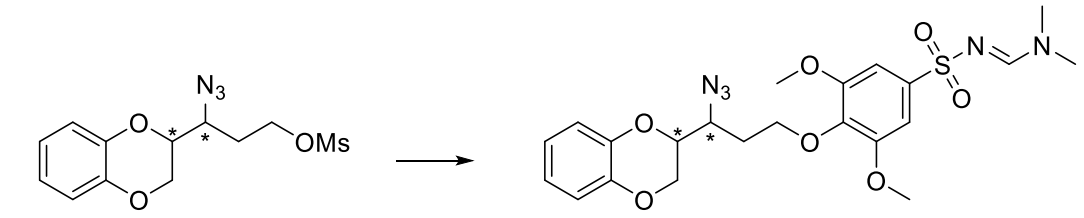

Chemical Formula:$C_{12}H_{15}N_3O_5S$
MW: 313,33

Chemical Formula:$C_{22}H_{27}N_5O_7S$
MW: 505,55

N,N-dimethylaminomethylene-3,5-dimethoxy-4-hydroxybenzensulfonamide (125 mg, 0.43 mmol) was treated with 62 mg K_2CO_3 (0,45 mmol) in 1 mL DMF and the suspension was stirred at rt for 30 minutes under a nitrogen atmosphere. Then a solution of 1-azido-1-(1,4-benzodioxan)-propylmethanesulfonate (122 mg, 0.39 mmol) in DMF (3 mL) was added dropwise and the reaction was stirred at 40°C until starting material was consumed (TLC monitoring)[58].

The reaction mixture was quenched with cold water and the precipitate formed was collected by filtration, dried under vacuo to afford 163 mg (0.32mmol).

Yield: 82%

m.p. 223°C (degradation)

^{1}H NMR (CD_3OD): δ 8.16 (s, 1H), 7.11 (s, 2H), 6.96-6.70 (m, 4H), 4.43 3.97 (m, 5H), 3.87-3.74 (m, 1H), 3.83-3.68 (m, 6H), 3.17 (s, 3H), 3.00 (s, 3H), 2.28-2.02 (m, 1H), 2.00-1.77 (m, 1H).

[58] Dichloromethane/methanol 95:5. R_f starting material = 0.78; R_f product = 0.88.

Compound XIII

3,5-dimethoxy-4-(3-azido-3-(1,4-benzodioxan)propoxy)benzene sulfonamide

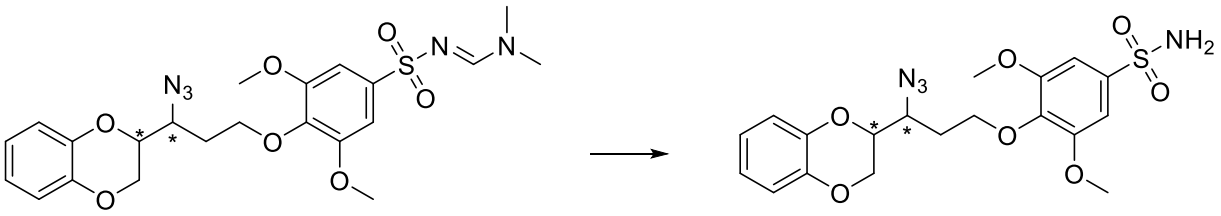

Chemical Formula:$C_{22}H_{27}N_5O_7S$
MW: 505,55

Chemical Formula:$C_{19}H_{22}N_4O_7S$
MW: 450,47

Hydrazine hydrate (0.17 mL, 3.58 mmol) was added at room temperature to a stirred mixture of 159 mg of N,N-dimethylaminomethylene-3,5-dimethoxy-4-(3-azido-3-(1,4-benzodioxan)propoxy) benzenesulfonamide (0.31 mmol) in methanol (4 mL). The reaction mixture was stirred until starting material was consumed (TLC monitoring)[59]. Then the mixture was evaporated to dryness under reduced pressure in order to obtain 161 mg of the pure product (0.35 mmol) as a white solid.

Yield: 100%

m.p. = 128°C

HRMS: *m/z* 449.1142 ($[M+H]^-$

^{1}H NMR (CD_3OD): δ 7.20 (s, 2H), 7.00-6.71 (m, 4H), 4.41-4.00 (m, 5H), 3.84 (m, 6H), 3.77-3.70 (m, 1H), 2.25-2.00 (m, 1H), 2.02-1.65 (m, 1H).

^{13}C NMR (CD_3OD): δ 153.23, 143.39, 143.24, 138.90, 121.07, 116.90, 116.57, 103.23, 75.55, 70.11, 65.56, 55.43, 49.06, 32.46.

[59] Dichloromethane/methanol 98:2. R_f starting material = 0.88; R_f product = 0.48.

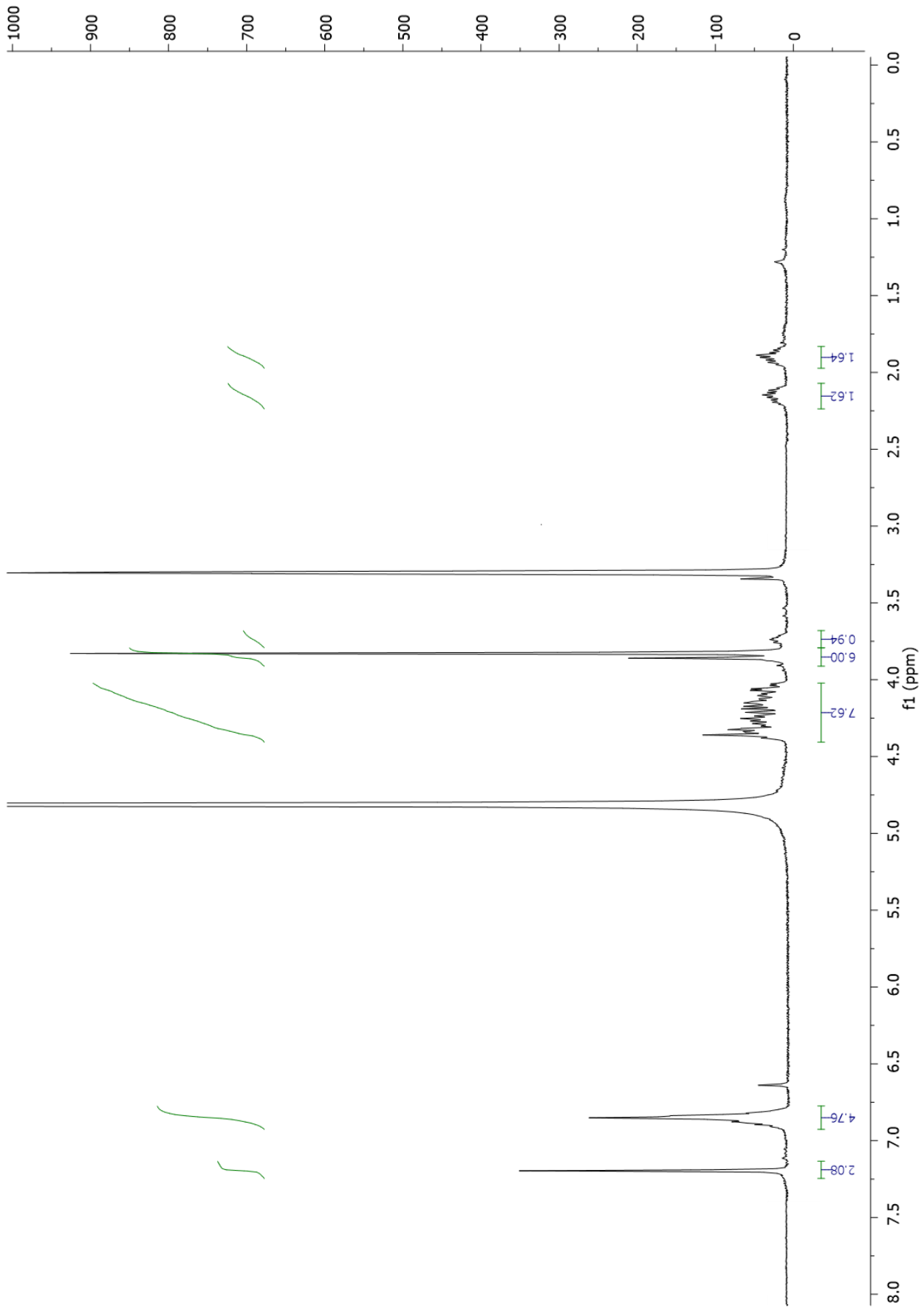
1000
900
800
700
600
500
400
300
200
100
0
0.0
0.5
1.0
1.5
2.0
2.5
3.0
3.5
4.0
4.5
5.0
5.5
6.0
6.5
7.0
7.5
8.0
f1 (ppm)
1.64
1.62
0.94
6.00
7.62
4.76
2.08

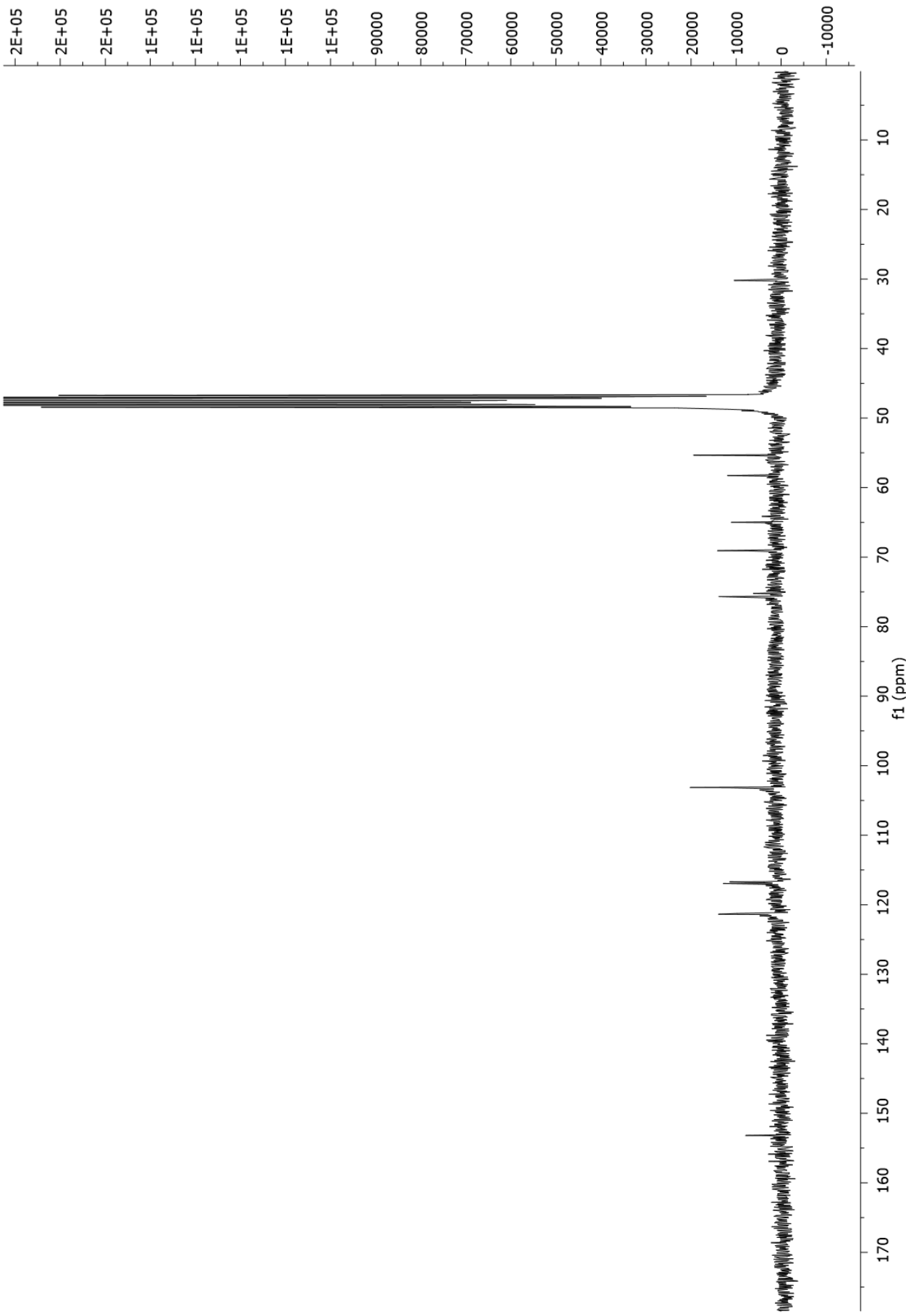
2E+05
2E+05
2E+05
1E+05
1E+05
1E+05
1E+05
1E+05
90000
80000
70000
60000
50000
40000
30000
20000
10000
0
-10000
10
20
30
40
50
60
70
80
90
100
110
120
130
140
150
160
170
f1 (ppm)

Compound XIV

3,5-dimethoxy-4-(3-amino-3-(1,4-benzodioxan)propoxy)benzene sulfonamide

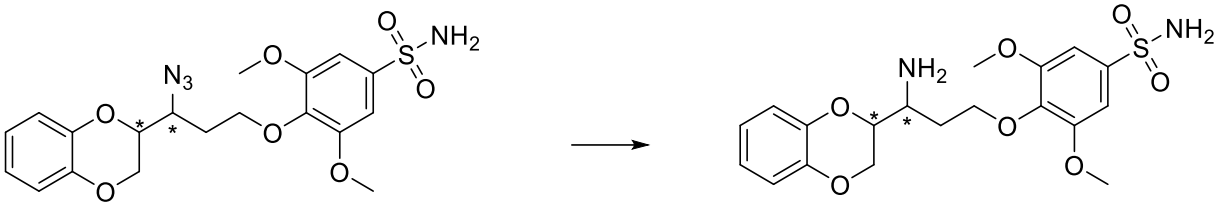

Chemical Formula:$C_{19}H_{22}N_4O_7S$
MW: 450,47

Chemical Formula:$C_{19}H_{24}N_2O_7S$
MW: 424,47

To a solution of 161 mg mmol of 3,5-dimethoxy-4-(3-azido-3-(1,4-benzodioxan)propoxy)benzene sulfonamide (0.35 mmol) in methanol (4 mL) was added 0.17 mL of hydrazine hydrate (3.5 mmol), and PdO (44 mg, 0.36 mmol). The mixture was then heated at reflux until starting material was consumed (TLC monitoring)[60]. After that, the solvent was evaporated under reduced pressure to obtain 124 mg of the pure product (0.29 mmol) as a pinkish solid.

Yield: 80%

m.p. = 138°C

HRMS: *m/z* 425.1371 ($[M+H]^+$

^{1}H NMR (CD_3OD): δ 7.22 (s, 2H), 6.92-6.75 (m, 4H), 4.50-4.29 (m, 1H), 4.29-4.01 (m, 4H), 3.88 (s, 6H), 3.49-3.36 (m, 1H), 2.28-2.01 (m, 1H), 2.02-1.77 (m, 1H).

^{13}C NMR (CD_3OD): δ 153.23, 143.39, 143.23, 138.90, 121.07, 116.90, 116.56, 103.21, 76.04, 75.54, 70.10, 65.56, 55.43, 32.46.

[60] Dichloromethane/methanol 98:2 + 1% NH_3. R_f starting material = 0.48; R_f product = 0.20.

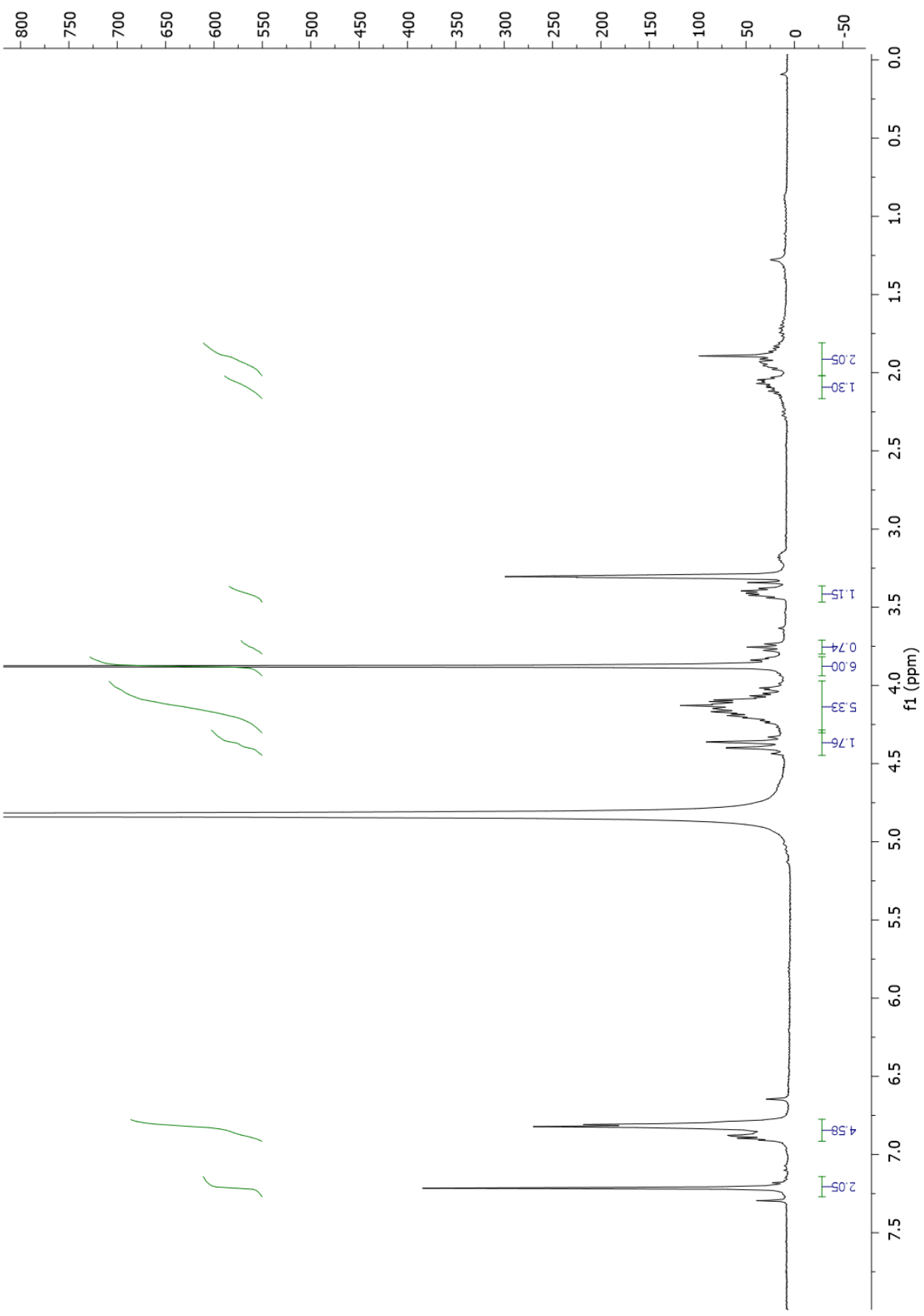
f1 (ppm)
2.05
1.30
1.15
0.74
6.00
5.33
1.76
4.58
2.05

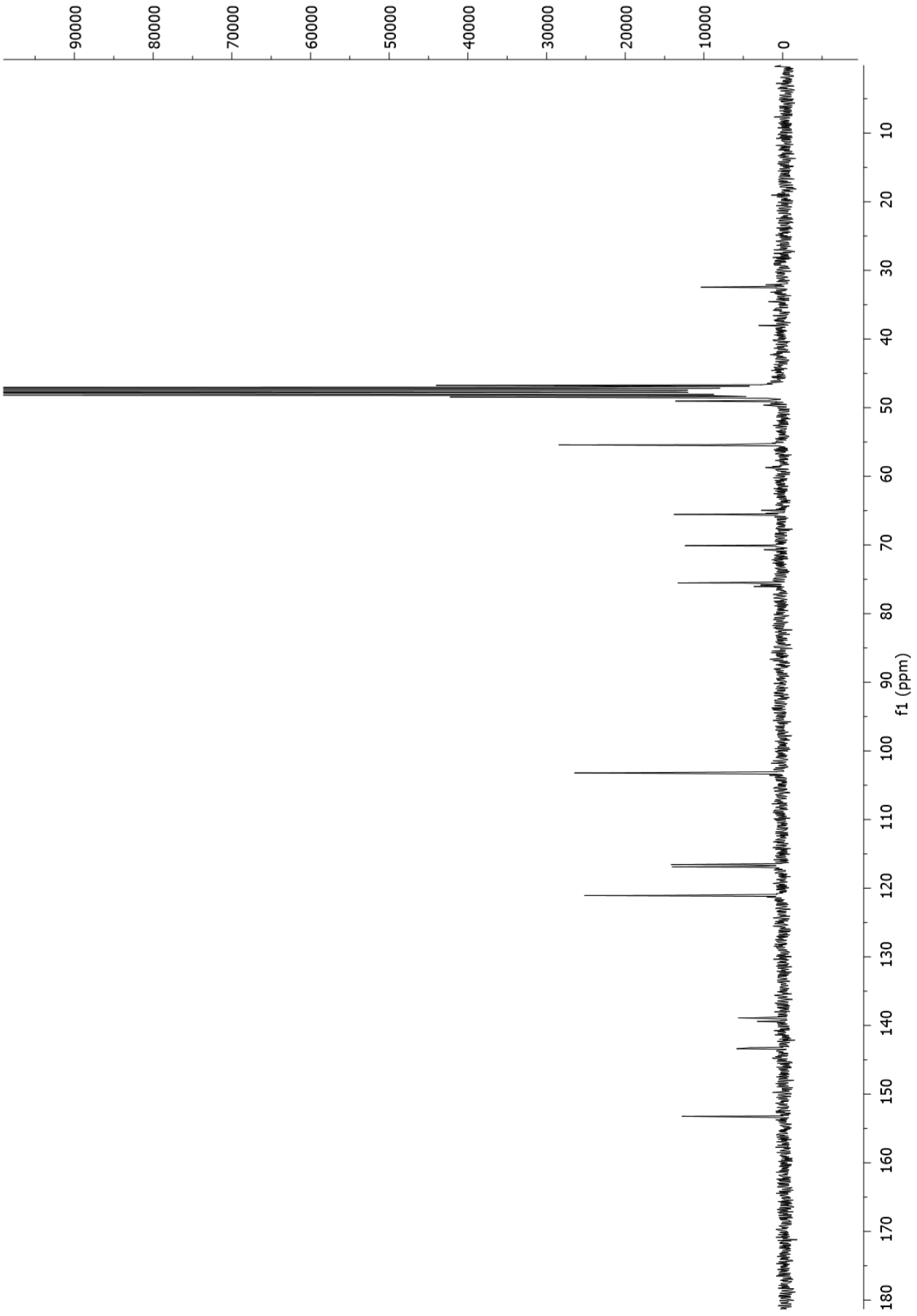
90000
80000
70000
60000
50000
40000
30000
20000
10000
0
10
20
30
40
50
60
70
80
90
100
110
120
130
140
150
160
170
180
f1 (ppm)

4-methanesulfonyloxy-1-butene

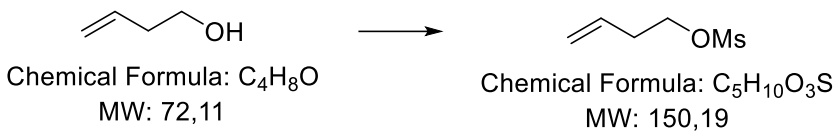

Chemical Formula: C_4H_8O
MW: 72,11

Chemical Formula: $C_5H_{10}O_3S$
MW: 150,19

6 g of 3 buten-1-ol (83.21 mmol) were dissolved in 50 ml of dichloromethane and the mixture was cooled down at 0°C in order to add 11.6 mL of triethylamine (83.21 mmol) under stirring. After that, 6.44 mL of methane sulfonyl chloride (83.21 mmol) were added dropwise. The mixture was stirred for one hour and the triethylamine hydrochloride was removed by filtration. The reaction mixture was washed with 10% aqueous solution of HCl, and then with brine. The organic phase was dried over anhydrous sodium sulfate and filtered and the solvent was evaporated in vacuo, providing the pure product as 11.15 mg of a colorless oil (74.23 mmol).

Yield: 89.2%

^{1}H NMR ($CDCl_3$): δ 5.86-5.50 (m, 1H), 5.22- 5.11 (m, 2H), 4.26 (t, *J*=6.7 Hz, 2H), 3.00 (s, 3H), 2.50 (ddt, *J*=13.4, 6.7, 1.3 Hz, 2H).

N,N-dimethylaminomethylene-4-(3-buten-1-oxy)benzenesulfonamide

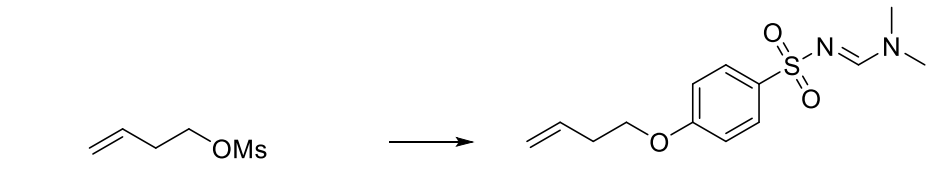

Chemical Formula: $C_5H_{10}O_3S$
MW: 150,19

Chemical Formula: $C_{13}H_{18}N_2O_3S$
MW: 282,36

Under a nitrogen atmosphere N,N-dimethylaminomethylene-4-hydroxybenzenesulfonamide (2.02 g, 8.86 mmol) was treated with 1.17 mg of K_2CO_3 (8.47 mmol) in 10 mL DMF and the suspension was stirred at room temperature for 30 minutes. Then a solution of 4-methanesulfonyloxy-1-butene (1.16 g, 7.70 mmol) in DMF (10 mL) was added dropwise and the reaction was stirred at 80°C until starting material was consumed (TLC monitoring)[61].

The reaction mixture was quenched with cold water and the white precipitate formed was collected by filtration, dried under vacuo to afford 25 mg (0.056 mmol).

Yield: 70.7%

m.p. 100°C

^{1}H NMR ($CDCl_3$): δ 8.11 (s, 1H), 7.80 (d, *J*=8.9 Hz, 2H), 6.92 (d, *J*=8.9 Hz, 2H), 5.86-5.50 (m, 1H), 5.24-5.04 (m, 2H), 4.04 (t, *J*=6.7 Hz, 2H), 3.11 (s, 3H), 3.00 (s, 3H), 2.54 (ddt, *J*=13.4, 6.7, 1.3 Hz, 2H).

[61] Toluene/ethyl acetate 1:1. R_f starting material = 0.12; R_f product = 0.32.

N,N-dimethylaminomethylene-4-(oxiranylethoxy)benzene sulfonamide

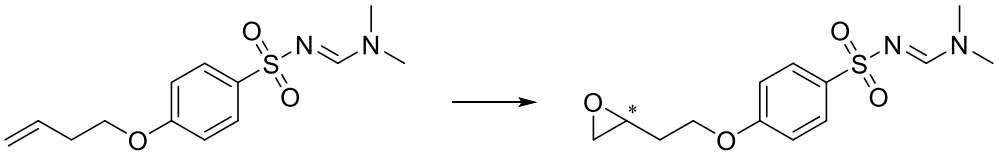

Chemical Formula: $C_{13}H_{18}N_2O_3S$
MW: 282,36

Chemical Formula: $C_{13}H_{18}N_2O_4S$
MW: 298,36

Under a nitrogen atmosphere *m*-chloroperbenzoic acid (1.43 g, 8.32 mmol) was added to a solution of N,N-dimethylaminomethylene-4-(3-buten-1-oxy)benzenesulfonamide (1.17 g, 4.16 mmol) in dichloromethane (30 mL) at 0°C. The reaction mixture was stirred at room temperature until TLC[62] indicated the disappearance of starting material. The mixture was washed with 10% aqueous solution of $Na_2S_2O_5$ and two times with 10% aqueous solution of $NaHCO_3$, and then with brine. The organic phase was dried over anhydrous sodium sulfate and filtered and the solvent was evaporated in vacuo, providing the pure product as 1.23 mg of a yellow gum (4.12 mmol).

Yield: 99.3%

^{1}H NMR ($CDCl_3$): δ 8.12 (s, 1H), 7.81 (d, *J*=8.4 Hz, 2H), 6.93 (d, *J*=8.4 Hz, 2H), 4.23-4.07 (m, 2H), 3.19-3.08 (m, 4H), 3.01 (s, 3H), 2.83 (t, *J*=4.6 Hz, 1H), 2.57 (dd, *J*=4.6, 2.6 Hz, 1H), 2.22-2.07 (m, 1H), 1.92 (m, 1H).

[62] Toluene/ethyl acetate 1:1. R_f starting material = 0.32; R_f product = 0.15.

N,N-dimethylaminomethylene-4-(3-hydroxy-4-phenoxybutoxy) benzenesulfonamide

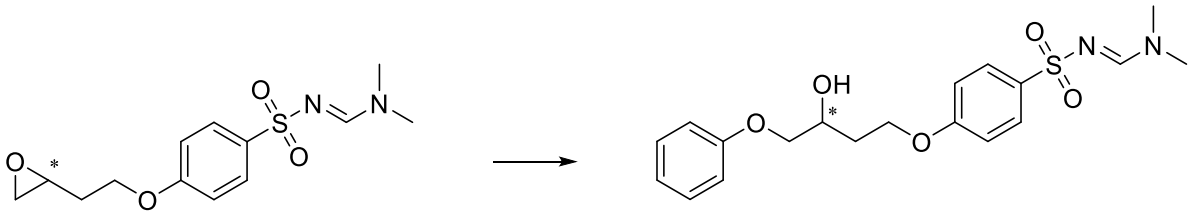

Chemical Formula: $C_{13}H_{18}N_2O_4S$
MW: 298,36

Chemical Formula: $C_{19}H_{24}N_2O_5S$
MW: 392,47

Under a nitrogen atmosphere phenol (610 mg, 6.53 mmol) was treated with 1.13 g of K_2CO_3 (8.15 mmol) in 10 mL DMF and the suspension was stirred at room temperature for 30 minutes. Then a solution of N,N-dimethylaminomethylene-4-(oxiranylethoxy)benzenesulfonamide (980 g, 3.26 mmol) in DMF (7 mL) was added dropwise and the reaction was stirred at 80°C until starting material was consumed (TLC monitoring)[63]. Afterward, the solvent was evaporated in vacuo and the crude was dissolved in ethyl acetate. The organic phase was washed with 10% aqueous solution of NaOH, and brine, dried over anhydrous sodium sulfate and filtered. The solvent was then evaporated in vacuo, providing a brown oil. Flash chromatography (dichloromethane/methanol 99:1) was performed in order to obtain 294 mg (0.75 mmol) of the pure product as a yellowish solid.

Yield: 70.7%

m.p. 100°C

^{1}H NMR ($CDCl_3$): δ 8.12 (s, 1H), 7.81 (d, *J*=6.9 Hz, 2H), 7.34-7.24 (m, 2H), 7.02-6.88 (m, 5H), 4.33-4.17 (m, 3H), 4.05 (ddd, *J*=9.3, 3.4, 1.8 Hz, 1H), 3.93 (ddd, *J*=9.3, 7.1, 1.8 Hz, 1H), 3.11 (s, 3H), 3.01 (s, 3H), 2.17-1.98 (m, 2H).

[63] Dichloromethane/methanol 95:5. R_f starting material: 0.64; R_f product: 0.45.

N,N-dimethylaminomethylene-*i4*-(3-methanesulfonate-4-phenoxy butoxy)benzenesulfonamide

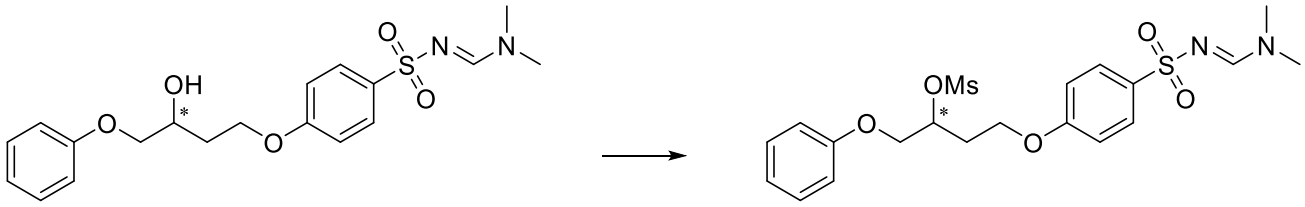

Chemical Formula: $C_{19}H_{24}N_2O_5S$
MW: 392,47

Chemical Formula: $C_{20}H_{26}N_2O_7S_2$
MW: 470,56

N,N-dimethylaminomethylene-4-(3-hydroxy-4-phenoxybutoxy)benzenesulfonamide (294 mg, 0.75 mmol) was dissolved in dichloromethane (5 mL), triethylamine (0.12 mL, 1.50 mmol) was added, and after the reaction mixture was cooled down to 0°C mesyl chloride (0.23 mL, 1.65 mmol) was added dropwise. The solution was stirred at room temperature until TLC[64] indicated the disappearance of starting material. The reaction mixture was washed with 10% aqueous solution of HCl 10%, aqueous solution of $NaHCO_3$, and then with brine. The organic phase was dried over anhydrous sodium sulfate and filtered and the solvent was evaporated in vacuo, providing the pure product as 305 mg of a yellow oil (0.65 mmol).

Yield: *86.6%*

^{1}H NMR ($CDCl_3$): δ 8.11 (s, 1H), 7.82 (d, *J*=8.9 Hz, 2H), 7.36-7.26 (m, 2H), 7.05-6.85 (m, 5H), 5.33-5.18 (m, 1H), 4.21 (m, 4H), 3.12 (s, 3H), 3.08 (s, 3H), 3.01 (s, 3H), 2.38-2.25 (m, 2H).

[64] Dichloromethane/methanol 95:5. R_f starting material = 0.45; R_f product = 0.71.

N,N-dimethylaminomethylene-4-(3-azido-4-phenoxybutoxy)benzene sulfonamide

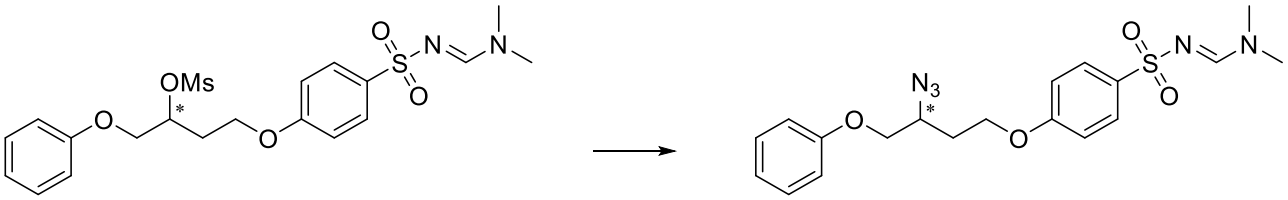

Chemical Formula: $C_{20}H_{26}N_2O_7S_2$
MW: 470,56

Chemical Formula: $C_{19}H_{23}N_5O_4S$
MW: 417,48

Sodium azide (423 mg, 6.50 mmol) was added to a solution of N,N-dimethylaminomethylene-4-(3-methanesulfonate-4-phenoxybutoxy)benzenesulfonamide (305 mg, 0.65 mmol) in DMF (20 mL) and water (3.8 mL). Then, the reaction mixture was refluxed, under stirring, until TLC[65] indicated the disappearance of starting material.

Afterward, the solution was evaporated in vacuo and the crude was dissolved in acetone. The formed precipitate was removed by filtration and then the solvent was evaporated in vacuo, providing the pure product as a yellow oil (239 mg, 0.57 mmol)

Yield = 88.3%

^{1}H NMR ($CDCl_3$): δ 8.12 (s, 1H), 7.82 (d, *J*=8.7 Hz, 2H), 7.36-7.26 (m, 2H), 7.04-6.88 (m, 5H), 4.25-4.00 (m, 5H), 3.11 (s, 3H), 3.00 (s, 3H), 2.21-2.08 (m, 1H), 2.08-1.91 (m, 1H).

[65] Dichloromethane/methanol 95:5. R_f starting material = 0.71; R_f product = 0.85.

Compound XV

4-(3-azido-4-phenoxybutoxy)benzenesulfonamide

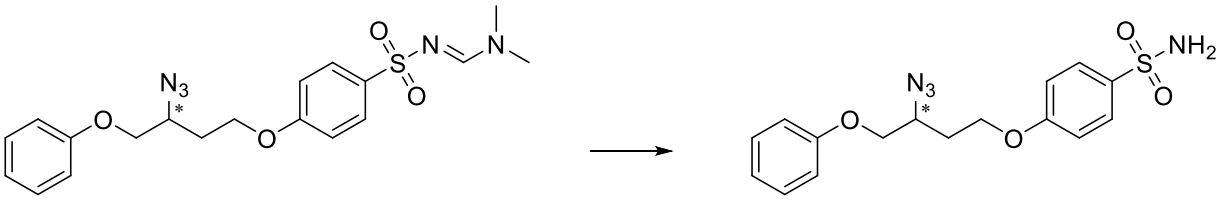

Chemical Formula: $C_{19}H_{23}N_5O_4S$
MW: 417,48

Chemical Formula: $C_{16}H_{18}N_4O_4S$
MW: 362,40

Hydrazine hydrate (0.28 mL, 5.74 mmol) was added at room temperature to a stirred mixture of 239 mg of N,N-dimethylaminomethylene-4-(3-azido-4-phenoxybutoxy)benzenesulfonamide (0.57 mmol) in methanol (7.5 mL). The reaction mixture was stirred until starting material was consumed (TLC monitoring)[66]. Then the mixture was evaporating to dryness under reduced pressure in order to obtain an orangish oil. Flash chromatography (dichloromethane/methanol 98:2) was performed in order to obtain 154 mg (0.43 mmol) of the pure product as a white solid.

Yield: 74.6%

m.p. 99°C

HRMS: *m/z* 361.0958 ($[M+H]^-$

^{1}H NMR (CD_3OD): δ 7.83 (d, *J*=7.4 Hz, 2H), 7.29 (dt, *J*=7.4, 1.0 Hz, 2H), 7.07 (d, *J*=7.4 Hz, 2H), 6.99-6.92 (m, 3H), 4.32-4.17 (m, 3H), 4.14-3.99 (m, 2H), 2.24-2.09 (m, 1H), 2.07-1.92 (m, 1H).

^{13}C NMR (CD_3OD): δ 161.60, 158.39, 135.52, 129.16, 127.85, 120.88, 114.19, 70.53, 64.52, 58.34, 29.95.

[66] Dichloromethane/methanol 95:5. R_f starting material = 0.85; R_f product = 0.40.

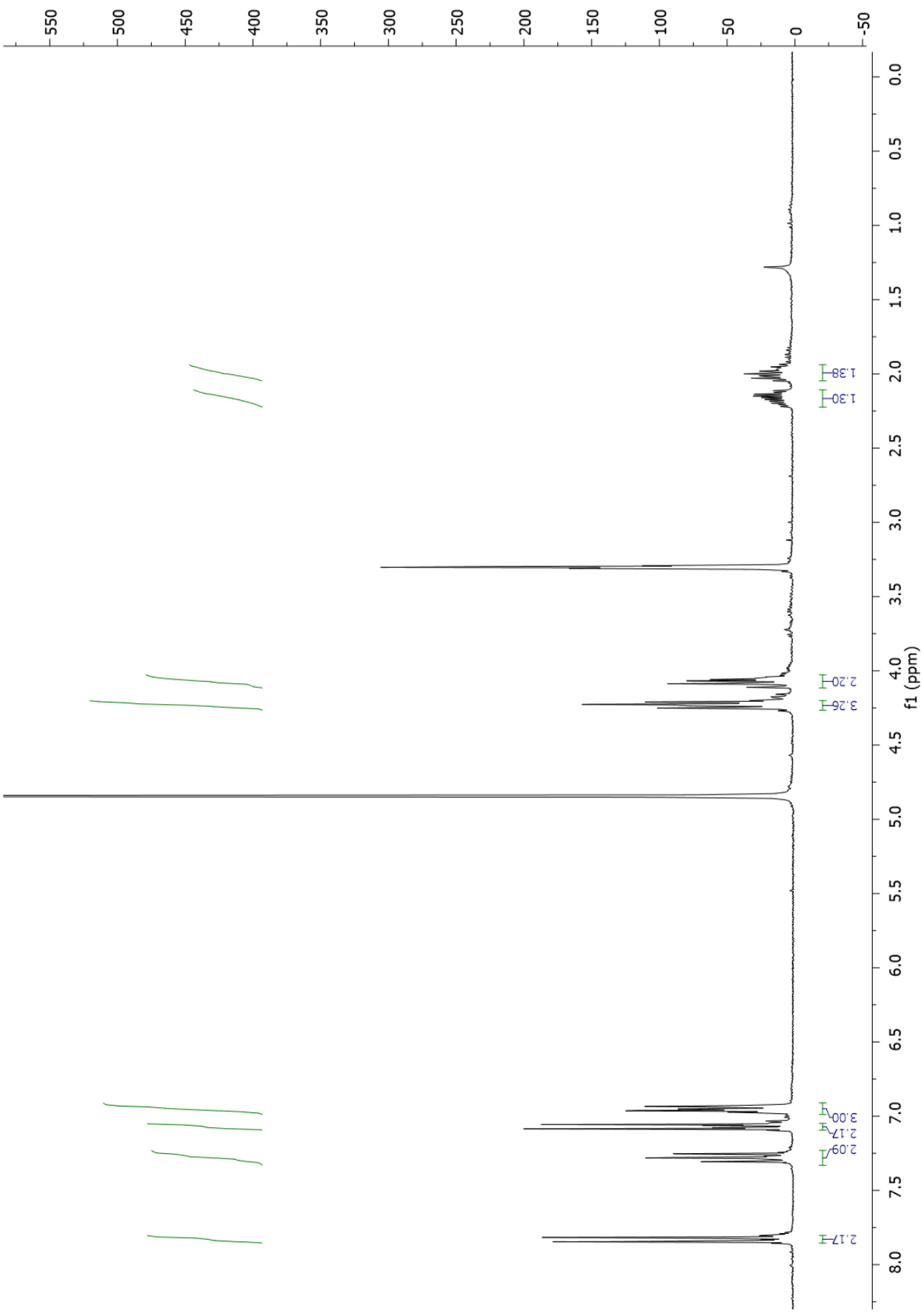
f1 (ppm)
1.38
1.30
2.20
3.26
3.00
2.17
2.09
2.17

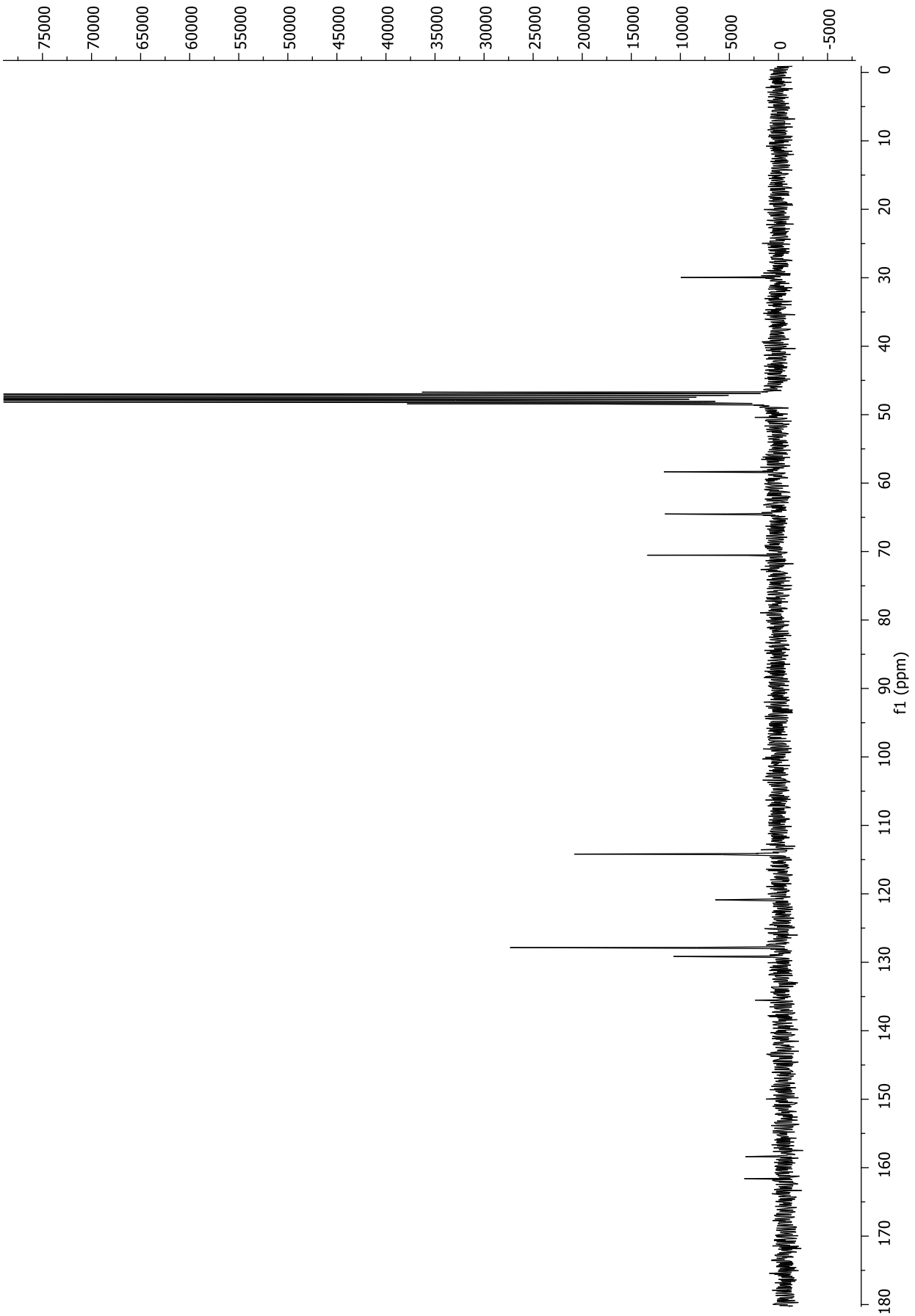
75000
70000
65000
60000
55000
50000
45000
40000
35000
30000
25000
20000
15000
10000
5000
0
-5000
0
10
20
30
40
50
60
70
80
90
100
110
120
130
140
150
160
170
180
f1 (ppm)

Compound XVI

4-(3-amino-4-phenoxybutoxy)benzenesulfonamide

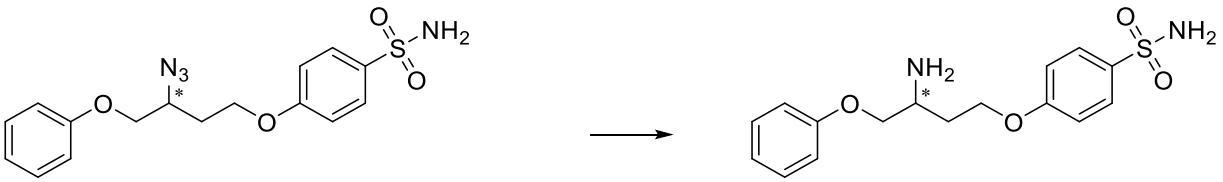

Chemical Formula: $C_{16}H_{18}N_4O_4S$
MW: 362,40

Chemical Formula: $C_{16}H_{20}N_2O_4S$
MW: 336,41

To a solution of 154 mg of 4-(3-azido-4-phenoxybutoxy)benzenesulfonamide (0.43 mmol) in methanol (4 mL) was added 86 mg of Pd/C 5%. The mixture was then vigorously shaken under hydrogen atmosphere at room temperature until starting material was consumed (TLC monitoring)[67]. After filtering on a celite pad, the solvent was evaporated under reduced pressure to obtain 85 mg (0.25 mmol) of the desired product as a white solid.

Yield: 58.5%

m.p. 154°C

HRMS: *m/z* 337.1231 ($[M+H]^+$

^{1}H NMR (CD_3OD): δ 7.82 (d, *J*=8.9 Hz, 2H), 7.30-7.22 (m, 2H), 7.05 (d, *J*=8.9 Hz, 2H), 6.98-6.88 (m, 3H), 4.24 (t, *J*=6.3 Hz, 2H), 4.02 (dd, *J*=9.4, 4.6 Hz, 1H), 3.89 (dd, *J*=9.4, 6.3 Hz, 1H), 3.44-3.33 (m, 1H), 2.19-2.05 (m, 1H), 2.02-1.87 (m, 1H).

^{13}C NMR (CD_3OD): δ 161.73, 158.79, 135.40, 129.08, 127.79, 120.59, 114.18, 71.64, 65.34, 32.51.

[67] Dichloromethane/methanol 95:5 + 1% NH_3. R_f starting material = 0.60; R_f product = 0.16.

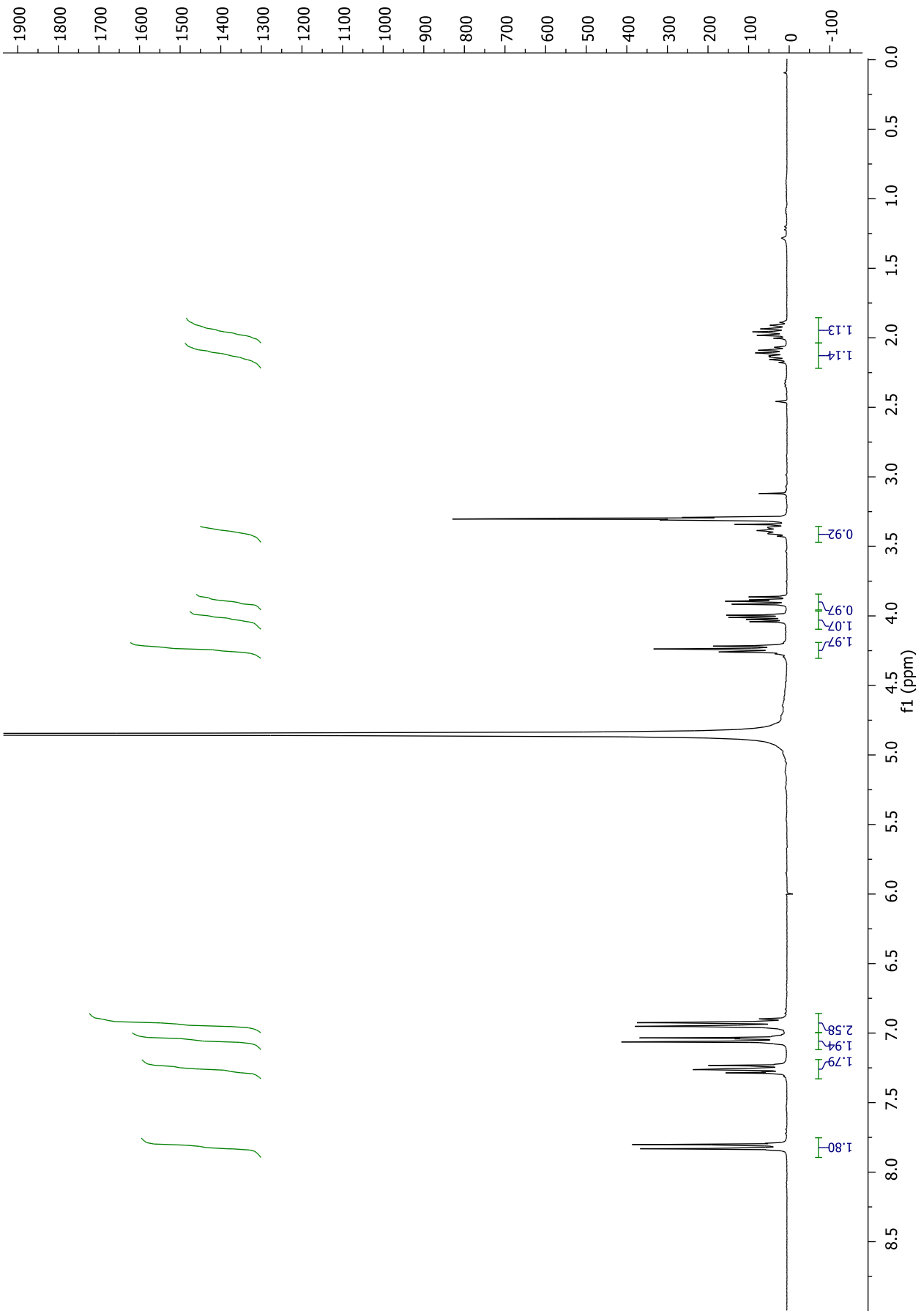
1.13
1.14
0.92
0.97
1.07
1.97
2.58
1.94
1.79
1.80
f1 (ppm)

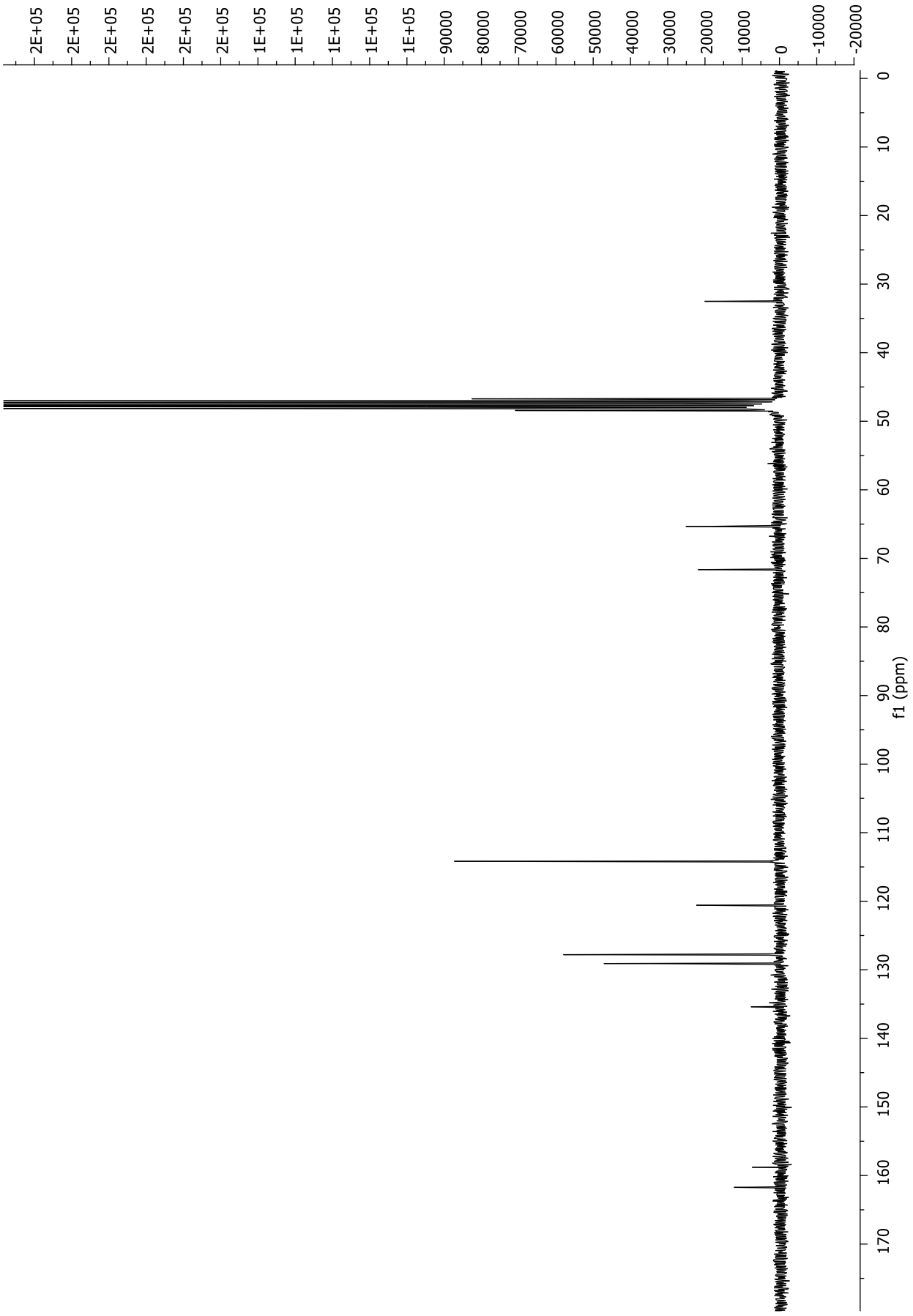
2E+05
2E+05
2E+05
2E+05
2E+05
2E+05
1E+05
1E+05
1E+05
1E+05
1E+05
90000
80000
70000
60000
50000
40000
30000
20000
10000
0
-10000
-20000
0
10
20
30
40
50
60
70
80
90
100
110
120
130
140
150
160
170
f1 (ppm)

N,N-dimethylaminomethylene-4-(3-hydroxy-4-(2-methoxyphenoxy) butoxy)benzenesulfonamide

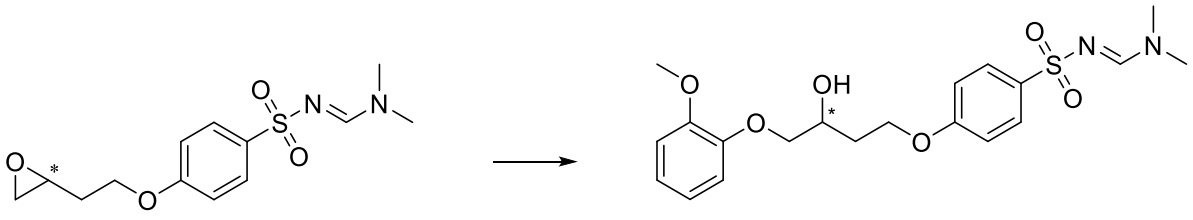

Chemical Formula: $C_{13}H_{18}N_2O_4S$
MW: 298,36

Chemical Formula: $C_{20}H_{26}N_2O_6S$
MW: 422,50

Under a nitrogen atmosphere guaiacol (810 mg, 6.53 mmol) was treated with 1.13 g of K_2CO_3 (8.15 mmol) in 19 mL DMF and the suspension was stirred at room temperature for 30 minutes. Then a solution of N,N-dimethylaminomethylene-4-(oxiranylethoxy)benzenesulfonamide (980 mg, 3.26 mmol) in DMF (7 mL) was added dropwise and the reaction was stirred at 80°C until starting material was consumed (TLC monitoring)[68]. Afterward, the solvent was evaporated in vacuo and the crude was dissolved in ethyl acetate. The organic phase was washed with 10% aqueous solution of NaOH, and brine, dried over anhydrous sodium sulfate and filtered. The solvent was then evaporated in vacuo, providing a dark oil. Flash chromatography (dichloromethane/methanol 99:1) was performed in order to obtain 322 mg (0.76 mmol) of the pure product as a red oil.

Yield: 24.8%

^{1}H NMR ($CDCl_3$): δ 8.11 (s, 1H), 7.79 (d, *J*=8.9 Hz, 2H), 7.02-6.86 (m, 6H), 4.32-4.14 (m, 3H), 4.09 (dd, *J*=9.8, 3.2 Hz, 1H), 3.93 (dd, *J*=9.8, 7.7 Hz, 1H), 3.84 (s, 3H), 3.10 (s, 3H), 3.00 (s, 3H), 2.11-1.93 (m, 2H).

[68] Dichloromethane/methanol 95:5. R_f starting material: 0.64; R_f product: 0.46.

N,N-dimethylaminomethylene-4-(3-mesyloxy-4-(2-methoxyphenoxy) butoxy)benzenesulfonamide

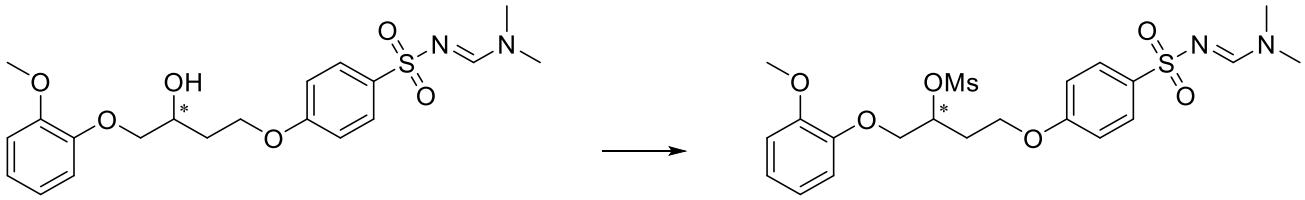

Chemical Formula: $C_{20}H_{26}N_2O_6S$
MW: 422,50

Chemical Formula: $C_{21}H_{28}N_2O_8S_2$
MW: 500,58

N,N-dimethylaminomethylene-4-(3-hydroxy-4-(2-methoxyphenoxy)butoxy)benzenesulfonamide (310 mg, 0.73 mmol) was dissolved in dichloromethane (4 mL), triethylamine (0.22 mL, 1.61 mmol) was added, and after the reaction mixture was cooled down to 0°C mesyl chloride (0.12 mL, 1.47 mmol) was added dropwise. The solution was stirred at room temperature until TLC[69] indicated the disappearance of starting material. The reaction mixture was washed with 10% aqueous solution of HCl 10%, aqueous solution of $NaHCO_3$, and then with brine. The organic phase was dried over anhydrous sodium sulfate and filtered and the solvent was evaporated in vacuo, providing the pure product as 365 mg of a reddish oil (0.73 mmol).

Yield: *100%*

^{1}H NMR ($CDCl_3$): δ 8.11 (s, 1H), 7.82 (d, *J*=8.3 Hz, 2H), 7.01-6.84 (m, 6H), 5.32-5.21 (m, 1H), 4.28-4.15 (m, 4H), 3.81 (s, 3H), 3.19 (s, 3H), 3.13 (s, 3H), 3.02 (s, 3H), 2.35-2.23 (m, 2H).

[69] Dichloromethane/methanol 95:5. R_f starting material = 0.46; R_f product = 0.70.

N,N-dimethylaminomethylene-4-(3-azido-4-(2-methoxyphenoxy) butoxy)benzenesulfonamide

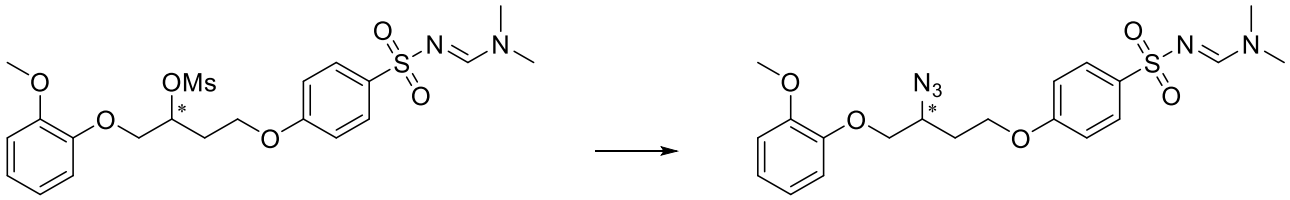

Chemical Formula: $C_{21}H_{28}N_2O_8S_2$
MW: 500,58

Chemical Formula: $C_{20}H_{25}N_5O_5S$
MW: 447,51

Sodium azide (527 mg, 8.11 mmol) was added to a solution of N,N-dimethylaminomethylene-4-(3-hydroxy-4-(2-methoxyphenoxy)butoxy)benzenesulfonamide (406 mg, 0.81 mmol) in DMF (14 mL) and water (4.4 mL). Then, the reaction mixture was refluxed, under stirring, until TLC[70] indicated the disappearance of starting material.

Afterward, the solution was evaporated in vacuo and the crude was dissolved in acetone. The formed precipitate was removed by filtration and then the solvent was evaporated in vacuo, providing the pure product as a yellow oil (321 mg, 0.72 mmol)

Yield = 98.0%

^{1}H NMR ($CDCl_3$): δ 8.12 (s, 1H), 7.82 (d, *J*=8.9 Hz, 2H), 7.02-6.86 (m, 6H), 4.28-4.04 (m, 5H), 3.84 (s, 3H), 3.12 (s, 3H), 3.01 (s, 3H), 2.29-2.07 (m, 1H), 2.10-1.91 (m, 1H).

[70] Dichloromethane/methanol 95:5. R_f starting material = 0.71; R_f product = 0.92.

Compound XVII

4-(3-azido-4-(2-methoxyphenoxy)butoxy)benzenesulfonamide

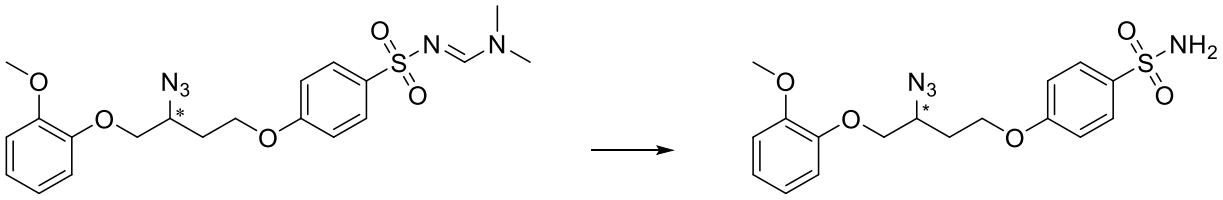

Chemical Formula: $C_{20}H_{25}N_5O_5S$
MW: 447,51

Chemical Formula: $C_{17}H_{20}N_4O_5S$
MW: 392,43

Hydrazine hydrate (0.70 mL, 14.34 mmol) was added at room temperature to a stirred mixture of 239 mg of N,N-dimethylaminomethylene-4-(3-hydroxy-4-(2-methoxyphenoxy)butoxy)benzene sulfonamide (14.34 mmol) in methanol (7.5 mL). The reaction mixture was stirred until starting material was consumed (TLC monitoring)[71]. Then the mixture was evaporating to dryness under reduced pressure in order to obtain an orangish oil.

Flash chromatography (dichloromethane/methanol 98:2) was performed in order to obtain 176 mg (0.45 mmol) of the pure product as a white solid.

Yield: 62.4%

m.p. 113℃

HRMS: *m/z* 391.1074 ($[M+H]^-$

^{1}H NMR (CD_3OD): δ 7.83 (d, *J*=8.8 Hz, 2H), 7.06 (d, *J*=8.8 Hz, 2H), 7.01-6.84 (m, 4H), 4.28-4.15 (m, 3H), 4.12-3.99 (m, 2H), 3.81 (s, 3H), 2.24-2.10 (m, 1H), 2.06-1.93 (m, 1H).

^{13}C NMR (CD_3OD): δ 161.61, 150.04, 147.99, 135.51, 127.83, 122.02, 120.73, 114.78, 114.21, 112.41, 71.95, 64.56, 58.49, 55.11, 30.05.

[71] Dichloromethane/methanol 95:5. R_f starting material = 0.92; R_f product = 0.74.

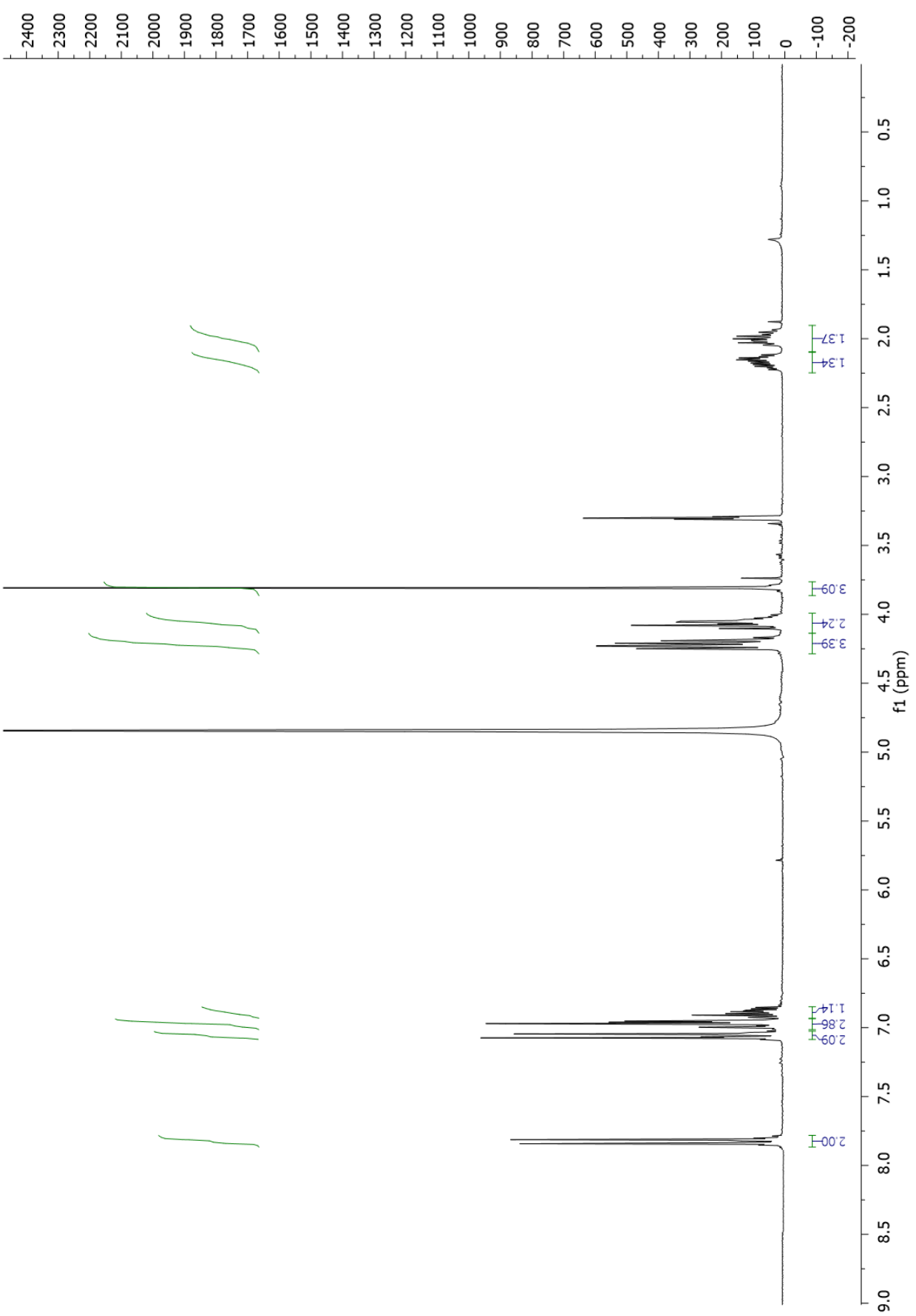
f1 (ppm)
1.37
1.34
3.09
2.24
3.39
1.14
2.86
2.09
2.00

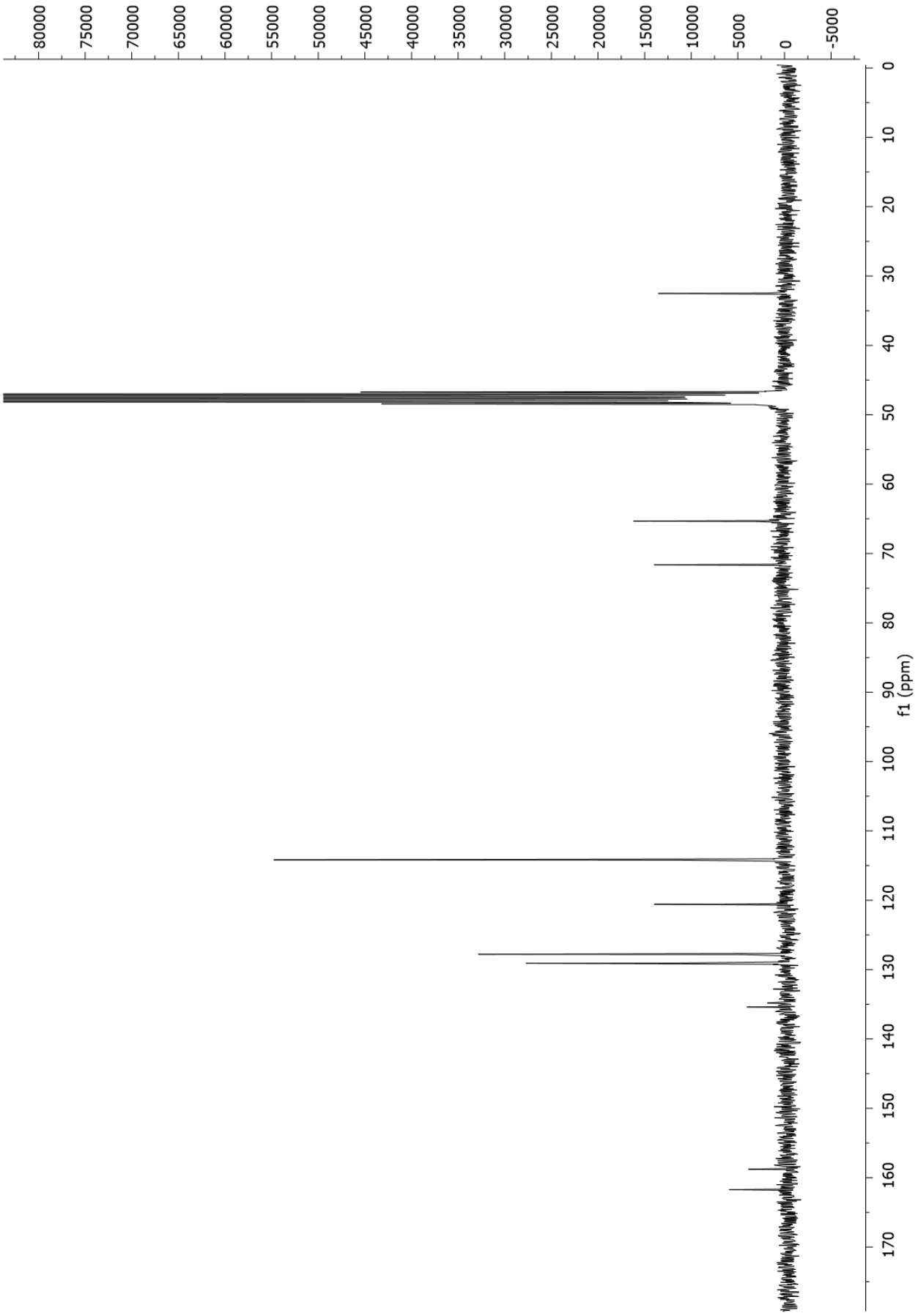
80000
75000
70000
65000
60000
55000
50000
45000
40000
35000
30000
25000
20000
15000
10000
5000
0
-5000
0
10
20
30
40
50
60
70
80
90
100
110
120
130
140
150
160
170
f1 (ppm)

Compound XVIII

4-(3-amino-4-(2-methoxyphenoxy)butoxy)benzenesulfonamide

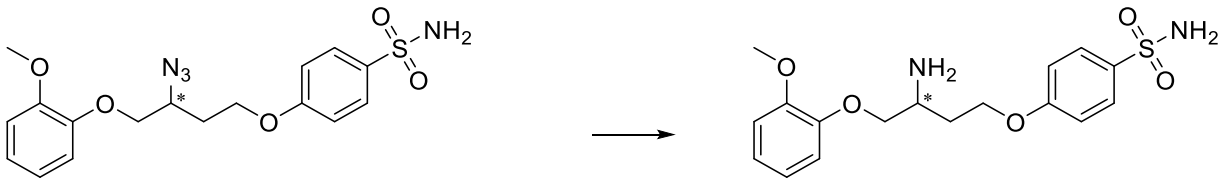

Chemical Formula: $C_{17}H_{20}N_4O_5S$
MW: 392,43

Chemical Formula: $C_{17}H_{22}N_2O_5S$
MW: 366,43

To a solution of 157 mg of 4-(3-azido-4-(2-methoxyphenoxy)butoxy)benzenesulfonamide (0.40 mmol) in methanol (4 mL) was added 80 mg of Pd/C 5%. The mixture was then vigorously shaken under hydrogen atmosphere at room temperature until starting material was consumed (TLC monitoring)[72]. After filtering on a celite pad, the solvent was evaporated under reduced pressure to obtain 111 mg (030 mmol) of the desired product as a white solid.

Yield: 76.1%

m.p. 132°C

HRMS: *m/z* 367.1334 ($[M+H]^+$

^{1}H NMR (CD_3OD): δ 7.81 (d, *J*=8.9 Hz, 2H), 7.04 (d, *J*=8.9 Hz, 2H), 7.01-6.83 (m, 4H), 4.25 (t, *J*=6.7 Hz, 2H), 4.05 (dd, *J*=9.6, 4.4 Hz, 1H), 3.91 (dd, *J*=9.6, 6.7 Hz, 1H), 3.82 (s, 3H), 3.46-3.35 (m, 1H), 2.20-2.05 (m, 1H), 2.03-1.90 (m, 1H).

^{13}C NMR (CD_3OD): δ 161.77, 149.73, 148.27, 135.37, 127.77, 121.52, 120.77, 114.24, 114.17, 73.59, 65.40, 54.99, 48.02, 32.61.

[72] Dichloromethane/methanol 98:2 + 1% NH_3. R_f starting material = 0.46; R_f product = 0.05.

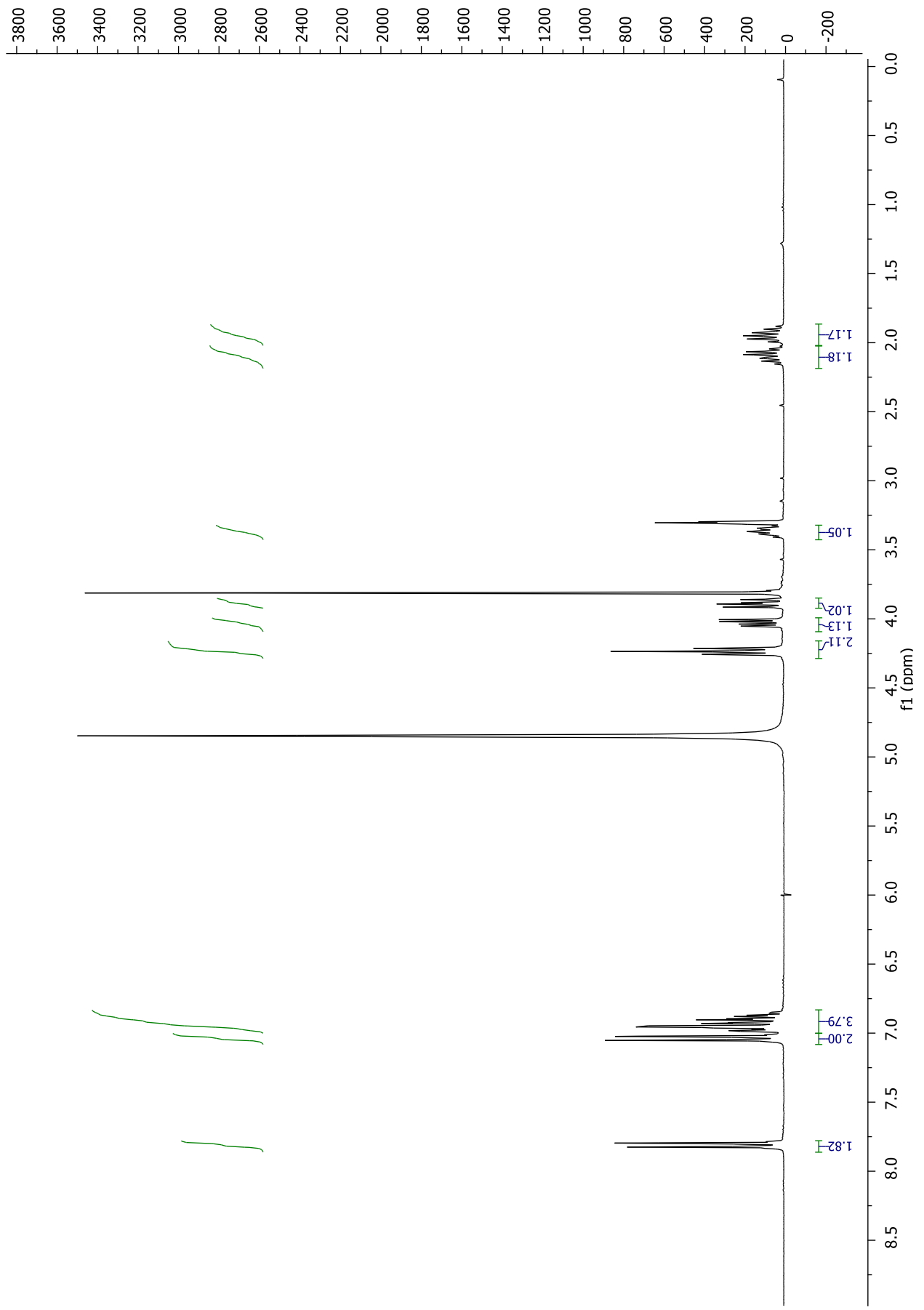
1.17
1.18
1.05
1.02
1.13
2.11
3.79
2.00
1.82
f1 (ppm)

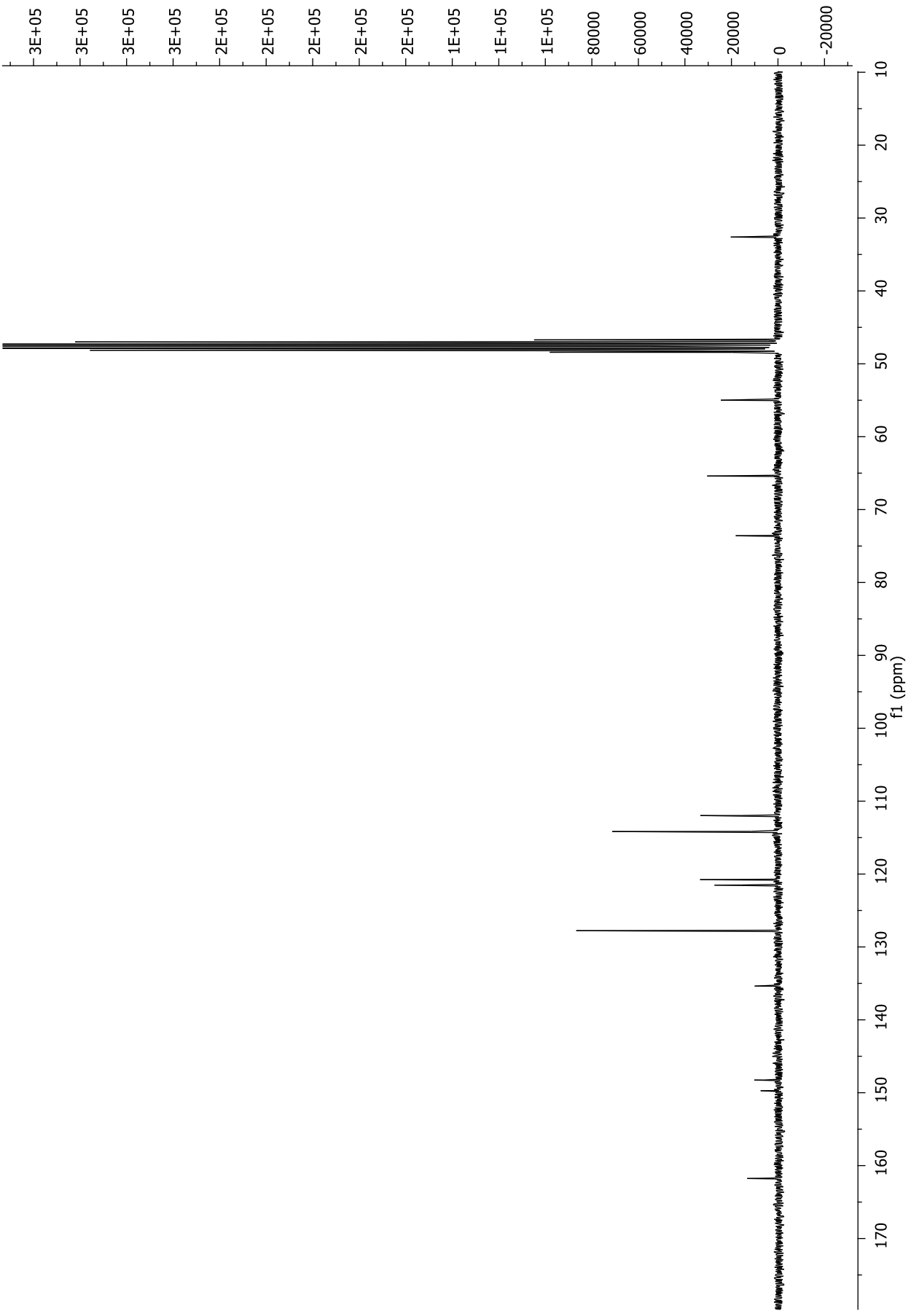
3E+05
3E+05
3E+05
3E+05
2E+05
2E+05
2E+05
2E+05
2E+05
1E+05
1E+05
1E+05
80000
60000
40000
20000
0
-20000
10
20
30
40
50
60
70
80
90
100
110
120
130
140
150
160
170
f1 (ppm)

o-2-methoxyethoxymethoxybenzaldehyde

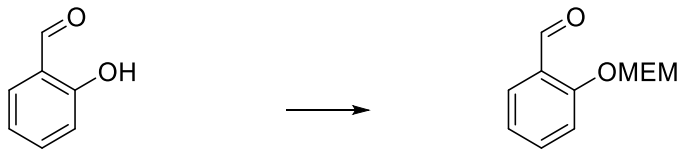

Chemical Formula: $C_7H_6O_2$
Molecular Weight: 122,12

Chemical Formula: $C_{11}H_{14}O_4$
Molecular Weight: 210,23

Under a nitrogen atmosphere a dichloromethane (10 mL) solution of 2-hydroxybenzaldehyde (1 mL, 9.38 mmol) was cooled to 0° C. and DIPEA (2.28 mL, 13.14 mmol) was added. Following the addition of MEM-Cl (1.28 mL, 13.14 mmol), the reaction mixture was allowed to stir, slowly warming to room temperature, until starting material was consumed (TLC monitoring)[73]. The reaction mixture was quenched by the addition of 10% aqueous solution of HCl. The organic layer was washed with washed with 10% aqueous solution of $NaHCO_3$, brine, dried over anhydrous sodium sulfate and filtered. The filtrate was concentrated under reduced pressure to provide the desired product as a yellow oil (1.96 g, 9.32 mmol)

Yield: 99.4%

^{1}H NMR ($CDCl_3$): δ 10.49 (s, *J*=0.8 Hz, 1H), 7.84 (dt, *J*=7.5, 1.7 Hz, 1H), 7.53 (ddt, *J*=9.0, 5.8, 1.7 Hz, 1H), 7.30-7.22 (m, 1H), 7.08 (t, *J*=7.5 Hz, 1H), 5.40 (d, *J*=1.5 Hz, 2H), 3.87 (ddd, *J*=6.1, 2.9, 1.5 Hz, 2H), 3.56 (ddd, *J*=6.1, 2.9, 1.5 Hz, 2H), 3.40-3.34 (s, 3H).

[73] Cyclohexane/ethyl acetate 7:3. R_f starting material = 0.70; R_f product = 0.70, stainer: cerium sulfate.

2-methoxyethoxymethyloxyphenol

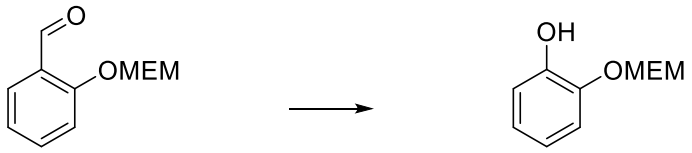

Chemical Formula: $C_{11}H_{14}O_4$
Molecular Weight: 210,23

Chemical Formula: $C_{10}H_{14}O_4$
Molecular Weight: 198,22

Under nitrogen atmosphere, *m*-chloroperbenzoic acid (2.18 g, 13.92 mmol) was added to a solution of *o*-2-methoxyethoxymethoxybenzaldehyde (2.09 g, 9.94 mmol) in dichloromethane (30 mL). The resulting reaction mixture was stirred at room temperature for 12 hours. Afterward, the mixture was cooled down to 0°C and the filtrate was diluted with dichloromethane and washed with a saturated aqueous solution of $Na_2S_2O_5$, a 10% aqueous solution of $NaHCO_3$ and then with brine. The organic phase was dried over anhydrous sodium sulfate, filtered and the solvent was evaporated in vacuo. The resulting residue was suspended in a methanolic (5 mL) solution of KOH (890 mg, 15.91 mmol) and the resulting reaction mixture was stirred at room temperature under stirring, until TLC[74] indicated the disappearance of starting material. Afterward, the mixture was concentrated in vacuo and the resulting residue was diluted with water (10 mL) and washed with diethyl ether. Upon phase separation, the aqueous phase was acidified with formic acid until pH 5 and extracted with ethyl acetate. The organic phase was dried over anhydrous sodium sulfate and filtered and the solvent was evaporated in vacuo, providing the pure product as a yellow oil (1.45 g, 7.31 mmol).

Yield: 73.0%

^{1}H NMR ($CDCl_3$): δ 7.07 (d, *J*=8.0 Hz, 1H), 6.94 (d, *J*=4.0 Hz, 2H), 6.86-6.77 (m, 1H), 5.27 (s, 2H), 3.98-3.78 (m, 2H), 3.66-3.53 (m, 2H), 3.41 (s, 3H)

[74] Cyclohexane/ethyl acetate 7:3. R_f starting material = 0.70; R_f product = 0.70, stainer: cerium sulfate.

N,N-dimethylaminomethylene-4-(3-hydroxy-4-(2-methoxyphenoxy) butoxy)benzenesulfonamide

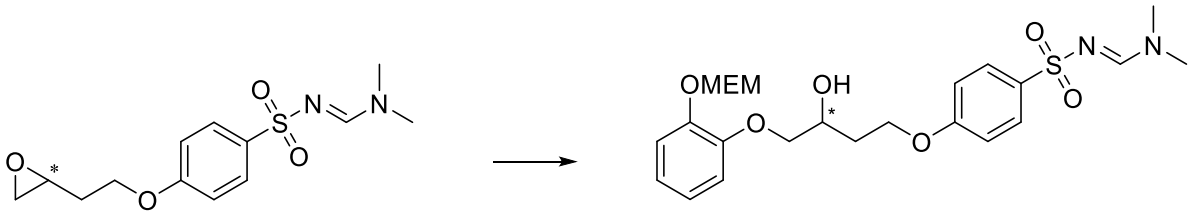

Chemical Formula: $C_{13}H_{18}N_2O_4S$
MW: 298,36

Chemical Formula: $C_{23}H_{32}N_2O_8S$
MW: 496,58

Under a nitrogen atmosphere 2-methoxyethoxymethyloxyphenol (1.48 mg, 7.47 mmol) was treated with 1.26 g of K_2CO_3 (9.14 mmol) in 15 mL DMF and the suspension was stirred at room temperature for 30 minutes. Then a solution of N,N-dimethylaminomethylene-4-(oxiranylethoxy)benzene sulfonamide (1.36 g, 4.57 mmol) in DMF (8 mL) was added dropwise and the reaction was stirred at 80°C until starting material was consumed (TLC monitoring)[75]. Afterward, the solvent was evaporated in vacuo and the crude was dissolved in ethyl acetate. The organic phase was washed with 10% aqueous solution of NaOH, and brine, dried over anhydrous sodium sulfate and filtered. The solvent was then evaporated in vacuo, providing a dark oil.

Flash chromatography (dichloromethane/methanol 98:2) was performed in order to obtain 775 mg (1.56 mmol) of the pure product as a red oil.

Yield: 34.1%

^{1}H NMR ($CDCl_3$): δ 8.11 (s, 1H), 7.80 (d, *J*=8.9 Hz, 2H), 7.18-7.12 (m, 1H), 7.00-6.89 (m, 5H), 5.28 (s, 2H), 4.30-4.14 (m, 3H), 4.10 (dd, *J*=9.7, 3.0 Hz, 1H), 3.93 (dd, *J*=9.7, 7.7 Hz, 1H), 3.88-3.82 (m, 2H), 3.60-3.50 (m, 2H), 3.35 (s, 3H), 3.11 (s, 3H), 3.00 (s, 3H), 2.12-1.92 (m, 2H).

[75] Dichloromethane/methanol 95:5. R_f starting material: 0.64; R_f product: 0.27.

N,N-dimethylaminomethylene-4-(3-mesyloxy-4-(2-methoxyethoxy methyloxyphenoxy)butoxy)benzenesulfonamide

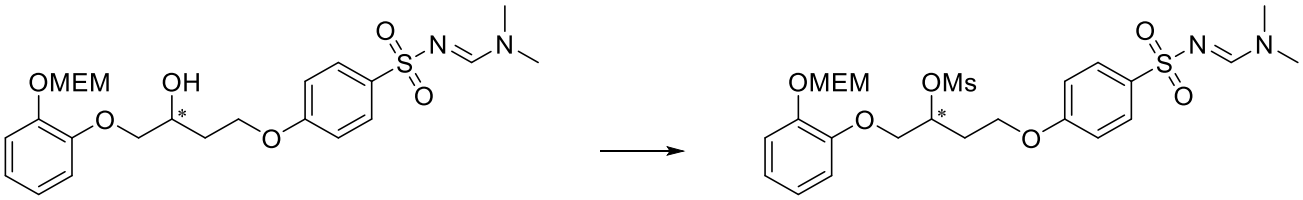

Chemical Formula: $C_{23}H_{32}N_2O_8S$
MW: 496,58

Chemical Formula: $C_{24}H_{34}N_2O_{10}S_2$
MW: 574,66

N,N-dimethylaminomethylene-4-(3-hydroxy-4-(2-methoxyphenoxy)butoxy)benzenesulfonamide (775 mg, 1.56 mmol) was dissolved in dichloromethane (5 mL), triethylamine (0.48 mL, 3.43 mmol) was added, and after the reaction mixture was cooled down to 0°C mesyl chloride (0.26 mL, 3.12 mmol) was added dropwise. The solution was stirred at room temperature until TLC[76] indicated the disappearance of starting material. The reaction mixture was washed with 10% aqueous solution of HCl 10%, aqueous solution of $NaHCO_3$, and then with brine. The organic phase was dried over anhydrous sodium sulfate and filtered and the solvent was evaporated in vacuo, providing the pure product as 776 mg of a yellow gum (1.35 mmol).

Yield: *86.6%*

^{1}H NMR ($CDCl_3$): δ 8.10 (s, 1H), 7.81 (d, *J*=8.8 Hz, 2H), 7.20-7.14 (m, 1H), 7.03-6.86 (m, 5H), 5.25 (m, 3H), 4.25-4.17 (m, 4H), 3.84-3.78 (m, 2H), 3.58-3.50 (m, 2H), 3.38 (s, 3H), 3.16 (s, 3H), 3.11 (s, 3H), 3.01 (s, 3H), 2.33-2.25 (m, 2H).

[76] Dichloromethane/methanol 95:5. R_f starting material = 0.27; R_f product = 0.68.

N,N-dimethylaminomethylene-4-(3-mesyloxy-4-(2-methoxyethoxy methyloxyphenoxy)benzenesulfonamide

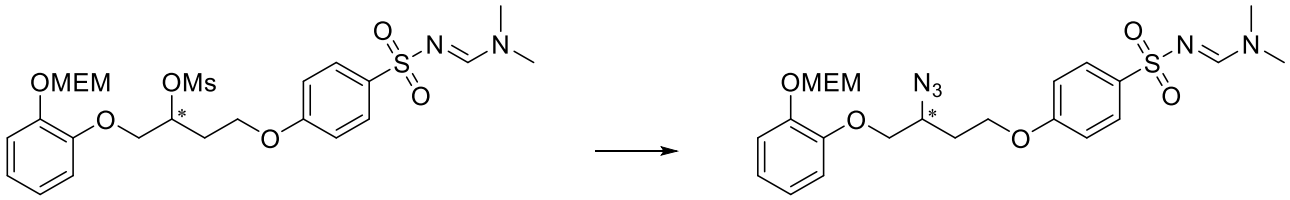

Chemical Formula: $C_{24}H_{34}N_2O_{10}S_2$
MW: 574,66

Chemical Formula: $C_{23}H_{31}N_5O_7S$
MW: 521,59

Sodium azide (877 mg, 13.5 mmol) was added to a solution of N,N-dimethylaminomethylene-4-(3-mesyloxy-4-(2-methoxyethoxymethyloxyphenoxy)butoxy)benzenesulfonamide (776 mg, 1.35 mmol) in DMF (18 mL) and water (5.6 mL). Then, the reaction mixture was refluxed, under stirring, until TLC[77] indicated the disappearance of starting material.

Afterward, the solution was evaporated in vacuo and the crude was dissolved in acetone. The formed precipitate was removed by filtration and then the solvent was evaporated in vacuo, providing a yellow oil. Flash chromatography (cyclohexane/acetone 6:4) was performed in order to obtain 290 mg (0.56 mmol) of the pure product as a colorless oil.

Yield = 41.2%

^{1}H NMR ($CDCl_3$): δ 8.12 (s, 1H), 7.82 (d, *J*=8.8 Hz, 2H), 7.18 (dd, *J*=7.2, 2.1 Hz, 1H), 7.01-6.88 (m, 5H), 5.28 (s, 2H), 4.25-4.01 (m, 5H), 3.86 (m, 2H), 3.60-3.51 (m, 2H), 3.37 (s, 3H), 3.12 (s, 3H), 3.01 (s, 3H), 2.25-2.09 (m, 1H), 2.04-1.92 (m, 1H).

[77] Dichloromethane/methanol 95:5. R_f starting material = 0.68; R_f product = 0.46.

Compound XIX

4-(3-azido-4-(2-hydroxyphenoxy)benzenesulfonamide

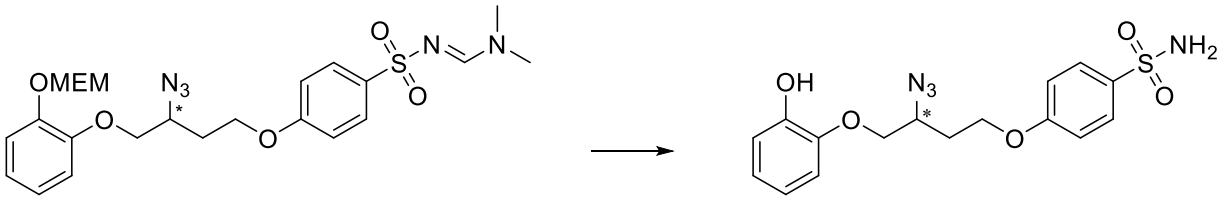

Chemical Formula: $C_{23}H_{31}N_5O_7S$
MW: 521,59

Chemical Formula: $C_{16}H_{18}N_4O_5S$
MW: 378,40

0.46 mL of HCl 37% (5.56 mmol) was added dropwise to a solution of N,N-dimethylaminomethylene-4-(3-mesyloxy-4-(2-methoxyethoxymethyloxyphenoxy)benzenesulfonamide (290 mg, 0.56 mmol) in methanol (4 mL). The resulting solution was vigorously stirred at 60°C, until TLC[78] indicated the disappearance of starting material. Afterward, methanol was removed from the reaction mixture in vacuo. Flash chromatography (dichloromethane/methanol 98:2) was performed in order to obtain 193 mg (0.51 mmol) of the pure product as a white solid.

Yield: 91.1%

m.p. 98°C (degradation)

HRMS: *m/z* 377.0911 ($[M+H]^-$

^{1}H NMR (CD_3OD): δ 7.83 (d, *J*=9.0 Hz, 2H), 7.07 (d, *J*=9.0 Hz, 2H), 6.99-6.93 (m, 1H), 6.86-6.74 (m, 3H), 4.30-4.04 (m, 5H), 2.28-2.13 (m, 1H), 2.08-1.94 (m, 1H).

^{13}C NMR (CD_3OD): δ 161.61, 146.85, 146.38, 135.54, 127.83, 121.93, 119.54, 115.58, 114.21, 71.66, 64.57, 58.51, 30.11.

[78] Dichloromethane/methanol 93:7. R_f starting material = 0.92; R_f product = 0.62.

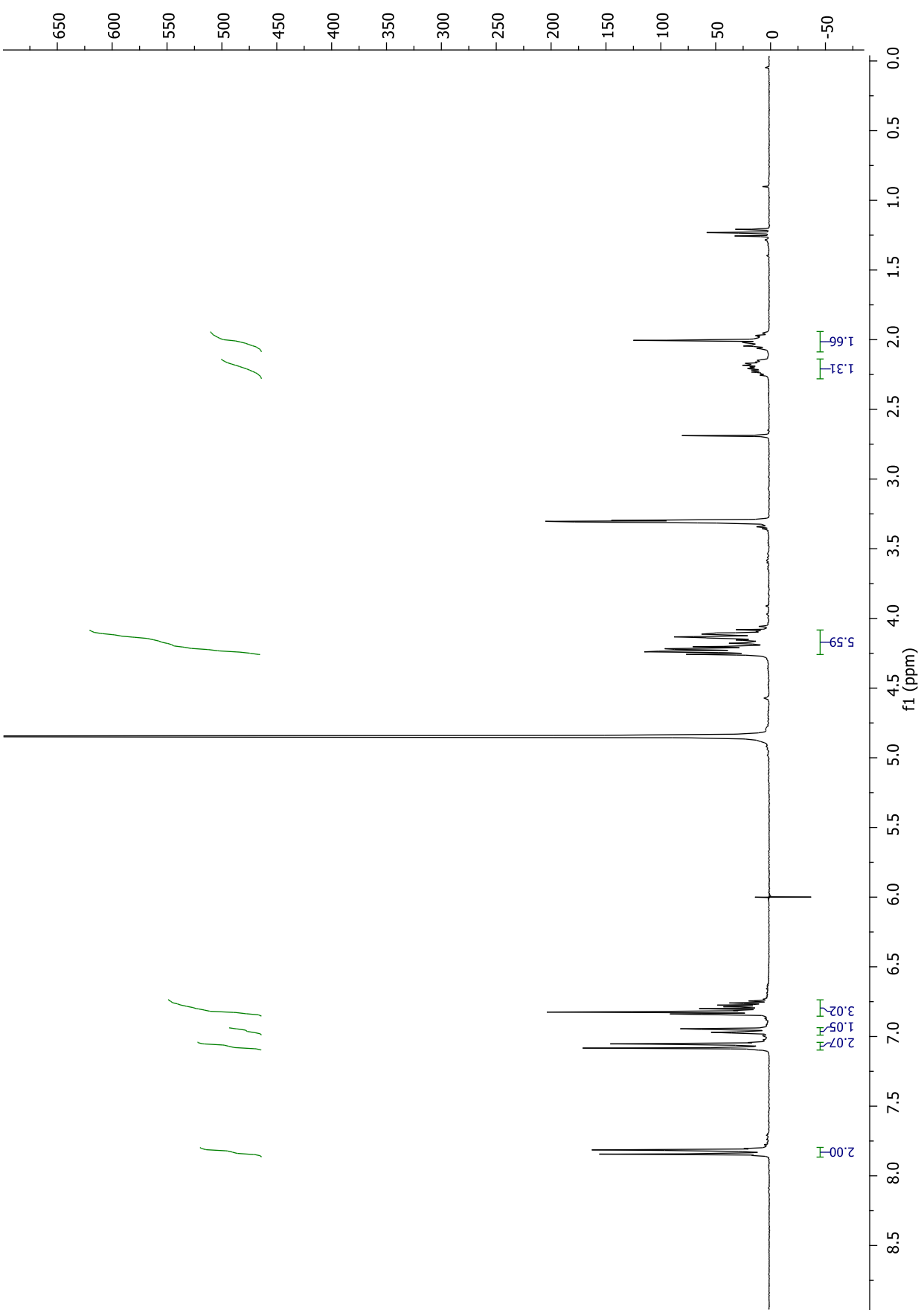
650
600
550
500
450
400
350
300
250
200
150
100
50
0
-50
0.0
0.5
1.0
1.5
2.0
2.5
3.0
3.5
4.0
4.5
5.0
5.5
6.0
6.5
7.0
7.5
8.0
8.5
f1 (ppm)
1.66
1.31
5.59
3.02
1.05
2.07
2.00

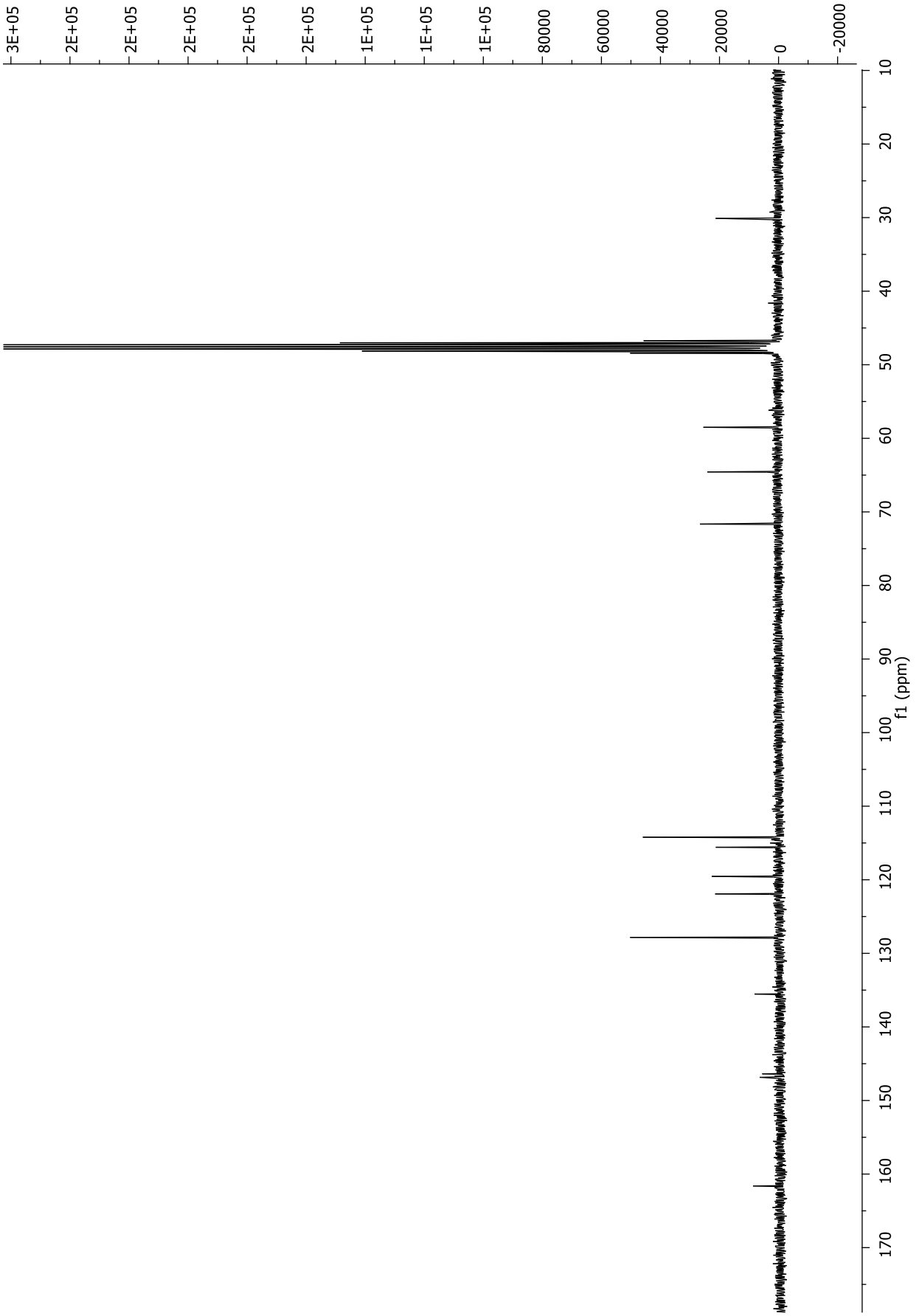
3E+05
2E+05
2E+05
2E+05
2E+05
2E+05
1E+05
1E+05
1E+05
80000
60000
40000
20000
0
-20000
10
20
30
40
50
60
70
80
90
100
110
120
130
140
150
160
170
f1 (ppm)

Compound XX

4-(3-amino-4-(2-hydroxyphenoxy)benzenesulfonamide

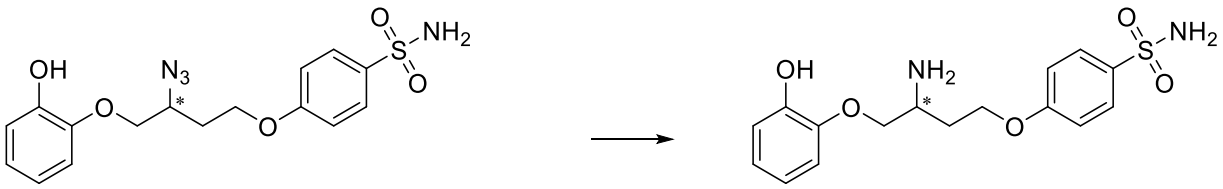

Chemical Formula: $C_{16}H_{18}N_4O_5S$
MW: 378,40

Chemical Formula: $C_{16}H_{20}N_2O_5S$
MW: 352,41

To a solution of 193 mg of 4-(3-azido-4-(2-hydroxyphenoxy)benzenesulfonamide (0.51 mmol) in methanol (4 mL) was added 100 mg of Pd/C 5%. The mixture was then vigorously shaken under hydrogen atmosphere at room temperature until starting material was consumed (TLC monitoring)[79]. After filtering on a celite pad, the solvent was evaporated under reduced pressure to obtain an yellow oil. Flash chromatography (ethyl acetate/methanol 8:2 + 1% NH_3) was performed in order to obtain 78 mg (0.22 mmol) of the pure product as a white solid.

Yield: 43.4%

m.p. = 126°C

HRMS: *m/z* 353.1177 ($[M+H]^+$

^{1}H NMR (CD_3OD): δ 7.81 (d, *J*=9.0 Hz, 2H), 7.04 (d, *J*=9.0 Hz, 2H), 6.94-6.88 (m, 1H), 6.82-6.71 (m, 3H), 4.23 (t, *J*=6.3 Hz, 2H), 4.08 (dd, *J*=9.6, 3.7 Hz, 1H), 3.88 (dd, *J*=9.6, 7.1 Hz, 1H), 3.46-3.36 (m, 1H), 2.16-1.87 (m, 2H).

^{13}C NMR (CD_3OD): δ 161.72, 146.78, 146.69, 135.42, 127.79, 121.33, 119.37, 115.39, 114.18, 113.00, 72.63, 65.37, 32.54.

[79] Dichloromethane/methanol 9:1 + 1% NH_3. R_f starting material = 0.88; R_f product = 0.42.

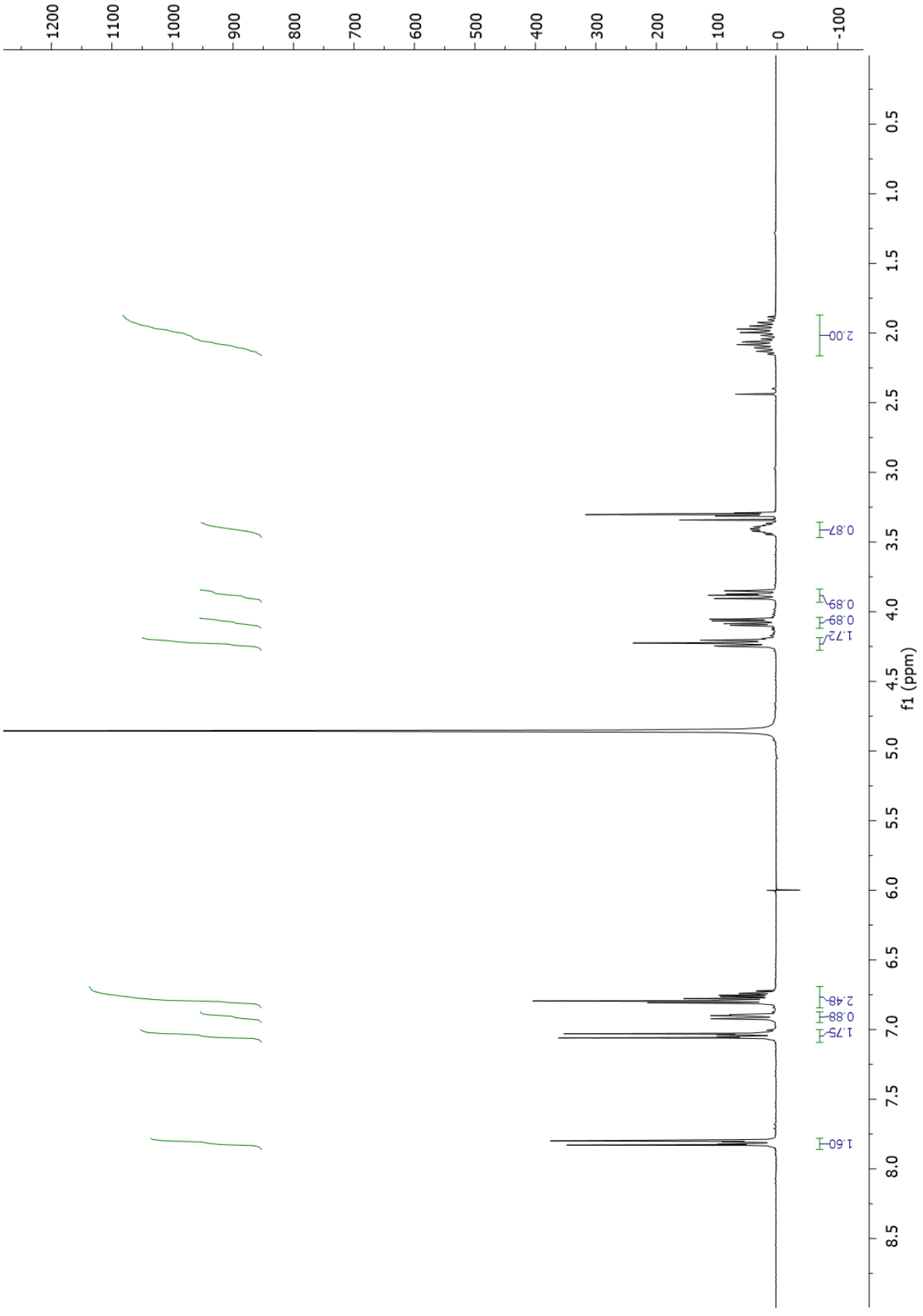
1200
1100
1000
900
800
700
600
500
400
300
200
100
0
-100
0.5
1.0
1.5
2.0
2.5
3.0
3.5
4.0
4.5
5.0
5.5
6.0
6.5
7.0
7.5
8.0
8.5
f1 (ppm)
2.00
0.87
0.89
0.89
1.72
2.48
0.88
1.75
1.60

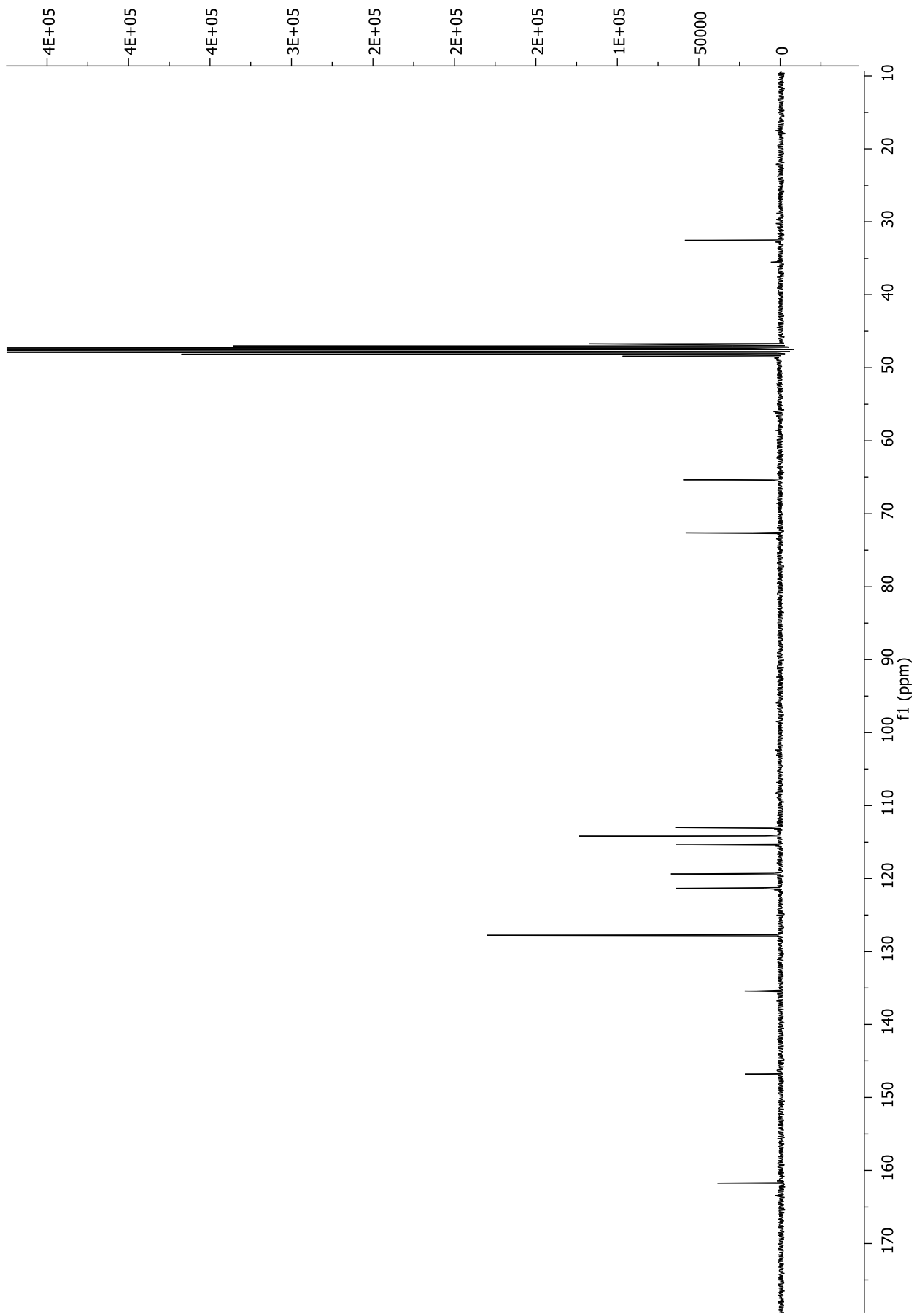
4E+05
4E+05
4E+05
3E+05
2E+05
2E+05
2E+05
1E+05
50000
0
10
20
30
40
50
60
70
80
90
100
110
120
130
140
150
160
170
f1 (ppm)

N,N-dimethylaminomethylene-4-(3-hydroxy-4-(2,6-dimethoxy phenoxy)butoxy)benzenesulfonamide

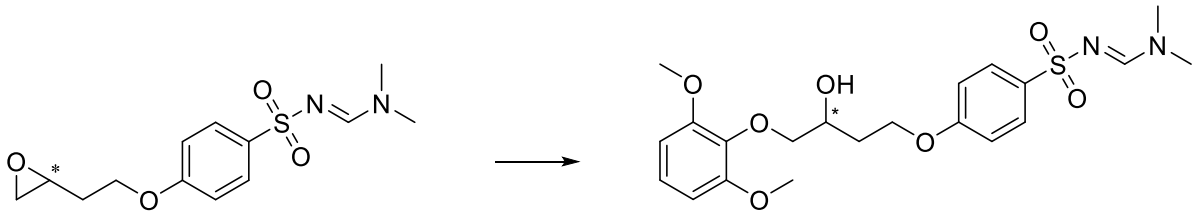

Chemical Formula: $C_{13}H_{18}N_2O_4S$
MW: 298,36

Chemical Formula: $C_{21}H_{28}N_2O_7S$
MW: 452,52

A solution of $PdCl_2$ (11 mg, 0.06 mmol), TBAB (435 mg, 1.35 mmol) and K_2CO_3 (186 mg, 1.35 mmol) in water was prepared and heated to 60°C. N,N-dimethylaminomethylene-4-(oxiranylethoxy)benzenesulfonamide (1.78 g, 5.96 mmol) was then added to the stirring mixture along with 2,6-dimethoxyphenol (835 mg, 5.42 mmol). The reaction was then stirred at 60°C until starting material was consumed (TLC monitoring)[80]. The product was then extracted three times using ethyl acetate. The combined organic layers were then dried over anhydrous sodium sulphate and concentrated under vacuum to yield the black crude product, which was then purified by flash chromatography (dichloromethane/methanol 98:2) to yield the product as a brown oil (570 mg, 1.26 mmol).

Yield: 23.2%

^{1}H NMR ($CDCl_3$): δ 8.11 (s, 1H), 7.79 (d, *J*=8.8 Hz, 2H), 7.01 (t, *J*=8.4 Hz, 1H), 6.92 (d, *J*=8.8 Hz, 2H), 6.59 (d, *J*=8.4 Hz, 2H), 4.29-4.13 (m, 3H), 4.11-4.01 (m, 1H), 3.86 (s, 6H), 3.82-3.69 (m, 1H), 3.11 (s, 3H), 3.00 (s, 3H), 1.98-1.86 (m, 2H).

[80] Dichloromethane/methanol 95:5. R_f starting material = 0.64; R_f product = 0.33.

N,N-dimethylaminomethylene-4-(3-mesyloxy-4-(2,6-dimethoxy phenoxy)butoxy)benzenesulfonamide

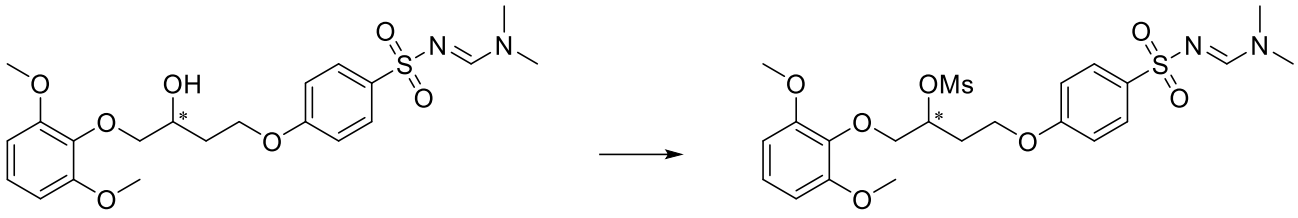

Chemical Formula: $C_{21}H_{28}N_2O_7S$
MW: 452,52

Chemical Formula: $C_{22}H_{30}N_2O_9S_2$
MW: 530,61

N,N-dimethylaminomethylene-4-(3-hydroxy-4-(2,6-dimethoxyphenoxy)butoxy)benzene sulfonamide (570 mg, 1.26 mmol) was dissolved in dichloromethane (12 mL), triethylamine (0.39 mL, 2.77 mmol) was added, and after the reaction mixture was cooled down to 0°C mesyl chloride (0.21 mL, 2.52 mmol) was added dropwise. The solution was stirred at room temperature until TLC[81] indicated the disappearance of starting material. The reaction mixture was washed with 10% aqueous solution of HCl 10%, aqueous solution of $NaHCO_3$, and then with brine. The organic phase was dried over anhydrous sodium sulfate and filtered and the solvent was evaporated in vacuo, providing the pure product as 644 mg of a yellow oil (1.21 mmol).

Yield: *96.4%*

^{1}H NMR ($CDCl_3$): δ 8.10 (s, 1H), 7.80 (d, *J*=8.9 Hz, 2H), 7.02 (t, *J*=8.4 Hz, 1H), 6.93 (d, *J*=8.9 Hz, 2H), 6.57 (d, *J*=8.4 Hz, 2H), 5.24 (m, 1H), 4.24-4.14 (m, 4H), 3.83 (s, 6H), 3.18 (s, 3H), 3.12 (s, 3H), 3.01 (s, 3H), 2.34-2.22 (m, 2H).

[81] Dichloromethane/methanol 95:5. R_f starting material = 0.33; R_f product = 0.60.

N,N-dimethylaminomethylene-4-(3-azido-4-(2,6-dimethoxyphenoxy) butoxy)benzenesulfonamide

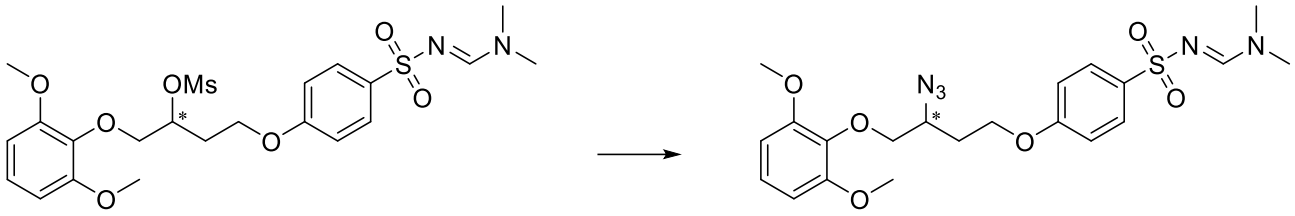

Chemical Formula: $C_{22}H_{30}N_2O_9S_2$
MW: 530,61

Chemical Formula: $C_{21}H_{27}N_5O_6S$
MW: 477,54

Sodium azide (789 mg, 12.14 mmol) was added to a solution of N,N-dimethylaminomethylene-4-(3-hydroxy-4-(2,6-dimethoxyphenoxy)butoxy)benzenesulfonamide (644 mg, 1.21 mmol) in DMF (25 mL) and water (7.8 mL). Then, the reaction mixture was refluxed, under stirring, until TLC[82] indicated the disappearance of starting material.

Afterward, the solution was evaporated in vacuo and the crude was dissolved in acetone. The formed precipitate was removed by filtration and then the solvent was evaporated in vacuo, providing a yellow oil. Flash chromatography (dichloromethane/methanol 98:2) was performed in order to obtain of the pure product as a white solid (321 mg, 0.72 mmol).

Yield = 68.9%

m.p. 118°C

^{1}H NMR ($CDCl_3$): δ 8.12 (s, 1H), 7.82 (d, *J*=8.9 Hz, 2H), 7.01 (t, *J*=8.4 Hz, 1H), 6.94 (d, *J*=8.9 Hz, 2H), 6.58 (d, *J*=8.4 Hz, 2H), 4.23-3.94 (m, 5H), 3.84 (s, 6H), 3.12 (s, 3H), 3.01 (s, 3H), 2.27-2.14 (m, 1H), 2.04-1.90 (m, 1H).

[82] Dichloromethane/methanol 95:5. R_f starting material = 0.60; R_f product = 0.66.

Compound XXI

4-(3-azido-4-(2,6-dimethoxyphenoxy)butoxy)benzenesulfonamide

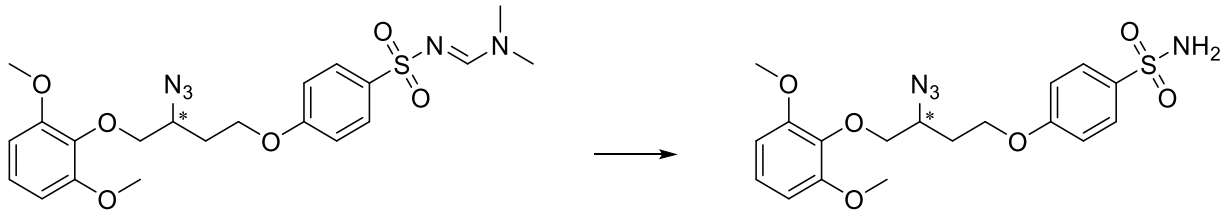

Chemical Formula: $C_{21}H_{27}N_5O_6S$
MW: 477,54

Chemical Formula: $C_{18}H_{22}N_4O_6S$
MW: 422,46

Hydrazine hydrate (0.81 mL, 16.74 mmol) was added at room temperature to a stirred mixture of 399 mg of N,N-dimethylaminomethylene-4-(3-hydroxy-4-(2,6-dimethoxyphenoxy)butoxy)benzene sulfonamide (0.84 mmol) in methanol (17 mL). The reaction mixture was stirred until starting material was consumed (TLC monitoring)[83]. Then the mixture was evaporating to dryness under reduced pressure in order to obtain an orangish oil.

Flash chromatography (dichloromethane/methanol 98:2) was performed in order to obtain 290 mg (0.69 mmol) of the pure product as a light yellow oil.

Yield: 82.6%

HRMS: *m/z* 421.1177 ($[M+H]^-$

^{1}H NMR (CD_3OD): δ 7.83 (d, *J*=8.9 Hz, 2H), 7.10-6.97 (m, 3H), 6.65 (d, *J*=8.4 Hz, 2H), 4.23 (dd, *J*=6.8, 5.5 Hz, 2H), 4.12-3.89 (m, 3H), 3.82 (s, 6H), 2.23-2.11 (m, 1H), 2.03-1.90 (m, 1H).

^{13}C NMR (CD_3OD): δ 161.65, 153.39, 136.54, 135.50, 127.84, 123.96, 114.20, 105.12, 74.78, 64.64, 58.99, 55.14, 55.12, 30.02.

[83] Dichloromethane/methanol 9:1. R_f starting material = 0.92; R_f product = 0.74.

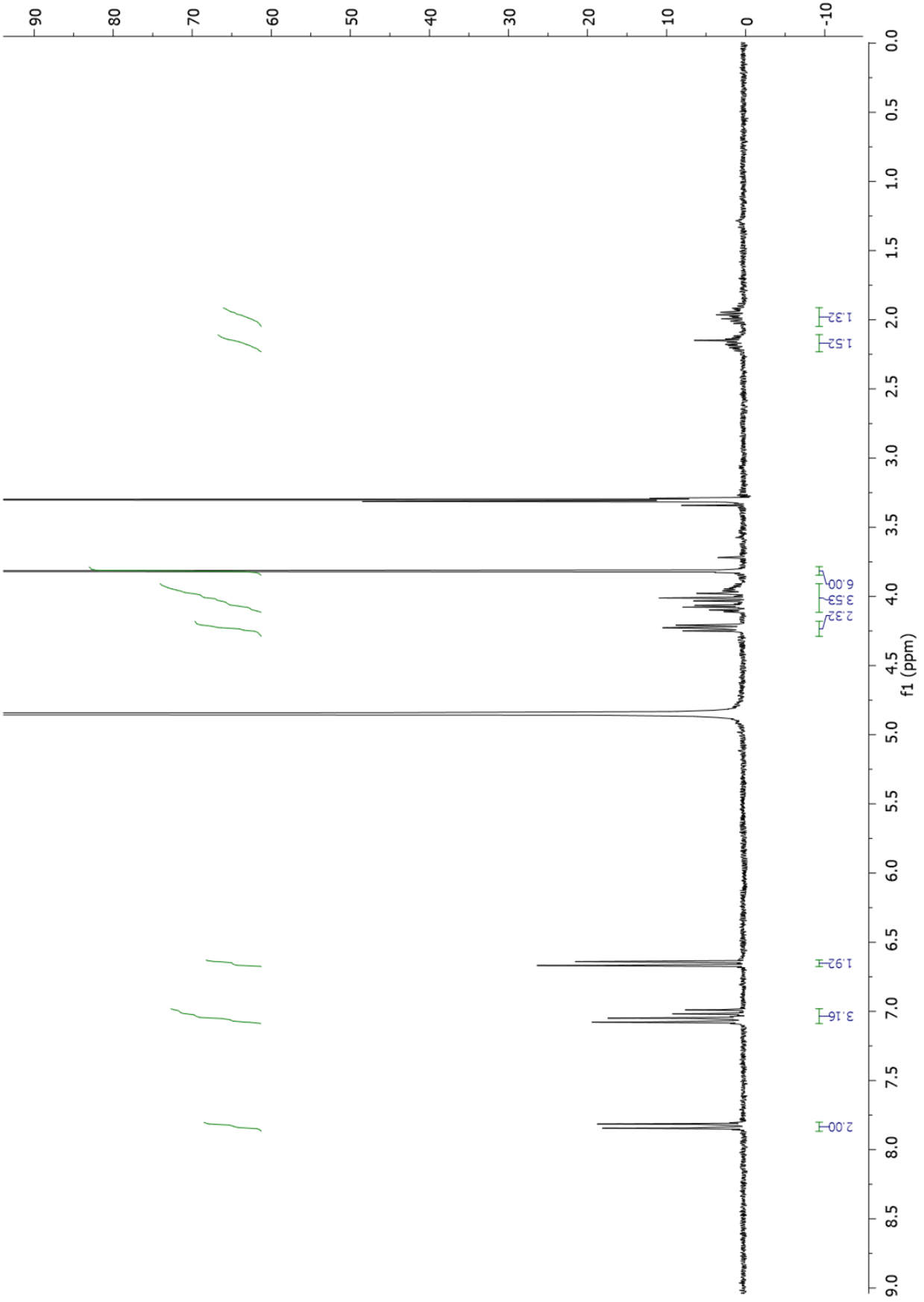
f1 (ppm)
1.32
1.52
6.00
3.53
2.32
1.92
3.16
2.00

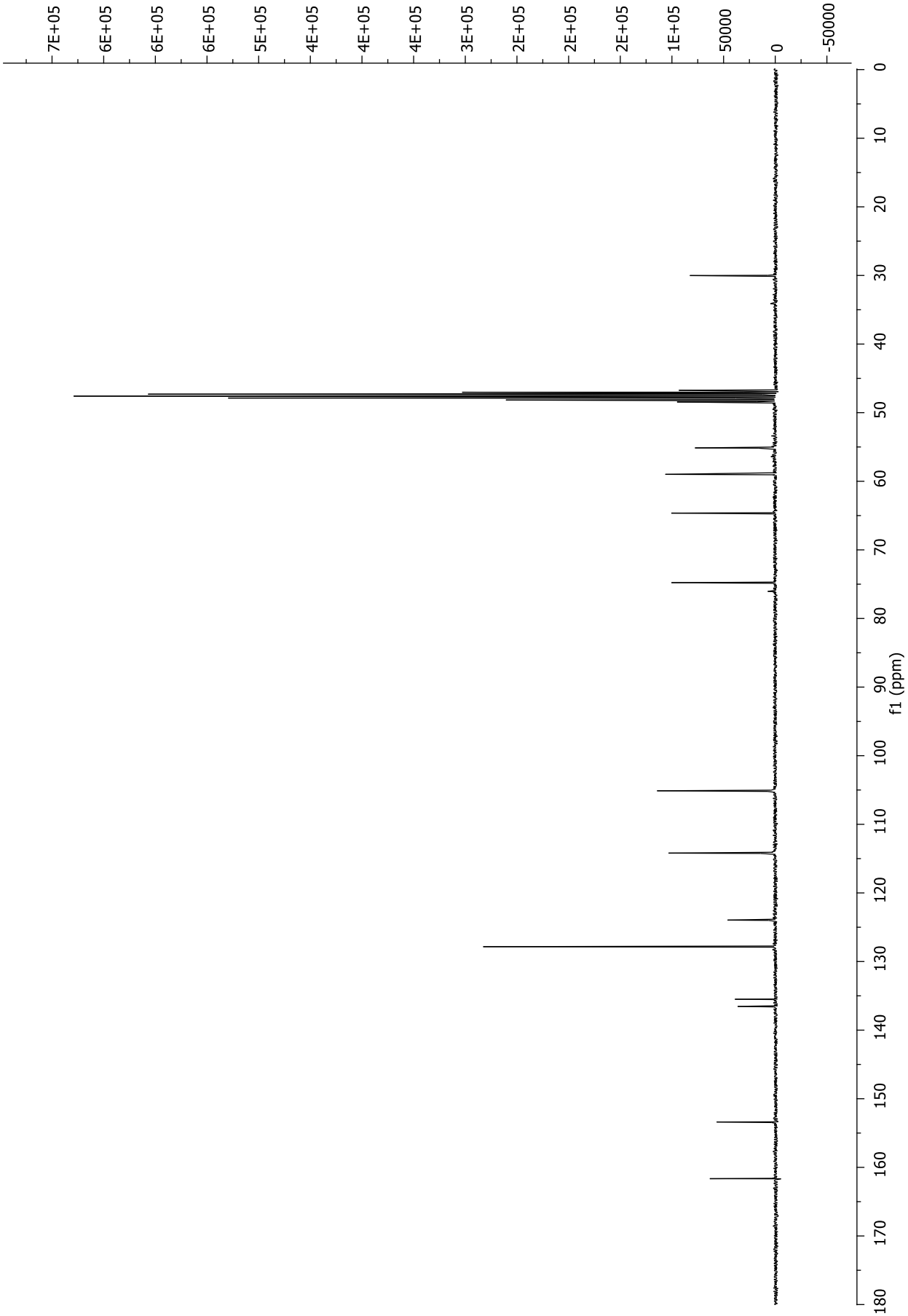
7E+05
6E+05
6E+05
6E+05
5E+05
4E+05
4E+05
4E+05
3E+05
2E+05
2E+05
2E+05
1E+05
50000
0
-50000
0
10
20
30
40
50
60
70
80
90
100
110
120
130
140
150
160
170
180
f1 (ppm)

Compound XXII

4-(3-amino-4-(2,6-dimethoxyphenoxy)benzenesulfonamide

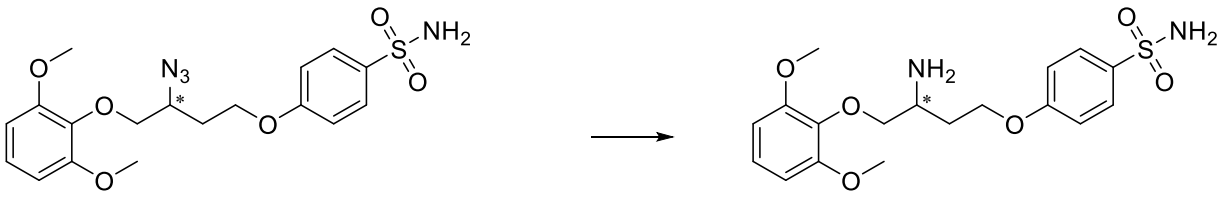

Chemical Formula: $C_{18}H_{22}N_4O_6S$
MW: 422,46

Chemical Formula: $C_{18}H_{24}N_2O_6S$
MW: 396,46

To a solution of 200 mg of 4-(3-azido-4-(2,6-dimethoxyphenoxy)benzenesulfonamide (0.47 mmol) in methanol (4 mL) was added 94 mg of Pd/C 5%. The mixture was then vigorously shaken under hydrogen atmosphere at room temperature until starting material was consumed (TLC monitoring)[84]. After filtering on a celite pad, the solvent was evaporated under reduced pressure to obtain an yellow oil. Flash chromatography (dichloromethane/methanol 98:2 + 1% NH_3) was performed in order to obtain 83 mg (0.21 mmol) of the pure product as a brownish clear oil.

Yield: 44.9%

HRMS: *m/z* 397.1439 ($[M+H]^+$

^{1}H NMR (CD_3OD): δ 7.82 (d, *J*=9.0 Hz, 2H), 7.07-6.97 (m, 3H), 6.65 (d, *J*=8.4 Hz, 2H), 4.21 (t, *J*=6.4 Hz, 2H), 4.08 (dd, *J*=10.0, 3.8 Hz, 1H), 3.81 (s, 6H), 3.79-3.69 (m, 1H), 3.28-3.17 (m, 1H), 2.10-1.94 (m, 1H), 1.94-1.79 (m, 1H).

^{13}C NMR (CD_3OD): δ 161.79, 153.34, 136.71, 135.35, 127.79, 123.74, 114.18, 105.05, 77.31, 65.45, 55.08, 32.15**.**

[84] Dichloromethane/methanol 9:1 + 1% NH_3. R_f starting material = 0.88; R_f product = 0.47.

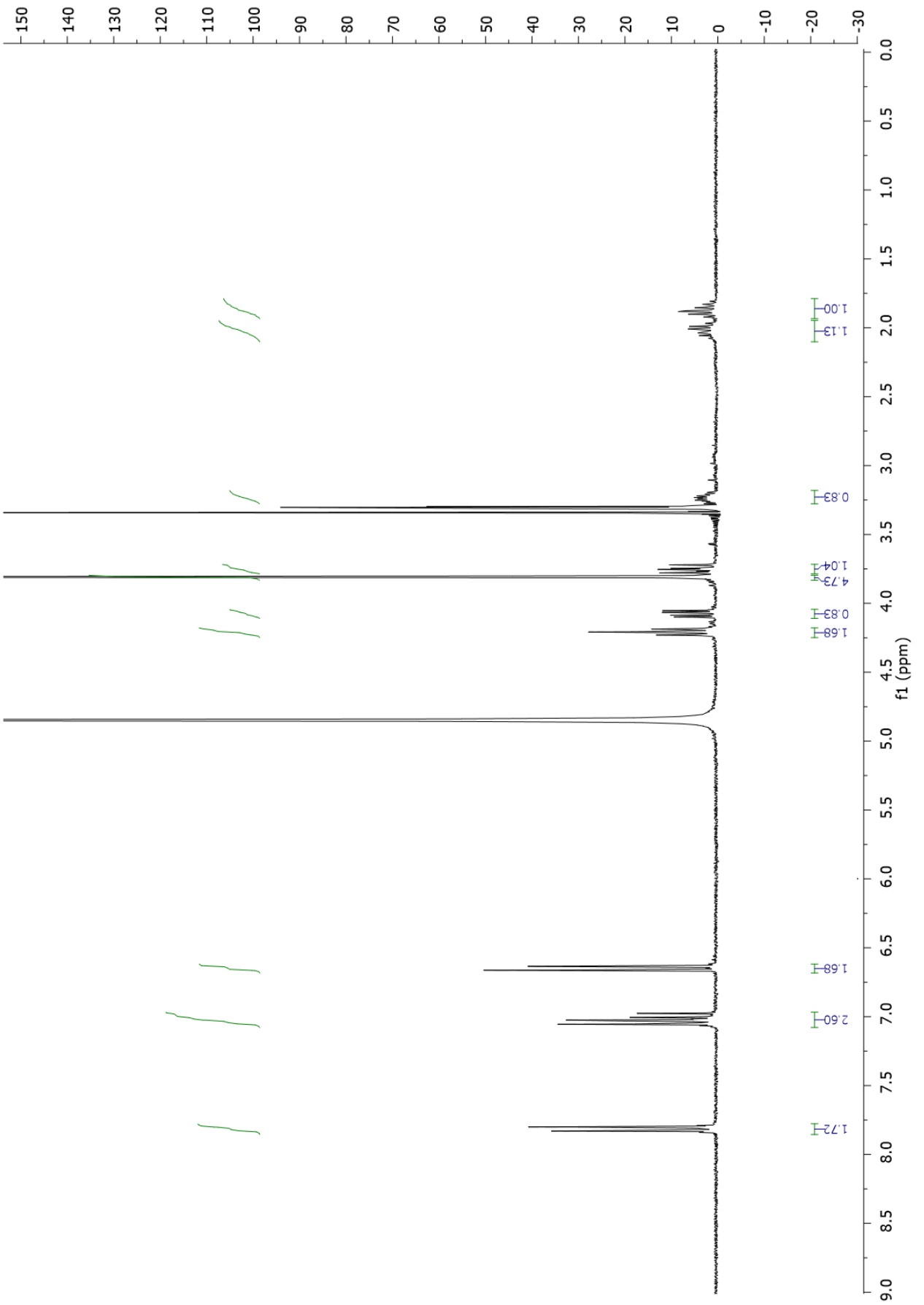
f1 (ppm)
1.00
1.13
0.83
1.04
4.73
0.83
1.68
1.68
2.60
1.72

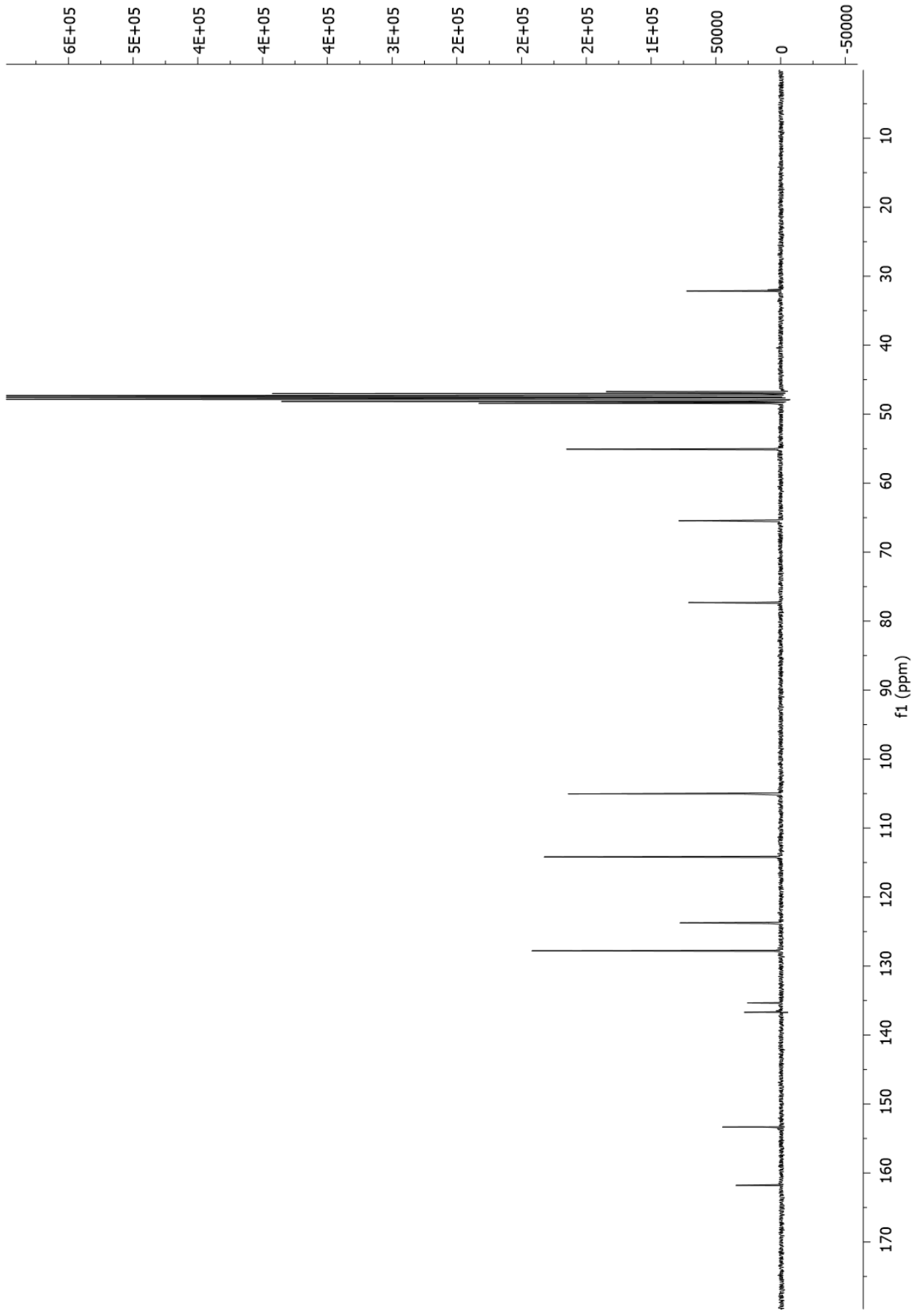
6E+05
5E+05
4E+05
4E+05
4E+05
3E+05
2E+05
2E+05
2E+05
1E+05
50000
0
-50000
10
20
30
40
50
60
70
80
90
100
110
120
130
140
150
160
170
f1 (ppm)

2-bromoresorcinol

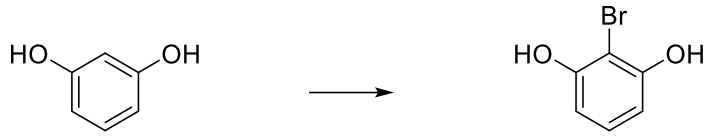

Chemical Formula: $C_6H_6O_2$
Molecular Weight: 110,11

Chemical Formula: $C_6H_5BrO_2$
Molecular Weight: 189,01

3 g (27.24 mmol) resorcinol were suspended in 45 mL chloroform and treated with 4.6 mL (89.89 mmol) of bromine. After heating to reflux until starting material was consumed (TLC monitoring)[85], the reaction was quenched with 10% solution of $Na_2S_2O_5$ and, upon separation, the organic layer was evaporated under reduced pressure. The residue was then dissolved in 13.5 mL MeOH and 67.5 mL H_2O. A solution of 6.86 g (54.48 mmol) Na_2SO_3 and 2.18 g (54.48 mmol) NaOH in 81 mL H_2O was added. It was stirred for at room temperature until TLC[86] indicated the disappearance of starting material and subsequently acidified with a 5% solution of HCl. The aqueous phase was extracted several times with ethyl ether and the combined organic phase was dried over anhydrous sodium sulfate, filtered and the solvent was evaporated in vacuo.
The crude was crystallized from chloroform/cyclohexane to obtain the pure product as a white solid (3.70 g, 19.58 mmol).

Yield: 71.8%

m.p. 102°C

^{1}H NMR ($CDCl_3$): δ 7.11 (t, *J*=8.2 Hz, 1H), 6.60 (d, *J*=8.2 Hz, 2H).

[85] Cyclohexane/ethyl acetate 8:2. R_f starting material = 0.13; R_f product = 0.37.
[86] Cyclohexane/ethyl acetate 8:2. R_f starting material = 0.37; R_f product = 0.30.

2-bromo-1,3-bis(2-methoxyethoxymethyloxy)resorcinol

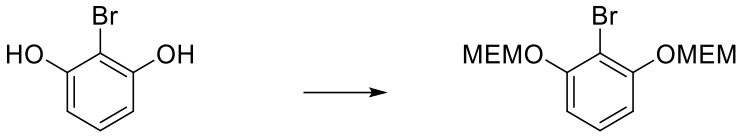

Chemical Formula: $C_6H_5BrO_2$
Molecular Weight: 189,01

Chemical Formula: $C_{14}H_{21}BrO_6$
Molecular Weight: 365,22

Under a nitrogen atmosphere a dichloromethane (10 mL) solution of 2-bromoresorcinol (1.04 g, 5.51 mmol) was cooled to 0°C. and DIPEA (2.11 mL, 12.13 mmol) was added. Following the addition of MEM-Cl (1.45 mL, 12.13 mmol), the reaction mixture was allowed to stir, slowly warming to room temperature, until starting material was consumed (TLC monitoring)[87]. The reaction mixture was quenched by the addition of 10% aqueous solution of HCl. The organic layer was washed with washed with 10% aqueous solution of NaOH, brine, dried over anhydrous sodium sulfate and filtered. The filtrate was concentrated under reduced pressure to provide a yellow oil. Flash chromatography (cyclohexane/ethyl acetate 8:2) was performed in order to obtain 1.3 g (3.56 mmol) of the pure product as a colorless oil.

Yield: 62.6%

^{1}H NMR ($CDCl_3$): δ 7.16 (t, *J*=8.3 Hz, 1H), 6.87 (d, *J*=8.3 Hz, 2H), 5.33 (s, 4H), 3.89-3.83 (m, 4H), 3.57-3.53 (m, 4H), 3.36 (s, 6H).

[87] Cyclohexane/ethyl acetate 7:3. R_f starting material = 0.45; R_f product = 0.43,

2,3-bis(2-methoxyethoxymethyloxy)phenol

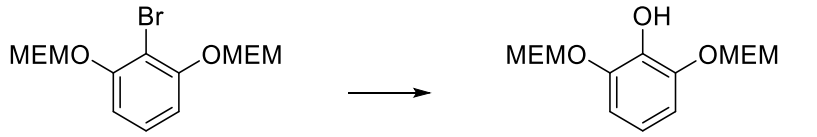

Chemical Formula: $C_{14}H_{21}BrO_6$
Molecular Weight: 365,22

Chemical Formula: $C_{14}H_{22}O_7$
Molecular Weight: 302,32

Under nitrogen atmosphere 1.6 M n-butyllithium (5 mL) was added to an ice-cooled solution of 2-bromo-1,3-bis(2-methoxyethoxymethyloxy)resorcinol (1.46 g, 4.00 mmol) in dry tetrahydrofuran (14.6 mL) at -78°C. After stirring for 1 hour at the same temperature, trimethyl borate (0.76 mL, 6.8 mmol) was added dropwise. After 30 minutes under stirring at room temperature the solution was concentrated reduced pressure and the crude residue was dissolved in 20% aqueous acetone (2.9 mL) containing $NaHCO_3$ (3.83 g). Afterward, Oxone (287 mg) was added and after 5 min the reaction was quenched with NaH_SO_3 (2.09 g). The reaction mixture was extracted with ethyl acetate and the organic layer dried over anhydrous sodium sulfate and filtered. Evaporation of the solvent gave an oil, which was purified by column chromatography. Eluting with cyclohexane/acetone (4:6) afforded the pure product[88] as a yellow oil (725 mg, 2.40 mmol).

Yield: 60.0%

^{1}H NMR ($CDCl_3$): δ 6.87-6.82 (m, 2H), 6.73 (dd, *J*=9.1, 7.3 Hz, 1H), 5.29 (s, 4H), 3.88 (dd, *J*=5.5, 3.7 Hz, 4H), 3.58 (dd, *J*=5.5, 3.7 Hz, 4H), 3.39 (s, 6H).

[88] Cyclohexane/ethyl acetate 1:1. R_f starting material = 0.55; R_f product = 0.13,

N,N-dimethylaminomethylene-4-(3-hydroxy-4-(2,3-bis-(2-methoxy ethoxymethyloxy)phenoxy)butoxy)benzenesulfonamide

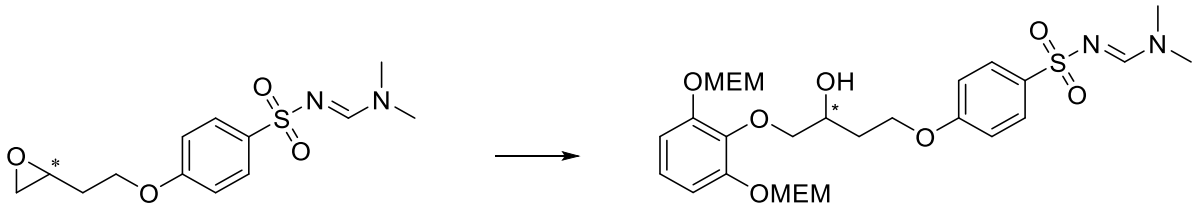

Chemical Formula: $C_{13}H_{18}N_2O_4S$
MW: 298,36

Chemical Formula: $C_{27}H_{40}N_2O_{11}S$
MW: 600,68

A solution of $PdCl_2$ (1.5 mg, 0.21 mmol), TBAB (68 mg, 0.21 mmol) and K_2CO_3 (29 mg, 0.21 mmol) in 3 mL of water was prepared and heated to 60°C. N,N-dimethylaminomethylene-4-(oxiranylethoxy)benzenesulfonamide (257 mg, 0.85 mmol) was then added to the stirring mixture along with 2,3-bis(2-methoxyethoxymethyloxy)phenol (277 mg, 0.93 mmol). The reaction was then stirred at 60°C until starting material was consumed (TLC monitoring)[89]. The product was then extracted three times using ethyl acetate. The combined organic layers were then dried over anhydrous sodium sulphate and concentrated under vacuum to yield the brown crude product, which was then purified by flash chromatography (cyclohexane/acetone 6:4) to yield the product as a yellow oil (115 mg, 0.19 mmol).

Yield: 20.4%

^{1}H NMR ($CDCl_3$): 8.10 (s, 1H), 7.78 (d, *J*=8.9 Hz, 2H), 7.00-6.84 (m, 5H), 5.29 (s, 4H), 4.29-4.13 (m, 4H), 4.13-4.02 (m, 1H), 3.88-3.78 (m, 4H), 3.56-3.48 (m, 4H), 3.35 (s, 6H), 3.10 (s, 3H), 2.99 (s, 3H), 2.02-1.81 (m, 2H).

[89] Cyclohexane/acetone 6:4. R_f starting material = 0.41; R_f product = 0.22.

N,N-dimethylaminomethylene-4-(3-mesyloxy-4-(2,3-bis-(2-methoxyethoxymethyloxy)phenoxy)butoxy)benzenesulfonamide

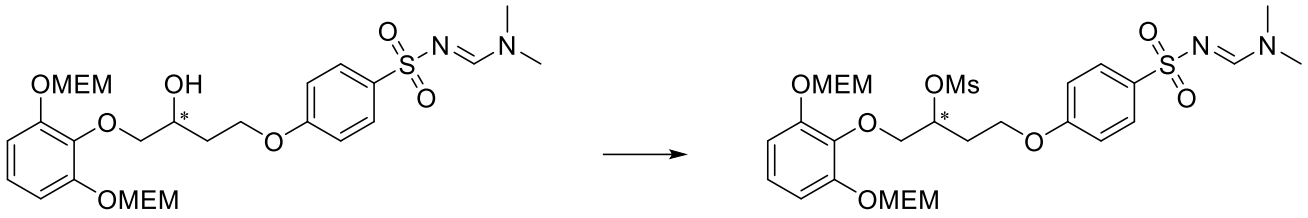

Chemical Formula: $C_{27}H_{40}N_2O_{11}S$
MW: 600,68

Chemical Formula: $C_{28}H_{42}N_2O_{13}S_2$
MW: 678,77

N,N-dimethylaminomethylene-4-(3-hydroxy-4-(2,3-bis-(2-methoxyethoxymethyloxy)phenoxy) butoxy)benzenesulfonamide (140 mg, 0.24 mmol) was dissolved in dichloromethane (1 mL), triethylamine (75 µL, 0.52 mmol) was added, and after the reaction mixture was cooled down to 0°C mesyl chloride (40 µL, 0.48 mmol) was added dropwise. The solution was stirred at room temperature until TLC[90] indicated the disappearance of starting material. The reaction mixture was washed with 10% aqueous solution of HCl 10%, aqueous solution of $NaHCO_3$, and then with brine. The organic phase was dried over anhydrous sodium sulfate and filtered and the solvent was evaporated in vacuo, providing the pure product as 146 mg of a yellow oil (0.22 mmol).

Yield: *91.6%*

^{1}H NMR ($CDCl_3$): δ 8.11 (s, 1H), 7.81 (d, *J*=8.9 Hz, 2H), 7.02-6.82 (m, 5H), 5.32-5.16 (m, 5H), 4.28-4.13 (m, 4H), 3.88-3.78 (m, 4H), 3.59-3.50 (m, 4H), 3.36 (s, 6H), 3.14 (s, 3H), 3.12 (s, 3H), 3.02 (s, 3H), 2.38-2.24 (m, 2H).

[90] Dichloromethane/methanol 95:5. R_f starting material = 0.39; R_f product = 0.49.

N,N-dimethylaminomethylene-4-(3-azido-4-(2,3-bis-(2-methoxyethoxymethyloxy)phenoxy)butoxy)benzenesulfonamide

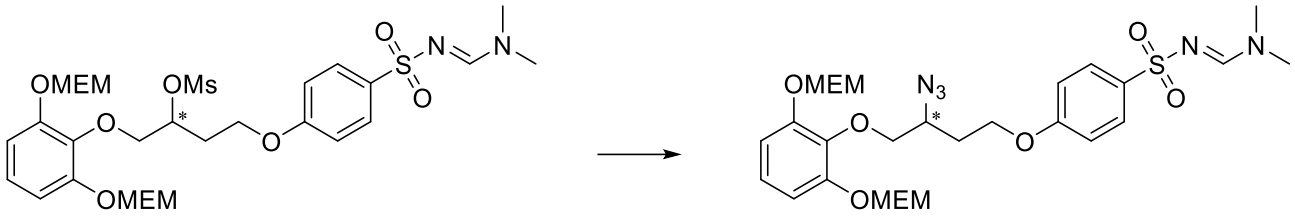

Chemical Formula: $C_{28}H_{42}N_2O_{13}S_2$
MW: 678,77

Chemical Formula: $C_{27}H_{39}N_5O_{10}S$
MW: 625,69

Sodium azide (133 mg, 2.04 mmol) was added to a solution of N,N-dimethylaminomethylene-4-(3-mesyloxy-4-(2,3-bis-(2-methoxyethoxymethyloxy)phenoxy)butoxy)benzenesulfonamide (141 mg, 0.20 mmol) in DMF (2.72 mL) and water (0.88 mL). Then, the reaction mixture was refluxed, under stirring, until TLC[91] indicated the disappearance of starting material.

Afterward, the solution was evaporated in vacuo and the crude was dissolved in acetone. The formed precipitate was removed by filtration and then the solvent was evaporated in vacuo, providing a yellow oil. Flash chromatography (cyclohexane/acetone 6:4) was performed in order to obtain of the pure product as a colorless oil (86 mg, 0.14 mmol).

Yield = 68.9%

^{1}H NMR ($CDCl_3$): δ 8.12 (s, 1H), 7.82 (d, *J*=8.8 Hz, 2H), 7.01–6.88 (m, 5H), 5.28 (s, 4H), 4.25–4.01 (m, 5H), 3.88–3.83 (m, 4H), 3.60–3.51 (m, 4H), 3.37 (s, 6H), 3.12 (s, 3H), 3.01 (s, 3H), 2.25–2.09 (m, 1H), 2.04–1.92 (m, 1H).

[91] Cyclohexane/Acetone 6:4. R_f starting material = 0.18; R_f product = 0.30.

Compound XXIII

4-(3-azido-4-(2,6-dihydroxyphenoxy)butoxy)benzenesulfonamide

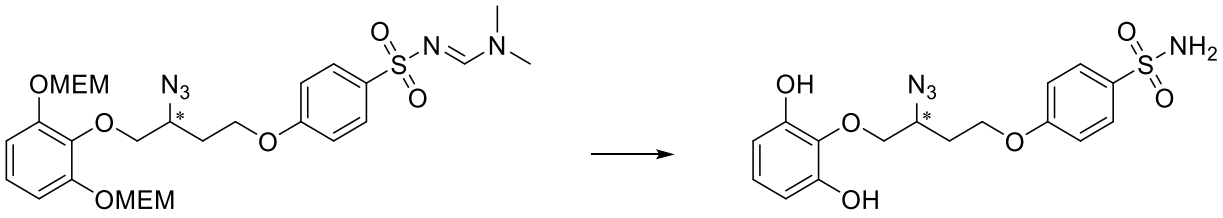

Chemical Formula: $C_{27}H_{39}N_5O_{10}S$
MW: 625,69

Chemical Formula: $C_{16}H_{18}N_4O_6S$
MW: 394,40

0.11 mL of HCl 37% (1.39 mmol) was added dropwise to a solution of N,N-dimethylaminomethylene-4-(3-azido-4-(2,3-bis-(2-methoxyethoxymethyloxy)phenoxy)butoxy)benzenesulfonamide (86 mg, 0.14 mmol) in methanol (1 mL). The resulting solution was vigorously stirred at 60°C, until TLC[92] indicated the disappearance of starting material. Afterward, methanol was removed from the reaction mixture in vacuo. Flash chromatography (cychlohexane/acetone 6:4) was performed in order to obtain 46 mg (0.12 mmol) of the pure product as a yellow oil.

Yield: 81.5%

HRMS: *m/z* 393.2113 ($[M+H]^-$

^{1}H NMR (CD_3OD): δ 7.83 (d, *J*=9.0 Hz, 2H), 7.07 (d, *J*=9.0 Hz, 2H), 6.99–6.93 (m, 1H), 6.86–6.74 (m, 2H), 4.30–4.04 (m, 5H), 2.28–2.13 (m, 1H), 2.08–1.94 (m, 1H).

^{13}C NMR (CD_3OD): δ 161.66, 150.49, 135.48, 134.24, 127.82, 123.71, 114.23, 107.32, 74.25, 64.66 59.26, 30.20.

[92] Cyclohexane/Acetone 6:4. R_f starting material = 0.30; R_f product = 0.20.

Compound XXIV

4-(3-amino-4-(2,6-dihydroxyphenoxy)benzenesulfonamide

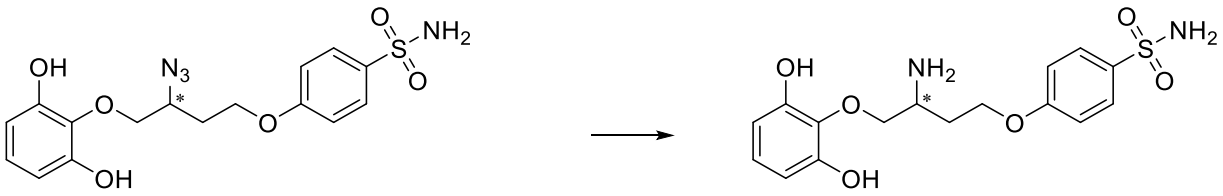

Chemical Formula: $C_{16}H_{18}N_4O_6S$
MW: 394,40

Chemical Formula: $C_{16}H_{20}N_2O_6S$
MW: 368,40

To a solution of 45 mg of 4-(3-azido-4-(2,6-dihydroxyphenoxy)benzenesulfonamide (0.12 mmol) in methanol (1 mL) was added 24 mg of Pd/C 5%. The mixture was then vigorously shaken under hydrogen atmosphere at room temperature until starting material was consumed (TLC monitoring)[93]. After filtering on a celite pad, the solvent was evaporated under reduced pressure to obtain an yellow oil. Preparative TLC chromatography (dichloromethane/methanol 90:10 + 1% NH_3) was performed in order to obtain 14 mg (0.03 mmol) of the pure product as a white waxy solid.

Yield: 25.0%

HRMS: *m/z* 369.1172 ($[M+H]^+$

^{1}H NMR (CD_3OD): δ δ 7.82 (d, *J*=8.9 Hz, 2H), 7.05 (d, *J*=8.9 Hz, 2H), 6.72 (t, J=8.2 Hz, 1H), 6.33 (d, *J*=8.2 Hz, 2H), 4.22 (t, *J*=6.1 Hz, 2H), 4.15 (dd, *J*=10.6, 3.2 Hz, 1H), 3.85 (dd, *J*=10.6, 8.0 Hz, 1H), 3.45 – 3.36 (m, 1H), 2.15 – 1.90 (m, 2H).

^{13}C NMR (CD_3OD): δ 161.76, 151.09, 135.437, 135.16, 127.78, 123.80, 114.21, 107.45, 76.75, 65.29, 32.30.

[93] Cyclohexane/Acetone 6:4 + 1% NH_3. R_f starting material = 0.20; R_f product = 0.11.

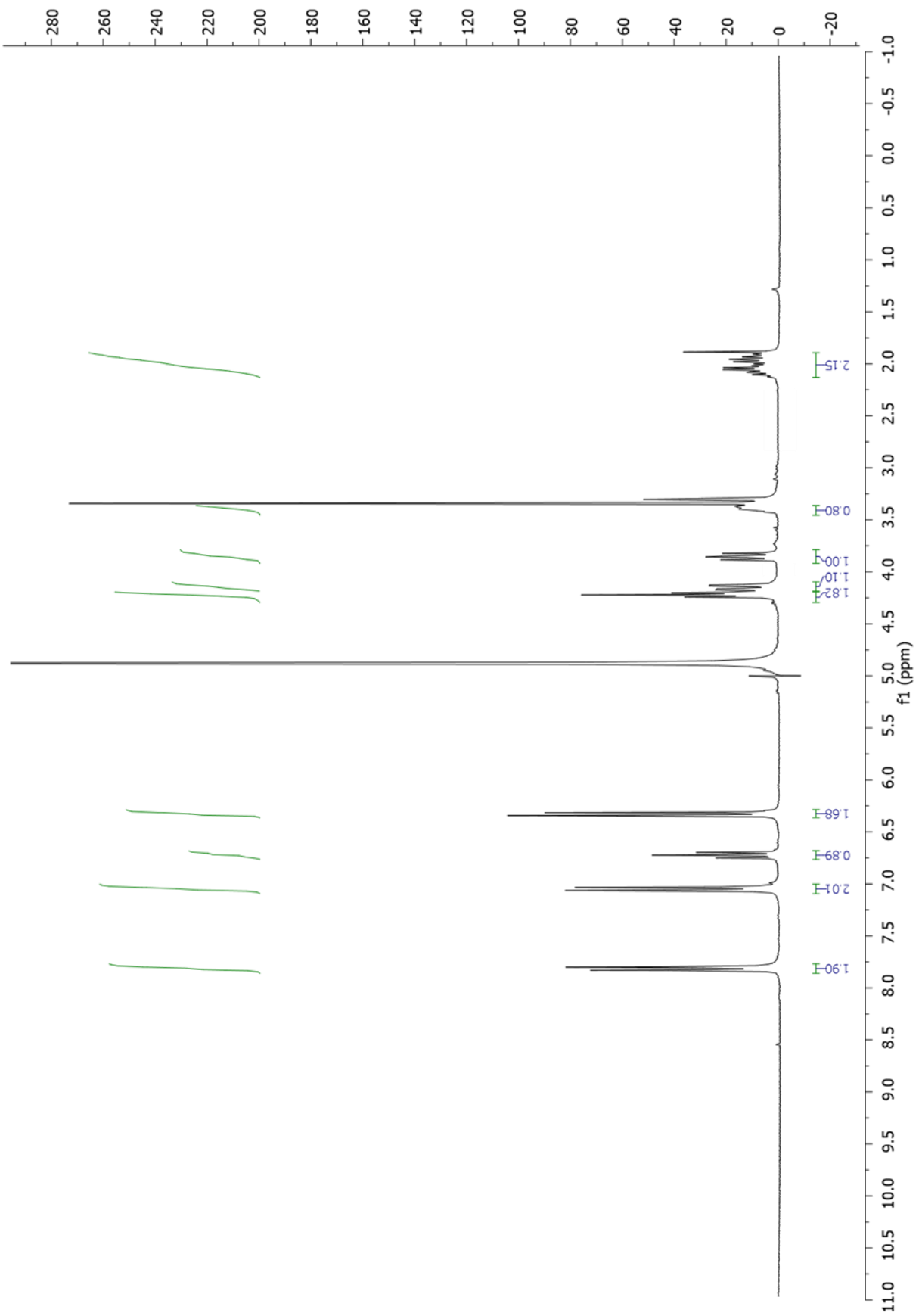
f1 (ppm)
2.15
0.80
1.00
1.10
1.82
1.68
0.89
2.01
1.90

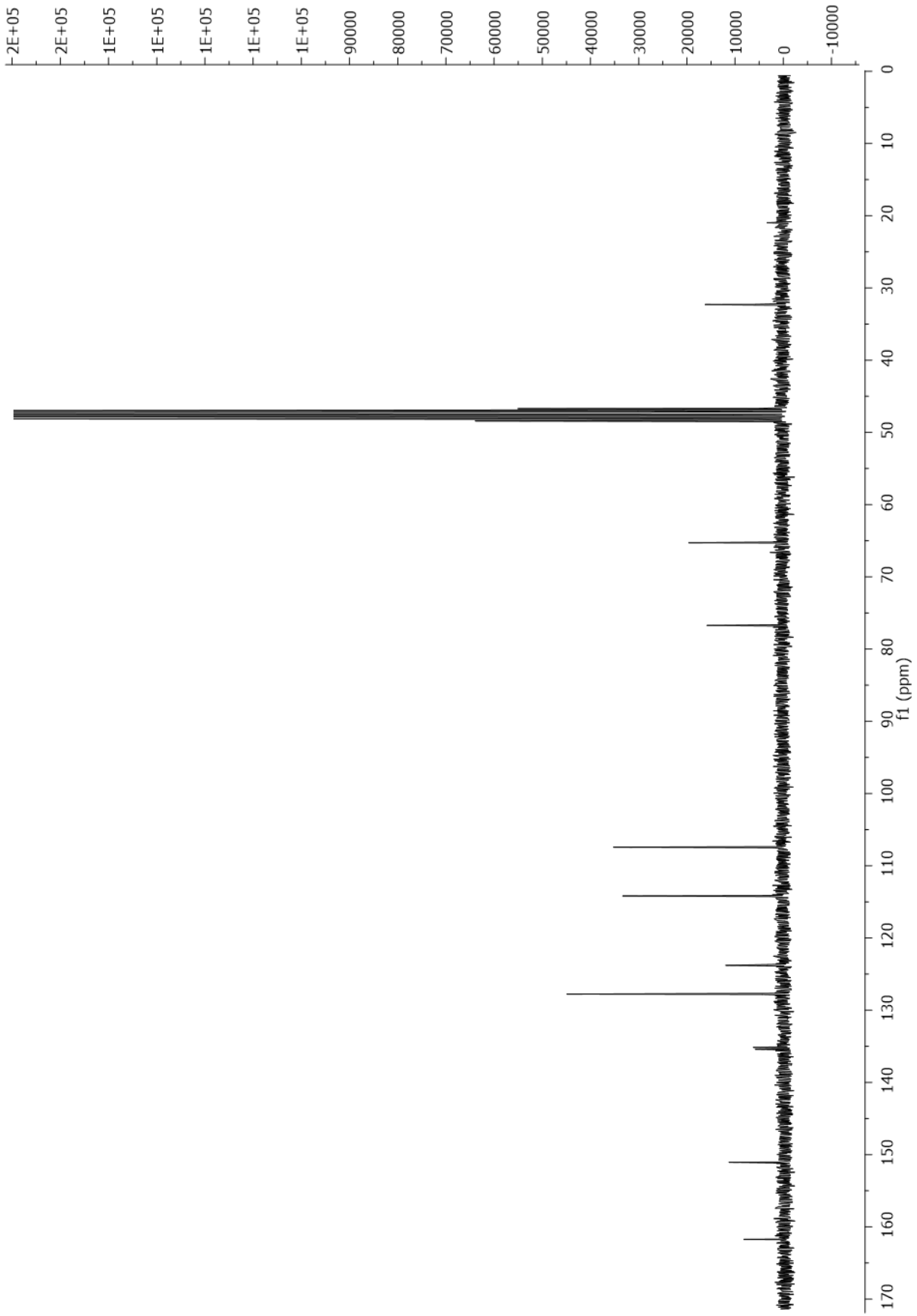
2E+05
2E+05
1E+05
1E+05
1E+05
1E+05
1E+05
90000
80000
70000
60000
50000
40000
30000
20000
10000
0
-10000
0
10
20
30
40
50
60
70
80
90
100
110
120
130
140
150
160
170
f1 (ppm)